Purkinje cell axonal torpedoes enhance axonal spike fidelity and cerebellar function

By

Daneck Lang-Ouellette

Department of Biology
McGill University
Montreal, Quebec, Canada
December 2020

A thesis submitted to the Faculty of Graduate and Postdoctoral Studies at McGill University in partial fulfillment of the requirements of the degree of

DOCTOR OF PHILOSOPHY

TABLE OF CONTENTS

LIST OF FIGURES

LIST OF TABLES

LIST OF ABBREVIATIONS

ACSF	artificial cerebrospinal fluid
AD	Alzheimer's disease
AIS	axon initial segment
ALS	amyotrophic lateral sclerosis
Aniso	anisomycin
ARSACS	autosomal recessive spastic ataxia of Charlevoix-Saguenay
ASD	autism spectrum disorder
Avg.	average
BC	basket cells
Ca^{2+}	calcium ions
Caspr	contactin-associated protein
CCD	Charged-coupled device
CDJ	Creutzfeldt-Jakob disease
CF	climbing fibers
CN	cerebellar nuclei
cm	centimeter
CTX	Ciguatoxin
CV	coefficient of variation
DHP	dihydropyridine
DPH	diphenylhydantoin
EM	electron microscopy
ER	endoplasmic reticulum
ET	essential tremor
FF	Firing frequency
Fig	Figure
g	gram
GABA	γ-aminobutyric acid
GC	granule cells
GCL	granule cell layer
GFP	green fluorescent protein
h	hour
HD	Huntington disease
Iba1	ionized calcium binding adaptor molecule 1
IDPN	β-iminodipropionitrile
ION	inferior olive nuclei
IP	intraperitoneal
IP_3	inositol-1,4,5-triphosphate
IP_3R	inositol-1,4,5-triphosphate receptor

kDa	kilodalton
kg	kilograms
L7 (pcp2)	Purkinje cell protein 2 specific promoter
LENAS	leukoencephalopathy with neuroaxonal spheroids
MBP	myelin basic protein
MF	mossy fibers
min	minute
mL	milliliter
ML	molecular layer
MLI	molecular layer interneuron
mM	millimolar
MS	multiple sclerosis
MSA-C	multiple system atrophy-cerebellar
MTCL1	microtubule cross-linking factor 1
µm	micrometer
µM	micromolar
mW	milliwatts
n	number
NF	neurofilament
NF-H	neurofilament-heavy chain
Ni^{2+}	Nickel ions
nm	nanometer
nM	nanomolar
NoR	Node of Ranvier
ns	not significant
OPCA	olivopontocerebellar atrophy
P#	post-natal day #
PB	phosphate buffer
PBS	phosphate buffer saline
PC	Purkinje cells
PCL	Purkinje cell layer
PD	Parkinson’s disease
PF	parallel fibers
PFA	paraformaldehyde
pH	potential of hydrogen
ROS	reactive oxygen species
RPM	revolutions per minute
RT	room temperature
SC	Stellate cells
SCA#	spinocerebellar ataxia type #

SER	smooth endoplasmic reticulum
SEM	standard error of the mean
SMI-34	hyperphosphorylated neurofilament (clone SMI-34)
STIM1	stromal interaction molecule 1
TTX	tetrodotoxin
VGCC (Cav#)	voltage-gated calcium channel
VGKC (Kv#)	voltage-gated potassium channel
VGSC (Nav#)	voltage-gated sodium channel
VOR	vestibular ocular reflex
WT	wildtype

ABSTRACT

Purkinje cells are the sole output of the cerebellar cortex, making them central to motor coordination. Purkinje cell focal axonal swellings, also called “torpedoes”, have been mainly observed in human post-mortem tissue of neurodegenerative diseases. The higher presence of torpedoes in diseased brains has led to the hypothesis that torpedoes contribute to pathophysiology.

This thesis represents one of the first functional investigations of axonal torpedoes in healthy mice. Using transgenic mice that express GFP specifically in Purkinje cells, I explored the functional properties underlying torpedoes in healthy brains. I recorded axonal propagation using dual-targeted soma and axon recordings. I discovered that axons with torpedoes propagated action potentials with fewer axonal failures than those without, suggesting that longstanding assumptions about the role of axonal torpedoes may be incorrect. By pharmacologically mimicking high axonal spike failures, I found that inducing axonal failures led to the formation of axonal swellings mediated by voltage-gated calcium channels. To determine whether the enhanced spike fidelity observed with axonal torpedoes was behaviorally relevant, we tested several cerebellar-related tasks. We found that mice displaying higher levels of cerebellar-related learning had more torpedoes than mice with lower levels of cerebellar-related learning.

In this Ph. D. thesis, I challenged the prevailing hypothesis that Purkinje cell axonal torpedoes are neurodegenerative. I proposed instead that they represent a neuroadaptive mechanism promoting axonal action potential propagation that enhances motor learning in animals. The results presented in this thesis broaden our fundamental understanding of Purkinje cell axonal torpedoes.

RÉSUMÉ

Les cellules de Purkinje sont la seule voie de sortie de l'information du cortex cérébelleux, ce qui en fait le centre de contrôle de la coordination motrice. Les enflements de l'axone des cellules de Purkinje, aussi appelés « Torpedoes », ont principalement été observés chez l'humain post-mortem atteint de maladies neurodégénératives. La présence accrue des torpedoes dans ces maladies neurodégénératives a mené à l'hypothèse que ceux-ci contribueraient à la physiopathologie.

Cette thèse présente l'une des premières investigations fonctionnelles sur des torpedoes chez des animaux en santé. L'utilisation de souris transgéniques, exprimant GFP dans les cellules de Purkinje, a permis d'explorer les torpedoes et leurs propriétés fonctionnelles sous-jacentes chez des souris saines. J'ai enregistré la propagation axonale en utilisant des enregistrements ciblés du soma et de l'axone. Ces enregistrements ont permis de découvrir que les axones ayant des torpedoes ont une propagation de potentielle d'action comportant moins d'erreur de propagation comparativement à ceux sans torpedoes. Ceci démontre une meilleure propagation de l'information chez les axones ayant un torpedo, suggérant que l'hypothèse neurodégénérative précédemment avancée à propos de la fonction des torpedoes pourrait être incorrecte. J'ai ensuite induit pharmacologiquement un haut niveau d'erreur de propagation de potentiel d'action. Ces expériences ont démontré qu'induire des erreurs de propagation mène à la formation d'enflements axonales et ce, grâce à des canaux calcium dépendants au voltage. Afin de déterminer si l'amélioration de la fidélité de propagation observée chez les torpedoes est pertinente au niveau du comportement animal, j'ai testé plusieurs tâches reliées au comportement moteur du cervelet. Ces résultats ont révélé que les souris démontrant un plus grand apprentissage au cours de ces

tâches corrèlent normalement avec un plus grand nombre de torpedoes que les souris ayant moins appris durant cette même tâche.

Cette thèse de doctorat, conteste l'hypothèse neurodégénérative initiale sur les torpedoes des cellules de Purkinje. Mes résultats mettent de l'avant un mécanisme neuro-adaptatif aidant la propagation axonale des potentiels d'actions afin d'améliorer l'apprentissage moteur chez les animaux. L'ensemble de la recherche présentée dans cette thèse approfondit notre compréhension fondamentale sur les enflements axonales des cellules de Purkinje.

DEDICATION

I would like to thank all my Montreal friends (you know who you are!) which made this time so much more enjoyable. Thanks to Sara Larivière, for making PN1 somehow pleasant and for the numerous card games nights. Special thanks to Dr. Nitin Kapadia for countless philosophical discussions (he would say “Arguments”, but what does he know!) about “contribution of chance in our life” and “free will”. His way of encouraging me to always push to better myself, will never be forgotten. Special thanks to Dr. Ziad El-Hajj, for having the terrible idea of introducing me to Scotch. Listening to me blow off steam or straight up complain, has made him a tremendous friend and confidant (he complains too!). Cheers guys!

I want to thank the Tremblay/Poirier family for their support throughout the last few years, but also for accepting me into their family.

Most importantly, I would like to thank all my family for their support, especially my parents, Joanne Lang and Robert Ouellette, and my siblings, Shannie and Nathaël for their constant encouragement. Although my research remains somewhat mysterious to them, their blind confidence and massive support in my success has undoubtedly been a driving force in this accomplishment.

Last but not least, I would like to express my sincere gratitude to Valérie Tremblay for her love, motivation, encouragement and support. Her unmatchable kindness towards others have made me rethink and transformed how I perceive our life in society. Having such a passionate, driven and compassionate partner is what made this journey so effortless.

ACKNOWLEDGEMENTS

First and foremost, I would like to express my sincere gratitude to my Ph.D. thesis advisor, Dr. Alanna J. Watt, for giving me this amazing opportunity, allowing me to grow as a scientist but also personally. Thank you for your constant support and encouragement through the hard times. I'll be forever grateful that you allowed and supported me in exploring different professional avenues. It was honestly an honor to work with you.

I want to thank my supervisory committee members, Dr. Alyson Fournier and Dr. Ed Ruthazer for their insightful input and support, which allowed me to make progress and reach all the milestones of the Ph.D. program. I would like to thank the Natural Sciences and Engineering Research Council (NSERC) for awarding me the Postgraduate-Doctoral Scholarship, and the Leonard and Kathleen O'Brien Humanitarian Trust for the postgraduate fellowship, which supported this work.

A special thanks to Dr. Per Jesper Sjöström for making custom data analysis software for this project. I would like to thank our collaborators Dr. Martijn Schonewille and his Ph.D. Student François G.C. Blot for their VOR experiment contribution.

I want to sincerely thank the former and current Watt lab members, for making my time in the lab an amazing experience. Special thanks to Dr. Sriram Jayabal, for mentoring me, but most importantly for his incomparable kindness and friendship. I would also like to acknowledge everyone that considerably helped advance this research project namely, Lovisa, Chloe, Carter, Connie, Pauline and Charlotte. Thanks to Kim, Brenda, Visou, Anna, Eviatar, Sophia and Amy for their support and constructive feedback on my research.

CONTRIBUTIONS TO ORIGINAL KNOWLEDGE

I, Daneck Lang-Ouellette, hereby claim the following parts of the thesis are distinct contributions to fundamental knowledge and original scholarship.

- Observed that Purkinje cells axonal torpedoes are not explicitly targeted by activated microglia for degradation, as a sign of inflammatory response.
- Described the morphological localization of torpedoes within the axons, showing that torpedoes are usually associated with the juxta-paranodal region of nodes of Ranvier, indicated by of Caspr protein staining.
- Characterized the somatic electrophysiological properties of Purkinje cells with and without axonal torpedoes, which were unaltered by the presence of Purkinje cells with axonal torpedoes.
- Demonstrated that Purkinje cells with axonal torpedoes have reduced axonal spike failures compared to control axons, in young and healthy L7(*pcp2*)-*tau*-GFP mice.
- Demonstrated that inducing artificial spike failures, by bath application of nanomolar concentration of TTX over a few hours, led to Purkinje cell axonal torpedo formation in live tissue.
- Characterized the mechanism of Purkinje cell axonal torpedo formation, which was entirely abolished in the absence of calcium ions, indicating the involvement of a calcium-dependent mechanism.
- Characterized the calcium dependent-mechanism of torpedo formation, by blocking voltage-gated calcium channels, using nickel ions. Voltage-gated calcium channels thus play a role in Purkinje cell axonal torpedo formation.

- Demonstrated that Purkinje cell torpedo formation does not require novel protein synthesis, since blocking this process does not alter the mechanism of torpedo formation.
- Demonstrated a positive correlation between motor coordination learning and the percentage of Purkinje cells with axonal torpedoes in specific regions of the cerebellum, using Rotarod and Erasmus Ladder assay.
- Described the distribution of axonal torpedoes across the whole cerebellar cortex of healthy L7(*pcp2*)-*tau*-GFP mice.

CONTRIBUTIONS OF AUTHORS

All experiments and analyses were performed by Daneck Lang-Ouellette unless stated otherwise below. Experimental designs were a collaboration between Daneck Lang-Ouellette and Dr. Alanna J. Watt.

CHAPTER 3: Purkinje cell myelin sheath (Fig 3.6) and neurofilament (Fig.3.2) immunohistochemistry were performed, collected and analyzed by Lovisa Ljungberg. Immunohistochemistry of Capsr (Fig. 3.7 and 3.9) and phosphorylated Neurofilaments (Fig 3.3) were performed and analyzed by Carter van Eitreim and Connie Li.

CHAPTER 4: Morphological measurements were done by Charlotte Rosen (Fig 4.1). Axonal reconstructions (Fig. 4.3) were done by Connie Li. T-type voltage-dependent calcium channel immunohistochemistry (Fig 4.9) was performed by Andy Huang.

CHAPTER 5: Rotarod assay (Fig 5.1) was performed by Pauline de Vanssay de Blavous. VOR assay (Fig 5.3) was a collaboration with Dr. Martijn Schonewille, and experiments were performed, and imaging data collection was done by Francois G.C. Blot. X-Clarity image processing and Rotarod (Fig 5.6) were done by Connie Li.

CHAPTER 1: INTRODUCTION

Movement coordination is essential for survival in the animal kingdom. From fish swimming, birds flying, monkeys climbing trees, to humans walking on two feet, well-coordinated sequences of repeated movements have allowed animals to not only evade predators but also to feed themselves and subsist. In modern life, coordination of movement does not necessarily hold the same critical role for human survival, primarily due to modern medicine and a comfortable lifestyle. However, the inability to move efficiently still greatly impacts a person's quality of life. Such motor coordination problems might arise from injuries as well as neurodegenerative diseases.

Understanding the basic functioning of the brain is instrumental in finding better ways to treat brain disorders. Each conscious and unconscious movement decision is processed and dictated by the brain. The coordination of movement has been associated with cerebellar cortical computational processing. Thus, establishing how information is transferred through the cerebellum is important. Information is transmitted through the cerebellar cortex exclusively via its output neurons, Purkinje cells. Sometimes these neurons display axonal swellings called "torpedoes", which may affect their ability to transfer information.

This dissertation will investigate axonal torpedoes to advance our understanding of their functional role in information processing, the molecular specializations of these structures, and their impact on motor learning.

CHAPTER 2: REVIEW OF LITERATURE

2.1 Cerebellum

2.1.1 Cerebellar Functions

The cerebellum is considered to be the center for coordinated voluntary movement because of the observation that damage to the cerebellar cortex leads to deficits in motor control, rather than paralysis, as observed following motor cortex damage (Kandel *et al.*, 2013). The cerebellum is involved in many motor-related diseases, notably the spinocerebellar ataxias (Schmahmann, 2004). Accumulating evidence suggests that the cerebellum contributes to higher cognitive function and is implicated in cognitive disorders such as autism spectrum disorder (ASD) (Verly *et al.*, 2014). The associations between specific cerebellar regions and behaviors in humans (King *et al.*, 2019) and mice (Reeber *et al.*, 2012) are well established in the literature, particularly for the flocculus and its role in the vestibular ocular reflex (VOR) (Lisberger & Fuchs, 1978). Although cerebellar regions have been functionally mapped, how the cerebellum integrates, and relays information is not fully understood.

2.1.2 Cerebellar Organization

The cerebellum is a highly organized structure divided into three distinct layers. The Purkinje cell layer is formed of a single sheet of Purkinje cell neurons. Surrounding the Purkinje cell layer are the superficial molecular layer and the deeper granule cell layer. The molecular layer contains molecular layer interneurons, like stellate cells and basket cells, which provide inhibitory input to the Purkinje cells. Purkinje cells also extend their dendrites into the molecular layer, where they receive most of their cerebellar input. The granule cell layer mainly contains densely packed

granule cells that extend their axons – the parallel fibers – through the Purkinje cell layer to the molecular layer, where they extend processes perpendicular to Purkinje cell dendrites, making synaptic connections with Purkinje cell dendritic arbors. Each Purkinje cell's dendritic tree integrates excitatory information from two different sources: parallel fibers, and a single climbing fiber. The climbing fibers originate from the inferior olivary nucleus, which is responsible for orchestrating motor coordination signals between the cerebellum and the spinal cord. Purkinje cell axons travel through the granule cell layer and converge in the white matter tract. From there, the axons project toward the cerebellar nuclei (CN), where they make synaptic connections with their postsynaptic targets in the CN (Fig 2.1). Purkinje cells are the sole output of the cerebellar cortex, and thus instrumental in maintaining motor coordination.

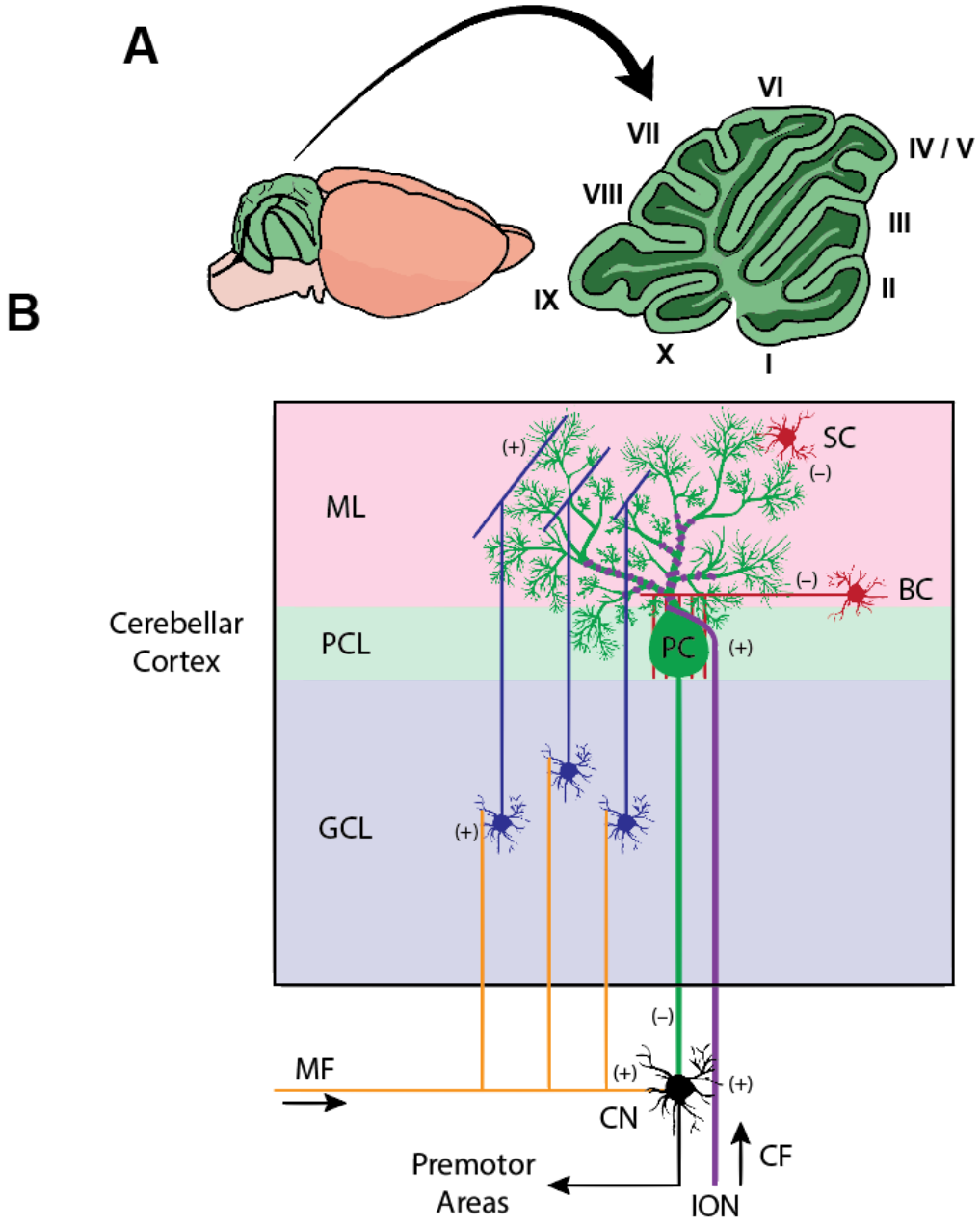

Figure 2.1: Cellular organization of the cerebellar cortex

(**A**) Schematic of a mouse brain, showing the cerebellum in green, a parasagittal cerebellar slice with the different lobules (arrow). (**B**) Schematic of the cerebellar cortex, showing the three layers; the molecular layer (ML), Purkinje cell layer (PCL), and the granule cell layer (GCL). Neuronal cell types are the Purkinje cell (PC; Green), the granule cell (GC; blue), the cerebellar nuclei neurons (CN; black) and the molecular layer interneuron like the stellate cell (SC) and basket cell (BC; red). Cerebellar external inputs come from the mossy fibers (MF) and the climbing fibers (CF) originating from various brainstem nuclei, and the inferior olive nuclei (ION), respectively. Excitatory (+) and inhibitory (-) connections within the cerebellar circuit.

2.2 Purkinje cells

Purkinje cells play a key role in the flow of information from the cerebellar cortex. There are approximately 200,000 Purkinje cells in the mouse cerebellum (Silvestri *et al.*, 2015). These cells possess the ability to fire action potentials spontaneously in the absence of any synaptic input (Thach, 1967). An action potential, also called a simple spike, is an electrical unit of information, which conveys information between Purkinje cells and CN neurons. Purkinje cell spontaneous activity or pacemaker activity can fire at frequencies ranging from 20 to 150 Hz (Raman & Bean, 1999). The ability to fire at such rates is mostly attributed to their large resurgent sodium current (Raman & Bean, 1997). Spontaneous activity is also facilitated by a fast potassium current after depolarization and the rapid deactivation of this potassium current. This fast potassium current prevents the over-hyperpolarization of Purkinje cells, allowing sodium channels to quickly depolarize the cells once more (Raman & Bean, 1999). Purkinje cells are GABAergic neurons, releasing synaptic vesicles containing the inhibitory neurotransmitter γ-aminobutyric acid (GABA) into the synaptic cleft (Person & Raman, 2012).

2.2.2 Axon Initial Segment

Purkinje cells are composed of a complex two-dimensional dendritic arbor, a relatively large cell body, and a long axon. The axon is divided into different sections, the first axon segment of 20-50 µm closest to the Purkinje cell body is unmyelinated and called the axon initial segment (AIS). Spikes are initiated in the AIS within 15-20 µm of the cell soma (Palmer *et al.*, 2010).

2.2.3 Myelin Sheath

Two well-characterized evolutionary mechanisms facilitate the propagation of action potentials after their initiation: (1) A large axon diameter, well described in famous experiments on the squid giant axon, which provides an escape mechanism with a fast reaction time (Young,

1938); and (2) an axon insulated by myelin, which reduces the axonal membrane capacitance. Oligodendrocytes are responsible for the formation of the myelin sheath around axons by extending their processes and tightly wrapping them around the axon. Purkinje cell myelination starts at postnatal day 6 (P6) in posterior lobules and gradually spreads to the anterior lobules by P10. By P12, most cerebellar axons are myelinated in mice (Foran & Peterson, 1992).

2.2.3 Nodes of Ranvier

The myelin sheath does not fully surround the whole axon; the formation of a myelin sheath around an axon leaves small unmyelinated gaps (~ 1 µm) called "Nodes of Ranvier" (Chapman & Hill, 2020). Since the myelin sheath insulates the axon, a large proportion of ionic channels are located within or near nodes of Ranvier. This narrow gap in the myelin sheath enables saltatory conduction, in which the action potential propagates its electrical charges by jumping from one node of Ranvier to the next one. Once voltage-gated sodium channels are activated, the axonal membrane (known as axolemma) at the node is depolarized. The electrical charge difference is propagated through the axon as current until it reaches another node of Ranvier. There, the axolemma is once again depolarized and the charge is thus propagated until it reaches its target.

Nodes of Ranvier are composed of three distinct sections: the node, the paranode, and the juxtaparanode (Fig 2.2). The node is the gap in the myelin sheath and contains a high density of voltage-gated sodium channels (VGSC), (Zonta *et al.*, 2011). The paranode is the end of the myelin sheath where it forms tight paranodal junctions with the axolemma. This junction is made by the coupling of the glial protein Neurofascin 155 to the Contactin/Caspr1 protein complex on the axonal membrane (Garcia-Fresco *et al.*, 2006). The juxtaparanode is the start of the myelinated segment, which contains voltage-gated potassium channels (VGKC) responsible for the repolarization phase of the action potential (Fehmi *et al.*, 2018; Hirono *et al.*, 2015).

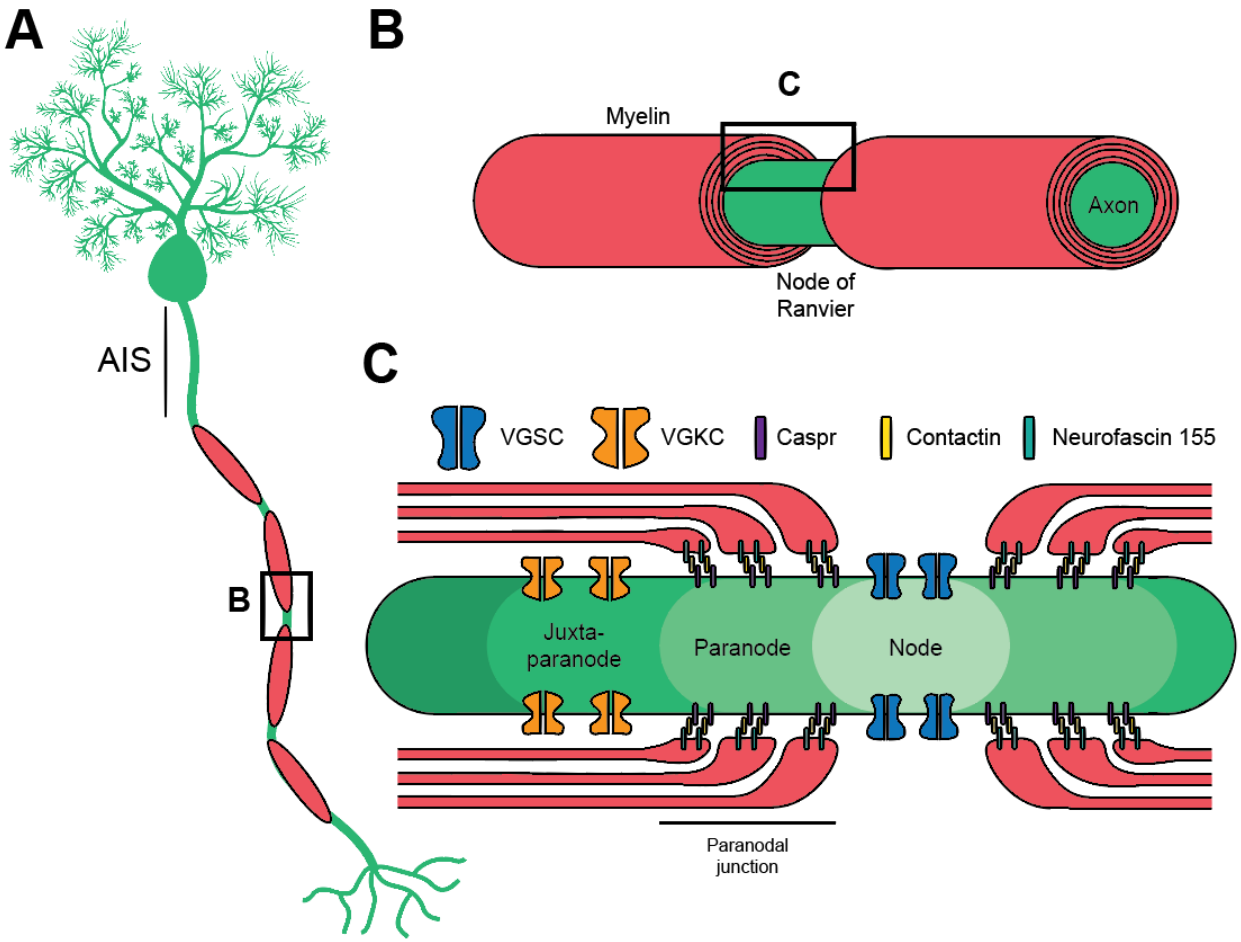

Figure 2.2: Axonal myelination and nodes of Ranvier
Schematic representation of a Purkinje cell with axon initial segment (AIS) and myelin sheath (**A**). (**B**) Overview of the myelin sheath surrounding the axon and a node of Ranvier, allowing for saltatory conduction of action potentials. (**C**) Structural organization of a node of Ranvier. Oligodendrocyte protrusion strongly adhering to the axolemma with a protein complex formed of Caspr, Contactin and Neurofascin 155 (Garcia-Fresco *et al.*, 2006). A simplified version of the voltage-gated sodium channel (VGSC) at nodes (e.g. $Na_V1.6$), forming a localized depolarization of the membrane and thus the propagation of an action potential (Zonta *et al.*, 2011). The presence of voltage-gated potassium channels (VGKC) at the juxtaparanode region allows for potassium release (e.g. $K_V1.2$) and rapid repolarisation of the membrane (Hirono *et al.*, 2015).

2.2.3 Axonal plasticity

One of the best-described mechanisms of axonal plasticity happens at the AIS. The AIS undergoes activity-dependent plasticity, showing a rearrangement of the AIS component away from the soma after high stimulation of hippocampal neurons (Grubb & Burrone, 2010). This AIS plasticity can be induced over a few hours of elevated activity (Evans *et al.*, 2015). Another study

showed that depriving auditory neurons of sensory inputs decreased their AIS length (Kuba *et al.*, 2010), while increase in calcium signaling through action potentials promotes myelin elongation (Krasnow *et al.*, 2018). The plasticity observed at the AIS could potentially apply to nodes of Ranvier, assuring a proper action potential conduction and velocity. A slight change in node of Ranvier length appears to regulate axonal propagation speed (Arancibia-Carcamo *et al.*, 2017). Recent experiments also showed that learning could increase the length of nodes of Ranvier (Cullen *et al.*, 2020). To my knowledge, however, such axonal plasticity mechanisms have yet to be observed in Purkinje cell axons.

2.2.4 Voltage-gated Ion Channels

The main cation channels responsible for the depolarization of neurons are voltage-gated sodium channels (VGSC). Purkinje cells go through developmentally regulated changes in sodium channel expression. During embryogenesis, Purkinje cells express mainly $Na_V1.3$ channels, which rapidly disappear after birth (Felts *et al.*, 1997). In contrast, $Na_V1.6$ channels are the main voltage-gated sodium channel expressed in Purkinje cell neurons throughout development (Felts *et al.*, 1997). $Na_V1.1$ has also been reported in Purkinje cells at P21, although its expression level is lower than $Na_V1.6$ (Schaller & Caldwell, 2003). Somatic expression has been observed for both $Na_V1.1$ and $Na_V1.6$ in Purkinje cells; however, only $Na_V1.6$ has been observed in the AIS and nodes of Ranvier (Vacher *et al.*, 2008).

Once a neuron depolarizes, voltage-gated potassium channels (VGKC) are responsible for repolarizing the membrane. The main voltage-gated potassium channel in Purkinje cells is $K_V3.3$, which is known for its fast inactivation properties (Chang *et al.*, 2007). $K_V7.2$, also known as a delayed rectifier channel, has also been reported in Purkinje cells (Cooper *et al.*, 2001). However, only Kv1.2 is located in the juxtaparanode regions of Purkinje cells (Hirono *et al.*, 2015).

Voltage-gated calcium channels (VGCC) are also highly expressed in Purkinje cells. The P/Q-type channel (i.e. $Ca_V2.1$), named "P" for "Purkinje," is the most highly-expressed voltage-gated calcium channel in Purkinje cells, and is responsible for generating complex spikes following climbing fiber activation of Purkinje cell dendrites (Davie *et al.*, 2008; Indriati *et al.*, 2013). Transient calcium channels, or T-type channels, have been observed in Purkinje cells, with $Ca_V3.1$ being by far the most highly expressed (Isope *et al.*, 2012; Talley *et al.*, 1999). Although the function of T-type calcium channels in Purkinje cells is not entirely clear, there is some evidence implicating them in motor learning (Ly *et al.*, 2013). The presence of L-type and R-type calcium channels has been demonstrated in Purkinje cells (Tringham *et al.*, 2007; Yokoyama *et al.*, 1995), but little is known about their function.

Table 2.1: Purkinje cell ion channel expression

Category	Type	Channel	Location	References
Voltage-gated	VGSC	$Na_V1.1$	Soma	(Kalume *et al.*, 2007)
		$Na_V1.6$	Soma/Dendrite/AIS/NoR	(Felts *et al.*, 1997), (Schaller & Caldwell, 2003)
	VGKC	$K_V1.2$	Juxtaparanodes	(Pan *et al.*, 2006), (Hirono *et al.*, 2015)
		$K_V3.3$	Soma/Dendrite/Axon	(Martina *et al.*, 2003), (Chang *et al.*, 2007)
		$K_V3.4$	Soma/Dendrite	(Martina *et al.*, 2003)
		$K_V7.2$ (KCNQ2)	Soma/AIS	(Cooper *et al.*, 2001), (Pan *et al.*, 2006)
		$K_V7.3$ (KCNQ3)	AIS	(Pan *et al.*, 2006)
	VGCC	$Ca_V1.2$ (L-type)	Soma/Dendrite	(Hell *et al.*, 1993)
		$Ca_V1.3$ (L-type)	Soma	(Hell *et al.*, 1993)
		$Ca_V2.1$ (P/Q type)	Soma/Dendrite/Axon	(Westenbroek *et al.*, 1995)
		Cav2.3 (R-type)	Soma/Dendrite	(Yokoyama *et al.*, 1995)
		$Ca_V3.1$ (T-type)	Soma/Dendrite	(Isope *et al.*, 2012)
		$Ca_V3.3$ (T-type)	Soma/Dendrite	(Molineux *et al.*, 2006)
Calcium-gated	BK	$K_{Ca}1.1$ (Slo1)	Soma/Dendrite/Paranodes	(Hirono *et al.*, 2015)
	IK	$K_{Ca}3.1$ (SK4)	NoR	(Grundemann & Clark, 2015)
	SK	$K_{Ca}2.2$ (SK2)	Soma/Dendrite	(Stocker & Pedarzani, 2000), (Hosy *et al.*, 2011)
Organelle	ER	IP3R1	Soma/Dendrite/Axon	(Sharp *et al.*, 1999)
		STIM1	Soma/Dendrite	(Hartmann *et al.*, 2014)
		RyR1	Soma/Dendrite	(Sawada *et al.*, 2008)

AIS, Axon initial segment; NoR, Node of Ranvier; ND, Not Determined

2.2.5 Calcium Signaling

Calcium plays an essential role as a signaling molecule. The following section is a review of calcium signaling, and, while covering the features of calcium signaling that are relevant for this thesis, is by no means exhaustive. Refer to (Brini *et al.*, 2014) for a complete review of calcium signaling in neurons. Calcium is a key signaling molecule in several biological processes, such as muscle contraction, bone formation, and release of neurotransmitters. Calcium concentration in the cytoplasm (~ 1µM) is approximately 2,000 times lower than in the extracellular milieu, making neurons highly vulnerable to calcium modulation (Fierro *et al.*, 1998).

One way that neurons control for calcium influx and maintain proper intracellular calcium homeostasis is through calcium buffering. Purkinje cell neurons express both Parvalbumin and Calbindin D-28k, which are calcium-binding proteins that act as calcium buffering systems (Celio, 1990). Maintaining an appropriate intracellular calcium concentration is crucial for proper cellular function. Calcium is stored inside organelles and intracellular signaling can be achieved by releasing it from these stores. The major calcium storage is the endoplasmic reticulum (ER), which uses stromal interaction molecule 1 (STIM1) for calcium uptake (Ryu *et al.*, 2017). Binding of inositol 1,4,5-triphosphate (IP_3) with its receptor (IP_3R), which is located on the ER membrane, releases calcium from the ER store (Berridge *et al.*, 2000; Koch, 1990). IP_3R can be found in axons, and intriguingly, it was recently showed that IP_3R activation in the Purkinje cell AIS leads to the inhibition of Purkinje cell firing (Gomez *et al.*, 2020).

Intracellular calcium also activates calcium-dependent potassium channels, which are identified by their conductance capacity (i.e. Big – BK, Intermediate – IK, and Small – SK channels). BK, or $K_{Ca}1.1$ are located in Purkinje cell paranodal junctions, and blocking axonal BK channels increases Purkinje cell failure rates (Hirono *et al.*, 2015). The IK (i.e. $K_{Ca}3.1$) channels

are located within the nodes of Ranvier of Purkinje cells. They are primarily responsible for increasing sodium channel availability, which ensures high axonal propagation fidelity (Grundemann & Clark, 2015).

2.3 Axonal swellings

Axonal swellings have been observed across the central nervous system, usually called "varicosities" when small and numerous, and "spheroids" on unmyelinated axons outside the cerebellar cortex. The presence of axonal swellings has also been reported in the peripheral nervous system, more precisely in the sciatic (Mendell *et al.*, 1977) and saphenous nerves (Tsukita & Ishikawa, 1980). Axonal swellings are also widely observed in the central nervous system, such as in the cerebral white matter (Jin *et al.*, 2015; Trapp *et al.*, 1998), the basal ganglia (Ohgami *et al.*, 1992), the corpus callosum (Newell *et al.*, 1999), the hippocampus (Galvin *et al.*, 1999), the brain stem (Liberski & Budka, 1999), the spinal cord (Carpenter, 1968; Clark *et al.*, 1984), the optic nerve (Yin *et al.*, 2016) and the retina (Risner *et al.*, 2018). Notably, some axonal swellings resemble axonal boutons, which are pre-synaptic terminals. These axonal boutons have been observed widely across the nervous system, for example, in hippocampal mossy fibers (Chamberland *et al.*, 2018) and CA3 neurons (Chereau *et al.*, 2017). However, axonal swellings generally refer to structures that are not pre-synaptic terminals. My Ph.D. research focused on the functional properties of Purkinje cell axonal swellings. It is an exciting but so-far unanswered question as to whether axonal swellings observed in different brain regions share functional similarities with Purkinje cell axonal swellings.

Purkinje cell axonal swellings were first drawn more than 100 years ago (Fig 2.3), by Santiago Ramon y Cajal in 1904 (Cajal, 1907; Cajal *et al.*, 1991). However, in 1918, Leendert

Bouman, who was later named one of the founding fathers of psychological psychiatry (Belzen, 1998), was the first to coin the term "torpedoes" for these structures (Bouman, 1918).

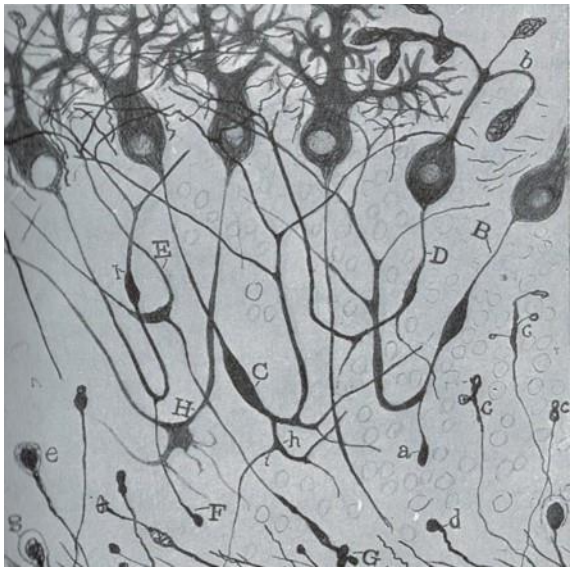

Figure 2.3: Original hand drawing of Purkinje cells with axonal swellings
Drawing made by Santiago Ramón y Cajal, "The father of modern Neuroscience," in 1904 (Cajal *et al.*, 1991).

During the 20th century, numerous articles showed the presence of torpedoes in a variety of conditions. For example, the formation of torpedo-like structures was reported in models of vitamin E deficiency (Lampert *et al.*, 1964; Lampert, 1967; Pentschew & Schwarz, 1962), where vitamin E was shown to have antioxidant properties (Gugliandolo *et al.*, 2017). Drug treatments like β-iminodipropionitrile (IDPN), which impairs axonal transport (Chou & Hartmann, 1965; Griffin *et al.*, 1978) or diphenylhydantoin (DPH), an anticonvulsant drug (Volk & Kirchgassner, 1985), also led to the formation of axonal swellings. Furthermore, electrical stimulation of cerebellar brain slices for 2h also caused Purkinje cell axonal swellings to form (Friede, 1964). Thus, several different types of cellular insults produce these axonal torpedoes.

2.3.1 Human neurodegeneration

To this day, Purkinje cell torpedoes have been mainly studied in human post-mortem tissue. Torpedoes have been observed in Arnold-Chiari malformation, which causes the extrusion of the cerebellum by the foramen magnum (Aring, 1938).They have also been recorded in different types of cerebellar atrophy, including cases of olivopontocerebellar atrophy (OPCA) (Ferrer *et al.*, 1994; Petito *et al.*, 1973) and multiple system atrophy-cerebellar (MSA-C) (Louis *et al.*, 2014a), all of which are characterized by cerebellar degeneration. Since the cerebellum was initially identified as a center for motor control, it was not surprising to observe torpedoes in motor-related diseases. In many cases, torpedoes were observed in illnesses related to motor dysfunction such as those that impact posture, gait and balance, including various types of ataxias (Corral-Juan *et al.*, 2018; Kemp *et al.*, 2016; Louis *et al.*, 2019; Norman, 1940; Sasaki *et al.*, 1998; Yang *et al.*, 2000). Figure 2.4 demonstrates the observation of torpedoes in the granule cell layer of a human post-mortem case of Friedreich's ataxia. Torpedoes have also been reported in other motor control diseases which are not classically cerebellar diseases, like Parkinson's disease (PD) (Louis *et al.*, 2009b), Huntington's disease (HD) (Sakai *et al.*, 2015), and amyotrophic lateral sclerosis (ALS) (Hirano *et al.*, 1967). Torpedoes have been extensively studied in essential tremor (ET) and are thought to be the primary pathological hallmark of this disorder (Axelrad *et al.*, 2008; Babij *et al.*, 2013; Louis *et al.*, 2009b; Louis *et al.*, 2019; Louis *et al.*, 2014a; Louis *et al.*, 2014b; Louis *et al.*, 2006; Louis *et al.*, 2009c). Taken together, the observation of torpedoes in so many diverse human diseases have reinforced the idea that torpedoes are associated with cerebellar motor dysfunction.

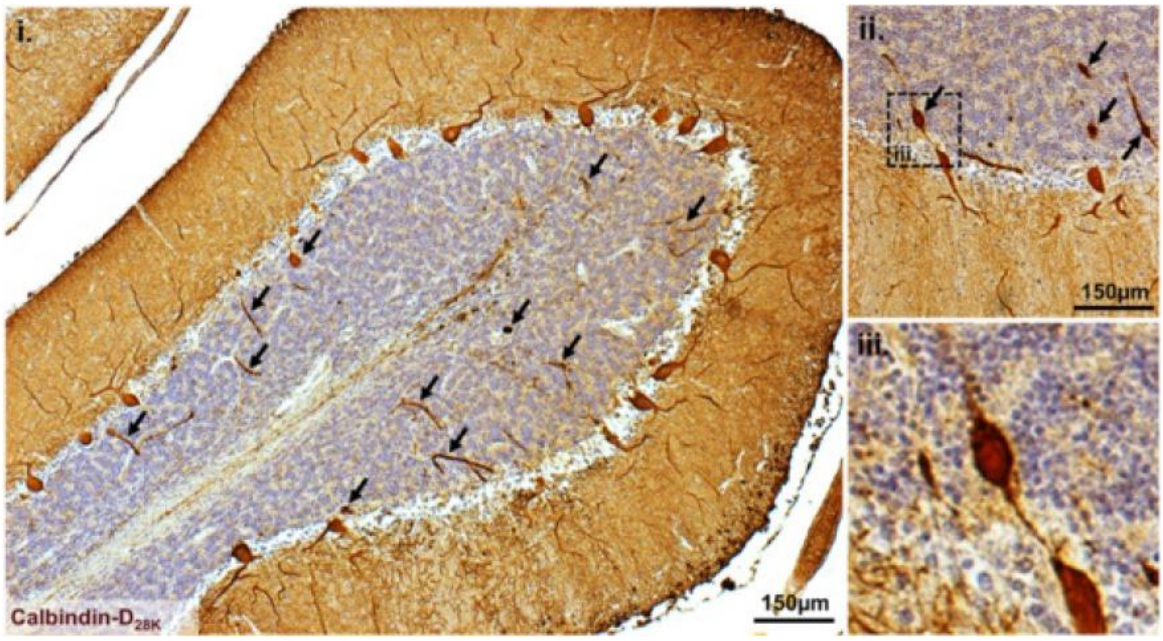

Figure 2.4: Post-mortem human axonal torpedoes
Post-mortem human case of Friedreich's ataxia stain with Calbindin-D28k. (i) Whole cerebellar lobule with many hypertrophic axons in the granule cell layer (arrows). (ii) Purkinje cells harboring a torpedo at proximities of the cell soma (arrows). (iii) Higher magnification of the torpedo in (ii). Image is taken from (Kemp *et al.*, 2016).

It has recently been established that the cerebellum is not implicated only in the coordination of movement, but also in a broad spectrum of behaviors. This may explain why torpedoes have also been reported in several non-motor human diseases, such as Tay-Sachs disease, a mutation of a lysosomal enzyme leading to neuronal toxicity (Terry & Weiss, 1963), progressive supranuclear palsy, caused by *tau* protein accumulation (Matsumoto *et al.*, 1996), Alzheimer's disease (AD) which is characterized by the presence of β-amyloid plaques and cognitive impairment (Louis *et al.*, 2009b), and fragile X syndrome, which causes intellectual disability (Greco *et al.*, 2002; Sabaratnam, 2000).

Perhaps more surprisingly, given their less apparent cerebellar physiopathology, torpedoes have been observed in Kuru-like encephalopathy (Yagishita, 1978), better known as the prion disease Creutzfeldt-Jakob disease (CJD) (Ferrer *et al.*, 2000), and also in cervical dystonia, also

described as spasmodic torticollis (Prudente *et al.*, 2013), both of which are diseases less typically associated with the cerebellum.

Interestingly, damage to Purkinje cell axons is sufficient to produce an increase in torpedoes. Fatal brain injury (Rand & Courville, 1934) or cerebellar white matter lesion patients (Takahashi *et al.*, 1992) exhibit torpedoes at close proximity to the damaged region. Additionally, torpedoes are prevalent in diseases that affect the myelination of Purkinje cells axons, such as in cases of leukoencephalopathy with neuroaxonal spheroids (LENAS) (Moro-de-Casillas *et al.*, 2004), and in multiple sclerosis (MS) (Kutzelnigg *et al.*, 2007; Redondo *et al.*, 2015). These observations suggest that localized axonal damage and axonal demyelination may contribute to torpedo formation.

Taken together, torpedoes have been studied in a wide range of neurological disorders, both motor and non-motor. This broad spectrum of disease suggests that torpedoes are not the hallmark of a single physiopathology. This array of evidence has led to the hypothesis that Purkinje cell axonal torpedoes are pathological hallmarks of a dysfunctional cerebellar cortex.

Table 2.2: Human pathologies with reported torpedoes

Symptoms	Human diseases	References
Cerebellar Atrophy	Olivopontocerebellar atrophy	(Petito *et al.*, 1973), (Ferrer *et al.*, 1994)
	Multiple system atrophy cerebellar	(Louis *et al.*, 2014a), (Louis *et al.*, 2019)
Ataxia	Familial congenital cerebellar ataxia	(Norman, 1940)
	Spinocerebellar ataxia type 1	(Louis *et al.*, 2019)
	Spinocerebellar ataxia type 2	(Louis *et al.*, 2019)
	Spinocerebellar ataxia type 3	(Louis *et al.*, 2019)
	Spinocerebellar ataxia type 6	(Sasaki *et al.*, 1998), (Yang *et al.*, 2000)
	Spinocerebellar ataxia type 37	(Corral-Juan *et al.*, 2018)
	Friedreich's ataxia	(Kemp *et al.*, 2016)
Motor dysfunction	Huntington disease	(Sakai *et al.*, 2015)
	Amyotrophic lateral sclerosis	(Hirano *et al.*, 1967), (Okamoto *et al.*, 1990)
	Parkinson's disease	(Louis *et al.*, 2009b), (Louis *et al.*, 2019)
	Essential tremor	(Louis *et al.*, 2006), (Axelrad *et al.*, 2008), (Louis *et al.*, 2009c), (Louis *et al.*, 2009b), (Babij *et al.*, 2013), (Louis *et al.*, 2014a), (Louis *et al.*, 2014b), (Louis *et al.*, 2019)
Dementia	Alzheimer's disease	(Louis *et al.*, 2009b)
Intellectual disability	Fragile X syndrome	(Sabaratnam, 2000), (Greco *et al.*, 2002)
Injury	Brain Injury	(Rand & Courville, 1934), (Ryu *et al.*, 2014)
	Cerebellar white matter lesion	(Takahashi *et al.*, 1992)
Demyelination	Leukoencephalopathy with neuroaxonal spheroids	(Moro-de-Casillas *et al.*, 2004)
	Multiple Sclerosis	(Kutzelnigg *et al.*, 2007), (Redondo *et al.*, 2015)
Prion	Creutzfeldt-Jakob disease	(Yagishita, 1978), (Ferrer *et al.*, 2000)
Rare diseases	Arnold-Chiari malformation	(Aring, 1938)
	Cervical dystonia	(Prudente *et al.*, 2013), (Louis *et al.*, 2019)
	Tay-Sachs disease	(Terry & Weiss, 1963)

2.3.2 Animal Models

Since studying Purkinje cell axonal torpedoes in human post-mortem tissue presents some experimental limitations, many researchers use animal models to improve experimental quality. Researchers have shown the presence of torpedoes in animal models of several of the human neurodegenerative diseases mentioned above. For example, torpedoes have been extensively described in animal models of ataxia. They were widely found in the Groggy mutant rat, studied as a model of ataxia (Takeuchi *et al.*, 1995), but also in a separate spontaneously arising mouse model of ataxia known as the Sticky mouse (Sarna & Hawkes, 2011). Furthermore, torpedoes have been found in the autosomal recessive spastic ataxia of Charlevoix-Saguenay (ARSACS) mouse model (Lariviere *et al.*, 2015) and SCA6 (Ljungberg *et al.*, 2016).

In animal models displaying motor control deficits, torpedoes have been observed in the Weaver mouse model usually used to study Parkinson's disease (Hirano & Dembitzer, 1973), as well as in the Quaking mouse, which has a deletion of the parkin gene that leads to juvenile parkinsonism (Suzuki & Zagoren, 1975). The overexpression of α-internexin, an intermediate neurofilament that is a cellular hallmark of Parkinson's disease and amyotrophic lateral sclerosis (ALS), leads to a high density of Purkinje cell axonal torpedoes (Ching *et al.*, 1999).

In several diseases in which Purkinje cells eventually die, axonal swellings have been observed prior to cell death, suggesting that torpedoes may contribute to cell death. Torpedoes have been found in the hyperspiny Purkinje cell mouse, which shows considerable Purkinje cell death (Sotelo, 1990), as well as in the Purkinje cell degeneration mouse (Baurle *et al.*, 1997). The MFP2 knockout mice, a Purkinje cell specific peroxisomal β-oxidation mutant, with high level of reactive oxygen species (ROS), also showed abundant torpedoes and Purkinje cell death (De Munter *et al.*, 2018). However, torpedoes have also been observed on the Purkinje cells that

survive insult, such as in rats injected with the glutamate agonist kainic acid, which causes seizures and Purkinje cell loss at injection sites (Rossi *et al.*, 1994). Do torpedoes appear on dying cells before cell death, on surviving cells, or both? From the literature, the relationship between torpedoes and Purkinje cell death remains unclear.

Torpedoes have also been seen in animal models of non-motor related diseases where axonal lesions and demyelination occur. Axonal degeneration caused by either axotomy in WT rat (Dusart & Sotelo, 1994), or mutation of the *Chp1* gene in mice (Liu *et al.*, 2013), led to elevated torpedo numbers. Both the Jimpy mice (Rosenfeld & Freidrich, 1983) and the Long Evans Shaker mice (Barron *et al.*, 2018), which show myelination defects, also displayed torpedoes. They were also observed in a proteolipid protein mutated mouse (Griffiths *et al.*, 1998), and in a mouse containing a mutated cerebroside sulfotransferase (Ishibashi *et al.*, 2015), which showed myelination defects and paranodal junction impairment, respectively. The *mtcl1* knockdown mouse, mutated for the microtubule cross-linking factor 1 (MTCL1) protein and causes disruption in the AIS formation, showed an elevated number of axonal swellings and ataxic motor symptoms (Satake *et al.*, 2017). The torpedoes resulting from myelination defects in these animal models resemble torpedoes found in human MS.

Taken together, these animal studies corroborate results from human tissue that show that torpedoes arise in response to a variety of neuronal insults, from ataxia and Parkinson's disease to Purkinje cell death and myelination problems. Moreover, torpedoes have also been reported in mice with axonal transport defects like the JIP1 and JSAP1 double mutant, which are associated with the motor protein kinesin (Sato *et al.*, 2015), and the Elavl3 knockout mouse, an RNA-binding protein affecting proper regulation of RNA splicing (Ogawa *et al.*, 2018). Torpedoes have also been described in gangliosidosis, a lipid storage disorder in cats (Walkley *et al.*, 1991). This work

leads to questions about whether torpedoes are related to different dysfunctional cellular pathways, like axonal transport and protein synthesis.

Table 2.3: Animal models with reported torpedoes

Defects/Diseases	Animal models	Gene mutated	References
PD and ALS	Weaver mice	*girk2*	(Hirano & Dembitzer, 1973)
	Quaking mice	*parkin*	(Suzuki & Zagoren, 1975)
	α-internexin overexpression	*α-internexin*	(Ching *et al.*, 1999)
Ataxia	Groggy rat	*cacna1*	(Takeuchi *et al.*, 1995)
	Sticky mice	*alanyl-tRNA synthetase*	(Sarna & Hawkes, 2011)
	MFP2 Knockout	*mfp2*	(De Munter *et al.*, 2018)
	ARSACS	*sacsin*	(Lariviere *et al.*, 2015)
	$SCA6^{84Q/84Q}$	*cacna1a*	(Ljungberg *et al.*, 2016)
	Tottering mice	*cacna1a*	(Rhyu *et al.*, 1999), (Hoebeek *et al.*, 2008) (Meier & MacPike, 1971)
Cell death	Hyperspiny Purkinje cell	*hps6*	(Sotelo, 1990)
	Purkinje cell degeneration		(Baurle *et al.*, 1997)
Axonal damage	vac mice	c*hip*	(Liu *et al.*, 2013)
	WT rat (chemical and physical lesion)	N/A	(Dusart & Sotelo, 1994), (Gianola & Rossi, 2001), (Gianola *et al.*, 2003)
Myelin defect	Jimpy mice	*plp*	(Rosenfeld & Freidrich, 1983)
	Long Evans Shaker	*mbp*	(Barron *et al.*, 2018)
	proteolipid protein knockout	*plp*	(Griffiths *et al.*, 1998)
	cerebroside sulfotransferase	*cerebroside sulfotransferase*	(Ishibashi *et al.*, 2015)
	mtcl1 knockdown mice	*mtcl1*	(Satake *et al.*, 2017)
	Contactin Knockout	*contactin*	(Berglund *et al.*, 1999)
	EL-deficient mice	*dapat*	(Teigler *et al.*, 2009)
Axonal transport	Jip1 and Jsap1	*jip1* & *jsap1*	(Sato *et al.*, 2015)
RNA splicing	Elavl3 Knockout	*elavl3*	(Ogawa *et al.*, 2018)
Seizure	WT rat (injection of Kainic Acid)	N/A	(Rossi *et al.*, 1994)

N/A, Not applicable

2.3.3 Torpedoes across the lifespan

Torpedoes transiently appear during normal development of healthy animals. Focal axonal swellings were reported during the second postnatal week of development, peaking in both rats (Gravel *et al.*, 1986) and mice (Ljungberg *et al.*, 2016) at postnatal day 11 (P11).

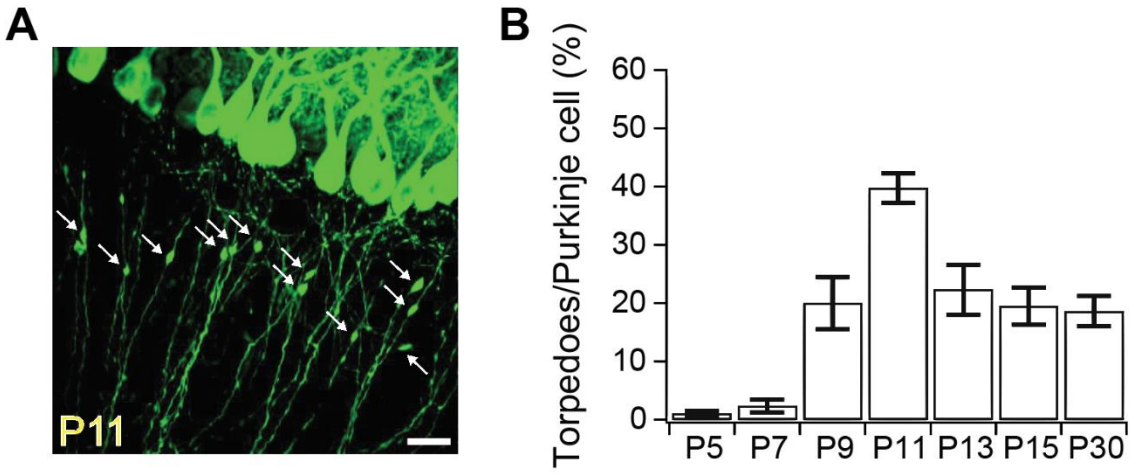

Figure 2.5: Developmental torpedoes in mice
(A) L7-tau-eGFP mice expressing GFP in Purkinje cell soma and axon, showing developmental torpedoes at P11. (B) Quantification of torpedoes during the first two postnatal weeks and at one month old, showing a peak in torpedoes at P11. Images were taken and adapted from (Ljungberg *et al.*, 2016).

Although these developmental torpedoes were smaller, some of them persisted into adulthood (P30). The presence of torpedoes in healthy animals calls into question the hypothesis that torpedo function is exclusively related to disease. During early normal development, Purkinje cell death takes place to allows proper formation of Purkinje cell monolayers. However, developmental Purkinje cell death was shown to be completed by P9 in mice (Jankowski *et al.*, 2009), indicating that developmental Purkinje cell death has ended by the time most developmental torpedoes appear at P11. Since Purkinje cell numbers are fixed after the developmental Purkinje cell death, torpedoes that persist into adulthood cannot be associated with natural Purkinje cells death.

Torpedoes have also been reported in aged mice. The number of Purkinje cells with axonal torpedoes noticeably and progressively increases, starting at six months and continuing up to 32 months of age in otherwise healthy wildtype mice (Baurle & Grusser-Cornehls, 1994).

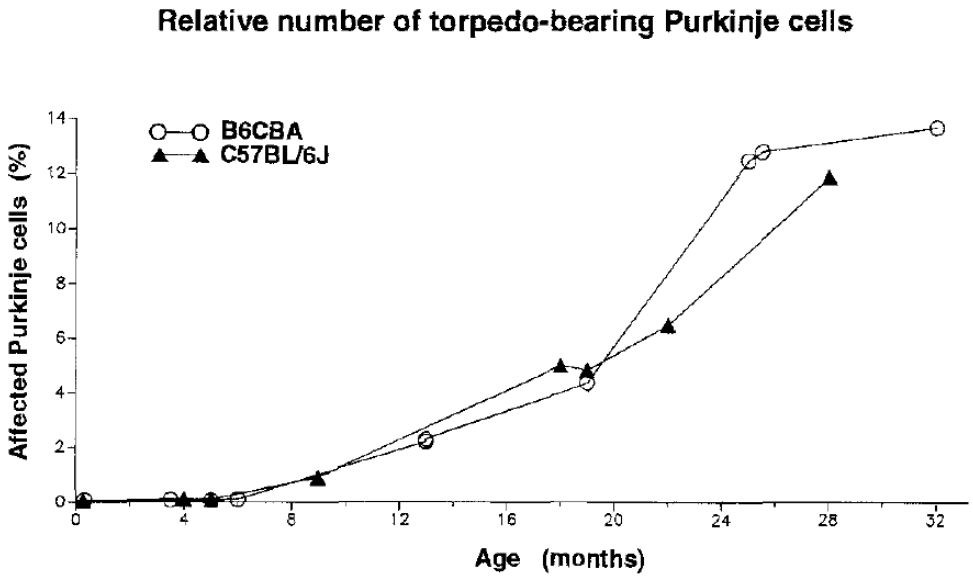

Figure 2.6: Torpedoes in wildtype aging mice
Assessment of the percentage of Purkinje cells with torpedoes in the cerebellar cortex throughout the lifespan of wildtype mice B6CBA (white circles) and C57BL6 (black triangles). Image is taken from (Baurle & Grusser-Cornehls, 1994).

The presence of human age-related Purkinje cell torpedoes has also been reported in post-mortem tissue (64-86 years old) (Kato & Hirano, 1985). Louis and colleagues found that in humans, the number of torpedoes correlates with aging, although they argue that the difference in the number of torpedoes between young (under 36-year-old) and older healthy patients (over 81-year-old) was negligible compared to what is observed in diseases (Louis *et al.*, 2009a). Age-related torpedoes have also been reported in the cerebellar cortex of a 12-year-old cow (midlife), showing a higher number of torpedoes compared to a 4 and a 6-years-old cows (young), without any sign of Purkinje cell loss (Ohfuji, 2017). Indeed, no direct evidence for torpedoes playing a role in aging and Purkinje cell loss has been demonstrated. In rats, Purkinje cell death is also minimal at the ages when the number of Purkinje cell torpedoes increases dramatically, between

10 and 42 months of age (Bakalian *et al.*, 1991). This suggests that the increment in torpedoes is not proportionally correlated with the amount of Purkinje cell death in healthy aging.

2.3.4 Ultrastructural characteristics of torpedoes

Torpedoes have been observed by electron microscopy (EM) in both human post-mortem tissue and animal models. One of the first human studies was reported in 1973, showing an enlargement of the axon, with the presence of mitochondria and endoplasmic reticulum (ER) (Petito *et al.*, 1973). Further studies followed, of which several confirmed the presence of mitochondria and ER inside torpedoes in addition to reporting the presence of disorganized neurofilament and of a myelin sheath surrounding most axonal torpedoes (Moro-de-Casillas *et al.*, 2004; Yagishita, 1979). One report observed the absence of a myelin sheath around a Purkinje cell axonal torpedo, where the authors raised the possibility that the torpedoes could have been located at the AIS (Louis *et al.*, 2009c), which is unmyelinated.

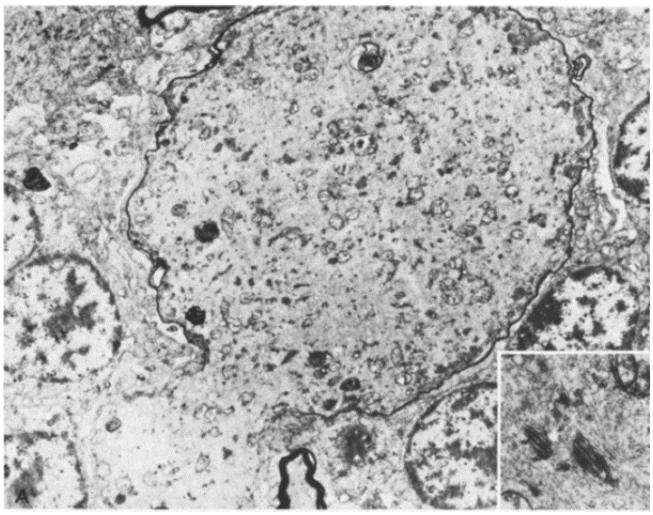

Figure 2.7: Ultrastructure of a torpedo in a human case of Creutzfeldt-Jakob disease
Transmission electron microscopy image of a torpedo in a human case of Kuru-like encephalopathy (also known as Creutzfeldt-Jakob disease). 4800x magnification. Thin myelin is present, with mitochondria inside the axon. Image is taken from (Yagishita, 1978).

Animal models of disease have also been imaged using EM. Most EM studies of torpedoes in animals showed the presence of a relatively normal myelin sheath (Dusart & Sotelo, 1994; Ishibashi *et al.*, 2015; Ogawa *et al.*, 2018). Although one study observed a marked thinning of the myelin sheath surrounding torpedoes, this was observed in the Quaking mice, which are characterized by a myelination defect (Suzuki & Zagoren, 1975). Subcellular organelle analysis confirmed the presence of mitochondria, smooth ER (SER) and disorganized neurofilaments in torpedoes in animal models of disease (Dusart & Sotelo, 1994; Ishibashi *et al.*, 2015; Ogawa *et al.*, 2018). The recurring presence of disorganized neurofilaments, typically caused by their phosphorylation, is associated with axonal transport defects. However, phosphorylated neurofilaments are also responsible for changes in axon caliber (Al-Chalabi & Miller, 2003). Therefore, disorganized neurofilaments in torpedoes could explain axonal enlargement and torpedo formation.

2.3.5 Computational axonal modeling

Axons are not simply morphological structures; they also serve as conduits for transmitting electrical information between cells. As mentioned in section 2.2, action potential speed of propagation can be increased by large axon diameter or by a myelin sheath. However, the biophysical implications of such focal axonal swellings remain elusive. Only a handful of computational models have tried to address the biophysical properties of torpedoes. One study predicted that a varicosity on the axon would create delays in action potential propagation. They also predicted that diffused axonal channel density would cause failures in propagating action potentials (Manor *et al.*, 1991). A more recent computational model of axonal injuries arrived at the same general conclusion: swellings resulted in either delays or failures of action potential propagation (Maia *et al.*, 2015). Since little physiological data is available regarding axonal

swellings, it is unclear how accurate these models are, or how representative they are of the biological phenomenon.

2.4 Axonal torpedoes: Current hypotheses

Focal axonal torpedoes have been observed on Purkinje cell axons for more than a century. Nevertheless, our understanding of the functional properties of these structures remains largely unclear. The current hypotheses for the functional role of Purkinje cell axonal torpedoes will be described in this section.

2.4.1 Purkinje cell death

Purkinje cell axonal torpedoes are usually described as a hallmark of cell death, due to the wide range of neurodegenerative diseases in which an increase in both axonal torpedoes and Purkinje cell death is observed after disease onset. This hypothesis is mainly based on correlative observation of an increase in torpedoes during disease progression, which inevitably proceeds to Purkinje cell death. To this day, few experiments provide direct evidence that torpedoes cause cell death. On the other hand, torpedoes have also been seen during development, reaching peak numbers after the natural developmental Purkinje cell death and after Purkinje cell numbers have stabilized. Purkinje cell death is also infrequent in healthy aged animals, where an increase in torpedoes has been observed. It remains unclear if torpedoes have a functional reason to exist, or if they are merely the natural effect of Purkinje cell death.

2.4.2 Axonal demyelination

Purkinje cell torpedoes have been observed at sites of demyelination. Animal models of MS showed large swollen axons in regions devoid of myelin. MS is an autoimmune disease which causes an inflammatory response towards myelin sheaths in the central nervous system. Thus,

axonal torpedoes have been associated with an inflammatory response, suggesting that torpedoes are sites of attack by the immune system, most likely for degradation. This would suggest that torpedoes form at unmyelinated sites as observed in MS patients (Trapp *et al.*, 1998), yet most studies describing axonal torpedoes show that myelin is unaffected around these swellings (Moro-de-Casillas *et al.*, 2004; Sasaki *et al.*, 1998; Terry & Weiss, 1963).

2.4.3 Axonal degeneration (Wallerian degeneration)

As described above (section 2.3.1), Purkinje cell axonal torpedoes have been widely studied in human post-mortem tissue. One major caveat of human post-mortem studies is that only a single time point is investigated, which is typically at a late disease stage. Observation of axonal torpedoes in human cerebellar cortex eventually led to the hypothesis that torpedoes could be a mechanism of axonal degeneration. This is also supported by the fact that it is not uncommon after slicing live tissue, to see cut axons form a spherical ball at the end of the cut axon, called "terminal clubs" by (Cajal *et al.*, 1991), or more commonly known as "end bulbs." Moreover, axonal degeneration mechanisms, like Wallerian degeneration, have been described as controlled axon death akin to apoptosis for cells. Wallerian degeneration is observed following axonal injury (1.5 days later) or after protein synthesis inhibition (Gilley & Coleman, 2010). Axon degeneration starts at the distal end and move retrogradely towards the cell body (Coleman, 2005). Following axolemma degeneration, the cytoskeletal structure and organelles begin to disintegrate and activated microglia start clearing debris (Wang *et al.*, 2012). Although the underlying mechanism for Wallerian degeneration remains incompletely understood, evidence implicates a calcium-dependent mechanism for the phenomenon (Coleman & Freeman, 2010). Importantly, since most axonal torpedo studies have been done in fixed tissue, little to nothing is known about the dynamics

of axonal torpedoes in the living cerebellar cortex. Do torpedoes show characteristics of Wallerian degeneration?

2.4.4 Axonal transport defect

Purkinje cells are large neurons with very intricate dendritic arborization and a long axon that can span great distances. These neurons need an efficient way of transporting essential material like organelles and new proteins to their extremities. For axons, materials are transported on extended microtubule tracks with motor proteins like kinesin and dynein for anterograde and retrograde transport, respectively. Since most EM studies reported the presence of dysregulated neurofilaments in torpedoes, many have suggested a possible issue or complete blockade in axonal transport. Treatment with colchicine, an axonal transport blocker, caused an accumulation of the transported materials leading to torpedo-like structure formation in cultured neurons (Horie *et al.*, 1983) and Purkinje cells (Pioro & Cuello, 1988). Defective axonal transport has therefore been hypothesized to be a major cause of torpedo formation.

2.4.5 Axonal compensatory mechanism

Lastly, due to the presence of torpedoes in a broad range of neurological diseases as well as in healthy animals, some researchers have speculated that torpedoes might act as a compensatory mechanism. In this scenario, torpedo formation would compensate for some loss of function during disease progression, which would occur more rarely in healthy animals. To my knowledge, Baurle and colleagues were the first to present such hypotheses. They studied the *pcd* mouse, which displayed massive Purkinje cell death. Interestingly, the surviving Purkinje cells frequently had axonal torpedoes. Since only moderate motor impairment was observed in these mice, despite the massive cell loss, the authors suggested that axonal plasticity in the form of torpedoes could be compensating for the Purkinje cell death, thereby explaining the discrepancy

found between their histological observations and their behavioral result (Baurle *et al.*, 1997). However, to date, there is little experimental evidence to support this compensatory mechanism hypothesis.

Throughout this thesis, I address some of these hypotheses. I present novel evidence regarding axonal torpedo function in healthy axons, supporting the axonal compensatory mechanism hypothesis. To date, we have no evidence that our characterization of torpedo function in young healthy tissue can also be applied to disease-related torpedoes. Nonetheless, most results do not contradict previous findings observed in disease-related torpedoes. My findings suggest that torpedoes are beneficial for the development and maintenance of proper cerebellar performance in healthy mice.

CHAPTER 3: MORPHOLOGICAL AND FUNCTIONAL STUDY OF PURKINJE CELL AXONAL TORPEDOES

3.1 Introduction

Purkinje cells axonal torpedoes have been observed in several human neurological diseases and animal models, as described in Chapter 2. Most studies have reported the presence of a myelin sheath surrounding Purkinje cell torpedoes. However, diseases involving myelin degeneration have also reported the presence of torpedoes on axons segment denuded of myelin sheath. Previous studies have also shown evidence for disorganized neurofilament, smooth endoplasmic reticulum (SER), and mitochondria in disease-related torpedoes (Dusart & Sotelo, 1994; Ishibashi *et al.*, 2015; Ogawa *et al.*, 2018). However, little is known about the functional role of torpedoes in healthy animals. The primary role of Purkinje cells is to integrate all information within the cerebellar cortex and transfer this information to other brain regions. Purkinje cells output information in the form of action potentials, which propagate along the Purkinje cell axon. Do torpedoes impact Purkinje cells information transfer to their postsynaptic targets? It has previously been hypothesized based on computational models that swellings negatively impact axonal propagation (Maia *et al.*, 2015; Manor *et al.*, 1991), but this has not been experimentally tested before now.

To address that, we used immunohistochemistry to look at torpedoes in healthy mice and investigated their morphological similarity to disease-related torpedoes. I also evaluated the electrophysiological properties of Purkinje cells with torpedoes, in hope of providing some new

molecular and physiological insight into torpedoes function. In this chapter, I am reporting some similarities between healthy torpedoes and previously obtained molecular results from torpedoes found in disease models. My data show that torpedoes are not sites of inflammation targeted by activated microglia and myelination appears normal. I showed that torpedoes are located within close proximity to nodes of Ranvier. Furthermore, I investigated the functional properties of Purkinje cell axonal torpedoes by performing simultaneous-dual recordings of individual Purkinje cell soma and its axon. My data shows that Purkinje cells with torpedoes have a higher fidelity rate, displaying fewer spike failures compared to control axons. This suggests that the presence of torpedoes improves information transfer in the cerebellum.

3.2 Materials & Methods

3.2.1 Animal

L7(*pcp2*)*-tau-eGFP* mice (Sekirnjak *et al.*, 2003; Watt *et al.*, 2009) were used to characterize the functional properties of axonal swellings. All animal procedures were approved by the McGill Animal Care Committee in accordance with the guidelines established by the Canadian Council on Animal Care.

3.2.2 Acute cerebellar slice preparation

Acute slices were prepared from young juvenile mice (P10-14), when axonal swellings are numerous (Ljungberg *et al.*, 2016). Mice were deeply anesthetized using isoflurane and checked for foot-paw reflex. Mice were decapitated, and the brain quickly removed in ice-cold artificial cerebrospinal fluid (ACSF; in mM: 125 NaCl, 2.5 KCl, 2 CaCl2, 1 MgCl2, 1.25 NaH2PO4, 26 NaHCO3 and 20 glucose, bubbled with 95% O2 and 5% CO2 to maintain pH at 7.3; Osmolarity 320 ± 5 mOsmol/kg). Parasagittal cerebellar vermis slices (200 μm thick) were made using a Leica VT 1000S vibratome. Slices were incubated in ACSF at 37°C for 45 min and then incubated at

room temperature (RT) until used for experiments. All chemicals were purchased from Sigma-Aldrich.

3.2.3 Electrophysiology

All recordings were taken from lobule III, using a Multiclamp 700B amplifier (Molecular Devices), at 33°C. An upright microscope (Scientifica) combined with a custom-built two-photon Ti:Sapphire laser (MaiTai; Spectra Physics) was used to identify Purkinje cell somata with intact axons (GFP). Glass pipettes dipped in CdSeS/ZnS alloyed quantum dots (Sigma-Aldrich) were visually positioned using the scanning two-photon laser as previously described (Andrasfalvy *et al.*, 2014). Loose cell-attached or extracellular recording of Purkinje cell somata and axons was performed using a custom-designed Igor Pro acquisition software (Wavemetrics). Axons were recorded in the granule cell layer, downstream from axonal swellings (50-200 μm from the parent soma), or an equivalent distance from a control axon without swellings.

3.2.4 Immunohistochemistry

Mice were anesthetized using an intraperitoneal (IP) injection of Avertin (2,2,2-tribromoethanol; dosage: 0.25 mL/10 g body weight) and transcardially perfused with 4 % paraformaldehyde (PFA; Electron Microscopy Sciences, EMS). Perfused brains were removed and kept at 4°C on a rotary shaker at 70 RPM for 24 hours in 4 % PFA. Brains were then transferred into phosphate-buffered saline (PBS) with 0.05 % sodium azide. Vermis sections were obtained using a Leica vibratome 3000 to make 100 μm-thick parasagittal slices, while flocculus slices were obtained using a Leica Cryostat CM1950 to make 40 μm-thick coronal slices. The slices were stored at 4 ºC in PBS with 0.05% sodium azide. Antigen retrieval was performed by incubating brain slice in 0.25% pepsin, 0.001% HCl in PBS solution for 10 min at RT. Following the antigen retrieval, slices were washed three times in 0.4% Triton X in 0.01 M PBS solution. All staining

was done in blocking solution containing 5% BSA, 0.05% sodium azide and 0.4% Triton X in 0.01 M PBS. The primary anti-myelin basic protein antibody (MBP; 1:500, BioLegend, Cat. No.: 836501) was used to stain for Purkinje cells myelin sheath. Anti-CASPR (1:200, Antibodies Incorporated, Cat. No.: 75-001) was used to stain for the paranodal section of nodes of Ranvier. Anti-Iba1 antibody (1:500, Wako Chemicals, Cat. No.: 019-19741) was used to stain for activated microglia, as a sign of inflammation. Anti-Neurofilament antibody (NF-200k, 1:500, Millipore, Cat. No.: MAB5266) was used to stain for all neurofilament, while anti-SMI-34 (1:200, BioLegend, Cat. No.: 835503) was used to stain for phosphorylated neurofilament. Slices were incubated with primary antibody at 4 ºC for 72 h on a rotary shaker at 70 RPM. Slices were then washed three times with a solution of 0.01 M PBS with 0.4% Triton X. Corresponding secondary antibodies, including Alexa594 donkey anti-rabbit, Alexa594 donkey anti-rat or Alexa594 anti-mouse antibody were used at dilution between 1:200 to 1:500. Secondary staining was done at 4 ºC for 90 min on a rotary shaker at 70 RPM. Slices were rinsed with 0.4% Triton X in 0.01 M PBS and mounted on slides with Prolong gold anti-fade mounting media (Life Technologies).

3.2.5 Imaging

Slices were either imaged on a custom-built two-photon microscope (Scientifica) with a Ti:Sapphire laser (MaiTai; Spectra Physics) tuned to775 nm (Alexa594) and to 890 nm (GFP), or with a Zeiss LSM800 laser scanning confocal microscope (Zeiss). Image acquisition was done using ScanImage running in Matlab (Mathworks), or the Zen Blue (Zeiss) software for the images obtained using the confocal microscope. All imaging was done in lobule III of the cerebellar vermis unless indicated otherwise. For live imaging, cerebellar slices were kept alive by continuously perfusing oxygenated ACSF (with drugs) at 33°C.

3.2.6 Analysis

Image analysis was done using Fiji/ImageJ or Zen blue (Zeiss) software. Z-stack images were taken in animals at P11 and P30. For myelination analysis, the percentage of MBP coverage of GFP positive torpedoes was assessed and reported. For Caspr, distance between nodes of Ranvier and the torpedo, as well as the location of the node relative to the torpedo (i.e. closer to the cell body or closer to the white matter) was reported. Iba1 antibody, a marker for Microglia, was measure by quantifying activated microglia per volume of granule cell layer and by counting microglial branches surrounding torpedoes or the segment of control axon. Neurofilament content was assessed by measuring the percentage of staining colocalizing with torpedoes. For electrophysiological recording, Igor Pro software was used to extract firing frequency and coefficient of variation. A custom-build plug-in made by Dr. Jesper Sjöström, was used to identify spike failures, and each spike failure was then manually confirmed. Neurolucida software (MBF Bioscience, USA) was used for 3D-reconstructions of axonal torpedo formation. Graphs were made using Igor Pro, Python 3, and Adobe Illustrator.

3.2.7 Statistics

Statistical analysis was done using SPSS (IBM), data normality and variance equality were determined using Shapiro-Wilk and Levene's test, respectively. Comparisons were made using either repeated-measures ANOVA and paired or unpaired Student's *T*-tests for parametric data, or Mann-Whitney *U*-tests for non-parametric data. Full repeated-measures ANOVA statistical analyses are reported in Appendix I. Data are reported as mean ± SEM. Statistical comparisons were made with the level of significance (α) set at $P^* < 0.05$, $P^{**} < 0.01$, $P^{***} < 0.005$.

3.3 Results

As described in Chapter 2, Purkinje cell axonal torpedoes have been reported in previous post-mortem human studies and animal models in several neuropathological alterations and defects. Some molecular and morphological features appear to overlap across different neurological diseases. To better understand the function of Purkinje cell axonal torpedoes, we investigated healthy torpedoes using immunohistochemistry and compared them to previously published data from disease-related torpedoes.

In addition, axonal recording of Purkinje cell torpedoes has not been frequently performed to date. One reason for this is that many technical challenges may prevent the study of axonal propagation in slice preparations. To overcome these challenges, I have employed several experimental refinements. First, to be able to target Purkinje cell soma and their axons, I used a mouse line that expresses the enhanced green fluorescent protein (eGFP) specifically in Purkinje cells, achieved by using a Purkinje cell-specific promoter (Pcp2/L7), created by Dr. Du Lac. GFP expression in axons was further enhanced by fusing GFP to *tau* protein, widely expressed in the axons (Sekirnjak *et al.*, 2003). Second, the use of two-photon imaging, which allows deep imaging into a tissue while preventing bleaching. Lastly, I used quantum dot labeling of the pipette tips (Andrasfalvy *et al.*, 2014), which allowed for simultaneous visualization and positioning of both recording electrodes, to facilitate these challenging experiments.

3.3.1 Absence of inflammatory signals at axonal swellings

Since torpedoes have been found in the cerebellar cortex of many neurological disorders, we wondered whether torpedoes were signs of inflammation. Inflammation is widespread in neurodegenerative diseases like Alzheimer's disease (AD), multiple sclerosis (MS) and amyotrophic lateral sclerosis (ALS), which all show the presence of torpedoes in both human

disease and animal models. To investigate whether torpedoes were sites of inflammation, we stained for ionized calcium-binding adapter 1 (Iba1), a marker for activated microglia. I demonstrated the presence of activated microglia in the granule cell layer (Fig 3.1A), which slightly increase with age (unpaired two-tailed Student *T*-test, P = 0.045; Fig 3.1B). However, microglia were stochastically distributed within the granule cell layer (Fig 3.1C), with no significant difference in the number of microglia associated with torpedoes and control axons (P11, Mann Whitney *U*-test, P = 0.84; P30, Mann Whitney *U*-test, p = 0.84; Fig 3.1D). These results suggest that torpedoes are not distinct sites of inflammation targeted by microglia for degradation.

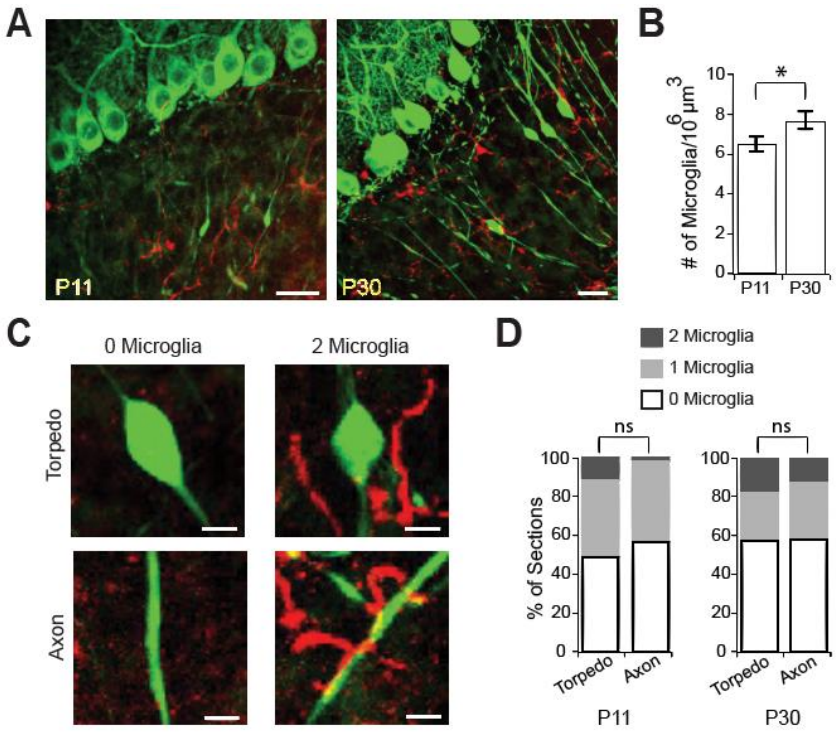

Figure 3.1: Torpedoes are not targeted by activated microglia for degradation
Activated microglia in the granule cell layer of the cerebellar cortex. (**A**) Representative images at P11 and P30 for activated microglia using Iba1 staining. Scale bar: 20 µm. (**B**) Comparison of microglia per volume of granule cell layer between P11 and P30 ($p^* < 0.05$). (**C**) Representative images showing torpedoes and control axons being contacted by microglia. Scale bar: 5 µm. (**D**) Quantification of microglia closely interacting with torpedoes and control axons at P11 and P30 ($p > 0.05$).

3.3.2 Presence of hyperphosphorylated neurofilaments

In the axoskeleton – the cytoskeleton of the axon – the presence of neurofilaments in axonal compartments is essential for the maintenance of axonal structures (Meller, 1987), probably even more so in structures like torpedoes. Given that disorganized neurofilament has been observed in disease-related torpedoes, we wondered if healthy torpedoes also contain disorganized neurofilaments. Lovisa Ljungberg, a former research assistant in our lab, used immunocytochemistry to detect neurofilament-200kD, the heavy chain (NF-H). We showed that a majority of torpedoes stained positively for neurofilaments both during development at P11 (64%; 51/80) and in young adults at P30 (78%; 85/109). The likelihood of NF-H being in a torpedo at different ages was not significantly different (P = 0.09; Fig 3.2B). Interestingly, neurofilament-positive torpedoes were significantly larger in size (NF+ width: 3.4 ± 0.2 µm) compare to torpedoes negative for neurofilaments (NF- width: 2.7 ± 0.1 µm; Mann-Whitney *U* test, P = 0.0007; Fig 3.2A). These results suggest that neurofilament enrichment might partially contribute to the enlargement of axonal swellings.

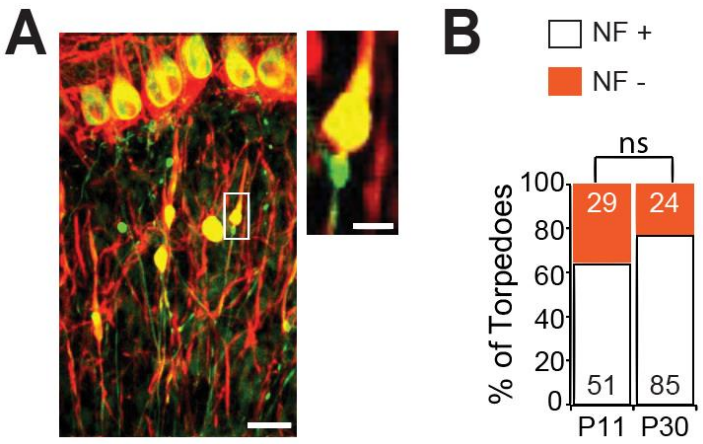

Figure 3.2: Presence of NF-H in Purkinje cells axonal torpedoes
Staining for NF-H was done on P11 mice. (**A**) Representative image of neurofilament staining (red) and the expression of GFP (green) in Purkinje cells. Scale bar: 20 µm. Inset shows neighboring torpedoes on the same axons, where a large torpedo is positive for NF-H (yellow) and

a small torpedo is negative (green). Scale bar in the inset: 5 µm. (**B**) Percentage of the torpedoes positive (white) and negative (orange) for neurofilaments at P11 and P30.

One major hallmark of torpedoes reported in diseases is the presence of disorganized neurofilaments. Disorganized neurofilaments are usually associated with phosphorylated neurofilament, which have been shown to cause axonal transport defects (Yuan *et al.*, 2017). However, neurodegenerative diseases are usually associated with the hyperphosphorylated form of neurofilaments. These hyperphosphorylated neurofilaments are thought to form neurofilament aggregates in diseases, such as Alzheimer's disease (Didonna & Opal, 2019). We thus wondered whether healthy torpedoes contain hyperphosphorylated neurofilament.

To address this question, we used an SMI-34 antibody, to stain for hyperphosphorylated neurofilaments (Redondo *et al.*, 2015). We observed that 45% (36/80) of torpedoes were positive for hyperphosphorylated neurofilament at P11 in healthy mice (Fig 3.3). Interestingly, similar incidents of hyperphosphorylated neurofilaments in torpedoes were observed in a mouse model of MS, where roughly 40% of axonal swellings were positive for SMI-34, compared with only 10% in control mice (Redondo *et al.*, 2015). This finding suggests that torpedoes in this MS model and in healthy animals with Purkinje cells specific eGFP expression might share some similarities. The phosphorylation of the C-terminus of neurofilament is required to form a healthy axoskeletal structure (Chen *et al.*, 2000). This indicates that the hyperphosphorylation of neurofilaments in torpedoes might cause the restructuring of this axonal compartment. Further investigation of hyperphosphorylated neurofilament is required to establish its function in healthy animals.

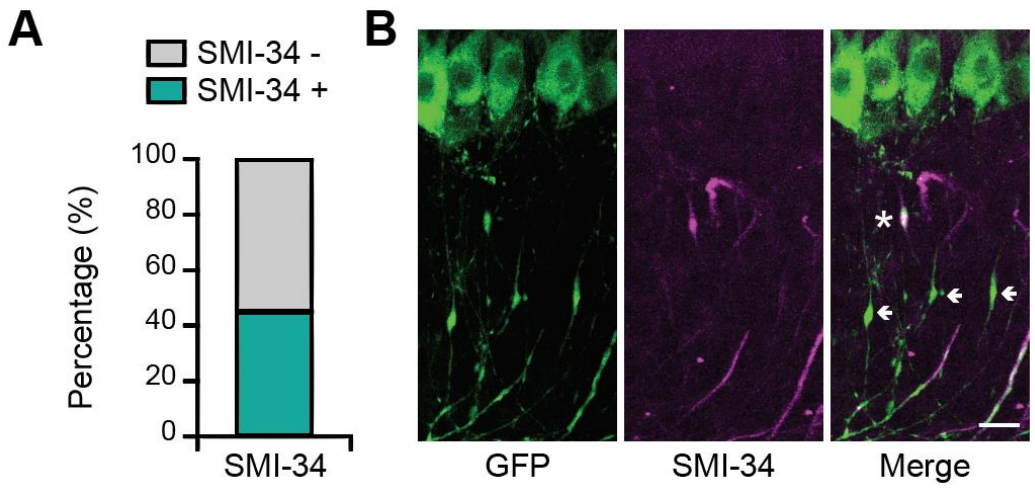

Figure 3.3: A subset of healthy torpedoes expresses hyperphosphorylated neurofilaments
(**A**) Percentage of SMI-34 positive torpedoes in P11 mice. (**B**) Representative image showing hyperphosphorylated torpedo in the cerebellar cortex. Co-localization of endogenous GFP in Purkinje cells (green) and the SMI-34 staining for hyperphosphorylated neurofilaments (magenta) in one torpedo is indicated by a star (*), while torpedoes without SMI-34 staining are indicated by arrows. Scale bar: 15 µm.

Only a subset of Purkinje cell axonal torpedoes were positive for hyperphosphorylated neurofilaments. We then decided to investigate the morphology of torpedoes. Since phosphorylation of neurofilament was shown to change axonal caliber (Nixon *et al.*, 1994), we wondered whether torpedoes tend to form on thicker axons compared to control axons. Using axonal tracing, we observed that the axon segments flanking torpedoes are not significantly different in diameter to neighboring control axons measured at a similar distance from the Purkinje cell layer (Mann-Whitney *U*-test, P = 0.224). Then, we wondered if axon segments from either side of a torpedo had any morphological differences, which might suggest defect in axonal transport. We showed that axonal segments before and after a torpedo were not significantly different (paired Student *T*-test, P = 0.119; Fig. 3.4).

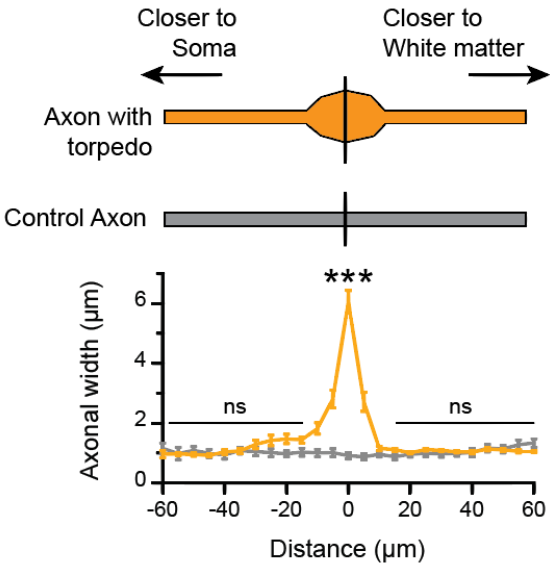

Figure 3.4: Morphology of torpedoes neighboring axon segments
Axonal tracing comparing axons with torpedoes (n = 15) to control axons (n = 13; Mann-Whitney U test, P > 0.05). Torpedoes (15 µm on both side of the torpedo center) were excluded from the analysis since axons were intentionally selected to have a size difference at this location.

3.3.3 Purkinje cells with and without torpedoes show no somatic recording differences

Since the literature surrounding torpedoes associated them with neurodegenerative disease, we wondered whether Purkinje cells with torpedoes had neuronal dysfunction, even in healthy mice. To address this, I recorded spontaneous action potentials from Purkinje cells with and without torpedoes. I measured firing frequency and the inter-spike interval coefficient of variation (CV), to determine whether these were altered, as they often are in neurodegenerative diseases (Ady et al., 2018; Jayabal et al., 2016). Interestingly, no significant differences were observed in either the firing frequency (Control axons: 45.16 ± 3.15 Hz and Torpedo axons: 44.32 ± 3.71 Hz; Mann-Whitney *U*-test, P = 0.70) (Fig 3.5A), or the CV of the inter-spike interval (Control axons: 0.29 ± 0.026 and Torpedo axons: 0.31 ± 0.053; Mann-Whitney *U*-test, p = 0.40; Fig 3.5B) of Purkinje cells with torpedoes compared to control Purkinje cells without torpedoes. This data

suggests that Purkinje cells with torpedoes display typical intrinsic firing properties and do not show early markers of dysfunction.

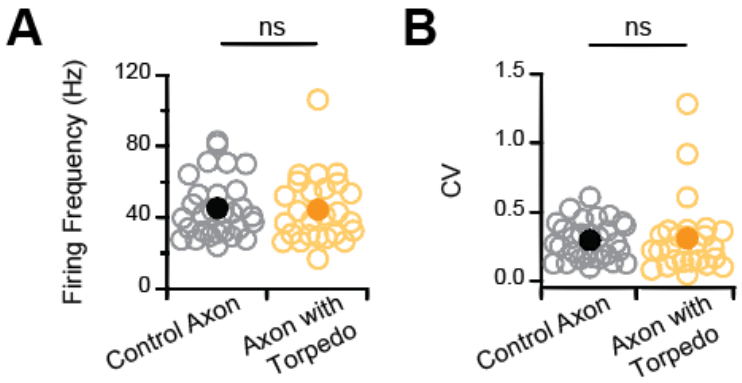

Figure 3.5: Firing frequency and regularity in Purkinje cells with/without torpedoes
(**A**) Firing frequency (Hz) and (**B**) coefficient of variation (CV) of inter-spike interval from Purkinje cell somatic recordings without (n = 29) and with axonal torpedoes (n = 26; Mann-Whitney *U*-test, P > 0.05).

3.3.4 Torpedoes are myelinated and have a close association with nodes of Ranvier

To further investigate the differences between previously studied disease torpedoes and healthy torpedoes in our mouse models, we wondered whether the myelin sheath was intact in torpedoes. To address that, Lovisa Ljungberg, a former research assistant in our lab, did immunohistochemistry of myelin basic protein (MBP; Fig 3.6A), a marker for the myelin sheath. The analysis was done on z-stack images to confirm the presence of myelin across the whole torpedo (Fig 3.6B). Our result confirmed that the vast majority of torpedoes were myelinated at P11 (84%; 102/122), while almost all torpedoes were myelinated at P30 (96%; 78/81). The small reduction of myelination surrounding torpedoes observed during development, although not significant, could be explained by the incomplete formation of the myelin sheath at P11 (P = 0.13; Fig 3.6C) which is not expected to be fully formed, as others have shown that myelin formation in rats is only completed at P15 (Gianola *et al.*, 2003).

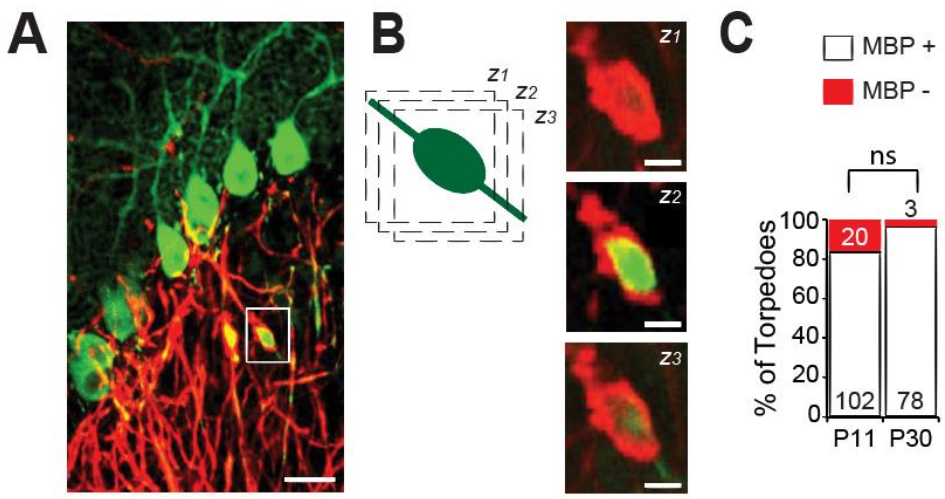

Figure 3.6: Myelination of Purkinje cell axonal torpedoes
Presence of myelin sheath surrounding the torpedoes in the acute cerebellar slices. (**A**) Representative image of the cerebellar cortex, showing the myelin sheath (MBP; Red) and the Purkinje cells (GFP; Green). Scale bar: 20 µm. (**B**) Myelin analysis was done by assessing the presence of MBP staining in z-stack images of torpedoes from top (Z1) to bottom (Z3). (**C**) Quantification of torpedoes covered in myelin showed that 84% of torpedoes are myelinated at P11, while 96% are myelinated at P30.

We then wondered whether torpedoes might be associated with axonal structures like node of Ranvier, which could arise because of molecular refinement at these sites. To address this, we used immunohistochemistry to label nodes of Ranvier in brain slices. This is challenging, and we had to explore multiple different antibodies and fixation protocols before we were successful in labeling paranodal structures at nodes of Ranvier in Purkinje cells. We used Caspr (Fig 3.7A), a paranodal membrane protein anchoring the axolemma (i.e. membrane of the axon) to the myelin sheath (see Fig 2.2). We showed that torpedoes are frequently located close to nodes of Ranvier, with more than half of the torpedoes we identified located less than 2 µm from a Caspr punctum (Fig 3.7B). This observation suggests that torpedoes are frequently associated with juxta-paranodal regions, which are typically enriched in potassium channels. This may influence the ability of the Purkinje cell axon to repolarize after an action potential, which is critical for its ability to propagate action potential with fidelity.

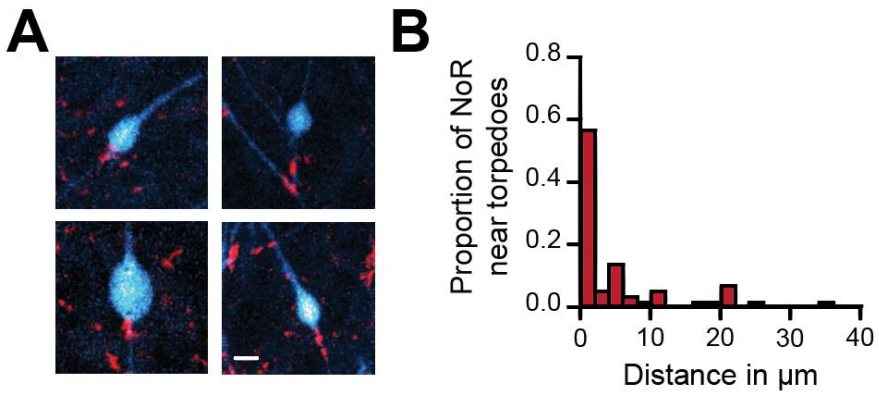

Figure 3.7: Torpedoes are located in close proximity to nodes of Ranvier
Presence of torpedoes at juxta-paranode sections of the node of Ranvier. (**A**) Representative images showing localization of paranodes (Caspr; Red) compared to torpedoes (GFP; Cyan). Scale bar: 5 µm (**B**) Proportion of nodes of Ranvier near torpedoes, with the majority being less than 2 µm from a torpedo.

Since torpedoes are frequently located in proximity to nodes of Ranvier, and it has been shown previously that the first and second nodes of Ranvier were located at ~ 80 µm and ~ 350 µm from the soma (Clark *et al.*, 2005), we wondered if Purkinje cell axon could harbor multiple torpedoes along the length of their axons. To address this, we followed GFP-expressing axons from the Purkinje cell layer to the white matter in 2-photon image stacks (beyond the white matter, it was difficult to follow single axons). We found that the presence of multiple torpedoes on the same axon within the granule cell layer is observed only rarely (1.35% or 13/963 torpedoes occur on an axon with a second torpedo; Fig 3.8). We previously showed that 40% (273 torpedoes/674 Purkinje cells) of Purkinje cells had torpedoes at P11 (Ljungberg *et al.*, 2016). This result suggests that most Purkinje cells have only one or zero torpedoes on their axon, at least within the granule cell layer, typically located near the first node of Ranvier. However, Purkinje cell axons may have additional torpedoes at distal locations through the white matter tract towards the CN neurons, possibly also in association with paranodal regions of nodes of Ranvier.

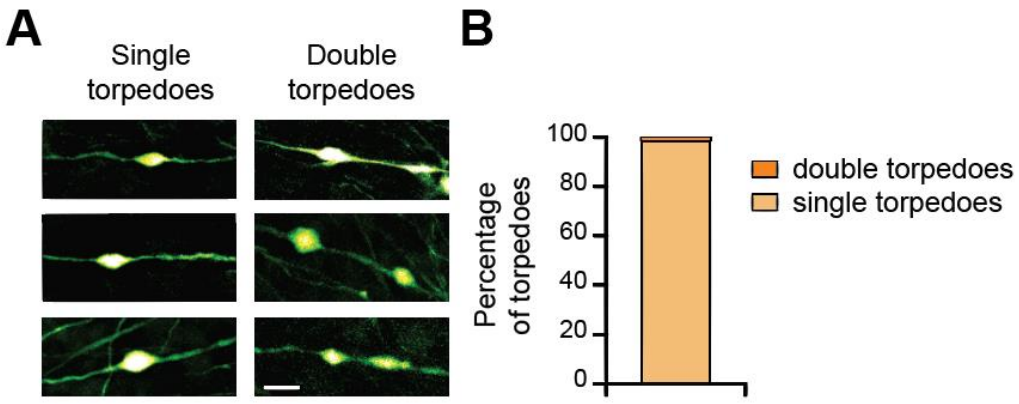

Figure 3.8: Rare occurrences of multiple torpedoes on the same axons
Purkinje cell axons rarely displayed multiple torpedoes within the granule cell layer. (**A**) Representative image showing single torpedoes and double torpedoes. Scale bar: 10 µm. (**B**) Percentage of single and double torpedoes on the same Purkinje cell axon (n = 963 torpedoes).

To better understand the association of torpedoes with the node of Ranvier, we wondered whether torpedoes were located upstream or downstream of the node of Ranvier. A more in-depth analysis of our Caspr immunocytochemistry images showed that torpedoes could be located upstream (i.e. closer to soma) or downstream (i.e. closer to white matter) of nodes of Ranvier, with a roughly equal proportion at 43% (25/58) and 57% (33/58), respectively (Fig 3.9B). No significant difference was observed between the distance of upstream and downstream nodes from a torpedo (Mann-Whitney *U* test, P = 0.866; Fig 3.9C). These results suggest that torpedoes appear to be forming on both sides of the node of Ranvier.

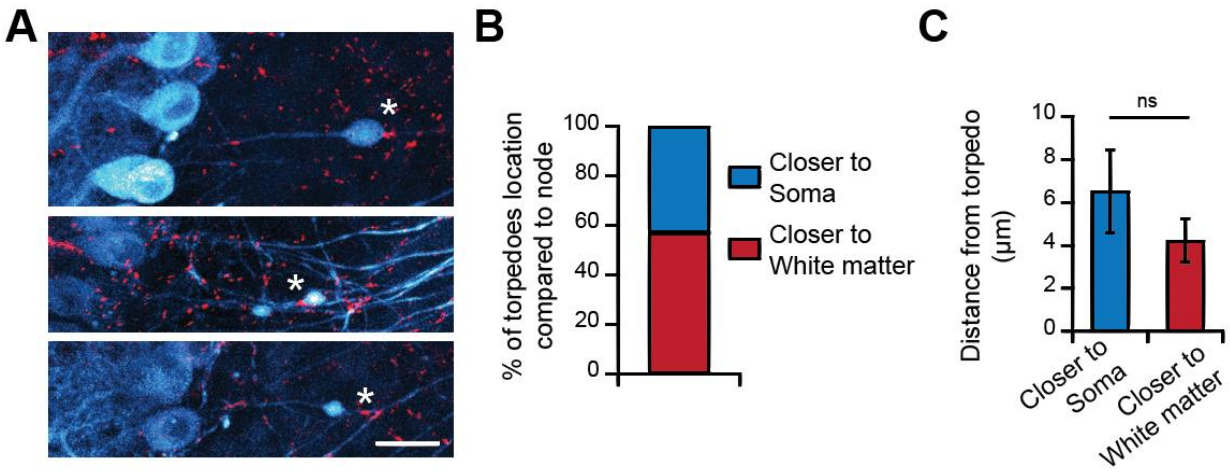

Figure 3.9: Torpedoes are equally distributed on both side of nodes of Ranvier
(**A**) Representative images showing localization of a node of Ranvier (Caspr; Red) on the Purkinje cell axon (GFP; Cyan). Scale bar: 20 µm (**B**) Percentage of torpedoes upstream (closer to the soma; Blue) or downstream (closer to the white matter; Red) of a node of Ranvier. (**C**) Distance between torpedoes and node of Ranvier, relative to the location of the node (Mann-Whitney U test, $P > 0.05$).

3.3.5 Purkinje cell axonal torpedoes show higher spiking fidelity compared to control axons

Since the close proximity of torpedoes to nodes of Ranvier may influence the ability of the Purkinje cell axon to propagate action potential with fidelity, we wondered if action potential propagation could be altered by the presence of axonal torpedoes. I recorded simultaneously from both Purkinje cell soma and axon from the same cell. This was challenging, but I was eventually able to successfully record simultaneously from Purkinje cell soma and the axon with a torpedo or the control axon (Fig 3.10).

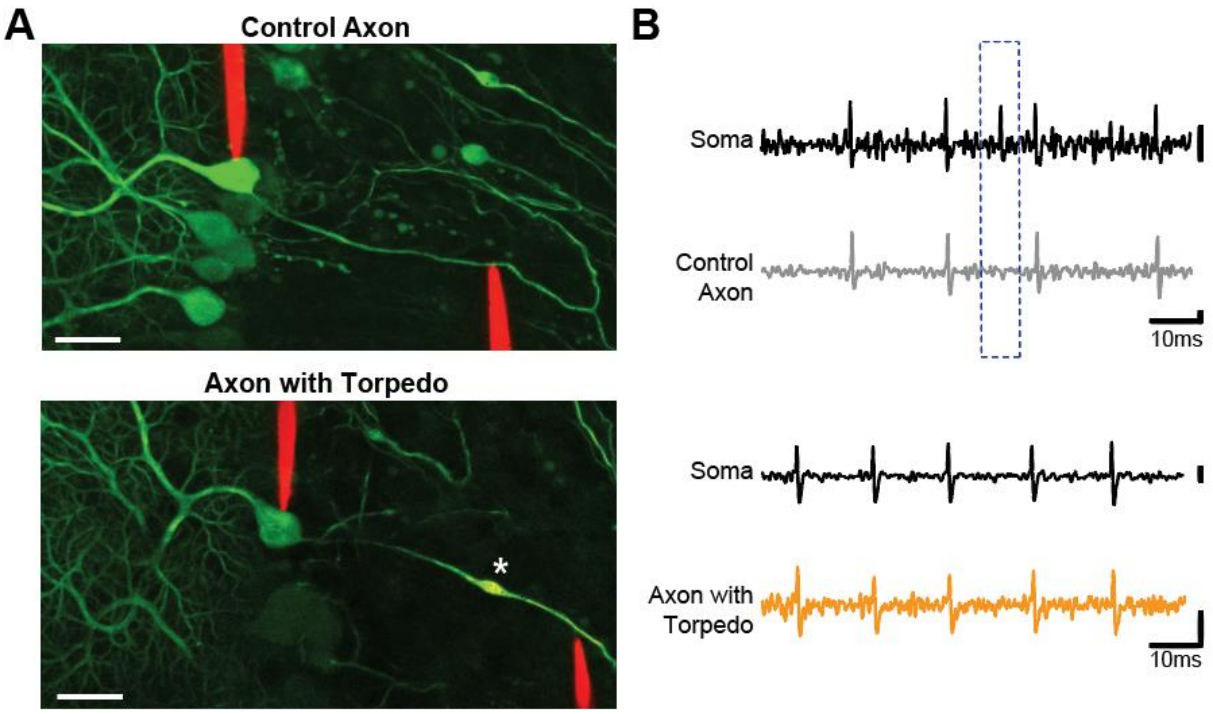

Figure 3.10: Simultaneous dual recordings of Purkinje cell soma and their axon
(**A**) Both electrodes are visually positioned using Quantum dots labeling. Scale bar: 25 µm. (**B**) Recording of soma (black) and its axon (Grey: Control axon; Orange: Axon with Torpedo). Top: Purkinje cell with a control axon without any torpedoes. Scale bar: 0.5 mV for two traces. Bottom: Purkinje cell with a torpedo on its axon (*). Scale bar: 1 mV and 0.5 mV.

In Purkinje cells without torpedoes, we observed a significant difference in the firing frequency recorded at the soma and at the axons (Mann-Whitney *U*-test, Control Axon, P = 0.038). In contrast, Purkinje cells with torpedoes did not show any difference in somatic and axonal firing frequency (Mann-Whitney *U*-test, Axon with Torpedo, P = 0.099; Fig 3.11A). No significant difference was observed in either control axon or axon with torpedo for the regularity of firing, quantified using CV of the inter-spike intervals (Mann-Whitney *U*-test, Control axon, P = 0.93; Axon with a torpedo, P = 0.49; Fig 3.11B). Further investigation of the difference in firing frequency in control axon allowed us to identify more action potential propagation failures in control axons compared to axons with a torpedo (Control axons: 5.69 ± 1.43 per 1000 spike; n =

11; axons with torpedo: 1.12 ± 0.41 per 1000 spikes; n = 9; Mann-Whitney *U*-test, p = 0.002; Fig 3.10B and Fig 3.11C). This means that Purkinje cells with torpedoes have a higher fidelity rate (where axons with high fidelity are defined as less than two failures per 1000 spikes) compare to control axons (Control axons: 18.2% high fidelity; Torpedo axons: 77.8% high fidelity; Mann-Whitney *U*-test, P = 0.022 (Fig 3.11D).

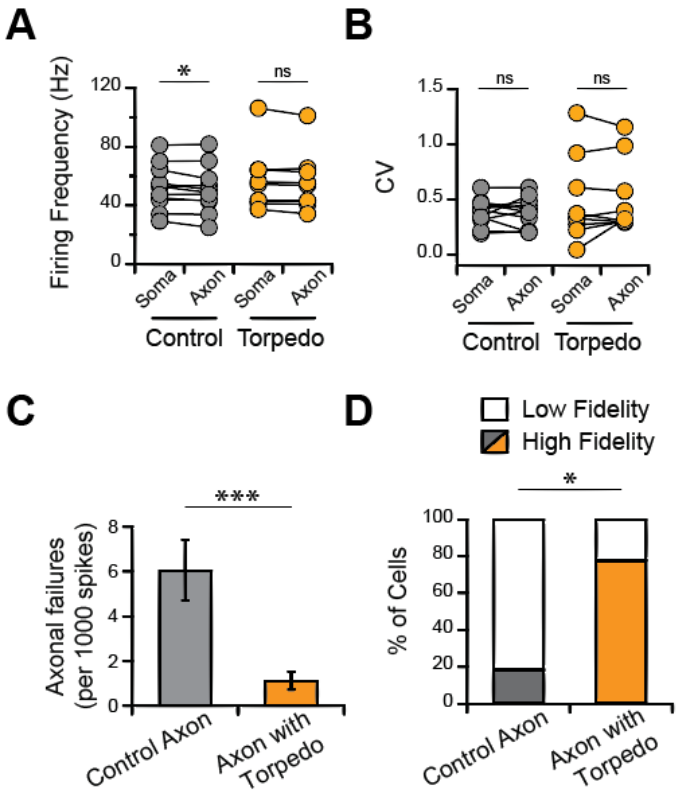

Figure 3.11:Axonal failures are predominant in control axons
(**A**) Firing frequency comparisons between somatic and axonal compartment within the same cells (Gray, Control: n = 11; Orange, Torpedo: n = 9; paired sample Student *T*-test, P > 0.05 and P* < 0.05). (**B**) CV comparisons between somatic and axonal compartment within the same cells (paired-sample Student *T*-test, P > 0.05). (**C**) Control axons display a higher axonal failure rate compared to axons with a torpedo (Mann-Whitney *U*-test; P*** < 0.005). (**D**) Percentage of Purkinje cells with low and high axonal fidelity (Low fidelity: avg. over 2 failures per 1000 spike; high fidelity: avg. less than 2 failures per 1000 spike; Mann-Whitney *U*-test; P* < 0.05).

Moreover, we showed that Purkinje cells with control axons display higher failure rates throughout their recording compared to Purkinje cell axons with torpedoes (Fig 3.12). Our data

suggest that torpedoes do not impair, but rather improve axonal propagation in healthy mice, contradicting many previous hypotheses presented in Chapter 2.

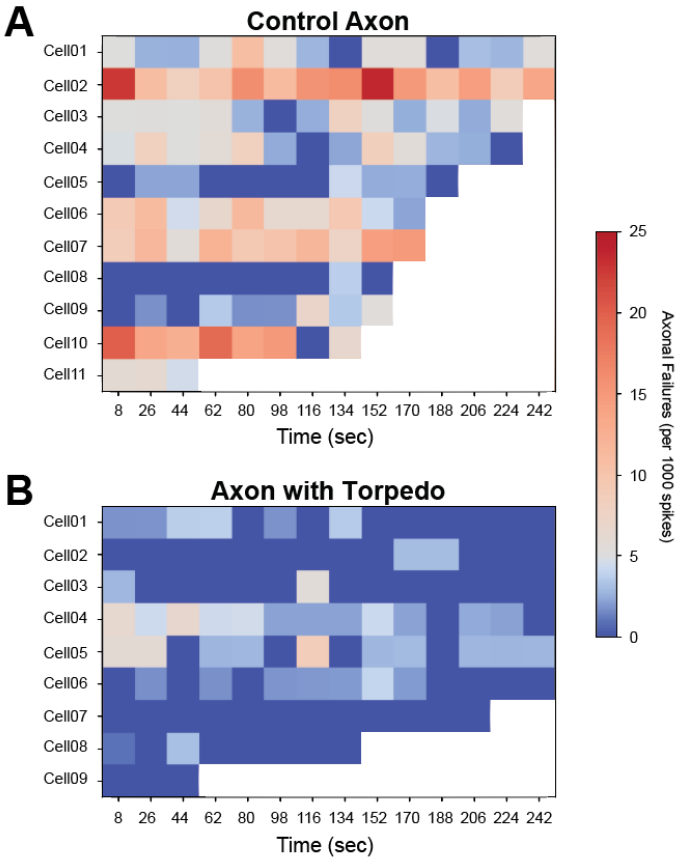

Figure 3.12: Axonal failure rate is consistent over time
Heatmaps are displaying the variability of axonal failures between each paired recording over time for control axons (**A**) and axons with a torpedo (**B**). Color gradient from low failures in blue to high failures in red.

A previous study showed that antidromic stimulation of Purkinje cell axons appears to induce more failures at high frequency (Hirono *et al.*, 2015). We wondered whether higher firing frequency in control axons could be related to higher propagation failures. We showed that control axons did not display higher failure rates due to overall higher spontaneous firing frequency compared to axons with a torpedo (Fig. 3.11C). Furthermore, we wondered if recording distances could affect axonal failures, hypothesizing that longer recording distances would have a higher

chance of axonal failure. We showed no link between axonal failures and recording distances of the electrodes (Fig 3.13B), as well as for firing frequency and recording distances (Fig 3.13C). Moreover, spike timing delay between somatic spiking and axonal spiking was observed and compared to recording distances. We observed no correlation between propagation delay and recording distances for both control axons and axons with a torpedo (Fig. 3.13D). Although negative propagation delays are usually observed in axonal recording near the soma, negative propagation delay has occasionally been observed in extracellular recording distances ranging from 50 to 200 µm (Palmer *et al.*, 2010). Based on the spike timing delays and recording distances, we were able to calculate the speed of propagation. We showed that the speed of propagation was not significantly different between control axons and axons with a torpedo (Control axon, 1.16 ± 0.44 m/s; Axon with a torpedo, 0.28 ± 0.75 m/s; unpaired Student *T*-test, P = 0.31; Fig. 3.13E).

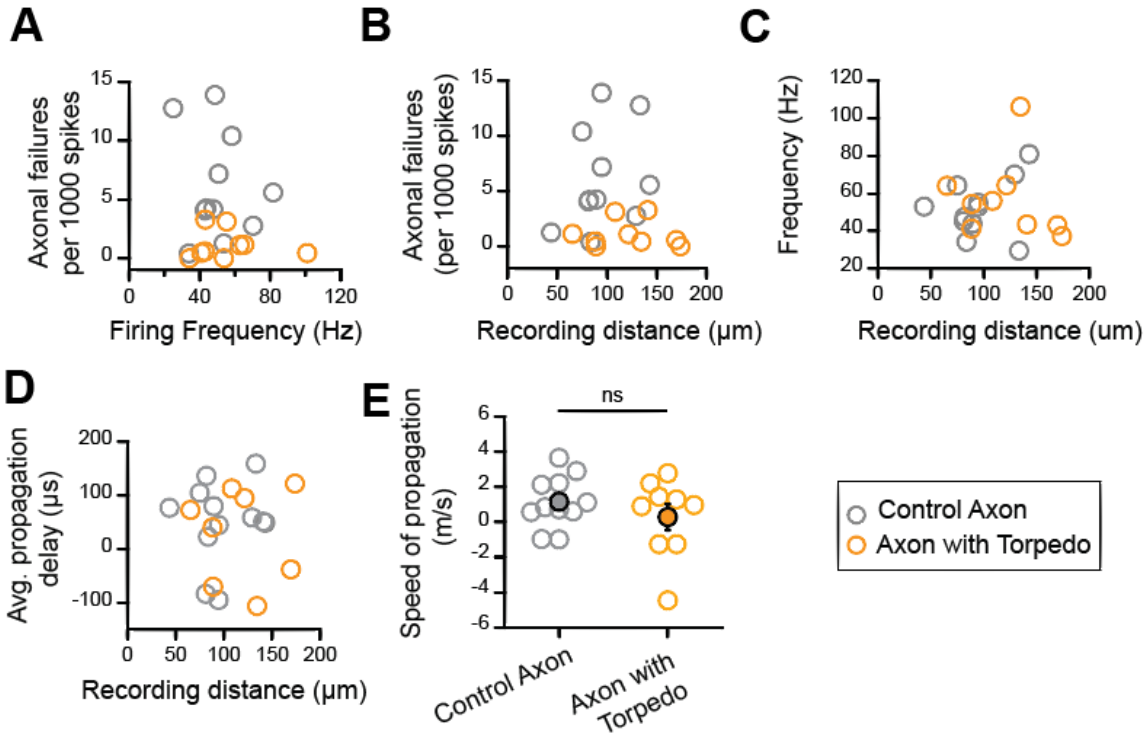

Figure 3.13: Propagation properties are unaltered in axons with/without torpedoes
(**A**) Distribution of the axonal failure rates and the firing frequency for all control axons and axons with a torpedo. (**B**) Distribution of axonal failures and recording distance between control axons

and axons with a torpedo. (**C**) Distribution of firing frequency and recording distance for each cell. (**D**) Distribution of propagation delay and recording distances. (**E**) Comparing speed of axonal propagation between control axons and axons with torpedo (Gray, Control: n = 11; Orange, Torpedo: n = 9; unpaired Student *T*-test, P > 0.05).

All electrophysiological properties of Purkinje cells with control axons and axons with a torpedo are reported in Table 3.1.

Table 3.1: Electrophysiological properties of control axons and axons with a torpedo

Properties	**Somatic value** Mean ± SEM (range, n)	**Control axons** Mean ± SEM (range, n)	**Axons with a torpedo** Mean ± SEM (range, n)	**P-value**
Somatic FF (Hz)		45.16 ± 3.15 (23.9 – 82.8, 29)	44.32 ± 3.71 (16.8 – 106.2, 26)	0.22
Dual-recording FF (Hz) - Control	52.33 ± 4.56 (29.4 – 80.9, 11)	50.51 ± 4.74 (24.9 – 81.6, 11)		*0.038*
Dual-recording FF (Hz) - Torpedo	56.63 ± 7.02 (37.3 – 106.2, 9)		55.43 ± 6.67 (34.2 – 100.9, 9)	*0.099*
Somatic CV		0.29 ± 0.026 (0.09 – 0.60, 29)	0.31 ± 0.053 (0.04 – 1.28, 26)	*0.40*
Dual-recording CV Control	0.38 ± 0.036 (0.19 – 0.61, 11)	0.38 ± 0.040 (0.20 – 0.61, 11)		*0.93*
Dual-recording CV Torpedo	0.49 ± 0.13 (0.044 – 1.28, 9)		0.54 ± 0.11 (0.29 – 1.16, 9)	*0.49*
Failure rates (Per 1000 spikes)		5.69 ± 1.43 (0.41 – 13.9, 11)	1.12 ± 0.41 *(0 – 3.28, 9)*	*0.0023*
Recording distance (µm)		95.3 ± 8.8 (43.5 – 142.8, 11)	121.2 ± 12.4 (65.1 – 173.8, 9)	0.098
Propagation delay (µs)		50.4 ± 24.1 (-95.0 – 159.0, 11)	30.9 ± 27.7 (-106.5 – 121.9, 9)	*0.60*
Speed of Propagation (m/s)		1.16 ± 0.44 (-0.99 – 3.65, 11)	0.28 ± 0.75 (-4.46 – 2.77, 9)	0.31

P-values are reported as Student's *T*-test when normally distributed, or Mann-Whitney *U*-test when not normally distributed. Abbreviations: CV, Coefficient of variation; FF, Firing frequency; SEM, Standard error of the mean.

3.4 Discussion

In this chapter, I investigated the molecular signature of Purkinje cell axonal torpedoes. I have shown that the torpedoes are not associated with sites of inflammation, as indicated by a normal density of activated microglia surrounding torpedoes. This result argue against torpedoes

being produced by an inflammatory response due to tissue swellings, which is observed in some neurodegenerative diseases (Cameron & Landreth, 2010; Jack *et al.*, 2005; Lecours *et al.*, 2018). Furthermore, we showed that most axons are myelinated, and axonal torpedoes have shown no signs of myelin degradation as characterized in diseases like multiple sclerosis.

We also found that ~60% of torpedoes were positive for heavy neurofilament (200-kDa). We know that neurofilaments (200-kDa) are one of the main axoskeletal proteins. However, phosphorylated neurofilaments have been associated with the formation of neurofilaments aggregates, causing axonal transport disruption (Schlaepfer, 1987). Interestingly, we observed that ~45% of torpedoes were positive for hyperphosphorylated neurofilaments, resembling the result obtained in a mouse model of MS (Redondo *et al.*, 2015). This result might suggest that disease-related torpedoes and healthy torpedoes are more alike than previously thought. Phosphorylation of neurofilament has been mainly associated with neurodegenerative diseases, but little is known about phosphorylated neurofilaments in healthy torpedoes. The possibility of phosphorylated neurofilament as part of the mechanism of torpedoes formation cannot be excluded since phosphorylation of neurofilament has been shown to modulate axonal caliber (Heimfarth *et al.*, 2016). This suggests that hyperphosphorylation of neurofilament may not be solely a sign of axonal pathology. It would be interesting to further test whether axonal transport is involved in torpedoes by using specific axonal transport blocker like Ciliobrevins, a dynein blocker (Roossien *et al.*, 2015), which is implicated in slow anterograde axonal transport of neurofilaments (Shah *et al.*, 2000).

Immunohistochemistry using Caspr antibody allowed us to localize nodes of Ranvier along Purkinje cell axons. We showed that torpedoes are usually within a few micrometers from nodes of Ranvier, most likely located in the juxta-paranodal region. Torpedoes close proximity to nodes

of Ranvier might indicate a possible modulation of juxta-paranode signaling molecule, which could impact the propagation of action potential.

To pursue this idea, I investigated the functional properties of Purkinje cell axonal swellings. Purkinje cell axonal torpedoes were shown to have higher propagation fidelity by showing fewer action potential propagation failures compared to control axons. This finding was highly unexpected since prior studies largely suggested a neurodegenerative role for Purkinje cell axonal torpedoes. Moreover, spike failures observed in control axons remain at just a few failing spikes per 1000 spikes. Our understanding of a single spiking event in Purkinje cell and its implication on the overall motor behavior remains incomplete. Some studies have shown that the introduction of an extra spike could largely predict monkey behavior (Chaisanguanthum *et al.*, 2014), suggesting that a single spike loss could have a meaningful effect on animal behavior as well. Furthermore, no other differences in electrophysiological properties were observed when comparing Purkinje cells with torpedoes to those without torpedoes. This contradict the neurodegenerative disease hypothesis for torpedoes, since many studies have shown a reduction in either Purkinje cell firing rate or regularity in animal models of diseases (Cook *et al.*, 2020).

Overall, this chapter presents evidence that torpedoes are not directly related to neurodegenerative disease but arise when axonal propagation fails and may help protect against such failures. Our results help explain why torpedoes are not a specific hallmark of a single disease, but more likely linked to several different insults that give rise to Purkinje cell axonal propagation failures.

CHAPTER 4: CHARACTERIZING THE MECHANISM OF TORPEDO FORMATION

4.1 Introduction

Purkinje cells are the sole output of the cerebellar cortex, meaning that their main role is to process all information within the cerebellar cortex and transfer this information to other brain regions. Purkinje cells output information in the form of action potentials. Action potentials are relayed as a chemical signal between their initiation site called the axon initial segment (AIS) and Purkinje cell terminals, where they make synaptic connections onto CN neurons. Purkinje cell axonal torpedoes were shown in Chapter 3 to prevent action potential propagation failures.

In this chapter, pharmacological approaches were used to generate spike failures, which induced the formation of axonal torpedoes. This approach was then utilized to identify the specific cellular mechanism behind torpedo formation. I found that torpedo formation requires calcium, and that voltage-gated calcium channels are likely responsible for torpedo formation. Immunohistochemistry was then used to confirm the presence of some voltage-gated calcium channels in torpedoes.

4.2 Materials & Methods

4.2.1 Animals

L7(*pcp2*)*-tau-eGFP* mice (Sekirnjak *et al.*, 2003; Watt *et al.*, 2009) were used to characterize the functional properties of axonal swellings. All animal procedures were approved by the McGill Animal Care Committee in accordance with the guidelines established by the Canadian Council on Animal Care.

4.2.2 Acute cerebellar slice preparation

Acute slices were prepared from young juvenile mice (P10-14), when axonal swellings are numerous (Ljungberg *et al.*, 2016). Mice were deeply anesthetized using isoflurane and checked for foot-paw reflex. Mice were decapitated, and the brain quickly removed in ice-cold artificial cerebrospinal fluid (ACSF; in mM: 125 NaCl, 2.5 KCl, 2 CaCl2, 1 MgCl2, 1.25 NaH2PO4, 26 NaHCO3 and 20 glucose, bubbled with 95% O2 and 5% CO2 to maintain pH at 7.3; Osmolarity 320 ± 5 mOsmol/kg). Parasagittal cerebellar vermis slices (200 μm thick) were made using a Leica VT 1000S vibratome. Slices were incubated in ACSF at 37°C for 45 min and then incubated at room temperature (RT) until used for experiments. All chemicals were purchased from Sigma-Aldrich.

4.2.3 Electrophysiology

All recordings were taken from lobule III, using a Multiclamp 700B amplifier (Molecular Devices), at 33°C. An upright microscope (Scientifica) combined with a custom-built two-photon Ti:Sapphire laser (MaiTai; Spectra Physics) was used to identify Purkinje cell somata with intact axons (GFP). Glass pipettes dipped in CdSeS/ZnS alloyed quantum dots (Sigma-Aldrich) were visually positioned using the scanning two-photon laser as previously described (Andrasfalvy *et al.*, 2014). Loose cell-attached or extracellular recording of Purkinje cell somata and axons was performed using a custom-designed Igor Pro acquisition software (Wavemetrics). Axons were recorded in the granule cell layer, downstream from axonal swellings (50-200 μm from the parent soma), or an equivalent distance from a control axon without torpedoes.

4.2.4 Immunohistochemistry

Mice were anesthetized using an intraperitoneal (IP) injection of Avertin (2,2,2-tribromoethanol; dosage: 0.25 mL/10 g body weight) and transcardially perfused with 4 %

paraformaldehyde (PFA; Electron Microscopy Sciences, EMS). Perfused brains were removed and kept at 4°C on a rotary shaker at 70 RPM for 24 hours in 4 % PFA. Brains were then transferred into phosphate-buffered saline (PBS) with 0.05 % sodium azide. Brains were sliced on a Leica vibratome 3000 into 100 μm-thick parasagittal slices for the vermis. The slices were stored at 4 ºC in PBS with 0.05% sodium azide. Antigen retrieval was performed by incubating slices in 0.25% pepsin, 0.001% HCl in PBS solution for 10 min at RT. Following the antigen retrieval, slices were washed 3 times in 0.4% Triton X in 0.01 M PBS solution. All staining was done in blocking solution containing 5% BSA, 0.05% sodium azide and 0.4% Triton X in 0.01 M PBS. The primary antibody for T-type voltage-gated calcium channels, namely anti-CACNA1G (Cav3.1), anti-CACNA1H (Cav3.2), and anti-CACNA1I (Cav3.3; 1:200, Alomone Labs, Cat. No.: ACC-021, ACC-025, ACC-009) were used to stain for these channels and identify their location within the cerebellar cortex. Slices were incubated with primary antibody at 4 ºC for 72 h on a rotary shaker at 70 RPM. Slices were then washed three times with a solution of 0.01 M PBS with 0.4% Triton X. Corresponding secondary antibodies, including Alexa594 donkey anti-rabbit, Alexa594 donkey anti-rat or Alexa594 anti-mouse antibody were used at dilution between 1:200 to 1:500. Secondary staining was done at 4 ºC for 90 min on a rotary shaker at 70 RPM. Slices were rinsed with 0.4% Triton X in 0.01 M PBS and mounted on slides with Prolong gold anti-fade mounting media (Life Technologies).

4.2.5 Imaging

For live imaging, cerebellar slices were kept alive by continuously perfusing buffered ACSF (with drugs) at 33°C. Images were taken using a custom-built two-photon microscope (Scientifica) with a Ti:Sapphire laser (MaiTai; Spectra Physics) tuned to 890 nm (GFP). Image acquisition was made using ScanImage running in MatLab (Mathworks). For fixed tissue, slides

were imaged on a Zeiss LSM800 laser scanning confocal microscope (Zeiss), using the Zen Blue software. All imaging was done in lobules III of the cerebellar vermis unless indicated otherwise.

4.2.6 Pharmacology

Tetrodotoxin (TTX; Biotium) was used at a concentration of 5 nM (*extra-low TTX*), 10 nM (*low TTX*) and 200 nM (*high TTX*), Nickel chloride (NiCl; Sigma-Aldrich) was used at concentrations of 100 µM and 1 mM, and Anisomycin (Aniso; MedChem Express) was used at a concentration of 25 µM in ACSF.

4.2.7 Analysis

For electrophysiological recording, Igor Pro software was used to extract firing frequency and coefficient of variation of inter-spike intervals. ImageJ/FIJI imaging software was used for all torpedo counts and Purkinje cell counts. *De novo* torpedo formation was counted and divided by Purkinje cell number observed in each time-lapse image. Neurolucida software (MBF Bioscience, USA) was used to do 3D-reconstruction of the axonal torpedo formation. Graphs were made using Igor Pro, Python 3, and Adobe Illustrator.

4.2.8 Statistics

Statistical analysis was performed using SPSS (IBM), data normality and variance equality were determine using Shapiro-Wilk and Levene's test, respectively. Multiple comparisons analyses were made using Repeated-measures ANOVA followed by Bonferroni corrected post-hoc test. Full repeated-measures ANOVA statistical analyses are reported in Appendix I. Comparisons were made with paired or unpaired Student's *T*-tests for parametric data, or Mann-Whitney *U*-tests for non-parametric data. Data were reported as mean ± SEM. Statistical comparisons were made with the level of significance (α) set at $P^* < 0.05$, $P^{**} < 0.01$, $P^{***} < 0.005$.

4.3 Results

As previously shown in Chapter 3, dual-simultaneous recording of soma and axon showed a reduced propagation failure in Purkinje cells with a torpedo compared to control axons. To better understand the function of Purkinje cell axonal torpedoes, we used pharmacology combined with live tissue imaging to explore the mechanism of *de novo* torpedo formation in healthy animals.

4.3.1 Purkinje cell axonal torpedoes are stable over hours

Purkinje cell axonal torpedoes were shown to improved axonal propagation in Chapter 3. We then wondered whether torpedoes were transiently observed on Purkinje cell axon to momentarily enhance axonal function, or if they were stable and conferred a long-lasting effect. To address this, I performed time-lapse two-photon imaging over 2 hours and measured axonal morphology over time.

To determine how dynamic torpedoes are, I repeatedly measured torpedo width in order to quantify any fluctuation in size. I observed that the average torpedo width was 5.04 ± 0.23 µm and showed minimal changes in width over time (Torpedo change in width at: 1h: 1.03 ± 0.016; 2h: 1.06 ± 0.019; n = 40; Fig 4.1B). At this resolution, a single pixel is equal to 0.37 µm. It could therefore be argued, that change within the average torpedo width ± the size of a pixel (i.e. 5.04 ± 0.37 µm) could not be counted as a significant change because this remained within our diffraction limit. Imaging in an acute slice over hours is typically associated with tissue swelling, which might change the morphology of small structures like torpedoes. Therefore, I measured the width of Purkinje cell somata and axons, as I expected these structures are relatively stable. Similarly to torpedoes, the changes observed were far within our diffraction limit in somata (Soma change in width: 1h: 1.01 ± 0.008 ; 2h: 1.01 ± 0.011; n = 36) and axons (Axon: 1h: 1.03 ± 0.021; 2h: 1.06 ± 0.025; n = 36; Fig 4.1B). This was adapted to the different cellular compartment measured (e.g.

Axon change in width at: 1.18 ± 0.37 µm). Since axonal retraction has previously been observed in cut axons and Wallerian degeneration (Coleman, 2005), we measured the distance between torpedoes and the Purkinje cell layer. We showed that the average distance between torpedoes and the Purkinje cell layer is 55.7 ± 3.2 µm (Fig. 4.1C), near the first node of Ranvier. Interestingly, we observed no evidence of axoplasm shift along the axon, or axonal retraction (Distance between soma and torpedo: 1h: 1.00 ± 0.008; 2h: 1.00 ± 0.011; n = 35; Fig 4.1D), which indicates that these torpedoes are not associated with such mechanisms. Most importantly, I found no evidence for new torpedoes forming or for torpedoes disappearing, suggesting that torpedoes are not highly dynamic in acute slices. We concluded that torpedoes were stable over 2h at physiological temperature.

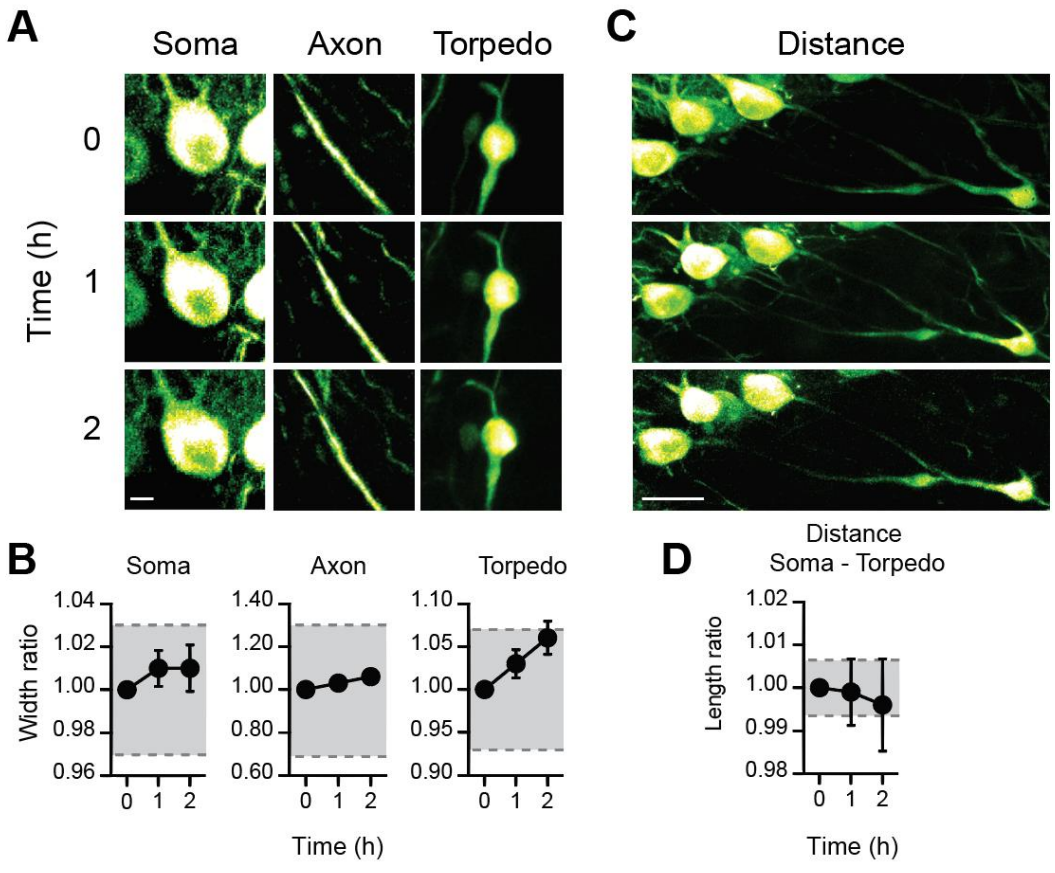

Figure 4.1: Stability of Purkinje cell axonal torpedoes at physiological temperature

(**A**) Representative time-lapse images of somata, axons, and torpedoes at a physiological temperature over 2 hours. Scale bar: 5 µm. (**B**) No change was observed in somata width (n = 36), in axons width (n = 36) and in torpedoes width (n = 40). (**C**) Representative time-lapse images of torpedoes displacement along Purkinje cell axons. Scale bar: 20 µm (**D)** No changes were observed between the soma and torpedo distances (n = 35). Gray dash lines represent a change of a single pixel (i.e. ± 0.37 µm) to the average width. Gray squares represent the diffraction limitation of this experiment for which we could not detect significant changes within these limits.

4.3.2 Pharmacological induction of spike failure leads to torpedo formation

In our healthy mice, we have found that torpedoes are not associated with axonal degeneration or deficits in spontaneous firing properties. On the contrary, our results suggest a functional improvement of axon propagation fidelity in axons with torpedoes. We wondered whether spike failures themselves led to the formation of axonal torpedoes, thereby causing a reduction in spike failures and improvement in axonal function. To address this, we pondered how we could pharmacologically reproduce an increase of spike failures in the axon. One way to block action potentials in neurons is with tetrodotoxin (TTX), which reversibly blocks voltage-gated sodium channels (Tsukamoto *et al.*, 2017). By applying a sub-saturating concentration of TTX ("*low TTX*"; 10nM) (Khaliq & Raman, 2006), I predicted to considerably reduced spiking events in the axon, due to fewer sodium channels, compared to the soma.

Using this pharmacological approach allowed us to observe the effect of increasing the axonal propagation failures in Purkinje cells. I found that a subset of control axons initially without axonal swellings formed new torpedoes in the presence of *low TTX* (7.11 ± 0.94 new torpedoes per 100 Purkinje cells; n = 38; Fig 4.2A). When we used regular ACSF, no new torpedo formations were observed ("*no TTX*": 1.45 ± 0.95 new torpedoes per 100 Purkinje cells; n = 6), as described previously. To determine whether this effect was due to blocking sodium channels themselves rather than differential firing between the axon and soma, we used a saturating concentration of

TTX (“*high TTX*”; 200 nM) and observed that the number of new torpedoes formed was low, and no higher than the *no TTX* condition (*high TTX*: 2.26 ± 0.79 new torpedoes per 100 Purkinje cells; n = 6; Fig 4.2A). This indicates that the complete blocking of sodium channels, and thus the complete absence of spiking events, cannot be responsible for torpedoes formation. The number of Purkinje cells with a newly formed torpedo increase by 5.7 % after bath applying *low TTX* for 3 hours (Fig 4.2B). We then wondered if we could increase the amount of Purkinje cells with newly formed torpedoes by incubating the slice in even lower TTX concentration (“*extra-low TTX*” at 5 nM). We showed that torpedo formation was still occurring at *extra low TTX* concentration, matching the result obtain with *low TTX* (*extra-low TTX*: 7.81 ± 2.65 new torpedoes per 100 Purkinje cells; n = 7; Fig 4.2B). Therefore, we pursued subsequent experiments using the *low TTX* concentration. This suggests that an increase in axonal propagation failures is at least in part responsible for the formation of new axonal torpedoes. In contrast, conditions that do not increase axonal failures such as *no TTX* (ACSF only) or *high TTX* are unable to produce new torpedoes in Purkinje cells.

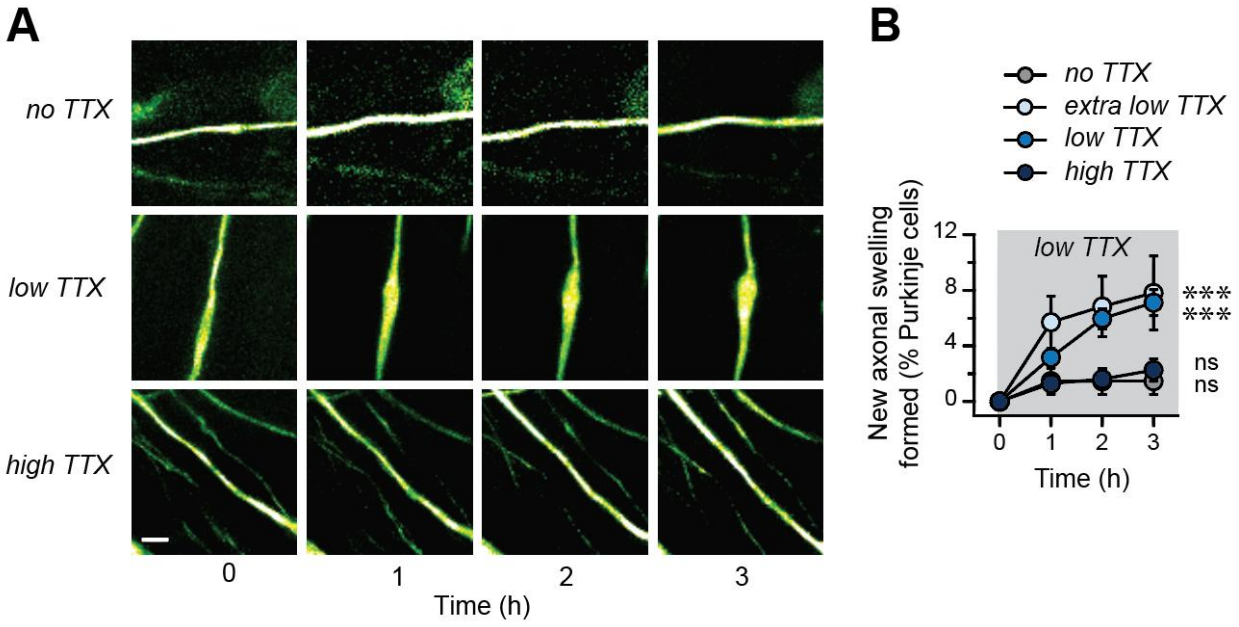

Figure 4.2: Low concentration of TTX induces torpedo formation in acute slices
(**A**) Representative time-lapse images of control axons in different conditions, ACSF without TTX (Top), ACSF with *low TTX* concentration, showing a torpedo forming (Middle), ACSF with *high TTX* concentration (Bottom). Scale bar: 5 µm. (**B**) Summary data showing an increase in newly formed torpedoes in *extra low TTX* and *low TTX* concentration compared to *no TTX* and *high TTX* (*no TTX*; n = 6 acquisitions; *extra low TTX*, n = 7; *low TTX*, n = 38; *high TTX*, n = 6; full repeated-measures ANOVA statistical analysis is shown in Appendix I, P > 0.05, P*** < 0.005).

Since torpedoes formed only on a subset of Purkinje cell axons, we wondered whether these axons could be morphologically identified before torpedo formation. To address this, we performed 3D-reconstructions of these newly formed axonal swellings and compared them to reconstruction made from images prior to torpedo formation. Interestingly, the initial volume of axons that later had torpedoes form on them was indistinguishable from neighboring axons that did not form torpedoes (Control axons: 12.5 ± 3.4 μm^3; axon before torpedo formed: 19.2 ± 7.7 μm^3; n = 8; compared at time 0; repeated-measures ANOVA, P = 0.44; Fig 4.3B). This also allowed us to examine whether axonal torpedoes could form by a local migration of axoplasm (i.e. axon cytoplasm), which should be evident in time-lapse images as axons become thinner or thicker. However, the formation of new torpedoes was focalized, with no apparent shift in axoplasm on neighboring axonal segments. Consistent with the formation of axonal torpedoes, a significant increase in volume was focally observed at the torpedo site compare to control axons (control axons: 20.9 ± 6.8 μm^3; axon with a newly formed torpedo: 71.4 ± 17.4 μm^3; n = 8; repeated-measures ANOVA, P = 0.017; Fig.4.3B). This suggests that the mechanism by which axonal torpedoes form may be focally restricted.

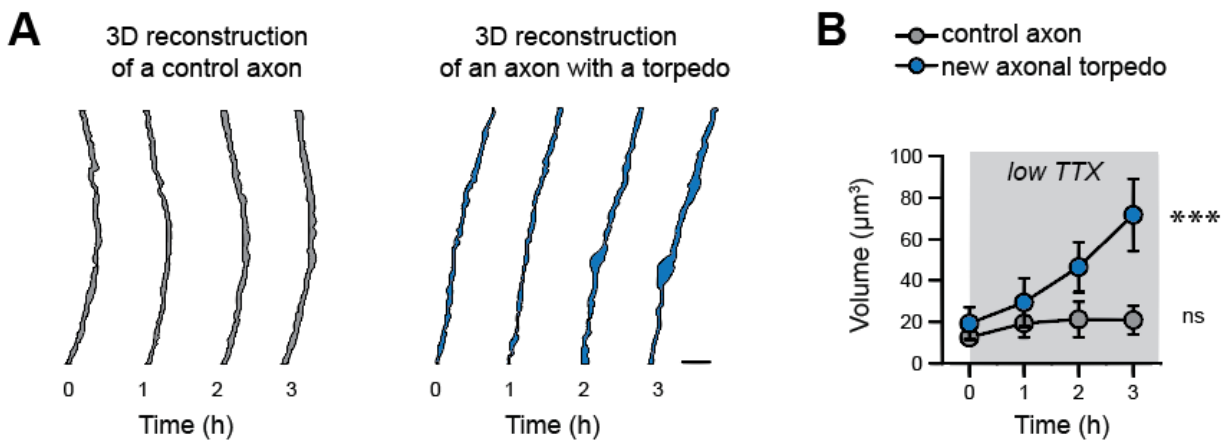

Figure 4.3: Three-dimensional reconstruction of a newly formed axonal swelling
(**A**) Representative changes in the volume of a control axon (left) and a control axon, which will form a new torpedo (right). Scale bar: 5 µm. (**B**) Progression of axonal volume during torpedo formation (full repeated-measures ANOVA statistical analysis is shown in Appendix I, $P > 0.05$, $P^{***} < 0.005$).

4.3.3 Exploring the effect of low TTX on torpedo formation

The bath application of *low TTX*, was predicted to considerably reduce spiking events in the axon, due to the presence of fewer sodium channels, compared to the soma. We wondered if this assumption was correct, and how Purkinje cell somata and axons reacted to the application of *low TTX*.

To address that, I performed simultaneous dual recordings of paired and unpaired soma and axon during bath application of *low TTX* over 1.5 hours. I showed that the firing frequency in the Purkinje cell soma was also largely reduced in *low TTX* (both somata and axons displayed reduced firing frequency in low TTX; repeated-measures ANOVA, $P < 0.001$, Fig 4.4B). However, somatic spiking events still occurred in comparison to control axons where spiking events could not be detected (repeated-measures ANOVA, $P = 0.003$). This suggests that *low TTX* induce a more sizeable reduction in Purkinje cell action potentials in axons compared to the soma, thereby mimicking high axonal failures (Fig 4.4A).

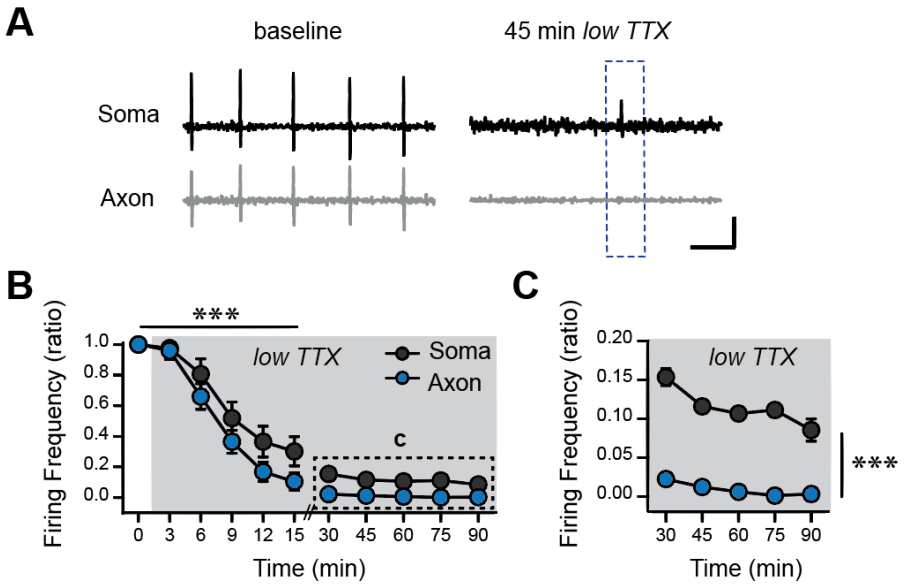

Figure 4.4: Effect of low TTX on Purkinje cell action potential propagation
(**A**) Simultaneous recording of Soma and Axon baseline (Left) and after 45min of *low TTX* perfusion (Right). Dash square indicates a spike failure. Scale bar, 1 mV, 25 ms. (**B**) Normalized effect of *low TTX* on Purkinje cells firing frequency (n = 17; repeated-measures ANOVA, P*** < 0.005). (**C**) Data inset showing the effect of low TTX on somata and axons firing frequency after 30 min perfusion (full repeated-measures ANOVA statistical analysis is shown in Appendix I, P > 0.05, P*** < 0.005).

Purkinje cell firing frequency is predominantly reduced in the first 30 min of *low TTX* incubation (Fig 4.4). Only occasional somatic spiking could be seen in the remaining recorded time. To look in more detail at the mechanism by which torpedoes form, we varied the duration of *low TTX* that was used to produce them. We wondered whether the mechanism of torpedo formation was engaged rapidly, eventually leading to the development of torpedoes over a few hours, or if Purkinje cells needed a long and persistent impairment of action potential propagation to form torpedoes.

To address this question, brain slices were placed in *low TTX* for half an hour to quickly increase axonal failures and then changed to *high TTX* concentration for 1.5 hours, to block all neuronal activity. We found that this short period of *low TTX* incubation followed by *high TTX* was not sufficient to induce torpedo formation (1.30 ± 0.50 new torpedo % Purkinje cell; n = 8; Fig 4.5A), similar to *high TTX* on its own (Fig 4.2). Although Purkinje cells have almost completely stopped firing after 30 min incubation in *low TTX* (Fig 4.4B), this shows that torpedo formation requires a longer exposure to *low TTX* concentration and that the initial firing frequency ramp down caused by *low TTX* in the first half-hour of this trial is not sufficient for torpedo formation. Similar experiments were then done where *high TTX* was perfused for half an hour, followed by *low TTX* for 1.5 hours. This protocol did not lead to torpedo formation either (0.93 ± 0.60 new torpedo % Purkinje cell; n = 6; Fig. 4.5B), indicating that sufficient failures are needed for torpedoes to form, which does not happen when *high TTX* is initially perfused, since this prevents torpedo formation completely even after changing the incubation solution for *low TTX* for one hour and a half. These experiments show that torpedo formation occurs following persistent axonal action potential failures.

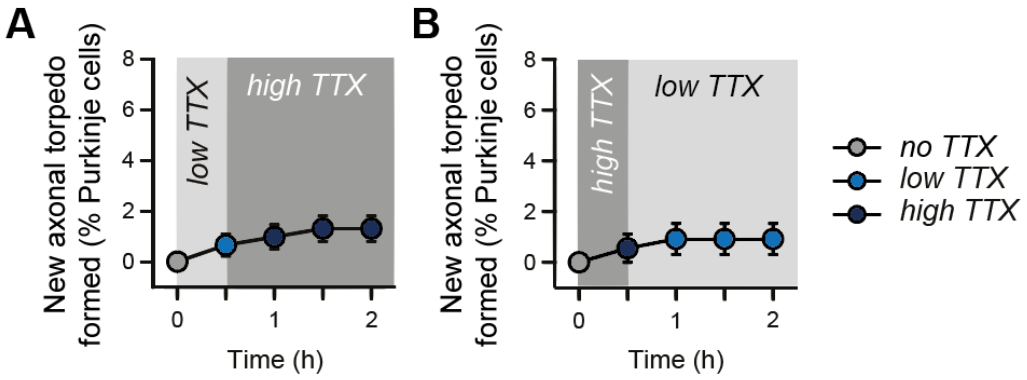

Figure 4.5: Brief application of low TTX is insufficient for torpedo formation

(**A**) No torpedo formation occurs when place in *low TTX* for 30 min and *high TTX* for 1.5 hours (n = 8). (**B**) No torpedo formation was observed when place in *high TTX* for 30 min and *low TTX* for 1.5 hours (n = 6).

4.3.4 Torpedo formation does not require proteins synthesis

Since axonal torpedoes lead to fewer spike failures, we hypothesized that proteins that could counteract spike failures, such as ion channels (i.e. VGSC or VGKC), in axons would be enriched in torpedoes, thereby facilitating axonal propagation. If this were true, it might indicate that major protein synthesis may be required for torpedo formation to occur and could explain the time delay for new torpedoes to form. To address that, we used Anisomycin (Aniso), a protein synthesis blocker, to block all novel protein synthesis in the cells (Karachot *et al.*, 2001). Live tissue imaging showed that Anisomycin (25µM) in the presence of *low TTX* (5.22 ± 1.33 new torpedoes % Purkinje cells; n = 10), did not alter torpedo formation from the *low TTX* condition (6.49 ± 1.28 new torpedoes % Purkinje cells; n = 18; Fig 4.6B), suggesting that protein synthesis is not required for torpedo formation. Interestingly Anisomycin on its own did not cause torpedo formation (2.20 ± 1.15 new torpedoes % Purkinje cells; n = 6; independent two-tailed Student's *T*-test, p = 0.14; Fig 4.6B), showing that axonal failures are required for torpedo formation. Our results showed that protein synthesis is not a major pathway implicated in torpedo formation, suggesting that novel protein formation inside axons is not the driving force for the axonal expansion observed in torpedo formation. Other pathways like axonal transport might be more important for allowing enlargement of axons and therefore improved axonal propagation fidelity in torpedoes. However, we cannot exclude the possibility that morphological changes observed in torpedo formation and their functional improvement of axonal propagation fidelity could be two distinct mechanisms. This indicates that *de novo* protein synthesis might still be required to improve action potential propagation.

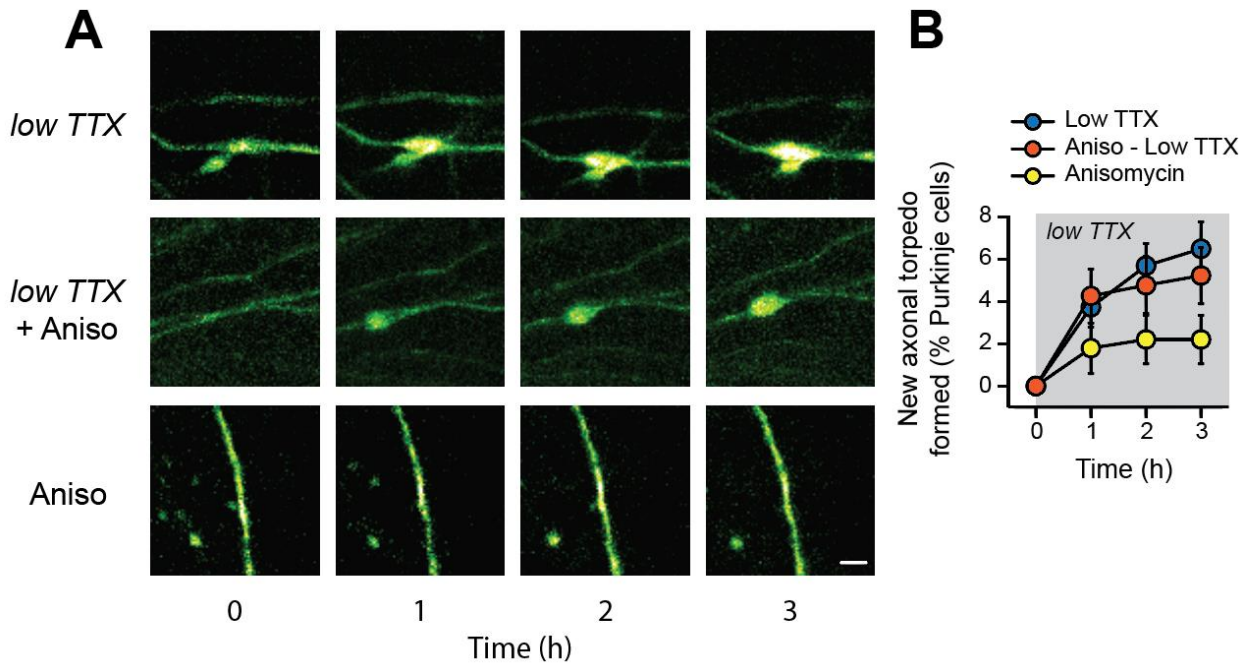

Figure 4.6: Protein synthesis is not required for torpedo formation
(**A**) Representative time-lapse images of axonal torpedoes formation in the absence of protein synthesis (*low TTX*, top; *low TTX* + Anisomycin, middle; and Anisomycin, bottom). Scale bar: 5 µm. (**B**) Summary representation of torpedoes formation in presence of Anisomycin (low TTX, n = 18; low TTX + Anisomycin, n = 10; Anisomycin, n = 6; full repeated-measures ANOVA statistical analysis is shown in Appendix I, $P > 0.05$).

4.3.5 Torpedo formation is mediated by voltage-gated calcium channels

To better understand the molecular mechanism of *de novo* torpedo formation, we wanted to know what signaling pathways might be involved in this process. We began by altering extracellular calcium, which is a major signaling molecule in the brain. We either excluded calcium entirely (0 mM Ca^{2+}) from our preparation or increased the concentration from 2 to 3 mM Ca^{2+} in the ACSF. We observed that torpedo formation rate is dependent on calcium concentration (Fig 4.7A). Torpedo formation rarely occurs in 0 mM Ca^{2+} concentration with *low TTX* (1.86 ± 0.58 new torpedoes % Purkinje cells; n = 15), compared to 0 mM Ca^{2+} alone (1.65 ± 0.56 new torpedoes % Purkinje cells; n = 12), which was significantly different from regular ACSF (with 2 mM Ca^{2+}) with *low TTX* (*low TTX* + 2 mM Ca^{2+}: 5.99 ± 1.14 new torpedoes % Purkinje cells; n = 14; Fig

4.7B). This shows that calcium is crucial for torpedo formation. We also found that an increase in ACSF calcium concentration to 3 mM Ca^{2+} with low TTX significantly elevated torpedo formation compared to 0 mM Ca^{2+} with low TTX (*low TTX* + 3 mM Ca^{2+}: 6.81 ± 1.23 new torpedoes % Purkinje cells; n = 12; Fig 4.7B), although this was not significantly different from ACSF with 2 mM Ca^{2+} in *low TTX*. These results show that extracellular calcium signaling is important for this torpedo formation mechanism.

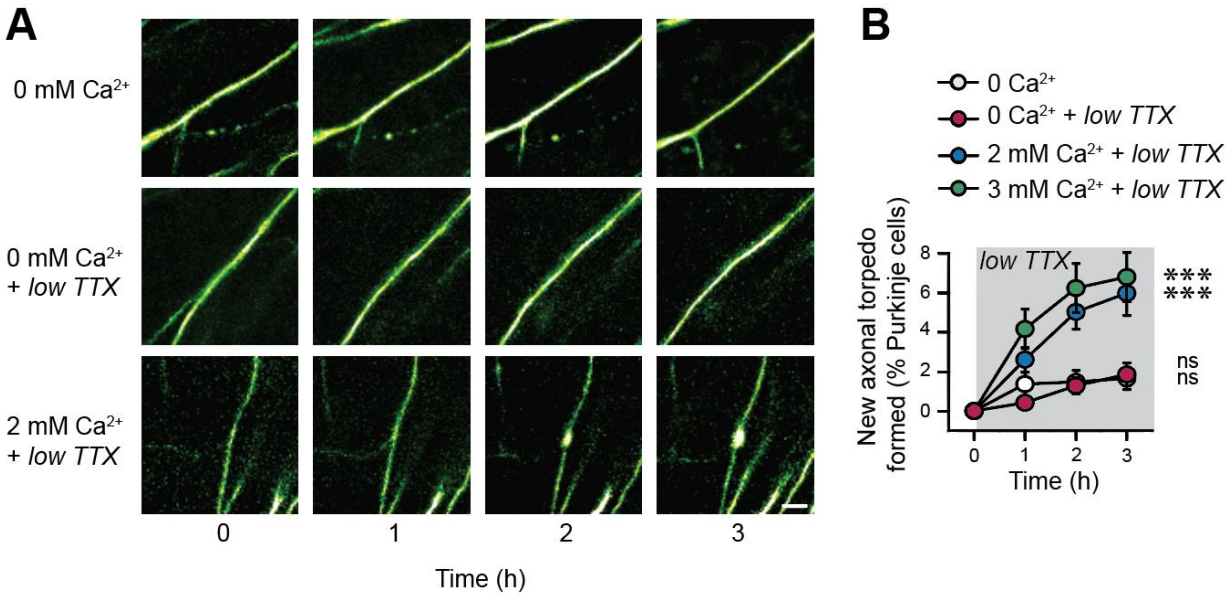

Figure 4.7: Torpedo formation in low TTX is calcium-dependent
(**A**) Representative time-lapse images of torpedo formation in different calcium concentrations in presences of low TTX. Scale bar: 5 µm. (**B**) New axonal torpedo formation over time showing the effect of different extracellular calcium concentrations on torpedo formation (0 mM Ca^{2+}; n = 12; 0 mM Ca^{2+} + *low TTX*; n = 15; 2 mM Ca^{2+} + *low TTX*; n = 14; 3 mM Ca^{2+} + *low TTX*; n = 12; full repeated-measures ANOVA statistical analysis is shown in Appendix I, P > 0.05, P*** < 0.005).

To further elucidate the role of calcium signaling in torpedo formation, we next investigated the involvement of calcium channels in this process. We used nickel ion (Ni^{2+}), which was initially identified as a T-type calcium channel (i.e. $Ca_V3.1$, $Ca_V3.2$, and $Ca_V3.3$) blocker. This has been shown to block Purkinje cell T-type currents at half the maximum inhibitory concentration (IC_{50}), which was equal to 110 µM in whole-cell recording (Isope *et al.*, 2012; Lee

et al., 1999). However, a presumably lower concentration of Ni^{2+} might display a similar blocking effect, due to lower numbers of ion channels in axons compared to Purkinje cell somata. While Ni^{2+} was first thought to predominantly block T-type channels, it has also been shown to block R-type and L-type, but not P/Q-type channels (Zamponi *et al.*, 1996). Thus, we interpreted Ni^{2+} to be a voltage-gated calcium channel blocker rather than a specific T-type channel blocker.

When we perfused 100 µM Ni^{2+} together with *low TTX*, we observed a reduction in torpedo formation (Fig 4.8A) of ~35% compared to *low TTX* alone (*low TTX* + 100 µM Ni^{2+}: 3.91 ± 0.98 new torpedoes % Purkinje cells; n = 6; *low TTX*: 6.09 ± 1.39 new torpedoes % Purkinje cells; n = 14), while torpedoes formed more frequently than with Ni^{2+} alone without *low TTX* (100 µM Ni^{2+}: 1.51 ± 0.94 new torpedoes % Purkinje cells; n = 5; Fig 4.8B). Furthermore, a higher Ni^{2+} concentration (1 mM), which likely blocks most voltage-gated calcium current, completely abolished torpedo formation in the presence of *low TTX* (Fig 4.8A). When 1 mM Ni^{2+} together with *low TTX* was compared to *low TTX* alone (*low TTX* + 1 mM Ni^{2+}: 1.19 ± 0.61 new torpedoes % Purkinje cells; n = 8; Fig 4.8C), it resembled the result when Ca^{2+} was not available (0 mM Ca^{2+} concentration; Fig 4.7). Our data suggest that torpedo formation is not dependent on P/Q-type calcium channel, but more likely involves other voltage-gated calcium channels, such as T-type, L-type, or R-type. Overall, this data suggests that torpedoes can be formed by spike failures in Purkinje cell axons, through a voltage-gated calcium channel dependent process.

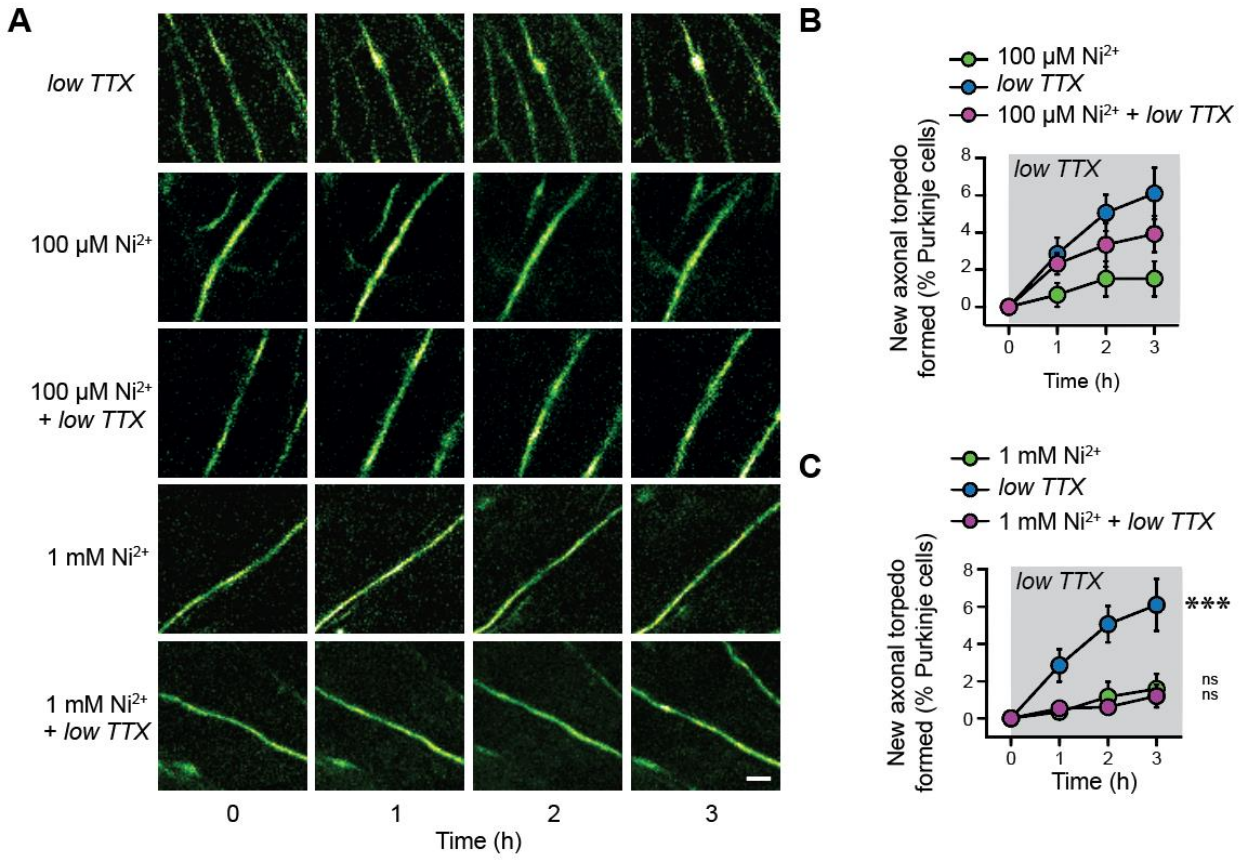

Figure 4.8: Torpedo formation is regulated by voltage-dependent calcium channels
(**A**) Representative time-lapse images of control axon without torpedo formation in the presence of Ni^{2+}. Scale bar: 5 µm. (**B**) New axonal torpedo formation over time, showing the effect of 100 µM Ni^{2+} on torpedo formation. (**C**) New axonal torpedo formation over time, showing the effect of 1 mM Ni^{2+} on torpedo formation (full repeated-measures ANOVA statistical analysis is shown in Appendix I, $P > 0.05$, $P^{***} < 0.005$).

4.3.6 Investigation of calcium channel in torpedoes

Our result showed that voltage-gated calcium channel is required for *de novo* torpedo formation, most likely through either T-type, L-type, and R-type calcium channels. We started by investigating T-type calcium channels since they had previously been reported to be the primary source of calcium influx at Purkinje cell nodes of Ranvier (Grundemann & Clark, 2015). To investigate which calcium channel is implicated in torpedoes formation, we labeled three different subtypes of T-type calcium channels: Cav3.1, Cav3.2 and Cav3.3. We found that all three T-type

calcium channel subtypes are expressed to varying levels in the cerebellar cortex. $Ca_V3.1$ has the highest expression in Purkinje cell somata and their dendrites, compared to $Ca_V3.2$ and $Ca_V3.3$ (Fig 4.9A). Furthermore, $Ca_V3.1$ was the only T-type channel subtype that was occasionally observed in torpedoes, as we observed staining in ~ 30% of torpedoes (Fig. 4.9B). These results suggest that T-type calcium channels are likely found in Purkinje cells, where they may contribute to torpedo formation. At this moment, further experimentation is required to evaluate the presence of L-type and R-type calcium channels in torpedoes.

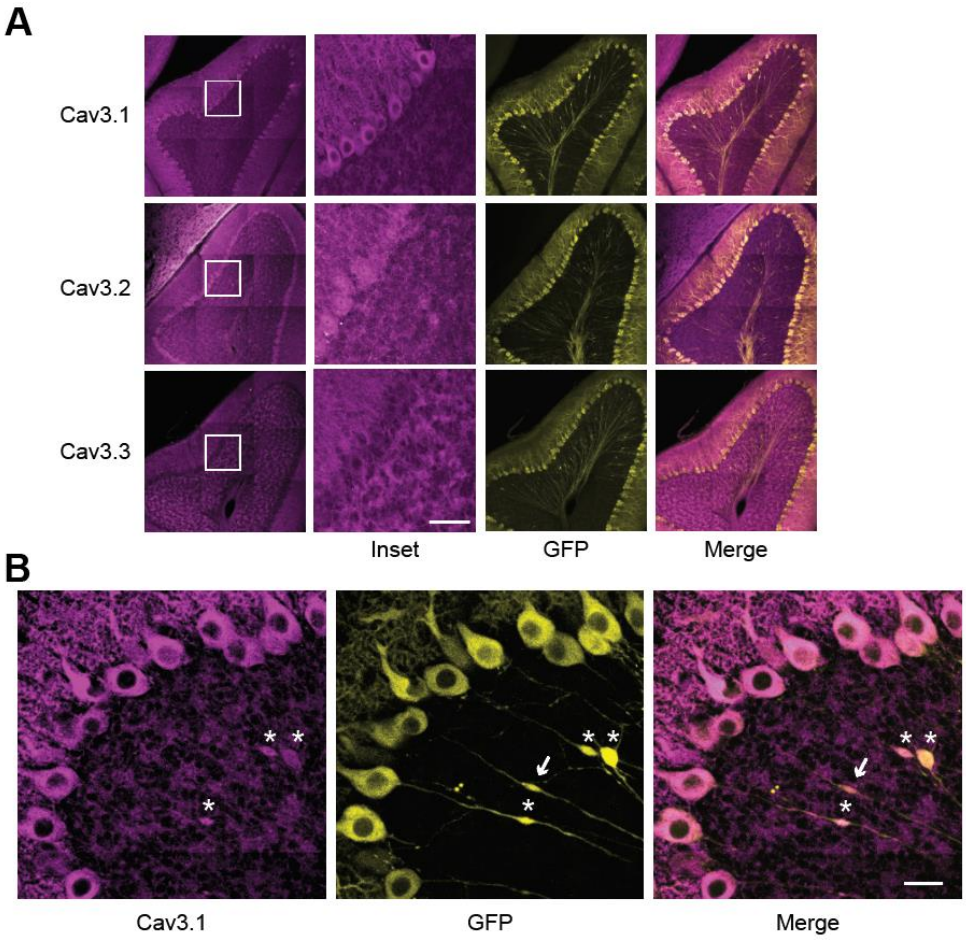

Figure 4.9: Distribution of T-type calcium channels expression in the cerebellar cortex
(**A**) Representative image showing the different T-type calcium channels present in the lobule III of the cerebellar cortex at P11. Scale bar: 200 µm (inset scale bar: 50 µm). (**B**) Representative images of Cav3.1 staining for torpedoes. Torpedoes positive for Cav3.1 are indicated by stars (*), while the arrow is a torpedo negative for Cav3.1. Scale bar: 25 µm.

4.4 Discussion

In this chapter, I investigated the mechanism of Purkinje cell axonal torpedo formation. Imaging of acute cerebellar slices in ACSF over 2-3 hours shows that Purkinje cells remain healthy during this time, without evidence of axonal retraction, torpedo formation, or elimination. However, when action potential failures were artificially reproduced using a sub-saturating concentration of TTX, new torpedoes appeared within a few hours on a subset of axons. Interestingly, torpedo formation was easily interrupted by *high TTX* (causing complete loss of action potentials) either at the beginning or at the end of the incubation. This shows that *low TTX*, producing sustained axonal action potential failures, is required for torpedo formation. Experiments on myelinated axons of frogs have shown a widening of nodes of Ranvier when neurons were placed in ciguatoxin (CTX), which reduces voltage-gated sodium channels (VGSC) threshold leading to hyper-excitability of the membrane (Mattei *et al.*, 2014). Although the effects of CTX on axonal spike propagation was not assessed, this result suggests that dysregulation of the firing pattern in neurons induces morphological restructuring in the axon, in a direction that promotes axonal function and homeostasis.

Protein synthesis was found not to be implicated in torpedo formation. This finding suggests that other mechanisms (e.g. axonal transport) are likely involved in torpedo formation. We found that torpedo formation was minimal in the absence of extracellular calcium, highlighting the importance of calcium signaling in torpedo formation. As described in Chapter 2, calcium has an extensive role as a signaling molecule in neurons. To further investigate how calcium signaling plays a role in torpedo formation, Ni^{2+} was used at both sub-saturating and saturating concentrations. The formation of new torpedoes was reduced by a third in sub-saturating Ni^{2+}. It was completely inhibited in saturating Ni^{2+}, suggesting that voltage-gated calcium channels are

likely to be involved in the torpedo formation mechanism. We also reported that only Cav3.1 was highly expressed in Purkinje cell somata and dendrites, as previously shown by (Isope *et al.*, 2012). Moreover, we observed Cav3.1 expression in Purkinje cell axonal torpedoes, suggesting that calcium influx through these channels may participate in torpedo formation and function.

An interesting future line of investigation would be to follow this with specific calcium channel blockers like Mibefradil for T-Type calcium channels, as well as staining for L-Type (Cav1.2 and Cav1.3) and R-type (Cav2.3) calcium channels, which would allow us to refine our understanding of the molecular pathway regulating torpedo formation.

Overall, this chapter presented evidence that torpedo formation is induced by the manipulation of Purkinje cell firing, such as by inducing propagation failures. Our results partly reveal the mechanism of torpedo formation, which appears to be regulated through voltage-gated T-type calcium channels. However, further experiments are required to elucidate the complete mechanism of torpedo formation and its function.

CHAPTER 5: IMPACT OF AXONAL TORPEDOES ON MOTOR LEARNING IN MICE

5.1 Introduction

Axonal torpedoes have been observed in both human disease and animal models of disease, leading to the hypothesis that they contribute to the pathophysiology underlying these diseases. The cerebellum is associated with coordination and motor control, and these cerebellar diseases usually lead to gait, balance, and motor coordination deficits. However, our results from Chapter 3 revealed that torpedoes in healthy animals were associated with an improvement in axonal spike failures. We therefore wondered how torpedoes in healthy animals might influence motor coordination.

In this chapter, I assessed motor coordination with different assays, which revealed a positive correlation between the amount of motor learning in task associated with the cerebellum and the density of torpedoes. By using a tissue clearing method, I was able to clear cerebella and morphologically map torpedoes in the vermis of the cerebellar cortex. I thus investigated the localization and density of torpedoes on the cerebellar cortex of healthy animals

5.2 Materials & Methods

5.2.1 Animals

Mice were used at 1-2 months of age for all behavioral studies. *L7*(*pcp2)-tau-eGFP* mice (Sekirnjak *et al.*, 2003; Watt *et al.*, 2009) were used to characterize axonal torpedoes. All animal procedures were approved by the McGill Animal Care Committee, in accordance with the

guidelines established by the Canadian Council on Animal Care. C57BL6/J mice were used for vestibular ocular reflex (VOR) behavioral study. Animal procedures for VOR were approved by the Dutch Ethical Committee for animal experiments in accordance with the Institutional Animal Care and Use Committee at the Erasmus Medical Centre.

5.2.2 Behavioral Assays

Rotarod Assay: We used a Rotarod (Stoelting Europe) as previously described (Jayabal *et al.*, 2016) to assess the natural variability of individual mice motor coordination. After an hour of acclimatization, mice were placed on an accelerating (from 4 to 40 RPM, over 5 min) rotating rod, and the latency to fall (4 trials/day for 7 days) was recorded. Motor learning was determined by subtracting the average time on the rod (last two trials) of day 1 from day 7 to determine the degree to which performance improved over the 7days. *Erasmus Ladder Assay*: We used the Erasmus Ladder (Noldus Inc.) to assess motor learning (Vinueza Veloz *et al.*, 2015). Mice walked across a horizontal ladder (42 trials/day for 4 days), which consisted of 2 parallel rows of 37 pressure monitored rungs between two dark chambers. Mice typically used short steps (stepping between two upper runs) to traverse the ladder. The change in the number of short steps across days was used to measure motor learning in individual animals. *VOR Assay*: Mice were equipped with a pedestal under general anesthesia with isoflurane/O2. After 2–3 days of recovery, mice were head-fixed with the body loosely restrained in a custom-made restrainer and placed in the center of a turntable (diameter: 63 cm) in the experimental set-up. A round screen (diameter 60 cm) with a random dotted pattern (‘drum’) surrounded the mouse during the experiment. VOR Phase reversal was induced by training mice over 4 days (6 x 5 min.) using in-phase sinusoidal drum and table rotation at 0.6 Hz (amplitude table 5°, drum 5° on day 1, 7.5° on day 2, 10° on day 3-4) and probed by recording VOR in the dark before and after training sessions. A CCD camera fixed to the

turntable monitored the eyes of the mice using eye-tracking software (ETL-200, ISCAN systems). For eye illumination during the experiments, two infrared emitters (output 600 mW, dispersion angle 7°, peak wavelength 880 nm) were fixed to the table and a third emitter, which produced the tracked corneal reflection, was mounted to the camera and aligned horizontally with the optical axis of the camera. Eye movements were calibrated by moving the camera left-right (peak-to-peak 20°) during periods that the eye did not move (Wu *et al.*, 2019). Gain and phase values of eye movements were calculated using custom-made Matlab routines (MathWorks).

5.2.3 Immunohistochemistry

L7-tau-eGFP mice were anesthetized using an intraperitoneal (IP) injection of Avertin (2,2,2-tribromoethanol; dosage: 0.25 mL/10 g body weight) and transcardially perfused with 4 % paraformaldehyde (PFA; Electron Microscopy Sciences, EMS). Perfused brains were removed and kept at 4°C on a rotary shaker at 70 RPM for 24 hours in 4 % PFA. Brains were then transferred into phosphate-buffered saline (PBS) with 0.05 % sodium azide. Brains were sliced on a Leica vibratome 3000 into 100 μm-thick parasagittal slices. The slices were stored at 4 ºC in PBS with 0.05% sodium azide. Antigen retrieval was performed by incubating slices in 0.25% pepsin, 0.001% HCl in PBS solution for 10 min at RT. Following the antigen retrieval, slices were washed 3 times in 0.4% Triton X in 0.01 M PBS solution. All staining was done in blocking solution containing 5% BSA, 0.05% sodium azide and 0.4% Triton X in 0.01 M PBS. Anti-inositol-triphosphate receptor antibody (IP_3R; 1:200, Abcam, Cat. No.: ab5804) was used to stain for IP_3R. Slices were incubated with primary antibody at 4 ºC for 72 h on a rotary shaker at 70 RPM. Slices were then washed three times with a solution of 0.01 M PBS with 0.4% Triton X. Corresponding secondary antibodies, including Alexa594 donkey anti-rabbit, Alexa594 donkey anti-rat or Alexa594 anti-mouse antibody were used at dilution between 1:200 to 1:500. Secondary staining

was done at 4 ºC for 90 min on a rotary shaker at 70 RPM. Slices were rinsed with 0.4% Triton X in 0.01 M PBS and mounted on slides with Prolong gold anti-fade mounting media (Life Technologies).

For C57BL6/J mice immunohistochemistry of the flocculus after VOR, mice were deeply anesthetized through IP administration of sodium pentobarbital, brains were post-fixed for 1 hour and were subsequently transferred to a 10% sucrose solution overnight at 4ºC. The following day they were embedded with 10% sucrose/14% gelatin (Wako) and placed in a 30% sucrose/10% formaldehyde for 1 hour at RT and switched to 30% sucrose solution overnight at 4ºC. Embedded brains were sectioned transversally into 40 μm-thick slices with a freezing microtome. Sections were rinsed with 0.1 M PB and incubated for 2 hours in 10 mM sodium citrate (pH 6) at 80 ºC for antigen retrieval. 10% of horse serum was used to block non-specific binding, and antibodies were applied for 2 days. Primary antibodies used were Calbindin (1:7000 mouse monoclonal, Sigma C9848), and IP3R (1:1000 rabbit polyclonal, Abcam 5804). Secondary antibodies used were coupled to Alexa Fluor-488 or Cy3 (1:200). Sections were mounted on coverslips in Chromaluin (genatin/chromate) and covered with Mowiol mounting medium (Polysciences Inc.).

5.2.4 Tissue Clearing

Mice were anesthetized using an intraperitoneal injection of Avertin (2,2,2-tribromoethanol; dosage: 0.25mL/10g body weight) and transcardially perfused with 4% paraformaldehyde (PFA; EMS). The brain was removed and transferred into 4% PFA and stored at 4°C on a rotary shaker at 70 RPM for 24 h after which the cerebellar cortex was isolated and transferred into a hydrogel solution (10% v/v 10X PBS, 10% v/v 40% Acrylamide; 0.025% v/v 10% VA-044 and filled up to 15ml with ddH2O) at 4°C for 24h. The cerebella were then transferred to the X-Clarity Polymerization system (Logos Biosystem) at 37°C, under 90 kPa

vacuum for 3h, followed by the X-Clarity Tissue Clearing system, using the electrophoretic tissue clearing solution (Logos Biosystem) set at a current of 1 Amp at 37°C for 24h.

5.2.5 Imaging

For fixed tissue, slices from the vermis were imaged on a custom-built two-photon microscope (Scientifica) with a Ti:Sapphire laser (MaiTai; Spectra Physics) tuned to 890 nm (GFP), while slices from the flocculus were imaged using an LSM700 or LSM800 laser scanning confocal microscope (Zeiss). Cleared cerebella were imaged using a Light sheet Z.1 ZEISS microscope with the Zen 2014 SP1 (black edition) software (Carl Zeiss) to image the whole cerebellum.

5.2.6 Analyses

Whole cerebellum images were first converted from CZI file into individual TIFF files. Image stacks were reconstructed from the individual TIFF files and stitched together to form the whole cerebellum image using Imaris Stitcher 9.2.1. Using Imaris 9.3 software, whole cerebellum images were cropped into different lobules to facilitate data manipulation. Manual surface creation was used to traces the boundaries of the granule cell layer. An automatic spot detection tool was used to identify torpedoes based on fluorescence intensity, area, and sphericity of the spot detected within the granule cells layer of each lobule. The total number of torpedoes was divided by the total granule cell layer area for each animal. Confocal images and 2-photon images were analyzed using Zen (blue edition; Zeiss) software and FIJI/ImageJ software, respectively.

5.3 Results

We previously showed that torpedoes are associated with reduced propagation failure of action potentials. Purkinje cells gather information from different sources (see Chapter 2) and are

the sole output of the cerebellar cortex. We wondered how spike failures along Purkinje cell axons could influence the behavioral output of animals, and whether a reduction in spike failures of the magnitude that we observed could impact animal behavior. To address that, we tested whether animal-to-animal variability in torpedo density influenced animal behavior. We also examined the variability of torpedo density across the cerebellar vermis using light-sheet imaging.

5.3.1 Motor learning is positively correlated with torpedoes

To better characterize the role of torpedoes on motor coordination learning, we wondered whether the number of torpedoes in the anterior lobules, which are known to be associated with motor coordination (Morton & Bastian, 2007), could influence the amount of learning on a motor coordination task. To address this, we tested mice over several days using an accelerating Rotarod assay and then quantified the number of torpedoes that each mouse had in lobule III. The Rotarod assay showed wide variability in motor performance across subjects (Day 1 ranged from 20 to 95%; Day 7 ranged from 56 to 97%, paired Student *T*-test, $P < 0.001$). The density of torpedoes in lobule III also showed a wide range of variability across animals (percentage of Purkinje cells with torpedo ranged from 12.5 to 57.1 %; Fig 5.1B). Remarkably, a positive correlation was observed between these measurements: mice that learned more tended to have a higher proportion of Purkinje cells with torpedoes (Pearson's correlation, $R = 0.54$, $P = 0.011$; Fig 5.1C). Mice were split between low and high learners, and we found that they had a significantly different number of torpedoes in lobule III (unpaired Student's *T*-test, $P = 0.046$; Fig 5.1E). These results suggest that Purkinje cell axonal torpedoes have a beneficial effect on learning motor coordination in lobule III and agree with our results that torpedoes reduce axonal failures.

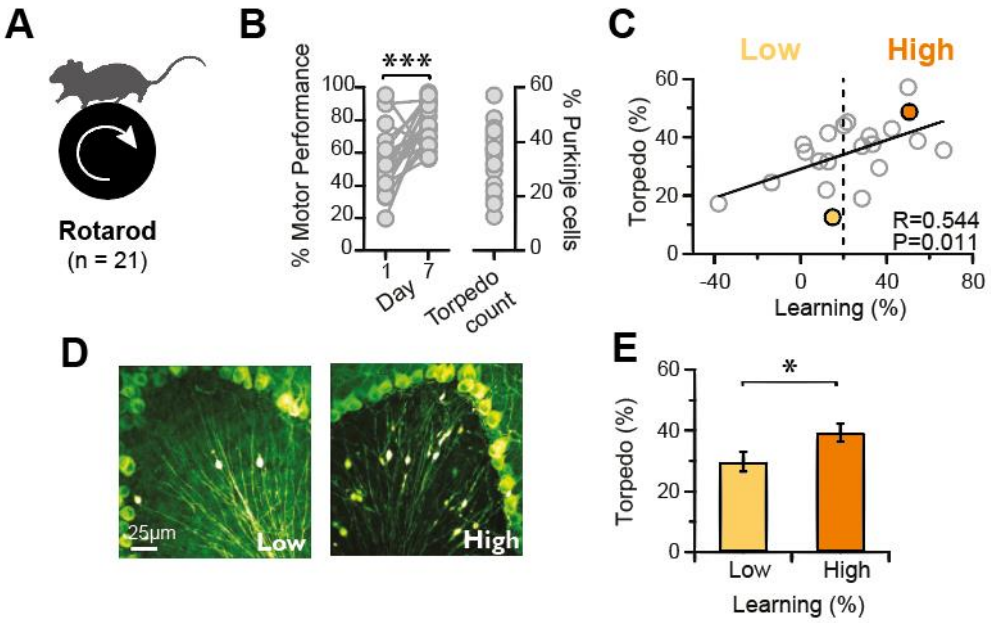

Figure 5.1: Rotarod motor learning and torpedoes

(**A**) Schematic representation of the Rotarod assay (N = 21). (**B**) Improvement of motor performance of individual animals on first (Day 1) and last day (Day 7; P*** < 0.005), and the distribution of Purkinje cells with torpedoes. (**C**) Correlation between motor learning and the percentage of cells with torpedoes (R = 0.54, P* < 0.05). (**D**) Representative images of Low (Left) and High (Right) learners with different torpedoes numbers. Scale bar = 25µm. (**E**) Low and High learners have a significant different percentage of Purkinje cells with torpedoes (P* < 0.05).

To better understand the involvement of cerebellar torpedoes in motor learning, we pursued a similar study with a different motor learning task. The Erasmus Ladder assay was developed as a motor assay that tests for cerebellar-related motor coordination and learning (Vinueza Veloz *et al.*, 2015). Mice run repeatedly over 8 days on the Erasmus ladder: the first 4 days of trials (day 1-4) were used to assess motor learning, while the last 4 days of trials (day 5-8) were used to assess cerebellar-related associative memory. When comparing the first and last day (day 1-4) of the motor learning Erasmus Ladder task, we observed some variability between animals (Day 1 ranged from 91.8 to 96.5%; Day 4 ranged from 95.4 to 99.4%, paired Student's *T*-test, P = 0.001), but also between the torpedo numbers (% of Purkinje cells with torpedoes ranged from 21.2 to 53.6%; Fig 5.2B). Interestingly, an even stronger correlation was observed between the axonal torpedoes

and motor learning (Pearson's correlation, R = 0.78, P = 0.008; Fig 5.2C), compared to the rotarod assay. The difference between low and high learners was also significantly different (unpaired Student *T*-test, P = 0.039; Fig 5.2E). The associative memory data (day 5-8) was difficult to interpret, because mice did not perform as expected on the task, and rather spent time freezing or hiding. Consistent with our empirical observations of the limits of this test, mice showed no associative learning memory over days (Day 5 ranged from 59.2 to 94.3%; Day 8 ranged from 36.5 to 98.0%, Wilcoxon signed-rank test, P = 0.11). Rather, some animals displayed worsening performance throughout the days. This did not correlate with torpedo density (Spearman's correlation, ρ = 0.20, P = 0.58; data not shown). These behavioral assays have both suggested that the presence of torpedoes in the anterior lobules of the cerebellar cortex has a significant impact on motor learning in animals.

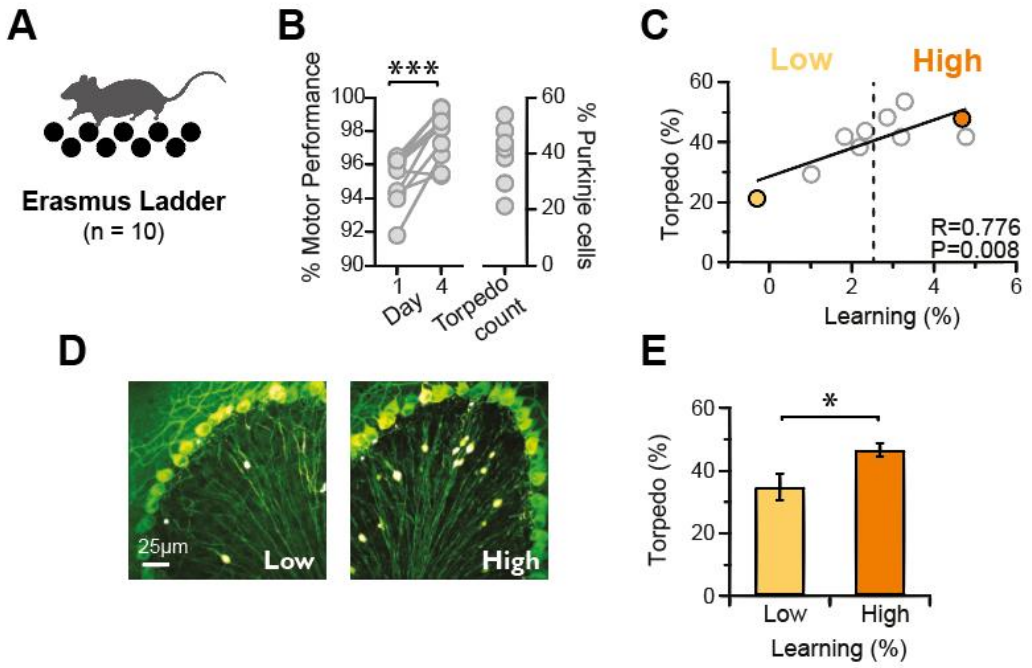

Figure 5.2: Erasmus Ladder motor learning and torpedoes
(**A**) Schematic representation of the Erasmus Ladder assay (n = 10). (**B**) Improvement of motor performance of individual animals on first (Day 1) and last day (Day 4; P*** < 0.005), and the distribution of Purkinje cells with torpedoes. (**C**) Correlation between the motor learning and the

percentage of cells with torpedoes (R = 0.78, P** < 0.01). (**D**) Representative images of low (Left) and high (Right) learners with different torpedoes numbers. Scale bar = 25µm. (**E**) Low and high learners have a significant difference in Purkinje cells with torpedoes (P* < 0.05).

5.3.3 Relationship between the vestibular ocular reflex and torpedoes in the flocculus

Since the presence of torpedoes has been associated with improved motor learning in the Rotarod and Erasmus ladder assays, we wondered if the presence of torpedoes could be associated with other cerebellar-related tasks. One of the best characterized regions of the cerebellum is the flocculus, which has been shown to be the locus of vestibular ocular reflex (Rambold *et al.*, 2002). In collaboration with the Schonewille Lab, we tested whether torpedoes in the flocculus might correlate with the eye movement learning in the vestibular ocular reflex. This was studied in wildtype (C57BL6/J) mice. Since wildtype mice do not endogenously label torpedoes as our L7-tau-eGFP mice do, the Schonewille Lab were using an antibody for inositol-triphosphate receptor (IP_3R) – an endoplasmic reticulum calcium channel – to identify torpedoes. To validate this method of identifying torpedoes, I stained cerebellar slices from the L7-tau-eGFP mice with this antibody and found that IP_3R stained accurately torpedoes in the vermis and the flocculus, with the majority (80%) of GFP positive torpedoes co-labeled with IP_3Rs (Fig 5.3).

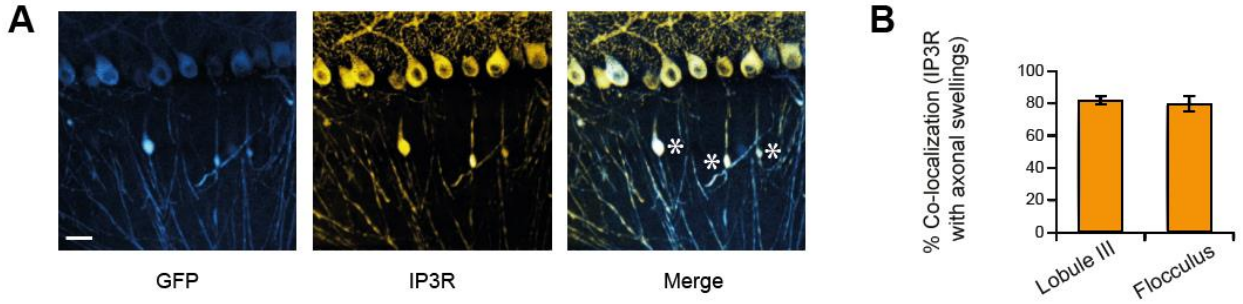

Figure 5.3: Purkinje cells axonal torpedoes colocalize with IP_3 receptors
Staining of torpedoes with the IP3R is indicative of ER in torpedoes. (A) Representative images, GFP (Left; Cyan), IP3R (Middle; Yellow), and merge (Right; torpedoes indicated by *). Scale bar

= 20 µm. (B) Percentage of torpedoes co-localizing both with GFP and IP3R, in the lobule III and the flocculus.

After behavioral testing was completed, mice were sacrificed and calbindin and IP_3R immunocytochemistry was performed to label Purkinje cell torpedoes. All control and untrained animals were discarded from this analysis since they were purposely prevented from learning the task, and all animals naturally display a varying degree of torpedoes (data not shown).As expected, the trained mice displayed learning, with a significant increase in the last two trials between the first (Day 1) and the last day (Day 4) (Day 1 ranged from 4.3 to 25.7%; Day 4 ranged from 72.1 to 98.8%, paired Student T-test, $P < 0.001$). However, a lower degree of variability in the density of torpedoes was observed in the flocculus compared to lobule III (% of Purkinje cells with torpedoes range from 10.3 to 22.5%; Fig 5.4B; compare to Fig 5.1 and 5.2). A weak, but not significant correlation was observed between VOR phase learning and torpedo density in the flocculus (Pearson's correlation, $R = 0.63$; $P = 0.052$). No significant difference was observed between torpedo numbers when the mice were split into low and high learners (unpaired Student *T*-test, $P = 0.12$). Thus, it appears that while the general trend is similar (Fig 5.4), there is at best a weak relationship between torpedo number and behaviour in the flocculus, perhaps because of the sparsity of torpedoes in that region overall. This suggests that cerebellar regions may form torpedoes at different rates, which may have a greater or weaker influence on associated behaviours.

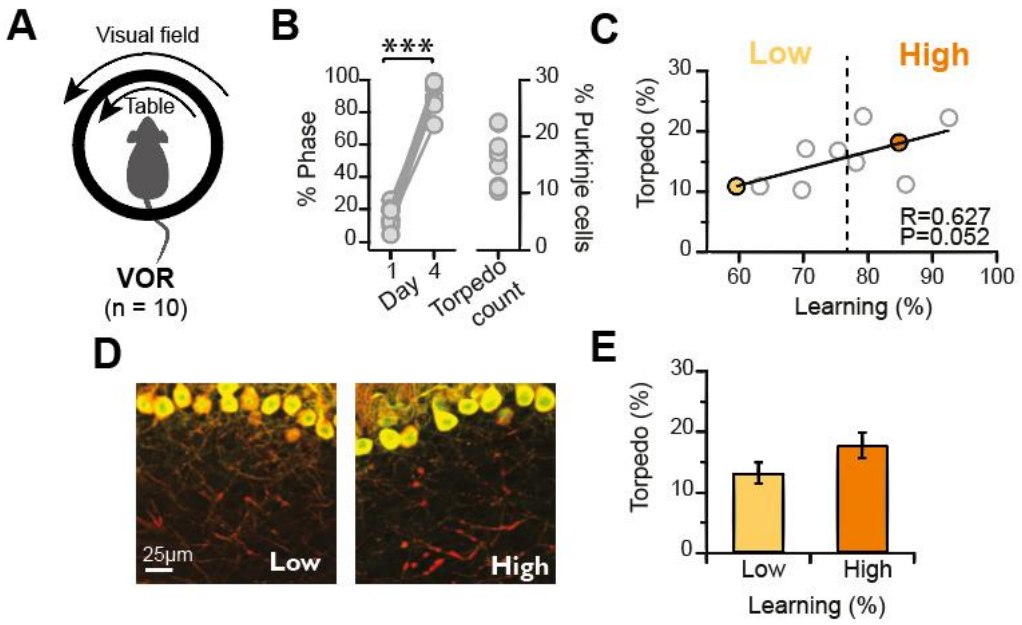

Figure 5.4: Vestibular ocular reflex and torpedoes
(**A**) Schematic representation of the VOR assay (N = 10). (**B**) Improvement of motor performance of individual animals on first (Day 1) and last day (Day 4; P*** < 0.005), and the distribution of Purkinje cells with torpedoes. (**C**) Correlation between motor learning and the percentage of cells with torpedoes (R = 0.63, P > 0.05). (**D**) Representative images of low (Left) and high (Right) learners with different numbers of torpedoes. Scale bar = 25µm. (**E**) Low and high learners have no significant difference in the percentage of Purkinje cells with torpedoes (P > 0.05).

5.3.1 Determination of torpedo localization in the cerebellar cortex

To gain insight into the behavioral consequences of torpedoes in the cerebellar cortex, I harnessed state-of-the-art technology to clear the cerebellar cortex. The clearing process fixes the cerebellar structural architecture using a hydrogel solution (Kim *et al.*, 2018). Subsequently, lipids are extracted using electrophoresis, while preserving the cellular structures and protein composition (Fig 5.5).

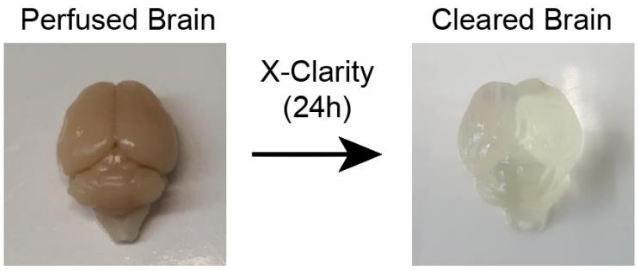

Figure 5.5: Whole mouse brain cleared using X-Clarity
(**A**) Left: Representative image of a perfused mouse brain. Right: representative image of a cleared brain, after 24h of X-Clarity electrophoresis, demonstrating the complete lipids extraction while preserving the cellular architecture of the brain.

Once the cerebellum was cleared, it was imaged using light-sheet microscopy. The challenge regarding the acquisition of whole cerebellum images is processing this data after acquisition. To accomplish this, each lobule of the vermis was cropped from the whole cerebellum image and processed separately (see Fig 5.6A, left image of lobule II). Once the individual lobules were isolated, I manually outlined the granule cell layer (Fig. 5.6A) to measure its volume. A spot detection tool was then used to automatically detect and count the number of torpedoes in the granule cell layer of each lobule, using parameters like fluorescence intensity, area, and sphericity to manually maximize detection and reduce noise. Four cerebella were processed this way, which revealed that there was a great deal of diversity in torpedo density across the cerebellar vermis. The density of torpedoes appeared higher in central lobules (avg. torpedo density per area for central lobules VI and VII is 1925 torpedo/mm^3), followed by anterior and posterior lobules (avg. torpedo density per area is 841 torpedoes/mm^3 for anterior lobules II to V and 862 torpedoes/$mm^3$for posterior lobule VIII) and finally, torpedo density appeared lowest in the nodular lobules (avg. torpedo density per area is 397 torpedoes/mm^3 for lobule IX; Fig 5.6B).

Furthermore, prior behavioral analyses were done on each of these animals, which allowed us to correlate the presence of torpedoes with their motor coordination abilities. We measured the

amount of motor learning and found that variability across individual animals was high (Day 1 ranged from 12.8 to 37.0%; Day 7 ranged from 49.6 to 87.5%, paired Student *T*-test, P = 0.026). As we observed in previous experiments where only a subset of torpedoes were analyzed, we observed a positive correlation between the total number of torpedoes in the vermis of the cerebellum and the amount of learning for each animal (Pearson's Correlation, R = 0.96, P = 0.045; Fig 5.6D). There are several possible explanations for these results: (1) rotarod learning involves the majority of the vermis, and thus total vermis numbers correlate with it, and/or (2) although the number of torpedoes differs across cerebellar regions, the differences observed across animals likely arises due to differences in the capacity of individual mice to form torpedoes, meaning that the variability across animals will be correlated with a number of different cerebellar behaviors, including rotarod. It will be interesting to explore further behavioral assays and perform light-sheet imaging on the cerebellum in order to determine how this relationship arises.

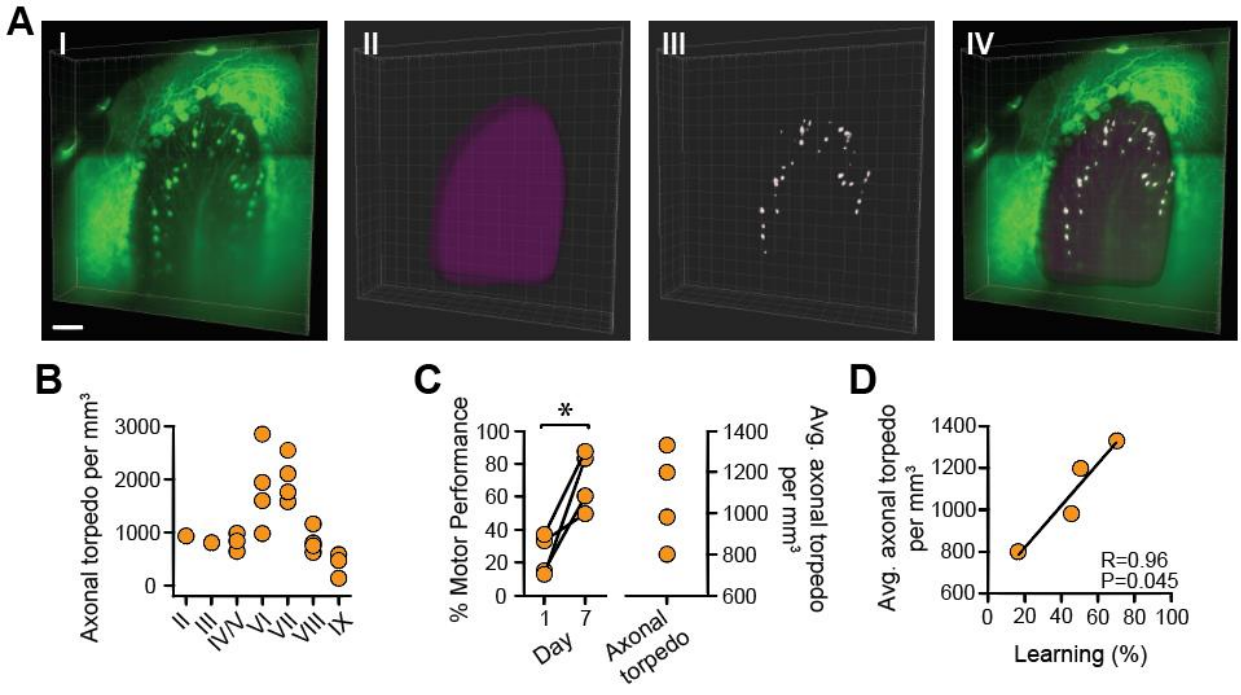

Figure 5.6: Whole cerebellar cortex torpedo distribution

(**A**) From left to right, (I) Representative images of isolated lobule II (Green; Purkinje cells expressing GFP), (II) tracing of the granule cell layer (Purple), (III) identification of torpedoes with spot detection tool (White) and (IV) merge of the previous images. Scale bar: 200 µm. (**B**) Distribution of torpedo density across the different lobules of the cerebellar cortex. (**C**) Motor performance on the first and last day of testing, showing the distribution of learning between animals ($P^* < 0.05$) and the average density of torpedoes between animals. (**D**) A strong correlation is observed showing that animals that display a larger amount of motor learning have a higher density of torpedoes.

5.4 Discussion

In this chapter, I have behaviorally tested animals using Rotarod and Erasmus Ladder assays. Interestingly, a positive correlation was observed between animal motor learning and the percentage of Purkinje cells with axonal torpedoes in lobule III for both assays. A similar positive trend, although not significant, was also observed between VOR learning and torpedoes in the flocculus. VOR showed a small variability in phase adaptation between animals and considering the low density of Purkinje cells with axonal torpedoes, this suggests that the flocculus may not be adapted to or does not require torpedoes to function properly. Further investigation is required to determine whether torpedoes in the flocculus also displayed a reduced propagation failure.

To better characterize the occupancy of torpedoes within the cerebellar cortex, I analyzed the distribution of torpedoes in the vermal region of the cerebellar cortex. A higher density of torpedoes was observed in central lobules, followed by anterior and posterior lobules and the lowest density was found in nodular lobules. It remains unclear why some cerebellar lobules contain more torpedoes than others. One simple explanation could be related to the differential gene expression of Purkinje cell sub-populations located in these different lobules. One of the best described differentially expressed genes is Zebrin II/Aldolase C, which shows small Zebrin II positive bands in the anterior lobules, while most Purkinje cells express Zebrin II in posterior and

nodular lobules (Fujita *et al.*, 2014). Other similar gene expression patterns might influence the density of torpedoes in specific cerebellar lobules.

We were intrigued to observe that the highest density of torpedoes was in central lobules. We have not yet used a behavioral test that we could correlate with these regions. Experimentally using a behavioral assay able to test these central lobules might strengthen our understanding of torpedoes effect on animal learning behavior. We would predict that these lobules might benefit the most from torpedoes or require more of them in order to function properly. Central lobules VI and VII were shown to have signs of hypoplasia (i.e. under-development) in autism spectrum disorder patients (Courchesne *et al.*, 1988). A recent study showed the implication of these same lobules in autistic mice as well as a behavioral rescue when these cerebellar regions were stimulated (Chao *et al.*, 2020). To behaviorally assess the involvement of torpedoes on lobules VI and VII, three chambers social test, elevated open platform, open field assay, or object-based attention test could be used in the future to assess the impact of torpedoes on animal social learning.

Overall, this chapter has shown the importance of Purkinje cell axonal torpedoes on animal behavioral output. Once again, our results in healthy young adult mice appear to contradict the neurodegenerative disease hypothesis for torpedo function. However, more direct evidence showing the impact of induced spike failures on animal learning behavior should be further investigated, particularly in animals with disease-related torpedoes.

CHAPTER 6: DISCUSSION

Purkinje cell axonal torpedoes were discovered at the beginning of the twentieth century. Since then, torpedoes have been observed in many human and animal neurological diseases. Due to this substantial presence in diseases, initial hypotheses proposed that torpedoes were implicated in axonal degeneration, eventually contributing to Purkinje cell death. Findings from this thesis suggest that, at least in healthy brains, this may not be true, since the presence of torpedoes enhances axonal and cerebellar function. These findings suggest that a torpedo is not necessarily a sign of degeneration but may rather be a neuronal mechanism providing improved axonal action potential propagation, thereby enhancing motor learning.

6.1 Results interpretation

6.1.1 Purkinje cell axonal torpedo morphology and function

Disease-related torpedoes were for a long time thought to serve a pathological role in the diseased brain. A review of the literature shows that torpedoes contain disorganized neurofilaments, mitochondria and ER. In some cases, torpedoes were myelinated, whereas in other reports, the myelin sheath was gone around torpedoes. This can be partly attributed to differences in diseases, since myelin degeneration is a key feature of some. We found similar results in the subcellular composition of torpedoes in healthy animals as what had been observed in a wide range of neurological diseases. The observation of hyperphosphorylated neurofilaments found in our torpedoes might suggest the disruption of axonal transport. However, the phosphorylation of neurofilaments has also been associated with other properties, such as axon caliber (Heimfarth *et al.*, 2016). Furthermore, although we observe disorganized neurofilaments in our torpedoes, we

suggest that this might be a morphological phenomenon associated with axonal caliber enlargement characterizing torpedoes rather than axonal transport disruption.

I showed that Purkinje cells that have torpedoes on their axons are indistinguishable in terms of firing frequency, inter-spike intervals, and speed of propagation from Purkinje cells without torpedoes. However, I observed that axons with torpedoes had reduced spike failures compared to control axons. Furthermore, we found that torpedoes are usually located in close proximity to nodes of Ranvier, making them well-placed to be involved in axonal action potential regulation. Torpedoes are located within the juxta-paranodal region of the node of Ranvier, where most potassium channels are located, and playing role in repolarizing the membrane (Hirono *et al.*, 2015). Purkinje cells contain a fast resurgent sodium current that allows them to fire at high frequency. The prevention of failures is associated with the presence of intermediate conductance calcium-dependent potassium channels ($K_{Ca}3.1$) at nodes of Ranvier; these channels hyperpolarize the axonal membrane, promoting excitability by increasing sodium channel availability and securing propagation. Blocking $K_{Ca}3.1$ was shown to leave sodium channels inactive at nodes of Ranvier (Grundemann & Clark, 2015), suggesting that $K_{Ca}3.1$ may be essential in regulating spike failures in Purkinje cells.

IP_3R have also been shown to be expressed in Purkinje cells torpedoes, both by us and by others (Gomez *et al.*, 2020). However, the impact of this enrichment of IP_3Rs in axonal torpedoes remain unclear. One explanation could be that IP_3Rs provide an internal calcium supply that contributes to the regulation of firing fidelity.

6.1.2 Mechanism of torpedo formation and axonal failure

I performed dual simultaneous recording from Purkinje cell soma and axons, which revealed a reduced axonal propagation failure along axons with an axonal torpedo. Next, I found

that pharmacologically producing spike failures using *low TTX* led to *de novo* formation of axonal torpedoes. Protein synthesis has been shown to modulate axonal remodeling, such as new axonal branch formation *in vivo* (Wong *et al.*, 2017). My research suggests, however, that torpedo formation does not require protein synthesis to occur.

Current results suggest that this mechanism requires extracellular calcium influx, which is regulated by voltage-gated calcium channels (VGCC). I next determined that T-type and L-type calcium channels were likely involved in this regulation using VGCC blockers. T-type calcium channels are low-voltage calcium channels, activated between -65mV to -20mV (Engbers *et al.*, 2013), thus matching the membrane potential of Purkinje cells when the axon fails to propagate action potential. We have shown that some Purkinje cell axonal torpedoes stained positively for the T-type calcium channel subunit $Ca_V3.1$. T-type calcium channels are coupled in Purkinje cells with the calcium-dependent potassium channel $K_{Ca}3.1$ (Engbers *et al.*, 2012). In the absence of extracellular calcium, we showed that torpedo formation is eliminated, even when spike failures were induced by *low TTX*. It is perhaps unexpected that calcium, which typically senses activity, is also a sensor in axonal failures, which is characterized by the absence of activity. It is possible that action potential failures are characterized by a small depolarization that is insufficient to remove the depolarization block on sodium channels. Thus, this small depolarization during axonal failures might be sufficient to activate T-type calcium channels, which would activate $K_{Ca}3.1$ channel, reducing the probability of further propagation failures. However, the possibility that calcium is continuously signaling during regular firing and brief imbalance during propagation failures is detected, leading to torpedo formation, is not excluded. Elucidating the full complement of ion channels located in torpedoes, for example, whether $K_{Ca}3.1$ channel are present, would allow us to better understand how torpedoes prevent spike failures.

L-type calcium channels are high-voltage calcium channels, and it is hard to envision a scenario where axonal failures would activate L-type calcium channels, although the fluctuation of an L-type calcium signal may be the signal that causes torpedo formation. L-type calcium channels have also been shown to couple with $K_{Ca}3.1$ in hippocampal neurons (Sahu *et al.*, 2019), suggesting that they are important for action potential repolarization. Future studies using specific calcium channel blockers, such as nifedipine or dihydropyridine (DHP) for L-type channels, mibefradil for T-type channels and TRAM-34 for the $K_{Ca}3.1$, will allow us to further elucidate the mechanisms by which torpedo formation occurs.

Interestingly, a recent paper reports calcium influx occurs through voltage-gated sodium channels in the AIS and nodes of Ranvier of L5 pyramidal cells that is amplified by intracellular signaling (Hanemaaijer *et al.*, 2020). This suggests that *low TTX* might not only induce spike failures but could also alter calcium signaling pathways in axons.

6.1.3 Impact of torpedoes on animal behaviors

Many cerebellar diseases lead to deficits in motor behavior. Surprisingly, we showed a positive correlation between the density of torpedoes in the cerebellum and motor learning tasks. This suggests that brains with a larger number of Purkinje cells with axonal torpedoes will have improved cerebellar information transmission, leading to enhanced behavioral output. Although we have not tested this experimentally, it is possible that increased failure rates in diseased brains causes enhanced torpedo formation in order to counteract pathophysiology by improving the failure rates in these cells. This could explain why torpedoes are prevalent in many cerebellar diseases. However, some questions remain unanswered. We do not yet understand how and over what time scale torpedoes are modulated in the intact animal. To test this, rotarod experiments could be conducted in parallel with *in vivo* imaging of the cerebellar cortex over many days. This

would allow us to assess torpedo number in a live animal and determine if and how they change during, and after a motor behavioral test.

6.3 Future perspectives

This research project has provided some novel insight into Purkinje cell axonal torpedoes in healthy animals. Further investigation is required to either confirm whether torpedoes function in a similar manner in animal models of diseases, or, if not, to determine what function(s) they play in disease. This thesis has increased our knowledge of torpedo composition. However, to fully understand the complexity of that structure, laser capture of single torpedoes followed by RNA sequencing (RNAseq) could be used. The high throughput of RNAseq could identify unique torpedo markers that might be central to our understanding of torpedo function. Furthermore, comparing RNAseq results from healthy and disease-related torpedoes could give us insight into the differences between them (if any).

Lastly, one proof of concept experiment would be to manipulate activity in a subset of Purkinje cells with optogenetics. For example, we could cross L7-tau-eGFP mice with L7-Cre mice. Animals could be virally injected with vectors containing a Floxed-Gq-Arch (ArchaeRhodopsin), an inhibitory opsin channel. Gq protein has recently been found to be uniquely localized within Purkinje cell myelinated axons (Gomez *et al.*, 2020), the authors of this manuscript have confirmed to us that torpedoes were labeled by Gq protein antibody (data not shown). All Purkinje cells would express eGFP, while a subset (i.e. those in the injected area) would express Arch only in the axons. An optic fiber emitting yellow light could be implanted in the cerebellum, which would precisely inhibit Purkinje cell axonal propagation in the Arch positive cells. *In vivo* imaging on a free moving animal could then be done to assess torpedo formation during behavior, while intermittently interrupting the firing pattern of Purkinje cell in a specific

region. This experiment would help answer whether torpedo numbers are static in live animals, as well as whether torpedo formation is driven by animal learning. If this works, an experimenter could then try to induce torpedo formation before the behavioral test to see if they can influence learning.

6.4 Closing remarks

In conclusion, the work presented in the thesis has helped to change our understanding of how Purkinje cell axonal torpedoes function. My work shows that torpedoes are a neuroadaptive mechanism that prevents axonal failures thereby improving motor learning in healthy animals. These results are intriguing and further investigation into torpedoes and their function is warranted. This will shed further light on how the brain adapts to challenges. A better understanding of such neuroadaptive mechanisms could lead to scientific breakthroughs that may advance how we treat neurological diseases.

REFERENCES

Al-Chalabi, A., & Miller, C. C. (2003). Neurofilaments and neurological disease. *Bioessays, 25*(4), 346-355. doi:10.1002/bies.10251

Andrasfalvy, B. K., Galinanes, G. L., Huber, D., Barbic, M., Macklin, J. J., Susumu, K., Delehanty, J. B., Huston, A. L., Makara, J. K., & Medintz, I. L. (2014). Quantum dot-based multiphoton fluorescent pipettes for targeted neuronal electrophysiology. *Nat Methods, 11*(12), 1237-1241. doi:10.1038/nmeth.3146

Arancibia-Carcamo, I. L., Ford, M. C., Cossell, L., Ishida, K., Tohyama, K., & Attwell, D. (2017). Node of Ranvier length as a potential regulator of myelinated axon conduction speed. *Elife, 6*. doi:10.7554/eLife.23329

Aring, C. D. (1938). Cerebellar Syndrome in an Adult with Malformation of the Cerebellum and Brain Stem (Arnold-Chiari Deformity), with a Note on the Occurrence of "Torpedoes" in the Cerebellum. *J Neurol Psychiatry, 1*(2), 100-109. doi:10.1136/jnnp.1.2.100

Axelrad, J. E., Louis, E. D., Honig, L. S., Flores, I., Ross, G. W., Pahwa, R., Lyons, K. E., Faust, P. L., & Vonsattel, J. P. (2008). Reduced Purkinje cell number in essential tremor: a postmortem study. *Arch Neurol, 65*(1), 101-107. doi:10.1001/archneurol.2007.8

Babij, R., Lee, M., Cortes, E., Vonsattel, J. P., Faust, P. L., & Louis, E. D. (2013). Purkinje cell axonal anatomy: quantifying morphometric changes in essential tremor versus control brains. *Brain, 136*(Pt 10), 3051-3061. doi:10.1093/brain/awt238

Bakalian, A., Corman, B., Delhaye-Bouchaud, N., & Mariani, J. (1991). Quantitative analysis of the Purkinje cell population during extreme ageing in the cerebellum of the Wistar/Louvain rat. *Neurobiol Aging, 12*(5), 425-430. doi:10.1016/0197-4580(91)90068-u

Barron, T., Saifetiarova, J., Bhat, M. A., & Kim, J. H. (2018). Myelination of Purkinje axons is critical for resilient synaptic transmission in the deep cerebellar nucleus. *Sci Rep, 8*(1), 1022. doi:10.1038/s41598-018-19314-0

Baurle, J., & Grusser-Cornehls, U. (1994). Axonal torpedoes in cerebellar Purkinje cells of two normal mouse strains during aging. *Acta Neuropathol, 88*(3), 237-245.

Baurle, J., Helmchen, C., & Grusser-Cornehls, U. (1997). Diverse effects of Purkinje cell loss on deep cerebellar and vestibular nuclei neurons in Purkinje cell degeneration mutant mice: a possible compensatory mechanism. *J Comp Neurol, 384*(4), 580-596.

Belzen, J. A. (1998). "Searching for the soul": religious factors in Leendert Bouman's development of a 'psychological psychiatry'. *Hist Psychiatry, 9*(35), 303-333. doi:10.1177/0957154X9800903503

Berglund, E. O., Murai, K. K., Fredette, B., Sekerkova, G., Marturano, B., Weber, L., Mugnaini, E., & Ranscht, B. (1999). Ataxia and abnormal cerebellar microorganization in mice with ablated contactin gene expression. *Neuron, 24*(3), 739-750. doi:10.1016/s0896-6273(00)81126-5

Berridge, M. J., Lipp, P., & Bootman, M. D. (2000). The versatility and universality of calcium signalling. *Nat Rev Mol Cell Biol, 1*(1), 11-21. doi:10.1038/35036035

Bouman, L. (1918). Die Histopathologie der Psychosen. *Amsterdam: Springer*.

Brini, M., Cali, T., Ottolini, D., & Carafoli, E. (2014). Neuronal calcium signaling: function and dysfunction. *Cell Mol Life Sci, 71*(15), 2787-2814. doi:10.1007/s00018-013-1550-7

Cajal, S. R. y. (1907). Note sur la dégénérescence traumatique des fibers nerveuses du cervelet et du cerveau. *Trabajos del Laboratorio de Investigaciones Biológicas de la Universidad de Madrid., 5*, 105-115.

Cajal, S. R. y., DeFelipe, J., & Jones, E. G. (1991). Cajal's Degeneration and Regeneration of the Nervous System.

Cameron, B., & Landreth, G. E. (2010). Inflammation, microglia, and Alzheimer's disease. *Neurobiol Dis, 37*(3), 503-509. doi:10.1016/j.nbd.2009.10.006

Carpenter, S. (1968). Proximal axonal enlargement in motor neuron disease. *Neurology, 18*(9), 841-851. doi:10.1212/wnl.18.9.841

Celio, M. R. (1990). Calbindin D-28k and parvalbumin in the rat nervous system. *Neuroscience, 35*(2), 375-475. doi:10.1016/0306-4522(90)90091-h

Chaisanguanthum, K. S., Joshua, M., Medina, J. F., Bialek, W., & Lisberger, S. G. (2014). The Neural Code for Motor Control in the Cerebellum and Oculomotor Brainstem. *eNeuro, 1*(1). doi:10.1523/ENEURO.0004-14.2014

Chamberland, S., Timofeeva, Y., Evstratova, A., Volynski, K., & Toth, K. (2018). Action potential counting at giant mossy fiber terminals gates information transfer in the hippocampus. *Proc Natl Acad Sci U S A, 115*(28), 7434-7439. doi:10.1073/pnas.1720659115

Chang, S. Y., Zagha, E., Kwon, E. S., Ozaita, A., Bobik, M., Martone, M. E., Ellisman, M. H., Heintz, N., & Rudy, B. (2007). Distribution of Kv3.3 potassium channel subunits in distinct neuronal populations of mouse brain. *J Comp Neurol, 502*(6), 953-972. doi:10.1002/cne.21353

Chao, O. Y., Marron Fernandez de Velasco, E., Pathak, S. S., Maitra, S., Zhang, H., Duvick, L., Wickman, K., Orr, H. T., Hirai, H., & Yang, Y. M. (2020). Targeting inhibitory cerebellar circuitry to alleviate behavioral deficits in a mouse model for studying idiopathic autism. *Neuropsychopharmacology, 45*(7), 1159-1170. doi:10.1038/s41386-020-0656-5

Chapman, T. W., & Hill, R. A. (2020). Myelin plasticity in adulthood and aging. *Neurosci Lett, 715*, 134645. doi:10.1016/j.neulet.2019.134645

Chen, J., Nakata, T., Zhang, Z., & Hirokawa, N. (2000). The C-terminal tail domain of neurofilament protein-H (NF-H) forms the crossbridges and regulates neurofilament bundle formation. *J Cell Sci, 113 Pt 21*, 3861-3869.

Chereau, R., Saraceno, G. E., Angibaud, J., Cattaert, D., & Nagerl, U. V. (2017). Superresolution imaging reveals activity-dependent plasticity of axon morphology linked to changes in action potential conduction velocity. *Proc Natl Acad Sci U S A, 114*(6), 1401-1406. doi:10.1073/pnas.1607541114

Ching, G. Y., Chien, C. L., Flores, R., & Liem, R. K. (1999). Overexpression of alpha-internexin causes abnormal neurofilamentous accumulations and motor coordination deficits in transgenic mice. *J Neurosci, 19*(8), 2974-2986.

Chou, S. M., & Hartmann, H. A. (1965). Electron microscopy of focal neuroaxonal lesions produced by beta-beta-iminodipropionitrile (IDPN) in rats. I. The advanced lesions. *Acta Neuropathol, 4*(6), 590-603. doi:10.1007/bf00691211

Clark, A. W., Parhad, I. M., Griffin, J. W., & Price, D. L. (1984). Neurofilamentous axonal swellings as a normal finding in the spinal anterior horn of man and other primates. *J Neuropathol Exp Neurol, 43*(3), 253-262. doi:10.1097/00005072-198405000-00004

Clark, B. A., Monsivais, P., Branco, T., London, M., & Hausser, M. (2005). The site of action potential initiation in cerebellar Purkinje neurons. *Nat Neurosci, 8*(2), 137-139. doi:10.1038/nn1390

Coleman, M. (2005). Axon degeneration mechanisms: commonality amid diversity. *Nat Rev Neurosci, 6*(11), 889-898. doi:10.1038/nrn1788

Coleman, M. P., & Freeman, M. R. (2010). Wallerian degeneration, wld(s), and nmnat. *Annu Rev Neurosci, 33*, 245-267. doi:10.1146/annurev-neuro-060909-153248

Cook, A. A., Fields, E., & Watt, A. J. (2020). Losing the Beat: Contribution of Purkinje Cell Firing Dysfunction to Disease, and Its Reversal. *Neuroscience*. doi:10.1016/j.neuroscience.2020.06.008

Cooper, E. C., Harrington, E., Jan, Y. N., & Jan, L. Y. (2001). M channel KCNQ2 subunits are localized to key sites for control of neuronal network oscillations and synchronization in mouse brain. *J Neurosci, 21*(24), 9529-9540.

Corral-Juan, M., Serrano-Munuera, C., Rabano, A., Cota-Gonzalez, D., Segarra-Roca, A., Ispierto, L., Cano-Orgaz, A. T., Adarmes, A. D., Mendez-Del-Barrio, C., Jesus, S., Mir, P., Volpini, V., Alvarez-Ramo, R., Sanchez, I., & Matilla-Duenas, A. (2018). Clinical, genetic and neuropathological characterization of spinocerebellar ataxia type 37. *Brain, 141*(7), 1981-1997. doi:10.1093/brain/awy137

Courchesne, E., Yeung-Courchesne, R., Press, G. A., Hesselink, J. R., & Jernigan, T. L. (1988). Hypoplasia of cerebellar vermal lobules VI and VII in autism. *N Engl J Med, 318*(21), 1349-1354. doi:10.1056/NEJM198805263182102

Cullen, C. L., Pepper, R. E., Clutterbuck, M. T., Pitman, K. A., Oorschot, V., Auderset, L., Tang, A. D., Ramm, G., Emery, B., Rodger, J., Jolivet, R. B., & Young, K. M. (2020). Periaxonal and nodal plasticity modulate action potential conduction in the adult mouse brain. *bioRxiv*.

Davie, J. T., Clark, B. A., & Hausser, M. (2008). The origin of the complex spike in cerebellar Purkinje cells. *J Neurosci, 28*(30), 7599-7609. doi:10.1523/JNEUROSCI.0559-08.2008

De Munter, S., Bamps, D., Malheiro, A. R., Kumar Baboota, R., Brites, P., & Baes, M. (2018). Autonomous Purkinje cell axonal dystrophy causes ataxia in peroxisomal multifunctional protein-2 deficiency. *Brain Pathol, 28*(5), 631-643. doi:10.1111/bpa.12586

Didonna, A., & Opal, P. (2019). The role of neurofilament aggregation in neurodegeneration: lessons from rare inherited neurological disorders. *Mol Neurodegener, 14*(1), 19. doi:10.1186/s13024-019-0318-4

Dusart, I., & Sotelo, C. (1994). Lack of Purkinje cell loss in adult rat cerebellum following protracted axotomy: degenerative changes and regenerative attempts of the severed axons. *J Comp Neurol, 347*(2), 211-232. doi:10.1002/cne.903470206

Engbers, J. D., Anderson, D., Asmara, H., Rehak, R., Mehaffey, W. H., Hameed, S., McKay, B. E., Kruskic, M., Zamponi, G. W., & Turner, R. W. (2012). Intermediate conductance calcium-activated potassium channels modulate summation of parallel fiber input in cerebellar Purkinje cells. *Proc Natl Acad Sci U S A, 109*(7), 2601-2606. doi:10.1073/pnas.1115024109

Engbers, J. D., Anderson, D., Zamponi, G. W., & Turner, R. W. (2013). Signal processing by T-type calcium channel interactions in the cerebellum. *Front Cell Neurosci, 7*, 230. doi:10.3389/fncel.2013.00230

Evans, M. D., Dumitrescu, A. S., Kruijssen, D. L. H., Taylor, S. E., & Grubb, M. S. (2015). Rapid Modulation of Axon Initial Segment Length Influences Repetitive Spike Firing. *Cell Rep, 13*(6), 1233-1245. doi:10.1016/j.celrep.2015.09.066

Fehmi, J., Scherer, S. S., Willison, H. J., & Rinaldi, S. (2018). Nodes, paranodes and neuropathies. *J Neurol Neurosurg Psychiatry, 89*(1), 61-71. doi:10.1136/jnnp-2016-315480

Felts, P. A., Yokoyama, S., Dib-Hajj, S., Black, J. A., & Waxman, S. G. (1997). Sodium channel alpha-subunit mRNAs I, II, III, NaG, Na6 and hNE (PN1): different expression patterns in developing rat nervous system. *Brain Res Mol Brain Res, 45*(1), 71-82. doi:10.1016/s0169-328x(96)00241-0

Ferrer, I., Genis, D., Davalos, A., Bernado, L., Sant, F., & Serrano, T. (1994). The Purkinje cell in olivopontocerebellar atrophy. A Golgi and immunocytochemical study. *Neuropathol Appl Neurobiol, 20*(1), 38-46. doi:10.1111/j.1365-2990.1994.tb00955.x

Ferrer, I., Puig, B., Blanco, R., & Marti, E. (2000). Prion protein deposition and abnormal synaptic protein expression in the cerebellum in Creutzfeldt-Jakob disease. *Neuroscience, 97*(4), 715-726. doi:10.1016/s0306-4522(00)00045-2

Fierro, L., DiPolo, R., & Llano, I. (1998). Intracellular calcium clearance in Purkinje cell somata from rat cerebellar slices. *J Physiol, 510 (Pt 2)*, 499-512. doi:10.1111/j.1469-7793.1998.499bk.x

Foran, D. R., & Peterson, A. C. (1992). Myelin acquisition in the central nervous system of the mouse revealed by an MBP-Lac Z transgene. *J Neurosci, 12*(12), 4890-4897.

Friede, R. L. (1964). Electrophoretic Production of "Reactive" Axon Swellings in Vitro and Their Histochemical Properties. *Acta Neuropathol, 3*, 217-228. doi:10.1007/bf00684397

Fujita, H., Aoki, H., Ajioka, I., Yamazaki, M., Abe, M., Oh-Nishi, A., Sakimura, K., & Sugihara, I. (2014). Detailed expression pattern of aldolase C (Aldoc) in the cerebellum, retina and other areas of the CNS studied in Aldoc-Venus knock-in mice. *PLoS One, 9*(1), e86679. doi:10.1371/journal.pone.0086679

Galvin, J. E., Uryu, K., Lee, V. M., & Trojanowski, J. Q. (1999). Axon pathology in Parkinson's disease and Lewy body dementia hippocampus contains alpha-, beta-, and gamma-synuclein. *Proc Natl Acad Sci U S A, 96*(23), 13450-13455. doi:10.1073/pnas.96.23.13450

Garcia-Fresco, G. P., Sousa, A. D., Pillai, A. M., Moy, S. S., Crawley, J. N., Tessarollo, L., Dupree, J. L., & Bhat, M. A. (2006). Disruption of axo-glial junctions causes cytoskeletal disorganization and degeneration of Purkinje neuron axons. *Proc Natl Acad Sci U S A, 103*(13), 5137-5142. doi:10.1073/pnas.0601082103

Gianola, S., & Rossi, F. (2001). Evolution of the Purkinje cell response to injury and regenerative potential during postnatal development of the rat cerebellum. *J Comp Neurol, 430*(1), 101-117. doi:10.1002/1096-9861(20010129)430:1<101::aid-cne1017>3.0.co;2-z

Gianola, S., Savio, T., Schwab, M. E., & Rossi, F. (2003). Cell-autonomous mechanisms and myelin-associated factors contribute to the development of Purkinje axon intracortical plexus in the rat cerebellum. *J Neurosci, 23*(11), 4613-4624.

Gilley, J., & Coleman, M. P. (2010). Endogenous Nmnat2 is an essential survival factor for maintenance of healthy axons. *PLoS Biol, 8*(1), e1000300. doi:10.1371/journal.pbio.1000300

Gomez, L. C., Kawaguchi, S. Y., Collin, T., Jalil, A., Gomez, M. D. P., Nasi, E., Marty, A., & Llano, I. (2020). Influence of spatially segregated IP3-producing pathways on spike generation and transmitter release in Purkinje cell axons. *Proc Natl Acad Sci U S A, 117*(20), 11097-11108. doi:10.1073/pnas.2000148117

Gravel, C., Leclerc, N., Plioplys, A., & Hawkes, R. B. (1986). Focal axonal swellings in rat cerebellar Purkinje cells during normal development. *Brain Res, 363*(2), 325-332.

Greco, C. M., Hagerman, R. J., Tassone, F., Chudley, A. E., Del Bigio, M. R., Jacquemont, S., Leehey, M., & Hagerman, P. J. (2002). Neuronal intranuclear inclusions in a new cerebellar

tremor/ataxia syndrome among fragile X carriers. *Brain, 125*(Pt 8), 1760-1771. doi:10.1093/brain/awf184

Griffin, J. W., Hoffman, P. N., Clark, A. W., Carroll, P. T., & Price, D. L. (1978). Slow axonal transport of neurofilament proteins: impairment of beta,beta'-iminodipropionitrile administration. *Science, 202*(4368), 633-635. doi:10.1126/science.81524

Griffiths, I., Klugmann, M., Anderson, T., Yool, D., Thomson, C., Schwab, M. H., Schneider, A., Zimmermann, F., McCulloch, M., Nadon, N., & Nave, K. A. (1998). Axonal swellings and degeneration in mice lacking the major proteolipid of myelin. *Science, 280*(5369), 1610-1613. doi:10.1126/science.280.5369.1610

Grubb, M. S., & Burrone, J. (2010). Channelrhodopsin-2 localised to the axon initial segment. *PLoS One, 5*(10), e13761. doi:10.1371/journal.pone.0013761

Grundemann, J., & Clark, B. A. (2015). Calcium-Activated Potassium Channels at Nodes of Ranvier Secure Axonal Spike Propagation. *Cell Rep, 12*(11), 1715-1722. doi:10.1016/j.celrep.2015.08.022

Gugliandolo, A., Bramanti, P., & Mazzon, E. (2017). Role of Vitamin E in the Treatment of Alzheimer's Disease: Evidence from Animal Models. *Int J Mol Sci, 18*(12). doi:10.3390/ijms18122504

Hanemaaijer, N. A., Popovic, M. A., Wilders, X., Grasman, S., Pavon Arocas, O., & Kole, M. H. (2020). Ca(2+) entry through NaV channels generates submillisecond axonal Ca(2+) signaling. *Elife, 9*. doi:10.7554/eLife.54566

Hartmann, J., Karl, R. M., Alexander, R. P., Adelsberger, H., Brill, M. S., Ruhlmann, C., Ansel, A., Sakimura, K., Baba, Y., Kurosaki, T., Misgeld, T., & Konnerth, A. (2014). STIM1 controls neuronal Ca(2)(+) signaling, mGluR1-dependent synaptic transmission, and cerebellar motor behavior. *Neuron, 82*(3), 635-644. doi:10.1016/j.neuron.2014.03.027

Heimfarth, L., da Silva Ferreira, F., Pierozan, P., Loureiro, S. O., Mingori, M. R., Moreira, J. C. F., da Rocha, J. B. T., & Pessoa-Pureur, R. (2016). Calcium signaling mechanisms disrupt the cytoskeleton of primary astrocytes and neurons exposed to diphenylditelluride. *Biochim Biophys Acta, 1860*(11 Pt A), 2510-2520. doi:10.1016/j.bbagen.2016.07.023

Hell, J. W., Westenbroek, R. E., Warner, C., Ahlijanian, M. K., Prystay, W., Gilbert, M. M., Snutch, T. P., & Catterall, W. A. (1993). Identification and differential subcellular localization of the neuronal class C and class D L-type calcium channel alpha 1 subunits. *J Cell Biol, 123*(4), 949-962. doi:10.1083/jcb.123.4.949

Hirano, A., & Dembitzer, H. M. (1973). Cerebellar alterations in the weaver mouse. *J Cell Biol, 56*(2), 478-486. doi:10.1083/jcb.56.2.478

Hirano, A., Kurland, L. T., & Sayre, G. P. (1967). Familial amyotrophic lateral sclerosis. A subgroup characterized by posterior and spinocerebellar tract involvement and hyaline inclusions in the anterior horn cells. *Arch Neurol, 16*(3), 232-243. doi:10.1001/archneur.1967.00470210008002

Hirono, M., Ogawa, Y., Misono, K., Zollinger, D. R., Trimmer, J. S., Rasband, M. N., & Misonou, H. (2015). BK Channels Localize to the Paranodal Junction and Regulate Action Potentials in Myelinated Axons of Cerebellar Purkinje Cells. *J Neurosci, 35*(18), 7082-7094. doi:10.1523/JNEUROSCI.3778-14.2015

Hoebeek, F. E., Khosrovani, S., Witter, L., & De Zeeuw, C. I. (2008). Purkinje cell input to cerebellar nuclei in tottering: ultrastructure and physiology. *Cerebellum, 7*(4), 547-558. doi:10.1007/s12311-008-0086-0

Horie, H., Takenaka, T., & Kaiho, M. (1983). Effects of disruption of microtubules on translocation of particles and morphology in tissue cultured neurites. *Brain Res, 288*(1-2), 85-93. doi:10.1016/0006-8993(83)90083-5

Hosy, E., Piochon, C., Teuling, E., Rinaldo, L., & Hansel, C. (2011). SK2 channel expression and function in cerebellar Purkinje cells. *J Physiol, 589*(Pt 14), 3433-3440. doi:10.1113/jphysiol.2011.205823

Indriati, D. W., Kamasawa, N., Matsui, K., Meredith, A. L., Watanabe, M., & Shigemoto, R. (2013). Quantitative localization of Cav2.1 (P/Q-type) voltage-dependent calcium channels in Purkinje cells: somatodendritic gradient and distinct somatic coclustering with calcium-activated potassium channels. *J Neurosci, 33*(8), 3668-3678. doi:10.1523/JNEUROSCI.2921-12.2013

Ishibashi, T., Kodama, A., & Baba, H. (2015). Disruption of paranodal axo-glial interaction and/or absence of sulfatide causes irregular type I inositol 1,4,5-trisphosphate receptor deposition in cerebellar Purkinje neuron axons. *J Neurosci Res, 93*(1), 19-27. doi:10.1002/jnr.23465

Isope, P., Hildebrand, M. E., & Snutch, T. P. (2012). Contributions of T-type voltage-gated calcium channels to postsynaptic calcium signaling within Purkinje neurons. *Cerebellum, 11*(3), 651-665. doi:10.1007/s12311-010-0195-4

Jack, C., Ruffini, F., Bar-Or, A., & Antel, J. P. (2005). Microglia and multiple sclerosis. *J Neurosci Res, 81*(3), 363-373. doi:10.1002/jnr.20482

Jankowski, J., Miething, A., Schilling, K., & Baader, S. L. (2009). Physiological purkinje cell death is spatiotemporally organized in the developing mouse cerebellum. *Cerebellum, 8*(3), 277-290. doi:10.1007/s12311-009-0093-9

Jayabal, S., Chang, H. H., Cullen, K. E., & Watt, A. J. (2016). 4-aminopyridine reverses ataxia and cerebellar firing deficiency in a mouse model of spinocerebellar ataxia type 6. *Sci Rep, 6*, 29489. doi:10.1038/srep29489

Jin, C., Washimi, Y., Yoshida, K., Hashizume, Y., & Yazawa, I. (2015). Characterization of spheroids in hereditary diffuse leukoencephalopathy with axonal spheroids. *J Neurol Sci, 352*(1-2), 74-78. doi:10.1016/j.jns.2015.03.033

Kalume, F., Yu, F. H., Westenbroek, R. E., Scheuer, T., & Catterall, W. A. (2007). Reduced sodium current in Purkinje neurons from Nav1.1 mutant mice: implications for ataxia in severe myoclonic epilepsy in infancy. *J Neurosci, 27*(41), 11065-11074. doi:10.1523/JNEUROSCI.2162-07.2007

Kandel, E. R., Schwartz, J. H., Jessell, T. M., Siegelbaum, S., Hudspeth, A. J., & Mack, S. (2013). Principles of neural science.

Karachot, L., Shirai, Y., Vigot, R., Yamamori, T., & Ito, M. (2001). Induction of long-term depression in cerebellar Purkinje cells requires a rapidly turned over protein. *J Neurophysiol, 86*(1), 280-289. doi:10.1152/jn.2001.86.1.280

Kato, T., & Hirano, A. (1985). A Golgi study of the proximal portion of the human Purkinje cell axon. *Acta Neuropathol, 68*(3), 191-195. doi:10.1007/BF00690193

Kemp, K. C., Cook, A. J., Redondo, J., Kurian, K. M., Scolding, N. J., & Wilkins, A. (2016). Purkinje cell injury, structural plasticity and fusion in patients with Friedreich's ataxia. *Acta Neuropathol Commun, 4*(1), 53. doi:10.1186/s40478-016-0326-3

Khaliq, Z. M., & Raman, I. M. (2006). Relative contributions of axonal and somatic Na channels to action potential initiation in cerebellar Purkinje neurons. *J Neurosci, 26*(7), 1935-1944. doi:10.1523/JNEUROSCI.4664-05.2006

Kim, J. H., Jang, M. J., Choi, J., Lee, E., Song, K. D., Cho, J., Kim, K. T., Cha, H. J., & Sun, W. (2018). Optimizing tissue-clearing conditions based on analysis of the critical factors affecting tissue-clearing procedures. *Sci Rep, 8*(1), 12815. doi:10.1038/s41598-018-31153-7

King, M., Hernandez-Castillo, C. R., Poldrack, R. A., Ivry, R. B., & Diedrichsen, J. (2019). Functional boundaries in the human cerebellum revealed by a multi-domain task battery. *Nat Neurosci, 22*(8), 1371-1378. doi:10.1038/s41593-019-0436-x

Koch, G. L. (1990). The endoplasmic reticulum and calcium storage. *Bioessays, 12*(11), 527-531. doi:10.1002/bies.950121105

Krasnow, A. M., Ford, M. C., Valdivia, L. E., Wilson, S. W., & Attwell, D. (2018). Regulation of developing myelin sheath elongation by oligodendrocyte calcium transients in vivo. *Nat Neurosci, 21*(1), 24-28. doi:10.1038/s41593-017-0031-y

Kuba, H., Oichi, Y., & Ohmori, H. (2010). Presynaptic activity regulates Na(+) channel distribution at the axon initial segment. *Nature, 465*(7301), 1075-1078. doi:10.1038/nature09087

Kutzelnigg, A., Faber-Rod, J. C., Bauer, J., Lucchinetti, C. F., Sorensen, P. S., Laursen, H., Stadelmann, C., Bruck, W., Rauschka, H., Schmidbauer, M., & Lassmann, H. (2007). Widespread demyelination in the cerebellar cortex in multiple sclerosis. *Brain Pathol, 17*(1), 38-44. doi:10.1111/j.1750-3639.2006.00041.x

Lampert, P., Blumberg, J. M., & Pentschew, A. (1964). An Electron Microscopic Study of Dystrophic Axons in the Gracile and Cuneate Nuclei of Vitamin E-Deficient Rats. *J Neuropathol Exp Neurol, 23*, 60-77. doi:10.1097/00005072-196401000-00005

Lampert, P. W. (1967). A comparative electron microscopic study of reactive, degenerating, regenerating, and dystrophic axons. *J Neuropathol Exp Neurol, 26*(3), 345-368.

Lariviere, R., Gaudet, R., Gentil, B. J., Girard, M., Conte, T. C., Minotti, S., Leclerc-Desaulniers, K., Gehring, K., McKinney, R. A., Shoubridge, E. A., McPherson, P. S., Durham, H. D., & Brais, B. (2015). Sacs knockout mice present pathophysiological defects underlying autosomal recessive spastic ataxia of Charlevoix-Saguenay. *Hum Mol Genet, 24*(3), 727-739. doi:10.1093/hmg/ddu491

Lecours, C., Bordeleau, M., Cantin, L., Parent, M., Paolo, T. D., & Tremblay, M. E. (2018). Microglial Implication in Parkinson's Disease: Loss of Beneficial Physiological Roles or Gain of Inflammatory Functions? *Front Cell Neurosci, 12*, 282. doi:10.3389/fncel.2018.00282

Lee, J. H., Gomora, J. C., Cribbs, L. L., & Perez-Reyes, E. (1999). Nickel block of three cloned T-type calcium channels: low concentrations selectively block alpha1H. *Biophys J, 77*(6), 3034-3042. doi:10.1016/S0006-3495(99)77134-1

Liberski, P. P., & Budka, H. (1999). Neuroaxonal pathology in Creutzfeldt-Jakob disease. *Acta Neuropathol, 97*(4), 329-334. doi:10.1007/s004010050995

Lisberger, S. G., & Fuchs, A. F. (1978). Role of primate flocculus during rapid behavioral modification of vestibuloocular reflex. I. Purkinje cell activity during visually guided horizontal smooth-pursuit eye movements and passive head rotation. *J Neurophysiol, 41*(3), 733-763. doi:10.1152/jn.1978.41.3.733

Liu, Y., Zaun, H. C., Orlowski, J., & Ackerman, S. L. (2013). CHP1-mediated NHE1 biosynthetic maturation is required for Purkinje cell axon homeostasis. *J Neurosci, 33*(31), 12656-12669. doi:10.1523/JNEUROSCI.0406-13.2013

Ljungberg, L., Lang-Ouellette, D., Yang, A., Jayabal, S., Quilez, S., & Watt, A. J. (2016). Transient Developmental Purkinje Cell Axonal Torpedoes in Healthy and Ataxic Mouse Cerebellum. *Front Cell Neurosci, 10*, 248. doi:10.3389/fncel.2016.00248

Louis, E. D., Faust, P. L., Vonsattel, J. P., & Erickson-Davis, C. (2009a). Purkinje cell axonal torpedoes are unrelated to advanced aging and likely reflect cerebellar injury. *Acta Neuropathol, 117*(6), 719-721. doi:10.1007/s00401-009-0534-z

Louis, E. D., Faust, P. L., Vonsattel, J. P., Honig, L. S., Rajput, A., Rajput, A., Pahwa, R., Lyons, K. E., Ross, W. G., Elble, R. J., Erickson-Davis, C., Moskowitz, C. B., & Lawton, A. (2009b). Torpedoes in Parkinson's disease, Alzheimer's disease, essential tremor, and control brains. *Mov Disord, 24*(11), 1600-1605. doi:10.1002/mds.22567

Louis, E. D., Kerridge, C. A., Chatterjee, D., Martuscello, R. T., Diaz, D. T., Koeppen, A. H., Kuo, S. H., Vonsattel, J. G., Sims, P. A., & Faust, P. L. (2019). Contextualizing the pathology in the essential tremor cerebellar cortex: a patholog-omics approach. *Acta Neuropathol, 138*(5), 859-876. doi:10.1007/s00401-019-02043-7

Louis, E. D., Kuo, S. H., Vonsattel, J. P., & Faust, P. L. (2014a). Torpedo formation and Purkinje cell loss: modeling their relationship in cerebellar disease. *Cerebellum, 13*(4), 433-439. doi:10.1007/s12311-014-0556-5

Louis, E. D., Lee, M., Babij, R., Ma, K., Cortes, E., Vonsattel, J. P., & Faust, P. L. (2014b). Reduced Purkinje cell dendritic arborization and loss of dendritic spines in essential tremor. *Brain, 137*(Pt 12), 3142-3148. doi:10.1093/brain/awu314

Louis, E. D., Vonsattel, J. P., Honig, L. S., Ross, G. W., Lyons, K. E., & Pahwa, R. (2006). Neuropathologic findings in essential tremor. *Neurology, 66*(11), 1756-1759. doi:10.1212/01.wnl.0000218162.80315.b9

Louis, E. D., Yi, H., Erickson-Davis, C., Vonsattel, J. P., & Faust, P. L. (2009c). Structural study of Purkinje cell axonal torpedoes in essential tremor. *Neurosci Lett, 450*(3), 287-291. doi:10.1016/j.neulet.2008.11.043

Ly, R., Bouvier, G., Schonewille, M., Arabo, A., Rondi-Reig, L., Lena, C., Casado, M., De Zeeuw, C. I., & Feltz, A. (2013). T-type channel blockade impairs long-term potentiation at the parallel fiber-Purkinje cell synapse and cerebellar learning. *Proc Natl Acad Sci U S A, 110*(50), 20302-20307. doi:10.1073/pnas.1311686110

Maia, P. D., Hemphill, M. A., Zehnder, B., Zhang, C., Parker, K. K., & Kutz, J. N. (2015). Diagnostic tools for evaluating the impact of Focal Axonal Swellings arising in neurodegenerative diseases and/or traumatic brain injury. *J Neurosci Methods, 253*, 233-243. doi:10.1016/j.jneumeth.2015.06.022

Manor, Y., Koch, C., & Segev, I. (1991). Effect of geometrical irregularities on propagation delay in axonal trees. *Biophys J, 60*(6), 1424-1437. doi:10.1016/S0006-3495(91)82179-8

Martina, M., Yao, G. L., & Bean, B. P. (2003). Properties and functional role of voltage-dependent potassium channels in dendrites of rat cerebellar Purkinje neurons. *J Neurosci, 23*(13), 5698-5707.

Matsumoto, R., Nakano, I., Arai, N., Suda, M., & Oda, M. (1996). Progressive supranuclear palsy with asymmetric lesions in the thalamus and cerebellum, with special reference to the unilateral predominance of many torpedoes. *Acta Neuropathol, 92*(6), 640-644. doi:10.1007/s004010050574

Mattei, C., Molgo, J., & Benoit, E. (2014). Involvement of both sodium influx and potassium efflux in ciguatoxin-induced nodal swelling of frog myelinated axons. *Neuropharmacology, 85*, 417-426. doi:10.1016/j.neuropharm.2014.06.001

Meier, H., & MacPike, A. D. (1971). Three syndromes produced by two mutant genes in the mouse. Clinical, pathological, and ultrastructural bases of tottering, leaner, and heterozygous mice. *J Hered, 62*(5), 297-302. doi:10.1093/oxfordjournals.jhered.a108176

Meller, K. (1987). The cytoskeleton of cryofixed Purkinje cells of the chicken cerebellum. *Cell Tissue Res, 247*(1), 155-165. doi:10.1007/BF00216558

Mendell, J. R., Sahenk, Z., Saida, K., Weiss, H. S., Savage, R., & Couri, D. (1977). Alterations of fast axoplasmic transport in experimental methyl n-butyl ketone neuropathy. *Brain Res, 133*(1), 107-118. doi:10.1016/0006-8993(77)90052-x

Molineux, M. L., McRory, J. E., McKay, B. E., Hamid, J., Mehaffey, W. H., Rehak, R., Snutch, T. P., Zamponi, G. W., & Turner, R. W. (2006). Specific T-type calcium channel isoforms are associated with distinct burst phenotypes in deep cerebellar nuclear neurons. *Proc Natl Acad Sci U S A, 103*(14), 5555-5560. doi:10.1073/pnas.0601261103

Moro-de-Casillas, M. L., Cohen, M. L., & Riley, D. E. (2004). Leucoencephalopathy with neuroaxonal spheroids (LENAS) presenting as the cerebellar subtype of multiple system atrophy. *J Neurol Neurosurg Psychiatry, 75*(7), 1070-1072. doi:10.1136/jnnp.2003.028431

Morton, S. M., & Bastian, A. J. (2007). Mechanisms of cerebellar gait ataxia. *Cerebellum, 6*(1), 79-86. doi:10.1080/14734220601187741

Newell, K. L., Boyer, P., Gomez-Tortosa, E., Hobbs, W., Hedley-Whyte, E. T., Vonsattel, J. P., & Hyman, B. T. (1999). Alpha-synuclein immunoreactivity is present in axonal swellings in neuroaxonal dystrophy and acute traumatic brain injury. *J Neuropathol Exp Neurol, 58*(12), 1263-1268. doi:10.1097/00005072-199912000-00007

Nixon, R. A., Paskevich, P. A., Sihag, R. K., & Thayer, C. Y. (1994). Phosphorylation on carboxyl terminus domains of neurofilament proteins in retinal ganglion cell neurons in vivo: influences on regional neurofilament accumulation, interneurofilament spacing, and axon caliber. *J Cell Biol, 126*(4), 1031-1046. doi:10.1083/jcb.126.4.1031

Norman, R. M. (1940). Primary degeneration of the granular layer of the cerebellum: An unusual form of familial cerebellar atrophy occurring in early life. *Brain, 63*, 365-379. doi:DOI 10.1093/brain/63.4.365

Ogawa, Y., Kakumoto, K., Yoshida, T., Kuwako, K. I., Miyazaki, T., Yamaguchi, J., Konno, A., Hata, J., Uchiyama, Y., Hirai, H., Watanabe, M., Darnell, R. B., Okano, H., & Okano, H. J. (2018). Elavl3 is essential for the maintenance of Purkinje neuron axons. *Sci Rep, 8*(1), 2722. doi:10.1038/s41598-018-21130-5

Ohfuji, S. (2017). Axonal and dendritic swellings on cerebellar Purkinje cells in a cow: a possible age-related change. *Comparative Clinical Pathology, 26*(6), 1381-1387. doi:10.1007/s00580-017-2544-x

Ohgami, T., Kitamoto, T., & Tateishi, J. (1992). Alzheimer's amyloid precursor protein accumulates within axonal swellings in human brain lesions. *Neurosci Lett, 136*(1), 75-78. doi:10.1016/0304-3940(92)90651-m

Okamoto, K., Hirai, S., Shoji, M., Senoh, Y., & Yamazaki, T. (1990). Axonal swellings in the corticospinal tracts in amyotrophic lateral sclerosis. *Acta Neuropathol, 80*(2), 222-226. doi:10.1007/BF00308929

Palmer, L. M., Clark, B. A., Grundemann, J., Roth, A., Stuart, G. J., & Hausser, M. (2010). Initiation of simple and complex spikes in cerebellar Purkinje cells. *J Physiol, 588*(Pt 10), 1709-1717. doi:10.1113/jphysiol.2010.188300

Pan, Z., Kao, T., Horvath, Z., Lemos, J., Sul, J. Y., Cranstoun, S. D., Bennett, V., Scherer, S. S., & Cooper, E. C. (2006). A common ankyrin-G-based mechanism retains KCNQ and NaV channels at electrically active domains of the axon. *J Neurosci, 26*(10), 2599-2613. doi:10.1523/JNEUROSCI.4314-05.2006

Pentschew, A., & Schwarz, K. (1962). Systemic axonal dystrophy in vitamin E deficient adult rats. *Acta Neuropathologica, 1*(4), 313-334.

Person, A. L., & Raman, I. M. (2012). Synchrony and neural coding in cerebellar circuits. *Front Neural Circuits, 6*, 97. doi:10.3389/fncir.2012.00097

Petito, C. K., Hart, M. N., Porro, R. S., & Earle, K. M. (1973). Ultrastructural studies of olivopontocerebellar atrophy. *J Neuropathol Exp Neurol, 32*(4), 503-522.

Pioro, E. P., & Cuello, A. C. (1988). Purkinje cells of adult rat cerebellum express nerve growth factor receptor immunoreactivity: light microscopic observations. *Brain Res, 455*(1), 182-186. doi:10.1016/0006-8993(88)90131-x

Prudente, C. N., Pardo, C. A., Xiao, J., Hanfelt, J., Hess, E. J., Ledoux, M. S., & Jinnah, H. A. (2013). Neuropathology of cervical dystonia. *Exp Neurol, 241*, 95-104. doi:10.1016/j.expneurol.2012.11.019

Raman, I. M., & Bean, B. P. (1997). Resurgent sodium current and action potential formation in dissociated cerebellar Purkinje neurons. *J Neurosci, 17*(12), 4517-4526.

Raman, I. M., & Bean, B. P. (1999). Ionic currents underlying spontaneous action potentials in isolated cerebellar Purkinje neurons. *J Neurosci, 19*(5), 1663-1674.

Rambold, H., Churchland, A., Selig, Y., Jasmin, L., & Lisberger, S. G. (2002). Partial ablations of the flocculus and ventral paraflocculus in monkeys cause linked deficits in smooth pursuit eye movements and adaptive modification of the VOR. *J Neurophysiol, 87*(2), 912-924. doi:10.1152/jn.00768.2000

Rand, C. W., & Courville, C. B. (1934). Histologic changes in the brain in cases of fatal injury to the head: V. Changes in the nerve fibers. *Archives of Neurology & Psychiatry, 31*(3), 527-555. doi:10.1001/archneurpsyc.1934.02250030067004

Redondo, J., Kemp, K., Hares, K., Rice, C., Scolding, N., & Wilkins, A. (2015). Purkinje Cell Pathology and Loss in Multiple Sclerosis Cerebellum. *Brain Pathol, 25*(6), 692-700. doi:10.1111/bpa.12230

Reeber, S. L., White, J. J., George-Jones, N. A., & Sillitoe, R. V. (2012). Architecture and development of olivocerebellar circuit topography. *Front Neural Circuits, 6*, 115. doi:10.3389/fncir.2012.00115

Rhyu, I. J., Abbott, L. C., Walker, D. B., & Sotelo, C. (1999). An ultrastructural study of granule cell/Purkinje cell synapses in tottering (tg/tg), leaner (tg(la)/tg(la)) and compound heterozygous tottering/leaner (tg/tg(la)) mice. *Neuroscience, 90*(3), 717-728. doi:10.1016/s0306-4522(98)00518-1

Risner, M. L., Pasini, S., Cooper, M. L., Lambert, W. S., & Calkins, D. J. (2018). Axogenic mechanism enhances retinal ganglion cell excitability during early progression in glaucoma. *Proc Natl Acad Sci U S A, 115*(10), E2393-E2402. doi:10.1073/pnas.1714888115

Roossien, D. H., Miller, K. E., & Gallo, G. (2015). Ciliobrevins as tools for studying dynein motor function. *Front Cell Neurosci, 9*, 252. doi:10.3389/fncel.2015.00252

Rosenfeld, J., & Freidrich, V. L., Jr. (1983). Axonal swellings in jimpy mice: does lack of myelin cause neuronal abnormalities? *Neuroscience, 10*(3), 959-966. doi:10.1016/0306-4522(83)90233-6

Rossi, F., Borsello, T., & Strata, P. (1994). Exposure to kainic acid mimics the effects of axotomy in cerebellar Purkinje cells of the adult rat. *Eur J Neurosci, 6*(3), 392-402. doi:10.1111/j.1460-9568.1994.tb00282.x

Ryu, C., Jang, D. C., Jung, D., Kim, Y. G., Shim, H. G., Ryu, H. H., Lee, Y. S., Linden, D. J., Worley, P. F., & Kim, S. J. (2017). STIM1 Regulates Somatic Ca(2+) Signals and Intrinsic Firing Properties of Cerebellar Purkinje Neurons. *J Neurosci, 37*(37), 8876-8894. doi:10.1523/JNEUROSCI.3973-16.2017

Ryu, J., Horkayne-Szakaly, I., Xu, L., Pletnikova, O., Leri, F., Eberhart, C., Troncoso, J. C., & Koliatsos, V. E. (2014). The problem of axonal injury in the brains of veterans with histories of blast exposure. *Acta Neuropathol Commun, 2*, 153. doi:10.1186/s40478-014-0153-3

Sabaratnam, M. (2000). Pathological and neuropathological findings in two males with fragile-X syndrome. *J Intellect Disabil Res, 44 (Pt 1)*, 81-85. doi:10.1046/j.1365-2788.2000.00261.x

Sahu, G., Wazen, R. M., Colarusso, P., Chen, S. R. W., Zamponi, G. W., & Turner, R. W. (2019). Junctophilin Proteins Tether a Cav1-RyR2-KCa3.1 Tripartite Complex to Regulate Neuronal Excitability. *Cell Rep, 28*(9), 2427-2442 e2426. doi:10.1016/j.celrep.2019.07.075

Sakai, K., Ishida, C., Morinaga, A., Takahashi, K., & Yamada, M. (2015). Case Study: Somatic Sprouts and Halo-Like Amorphous Materials of the Purkinje Cells in Huntington's Disease. *Cerebellum, 14*(6), 707-710. doi:10.1007/s12311-015-0678-4

Sarna, J. R., & Hawkes, R. (2011). Patterned Purkinje cell loss in the ataxic sticky mouse. *Eur J Neurosci, 34*(1), 79-86. doi:10.1111/j.1460-9568.2011.07725.x

Sasaki, H., Kojima, H., Yabe, I., Tashiro, K., Hamada, T., Sawa, H., Hiraga, H., & Nagashima, K. (1998). Neuropathological and molecular studies of spinocerebellar ataxia type 6 (SCA6). *Acta Neuropathol, 95*(2), 199-204. doi:10.1007/s004010050787

Satake, T., Yamashita, K., Hayashi, K., Miyatake, S., Tamura-Nakano, M., Doi, H., Furuta, Y., Shioi, G., Miura, E., Takeo, Y. H., Yoshida, K., Yahikozawa, H., Matsumoto, N., Yuzaki, M., & Suzuki, A. (2017). MTCL1 plays an essential role in maintaining Purkinje neuron axon initial segment. *EMBO J, 36*(9), 1227-1242. doi:10.15252/embj.201695630

Sato, T., Ishikawa, M., Yoshihara, T., Nakazato, R., Higashida, H., Asano, M., & Yoshioka, K. (2015). Critical role of JSAP1 and JLP in axonal transport in the cerebellar Purkinje cells of mice. *FEBS Lett, 589*(19 Pt B), 2805-2811. doi:10.1016/j.febslet.2015.08.024

Sawada, K., Hosoi, E., Bando, M., Sakata-Haga, H., Lee, N. S., Jeong, Y. G., & Fukui, Y. (2008). Differential alterations in expressions of ryanodine receptor subtypes in cerebellar cortical neurons of an ataxic mutant, rolling mouse Nagoya. *Neuroscience, 152*(3), 609-617. doi:10.1016/j.neuroscience.2007.12.048

Schaller, K. L., & Caldwell, J. H. (2003). Expression and distribution of voltage-gated sodium channels in the cerebellum. *Cerebellum, 2*(1), 2-9. doi:10.1080/14734220309424

Schlaepfer, W. W. (1987). Neurofilaments: structure, metabolism and implications in disease. *J Neuropathol Exp Neurol, 46*(2), 117-129.

Schmahmann, J. D. (2004). Disorders of the cerebellum: ataxia, dysmetria of thought, and the cerebellar cognitive affective syndrome. *J Neuropsychiatry Clin Neurosci, 16*(3), 367-378. doi:10.1176/jnp.16.3.367

Sekirnjak, C., Vissel, B., Bollinger, J., Faulstich, M., & du Lac, S. (2003). Purkinje cell synapses target physiologically unique brainstem neurons. *J Neurosci, 23*(15), 6392-6398.

Shah, J. V., Flanagan, L. A., Janmey, P. A., & Leterrier, J. F. (2000). Bidirectional translocation of neurofilaments along microtubules mediated in part by dynein/dynactin. *Mol Biol Cell, 11*(10), 3495-3508. doi:10.1091/mbc.11.10.3495

Sharp, A. H., Nucifora, F. C., Jr., Blondel, O., Sheppard, C. A., Zhang, C., Snyder, S. H., Russell, J. T., Ryugo, D. K., & Ross, C. A. (1999). Differential cellular expression of isoforms of inositol 1,4,5-triphosphate receptors in neurons and glia in brain. *J Comp Neurol, 406*(2), 207-220.

Silvestri, L., Paciscopi, M., Soda, P., Biamonte, F., Iannello, G., Frasconi, P., & Pavone, F. S. (2015). Quantitative neuroanatomy of all Purkinje cells with light sheet microscopy and high-throughput image analysis. *Frontiers in Neuroanatomy, 9*, 68. doi:10.3389/fnana.2015.00068

Sotelo, C. (1990). Axonal abnormalities in cerebellar Purkinje cells of the 'hyperspiny Purkinje cell' mutant mouse. *J Neurocytol, 19*(5), 737-755. doi:10.1007/bf01188042

Stocker, M., & Pedarzani, P. (2000). Differential distribution of three Ca(2+)-activated K(+) channel subunits, SK1, SK2, and SK3, in the adult rat central nervous system. *Mol Cell Neurosci, 15*(5), 476-493. doi:10.1006/mcne.2000.0842

Suzuki, K., & Zagoren, J. C. (1975). Focal axonal swelling in cerebellum of quaking mouse: light and electron microscopic studies. *Brain Res, 85*(1), 38-43.

Takahashi, N., Iwatsubo, T., Nakano, I., & Machinami, R. (1992). Focal appearance of cerebellar torpedoes associated with discrete lesions in the cerebellar white matter. *Acta Neuropathol, 84*(2), 153-156. doi:10.1007/bf00311388

Takeuchi, I. K., Aoki, E., & Takeuchi, Y. K. (1995). Axonal swellings in cerebellar white matter of groggy mutant rat. *Acta Neuropathol, 90*(5), 486-492. doi:10.1007/bf00294810

Talley, E. M., Cribbs, L. L., Lee, J. H., Daud, A., Perez-Reyes, E., & Bayliss, D. A. (1999). Differential distribution of three members of a gene family encoding low voltage-activated (T-type) calcium channels. *J Neurosci, 19*(6), 1895-1911.

Teigler, A., Komljenovic, D., Draguhn, A., Gorgas, K., & Just, W. W. (2009). Defects in myelination, paranode organization and Purkinje cell innervation in the ether lipid-deficient mouse cerebellum. *Hum Mol Genet, 18*(11), 1897-1908. doi:10.1093/hmg/ddp110

Terry, R. D., & Weiss, M. (1963). Studies in Tay-Sachs disease. II. Ultrastructure of the cerebrum. *J Neuropathol Exp Neurol, 22*, 18-55. doi:10.1097/00005072-196301000-00003

Thach, W. T., Jr. (1967). Somatosensory receptive fields of single units in cat cerebellar cortex. *J Neurophysiol, 30*(4), 675-696. doi:10.1152/jn.1967.30.4.675

Trapp, B. D., Peterson, J., Ransohoff, R. M., Rudick, R., Mork, S., & Bo, L. (1998). Axonal transection in the lesions of multiple sclerosis. *N Engl J Med, 338*(5), 278-285. doi:10.1056/NEJM199801293380502

Tringham, E. W., Payne, C. E., Dupere, J. R., & Usowicz, M. M. (2007). Maturation of rat cerebellar Purkinje cells reveals an atypical Ca2+ channel current that is inhibited by omega-agatoxin IVA and the dihydropyridine (-)-(S)-Bay K8644. *J Physiol, 578*(Pt 3), 693-714. doi:10.1113/jphysiol.2006.121905

Tsukamoto, T., Chiba, Y., Wakamori, M., Yamada, T., Tsunogae, S., Cho, Y., Sakakibara, R., Imazu, T., Tokoro, S., Satake, Y., Adachi, M., Nishikawa, T., Yotsu-Yamashita, M., & Konoki, K. (2017). Differential binding of tetrodotoxin and its derivatives to voltage-sensitive sodium channel subtypes (Nav 1.1 to Nav 1.7). *Br J Pharmacol, 174*(21), 3881-3892. doi:10.1111/bph.13985

Tsukita, S., & Ishikawa, H. (1980). The movement of membranous organelles in axons. Electron microscopic identification of anterogradely and retrogradely transported organelles. *J Cell Biol, 84*(3), 513-530. doi:10.1083/jcb.84.3.513

Vacher, H., Mohapatra, D. P., & Trimmer, J. S. (2008). Localization and targeting of voltage-dependent ion channels in mammalian central neurons. *Physiol Rev, 88*(4), 1407-1447. doi:10.1152/physrev.00002.2008

Verly, M., Verhoeven, J., Zink, I., Mantini, D., Van Oudenhove, L., Lagae, L., Sunaert, S., & Rommel, N. (2014). Structural and functional underconnectivity as a negative predictor for language in autism. *Hum Brain Mapp, 35*(8), 3602-3615. doi:10.1002/hbm.22424

Vinueza Veloz, M. F., Zhou, K., Bosman, L. W., Potters, J. W., Negrello, M., Seepers, R. M., Strydis, C., Koekkoek, S. K., & De Zeeuw, C. I. (2015). Cerebellar control of gait and interlimb coordination. *Brain Struct Funct, 220*(6), 3513-3536. doi:10.1007/s00429-014-0870-1

Volk, B., & Kirchgassner, N. (1985). Damage of Purkinje cell axons following chronic phenytoin administration: an animal model of distal axonopathy. *Acta Neuropathol, 67*(1-2), 67-74.

Walkley, S. U., Baker, H. J., Rattazzi, M. C., Haskins, M. E., & Wu, J. Y. (1991). Neuroaxonal dystrophy in neuronal storage disorders: evidence for major GABAergic neuron involvement. *J Neurol Sci, 104*(1), 1-8. doi:10.1016/0022-510x(91)90208-o

Wang, J. T., Medress, Z. A., & Barres, B. A. (2012). Axon degeneration: molecular mechanisms of a self-destruction pathway. *J Cell Biol, 196*(1), 7-18. doi:10.1083/jcb.201108111

Watt, A. J., Cuntz, H., Mori, M., Nusser, Z., Sjostrom, P. J., & Hausser, M. (2009). Traveling waves in developing cerebellar cortex mediated by asymmetrical Purkinje cell connectivity. *Nat Neurosci, 12*(4), 463-473. doi:10.1038/nn.2285

Westenbroek, R. E., Sakurai, T., Elliott, E. M., Hell, J. W., Starr, T. V., Snutch, T. P., & Catterall, W. A. (1995). Immunochemical identification and subcellular distribution of the alpha 1A subunits of brain calcium channels. *J Neurosci, 15*(10), 6403-6418.

Wong, H. H., Lin, J. Q., Strohl, F., Roque, C. G., Cioni, J. M., Cagnetta, R., Turner-Bridger, B., Laine, R. F., Harris, W. A., Kaminski, C. F., & Holt, C. E. (2017). RNA Docking and Local Translation Regulate Site-Specific Axon Remodeling In Vivo. *Neuron, 95*(4), 852-868 e858. doi:10.1016/j.neuron.2017.07.016

Wu, B., Blot, F. G., Wong, A. B., Osorio, C., Adolfs, Y., Pasterkamp, R. J., Hartmann, J., Becker, E. B., Boele, H. J., De Zeeuw, C. I., & Schonewille, M. (2019). TRPC3 is a major contributor to functional heterogeneity of cerebellar Purkinje cells. *Elife, 8*. doi:10.7554/eLife.45590

Yagishita, S. (1978). Morphological investigations on axonal swellings and spheroids in various human diseases. *Virchows Arch A Pathol Anat Histol, 378*(3), 181-197. doi:10.1007/bf00427359

Yagishita, S. (1979). Ultrastructural observations on axonal swelling in the human gracile nucleus. *Virchows Arch A Pathol Anat Histol, 382*(2), 217-226. doi:10.1007/bf01102876

Yang, Q., Hashizume, Y., Yoshida, M., Wang, Y., Goto, Y., Mitsuma, N., Ishikawa, K., & Mizusawa, H. (2000). Morphological Purkinje cell changes in spinocerebellar ataxia type 6. *Acta Neuropathol, 100*(4), 371-376. doi:10.1007/s004010000201

Yin, X., Kidd, G. J., Ohno, N., Perkins, G. A., Ellisman, M. H., Bastian, C., Brunet, S., Baltan, S., & Trapp, B. D. (2016). Proteolipid protein-deficient myelin promotes axonal mitochondrial dysfunction via altered metabolic coupling. *J Cell Biol, 215*(4), 531-542. doi:10.1083/jcb.201607099

Yokoyama, C. T., Westenbroek, R. E., Hell, J. W., Soong, T. W., Snutch, T. P., & Catterall, W. A. (1995). Biochemical properties and subcellular distribution of the neuronal class E calcium channel alpha 1 subunit. *J Neurosci, 15*(10), 6419-6432.

Young, J. Z. (1938). The Functioning of the Giant Nerve Fibres of the Squid. *Journal of Experimental Biology, 15*, 170-185.

Yuan, A., Rao, M. V., Veeranna, & Nixon, R. A. (2017). Neurofilaments and Neurofilament Proteins in Health and Disease. *Cold Spring Harb Perspect Biol, 9*(4). doi:10.1101/cshperspect.a018309

Zamponi, G. W., Bourinet, E., & Snutch, T. P. (1996). Nickel block of a family of neuronal calcium channels: subtype- and subunit-dependent action at multiple sites. *J Membr Biol, 151*(1), 77-90. doi:10.1007/s002329900059

Zonta, B., Desmazieres, A., Rinaldi, A., Tait, S., Sherman, D. L., Nolan, M. F., & Brophy, P. J. (2011). A critical role for Neurofascin in regulating action potential initiation through maintenance of the axon initial segment. *Neuron, 69*(5), 945-956. doi:10.1016/j.neuron.2011.02.021

APPENDIX I

Repeated-measures ANOVAs

Statistical Analyses

APPENDIX I

Fig 4.2 - TTX concentration

Repeated-measures ANOVA

	P-Value
Mauchly's Test of Sphericity	<0.001
(Greenhouse-Geisser)	0.513
Tests of Within-Subjects Effects	
(Greenhouse-Geisser correction)	
Time	<0.001
Time * Condition	0.016
Tests of Between-Subjects Effects	
Condition	0.031

Multivariate Tests (Wilk's Lambda)			P-Value
No TTX			0.770
Extra Low TTX			0.001
Low TTX			<0.001
High TTX			0.773
Pairwise Comparisons (Boneferroni correction)			
Condition	Time		
Low TTX	0	1	<0.001
		2	<0.001
		3	<0.001
	1	2	<0.001
		3	<0.001
	2	3	0.007
Extra Low TTX	0	1	<0.001
		2	0.001
		3	0.002
	1	2	1.00
		3	0.803
	2	3	1.00

Univariate Tests			P-Value
Time			
1			0.080
2			0.017
3			0.034
Pairwise Comparisons (Boneferroni correction)			
Time	Condition		
2	*No TTX*	*Extra Low TTX*	0.164
		Low TTX	0.116
		High TTX	1.00
	Extra Low TTX	*Low TTX*	1.00
		High TTX	0.190
	Low TTX	*High TTX*	0.142
3	*No TTX*	*Extra Low TTX*	0.246
		Low TTX	0.131
		High TTX	1.00
	Extra Low TTX	*Low TTX*	1.00
		High TTX	0.437
	Low TTX	*High TTX*	0.287

Pairwise Comparisons only shown for significant condition or time.

Fig 4.3 - Axonal reconstruction volume

Repeated-measures ANOVA

	P-Value
Mauchly's Test of Sphericity	0.021
(Greenhouse-Geisser)	0.589
Tests of Within-Subjects Effects	
(Greenhouse-Geisser correction)	
Time	<0.001
Time * Axon type	0.004
Tests of Between-Subjects Effects	
Axon type	0.093

Multivariate Tests (Wilk's Lambda)			P-Value
Control			0.471
Torpedo			0.002
Pairwise Comparisons (Boneferroni correction)			
Axon type	Time		
Torpedo	0	1	0.346
		2	0.007
		3	<0.001
	1	2	0.221
		3	0.003
	2	3	0.002

Univariate Tests			P-Value
Time			
0			0.441
1			0.470
2			0.107
3			0.017
Pairwise Comparisons (Boneferroni correction)			
Time	Axon type		
3	Control	Torpedo	0.017

Fig 4.4 - Dual-recording in low TTX

Repeated-measures ANOVA (FF Ramp down)

	P-Value
Mauchly's Test of Sphericity	0.018
(Greenhouse-Geisser)	0.780
(Huynh-Feldt)	0.933
Tests of Within-Subjects Effects	
(Huynh-Feldt correction)	
Time	<0.001
Time * Condition	0.466
Tests of Between-Subjects Effects	
Compartement	0.112

Multivariate Tests (Wilk's Lambda)			P-Value
Time			<0.001
Pairwise Comparisons (Boneferroni correction)			
Time (min)			
3	6		0.015
	9		<0.001
	12		<0.001
	15		<0.001
6	9		0.001
	12		<0.001
	15		<0.001
9	12		0.001
	15		<0.001
12	15		0.052

Repeated-measures ANOVA (long exposure)

	P-Value
Mauchly's Test of Sphericity	<0.001
(Greenhouse-Geisser)	0.577
Tests of Within-Subjects Effects	
(Greenhouse-Geisser correction)	
Time	<0.001
Time * Condition	0.023
Tests of Between-Subjects Effects	
Compartment	<0.001

Multivariate Tests (Wilk's Lambda)			P-Value
Soma			<0.001
Axon			0.109
Pairwise Comparisons (Boneferroni correction)			
Compartment	Time (min)		
Soma	30	45	0.001
		60	0.002
		75	0.002
		90	<0.001
	45	60	1.00
		75	1.00
		90	0.102
	60	75	1.00
		90	0.950
	75	90	0.209

Univariate Tests			P-Value
Time (min)			
30			<0.001
45			<0.001
60			<0.001
75			<0.001
90			<0.001
Pairwise Comparisons (Boneferroni correction)			
Time (min)	Condition		
30	Soma	Axon	<0.001
45	Soma	Axon	<0.001
60	Soma	Axon	<0.001
75	Soma	Axon	<0.001
90	Soma	Axon	<0.001

Pairwise Comparisons only shown for significant condition or time.

Fig 4.6 - Anisomycin

Repeated-measures ANOVA

		P-Value
Mauchly's Test of Sphericity		<0.001
Greenhouse-Geisser (Ɛ < 0.750)	0.597	
Tests of Within-Subjects Effects		
(Greenhouse-Geisser correction)		
Time		<0.001
Time * Condition		0.224
Tests of Between-Subjects Effects		
Condition		0.246

Multivariate Tests (Wilk's Lambda)			P-Value
Time			<0.001
Pairwise Comparisons (Boneferroni correction)			
Time			
0	1		0.001
	2		<0.001
	3		<0.001
1	2		0.128
	3		0.207
2	3		1.00

Pairwise Comparisons only shown for significant condition or time.

Fig 4.7 - Calcium concentration

Repeated-measures ANOVA

	P-Value
Mauchly's Test of Sphericity	<0.001
(Greenhouse-Geisser)	0.601
Tests of Within-Subjects Effects	
(Greenhouse-Geisser correction)	
Time	<0.001
Time * Condition	<0.001
Tests of Between-Subjects Effects	
Condition	<0.001

Multivariate Tests (Wilk's Lambda)	P-Value
0 mM Ca^{2+}	0.245
0 mM Ca^{2+} + *low TTX*	0.162
2 mM Ca^{2+} + *low TTX*	<0.001
3 mM Ca^{2+} + *low TTX*	<0.001

Pairwise Comparisons (Boneferroni correction)

Condition	Time		P-Value
2 mM Ca^{2+} + *low TTX*	0	1	0.001
		2	<0.001
		3	<0.001
	1	2	<0.001
		3	<0.001
	2	3	0.112
3 mM Ca^{2+} + *low TTX*	0	1	<0.001
		2	<0.001
		3	<0.001
	1	2	0.001
		3	0.003
	2	3	1.00

Univariate Tests Time	P-Value
1	0.001
2	<0.001
3	<0.001

Pairwise Comparisons (Boneferroni correction)

Time	Condition		P-Value
1	0 mM Ca^{2+}	0 mM Ca^{2+} + *low TTX*	1.00
		2 mM Ca^{2+} + *low TTX*	1.00
		3 mM Ca^{2+} + *low TTX*	0.027
	0 mM Ca^{2+} + *low TTX*	2 mM Ca^{2+} + *low TTX*	0.082
		3 mM Ca^{2+} + *low TTX*	0.001
	2 mM Ca^{2+} + *low TTX*	3 mM Ca^{2+} + *low TTX*	0.550
2	0 mM Ca^{2+}	0 mM Ca^{2+} + *low TTX*	1.00
		2 mM Ca^{2+} + *low TTX*	0.020
		3 mM Ca^{2+} + *low TTX*	0.001
	0 mM Ca^{2+} + *low TTX*	2 mM Ca^{2+} + *low TTX*	0.007
		3 mM Ca^{2+} + *low TTX*	<0.001
	2 mM Ca^{2+} + *low TTX*	3 mM Ca^{2+} + *low TTX*	1.00
3	0 mM Ca^{2+}	0 mM Ca^{2+} + *low TTX*	1.00
		2 mM Ca^{2+} + *low TTX*	0.011
		3 mM Ca^{2+} + *low TTX*	0.003
	0 mM Ca^{2+} + *low TTX*	2 mM Ca^{2+} + *low TTX*	0.010
		3 mM Ca^{2+} + *low TTX*	0.002
	2 mM Ca^{2+} + *low TTX*	3 mM Ca^{2+} + *low TTX*	1.00

Pairwise Comparisons only shown for significant condition or time.

Fig 4.8 - Nickel concentration

Repeated-measures ANOVA (100 µM Ni^{2+})

	P-Value	Multivariate Tests (Wilk's Lambda)		P-Value
Mauchly's Test of Sphericity	<0.001	Time		0.003
(Greenhouse-Geisser)	0.621			
		Pairwise Comparisons (Boneferroni correction)		
Tests of Within-Subjects Effects		Time		
(Greenhouse-Geisser correction)		0	1	0.021
Time	<0.001		2	0.001
Time * Condition	0.209		3	0.003
		1	2	0.114
Tests of Between-Subjects Effects			3	0.189
Condition	0.109	2	3	0.001

Repeated-measures ANOVA (1 mM Ni^{2+})

	P-Value	Multivariate Tests (Wilk's Lambda)		P-Value	Univariate Tests			P-Value
					Time			
Mauchly's Test of Sphericity	<0.001	1 mM Ni^{2+}		0.779	1			0.057
(Greenhouse-Geisser)	0.615	*low TTX*		<0.001	2			0.002
		1 mM Ni^{2+} + *low TTX*		0.792	3			0.015
		Pairwise Comparisons			**Pairwise Comparisons**			
		(Boneferroni correction)			**(Boneferroni correction)**			
Tests of Within-Subjects Effects		Condition	Time		Time	Condition		
(Greenhouse-Geisser correction)		*low TTX*	0	1	0.001	2	1 mM Ni^{2+}	*low TTX*	0.028
Time	<0.001			2	<0.001			1 mM Ni^{2+} + *low TTX*	1.00
Time * Condition	0.011			3	<0.001		*low TTX*	1 mM Ni^{2+} + *low TTX*	0.005
			1	2	0.005	3	1 mM Ni^{2+}	*low TTX*	0.083
Tests of Between-Subjects Effects				3	0.011			1 mM Ni^{2+} + *low TTX*	1.00
Condition	0.005		2	3	0.443		*low TTX*	1 mM Ni^{2+} + *low TTX*	0.030

Pairwise Comparisons only shown for significant condition or time.

ANNEX I

Title: Transient Developmental Purkinje cell axonal torpedoes in healthy and ataxic mouse cerebellum

Authors list: Lovisa Ljungberg, Daneck Lang-Ouellette, Angela Yang, Sriram Jayabal, Sabrina Quilez and Alanna J. Watt

Published in: Frontiers of Cellular Neuroscience

Date: November 2016

frontiers in Cellular Neuroscience

ORIGINAL RESEARCH
published: 02 November 2016
doi: 10.3389/fncel.2016.00248

Transient Developmental Purkinje Cell Axonal Torpedoes in Healthy and Ataxic Mouse Cerebellum

*Lovisa Ljungberg, Daneck Lang-Ouellette, Angela Yang, Sriram Jayabal, Sabrina Quilez and Alanna J. Watt**

Department of Biology, McGill University, Montreal, QC, Canada

Information is carried out of the cerebellar cortical microcircuit via action potentials propagated along Purkinje cell axons. In several human neurodegenerative diseases, focal axonal swellings on Purkinje cells – known as torpedoes – have been associated with Purkinje cell loss. Interestingly, torpedoes are also reported to appear transiently during development in rat cerebellum. The function of Purkinje cell axonal torpedoes in health as well as in disease is poorly understood. We investigated the properties of developmental torpedoes in the postnatal mouse cerebellum of wild-type and transgenic mice. We found that Purkinje cell axonal torpedoes transiently appeared on axons of Purkinje neurons, with the largest number of torpedoes observed at postnatal day 11 (P11). This was after peak developmental apoptosis had occurred, when Purkinje cell counts in a lobule were static, suggesting that most developmental torpedoes appear on axons of neurons that persist into adulthood. We found that developmental torpedoes were not associated with a presynaptic GABAergic marker, indicating that they are not synapses. They were seldom found at axonal collateral branch points, and lacked microglia enrichment, suggesting that they are unlikely to be involved in axonal refinement. Interestingly, we found several differences between developmental torpedoes and disease-related torpedoes: developmental torpedoes occurred largely on myelinated axons, and were not associated with changes in basket cell innervation on their parent soma. Disease-related torpedoes are typically reported to contain neurofilament; while the majority of developmental torpedoes did as well, a fraction of smaller developmental torpedoes did not. These differences indicate that developmental torpedoes may not be functionally identical to disease-related torpedoes. To study this further, we used a mouse model of spinocerebellar ataxia type 6 (SCA6), and found elevated disease-related torpedo number at 2 years. However, we found normal levels of developmental torpedoes in these mice. Our findings suggest that the transient emergence of Purkinje cell axonal torpedoes during the second postnatal week in mice represents a normal morphological feature in the developing cerebellar microcircuit.

Keywords: axon, pruning, microglia, synapse, myelin, neurofilament, ataxia, axonal swelling

OPEN ACCESS

Edited by:
Egidio D'Angelo,
University of Pavia, Italy

Reviewed by:
Richard Hawkes,
University of Calgary, Canada
Filippo Tempia,
University of Turin, Italy

****Correspondence:***
Alanna J. Watt
alanna.watt@mcgill.ca

Received: *24 August 2016*
Accepted: *10 October 2016*
Published: *02 November 2016*

Citation:
Ljungberg L, Lang-Ouellette D, Yang A, Jayabal S, Quilez S and Watt AJ (2016) Transient Developmental Purkinje Cell Axonal Torpedoes in Healthy and Ataxic Mouse Cerebellum. Front. Cell. Neurosci. 10:248. doi: 10.3389/fncel.2016.00248

INTRODUCTION

Purkinje cell axons convey information away from the cerebellar cortical microcircuit, and are thus critical for cerebellar function. Over a century ago, focal axonal swellings were identified along Purkinje cell axons (Ramon and Cajal, 1991). The term "torpedo" was used to identify these focal swellings in 1918 by the Dutch psychiatrist Leendert Bouman (Bouman, 1918), and

the term has been used since then to identify swellings or spheroids on Purkinje cell axons. Purkinje cell axonal torpedoes are observed in several diseases, including essential tremor (Louis et al., 2006, 2009, 2014), spinocerebellar ataxias (Sasaki et al., 1998; Yang et al., 2000; Louis et al., 2014), encephalopathy (Yagishita, 1978), and other cerebellar disorders (Hirano et al., 1973; Louis et al., 2014), and are especially prevalent in the cerebellar vermis (Louis et al., 2011). Torpedo-like swellings have also been observed in several spontaneously arising ataxic rodents, for e.g., *weaver* (Hirano et al., 1973), hyperspiny Purkinje cell (hpc) (Sotelo, 1990), and *sticky* mice (Sarna and Hawkes, 2011), *groggy* rats (Takeuchi et al., 1995), and in mouse models of disease such as Autosomal Recessive Ataxia of the Charlevoix-Saguenay Region (ARSACS) (Lariviere et al., 2015). Furthermore, torpedoes are enriched in rodent brains after chronic administration of certain chemicals, such as the anti-seizure medicine phenytoin (Volk and Kirchgassner, 1985), the excitotoxic kainic acid (Rossi et al., 1994), and molecules that interfere with microtubule transport (Pioro and Cuello, 1988). Purkinje cell axonal torpedoes have also been observed close to cerebellar lesions (Takahashi et al., 1992). Taken together, these observations have led to the belief that Purkinje cell axonal torpedoes are associated with cerebellar damage and degeneration. Indeed, torpedoes can be observed on the axons of surviving cells at the same time as Purkinje cell death is observed (Louis et al., 2014). This suggests that the relationship between cell death and Purkinje cell torpedo accumulation is complex. For example, torpedoes are numerous in the cerebella from essential tremor patients who have significant Purkinje cell loss, suggesting that torpedoes are prevalent on axons of Purkinje cell that do not die. However, in diseases such as multiple system atrophy-cerebellar, torpedoes are more prevalent when Purkinje cell loss is minimal. Multiple system atrophy-cerebellar patients that have greater Purkinje cell loss have fewer torpedoes, possibly because the neurons with torpedoes have died (Louis et al., 2014). It is thus an open question whether torpedoes cause neurodegeneration or are in fact neuroprotective (Babij et al., 2013). Interestingly, torpedoes also occur in healthy brains (Kato and Hirano, 1985), and there is some evidence that torpedoes accumulate with age in both human and rodent cerebellum (Baurle and Grusser-Cornehls, 1994). The presence of torpedoes in aging cerebellum may occur because of the accumulation of changes that are similar to those observed in neurodegenerative diseases but in an age-dependent manner.

In addition to torpedoes being prevalent in diseased and aged brains, focal swellings on Purkinje cell axons that at least superficially resemble Purkinje cell torpedoes have been observed in the developing rat, with a transient peak observed from the second to third postnatal week of development (Gravel et al., 1986). Even less is known about the properties or functions of these so-called developmental torpedoes.

We use a transgenic mouse that expresses an enhanced GFP fused to tau (Sekirnjak et al., 2003), which brightly labels Purkinje cell axons (Watt et al., 2009), to characterize developmental Purkinje cell torpedoes in mice. We find that developmental torpedoes are observed in the second and third postnatal week of development, at ages after developmental Purkinje cell death has occurred, and the total number of Purkinje cells is static. Purkinje cell developmental torpedoes are seldom associated with a collateral branch point, and microglia are not enriched around developmental torpedoes, suggesting that they are not likely to be associated with axonal pruning. They do not stain for an inhibitory presynaptic marker, which suggests that they are not the presynaptic element of transient inhibitory synapses. Developmental torpedoes appear largely on myelinated axons and, like disease-related torpedoes, most are enriched with neurofilament, although a sizeable fraction of neurofilament-negative developmental torpedoes were also observed. Finally, we report that although Purkinje cells had elevated number of torpedoes in a mouse model of spinocerebellar ataxia type 6 in aged mice, we found no differences in the number of developmental torpedoes in these mice, or when motor deficits are first observed. Taken together, these results suggest that developmental torpedoes are not pathophysiological but rather represent a normal morphological Purkinje cell axonal feature during the formation of the cerebellar microcircuit.

MATERIALS AND METHODS

Animals and Slice Preparation

We used L7-tau-gfp mice (Sekirnjak et al., 2003; Watt et al., 2009) (generous gifts from both S. du Lac and M. Häusser), and C57BL6/J mice (purchased from Jackson laboratories, Bar Harbor, ME, USA) to characterize developmental torpedoes. For the SCA6$^{84Q/84Q}$ disease model we used transgenic mice harboring a humanized 84-CAG repeat tract in the mouse *Cacna1a* locus (Jackson laboratories; strain B6.129S7-Cacna1a^{tm3Hzo}/J; stock number: 008683) (Watase et al., 2008). Mice [postnatal day (P)5-P15] were anesthetized with isoflurane, sacrificed, and the brain was rapidly removed into ice-cold ACSF (in mM) 125 NaCl, 2.5 KCl, 2 CaCl2, 1 MgCl2, 1.25 NaH2PO4, 26 NaHCO3, and 20 glucose. Mice (P15 and older) were transcardially perfused with 4% PFA (EMS, Hatfield, PA, USA) and the brains were quickly removed. In some cases, P30 mice were anesthetized with isoflurane, sacrificed, and the brain was rapidly removed into an ice-cold partial sucrose replacement solution (in mM) 111 Sucrose, 50 NaCl, 2.5 KCl, 0.65 CaCl2, 10 MgCl2, 1.25 NaH2PO4, 25 NaHCO3, and 25 glucose. For mice of all ages, the brains extracted (as above) were then quickly transferred into 4% PFA (EMS, Hartfield, PA, USA), and stored at 4°C on a rotary shaker at 70 RPM for at least 48 h, then transferred to PBS with 0.05% sodium azide. Results were compared for tissue prepared with and without perfusion, but no significant changes were observed and this data was pooled.

The vermis of the cerebellum was then submerged in 0.05% sodium azide in 0.01 M PBS and sliced into 100 μm parasagittal slices on a Leica Vibratome 3000 plus (Concord, ON, Canada). The slices were stored at 4°C in 0.05% sodium azide in 0.01 M PBS. Animal procedures were approved by the McGill Animal Care Committee and conform to the guidelines set in place by the Canadian Council on Animal Care.

Immunocytochemistry

All staining was performed in a blocking solution with 5% BSA, 0.05% sodium azide, and 0.4% Triton X in 0.01 M PBS. The primary antibodies used were mouse anti-Neurofilament 200 kD (1:500, Millipore, Temecula, CA, USA; Cat. No.: MAB5266), mouse anti-Myelin Basic Protein (MBP; 1:500, Biolegend, San Diego, CA, USA; Cat. No.: 836501), rabbit anti-Green Fluorescent Protein (1:500, Millipore, Temecula, CA, USA; Cat. No.: AB3080P) (in P5 and P7 animals to amplify the GFP signal), guinea pig anti- (1:500, Cedarlane, Burlington, Ontario, Canada; Cat. No.: 131004(SY)) rabbit anti-Iba1 (1:500, Wako Chemicals, Osaka, Japan, Cat. No.: 019-19741), and rabbit anti-Calbindin D-28k (1:1000, Swant, Switzerland; Cat. No.: CB38). The slices were incubated in primary antibody at 4°C for 72 h on a rotary shaker at 70 RPM. Slices were then rinsed three times in a solution containing 0.4% Triton X in 0.01 M PBS.

The secondary antibodies were used at dilutions corresponding to the primary antibody. The secondary antibodies used were Alexa Fluor 594 donkey anti-rabbit (Jackson ImmunoResearch, West Grove, PA, USA; Cat. No.: 711-585-152), Alexa Fluor 488 donkey anti-mouse (Jackson ImmunoResearch; Cat. No.: 715-545-150), Alexa Fluor 594 donkey anti-guinea pig (Jackson ImmunoResearch; Cat. No.: 706-585-1480) and Alexa Fluor 594 donkey anti-mouse (Jackson ImmunoResearch; Cat. No.: 715-585-10). AffiniPure Fab Fragment donkey anti-mouse (Jackson ImmunoResearch; Cat. No.: 715-007-003) was used during secondary staining with antibodies made in mouse to avoid cross reactivity. The secondary staining was performed at 4°C for 90 min on a rotary shaker at 70 RPM. Slices were rinsed with 0.4% Triton X in 0.01 M PBS, mounted onto slides with Prolong Gold Antifade mounting media (Invitrogen), and stored in the dark at 4°C. Chemicals were purchased from Sigma unless otherwise indicated.

Imaging

Slices were imaged with a custom-built two-photon microscope with a Ti:Sapphire laser (MaiTai; Spectra Physics, Santa Clara, CA, USA) tuned to either 890 nm (GFP) or 775 nm (non-GFP). Image acquisition was done using ScanImage running in Matlab (Mathworks, Natick, MA, USA) (Pologruto et al., 2003). All imaging was done in lobule III of the cerebellar vermis. Whole lobule images (**Figure 1**) were obtained with a Leica upright fluorescent microscope using GFP filter.

Data Analysis

Image analysis was performed in ImageJ. Torpedo density was measured as number of torpedoes/number of Purkinje cells per acquisition when signal to noise was high. However, for very young slices and very old slices, we found that Calbindin labeling gave high background, and we thus counted the number of torpedoes/section instead. Torpedo length was measured as the distance from the beginning to the end of the swelling parallel to the axon. Torpedo width was measured perpendicular to the length, and close to the widest point of the swelling. Axial ratio was defined as the length/width of each torpedo. To compare the density of microglia around torpedoes and axons, a 25 μm $\times$ 25 μm box was centered around either Purkinje cell axonal torpedoes or Purkinje cell axons without neighboring torpedoes while viewing only the green (Purkinje cell label) channel. Switching to the red channel, the red-labeled microglia that were in the boxed region were counted. To strengthen our analytical power, we performed analysis in tandem for key findings, including developmental torpedo count. Two individuals analyzed data images independently, and results were found to be consistent across experimenter. Data was collected from equal number of acquisitions from at least three animals from a minimum of two litters (typically three) for each comparison.

Statistics

Data are reported as Mean $\pm$ SEM or as percentage of totals for distributions. Comparisons were made using one-tailed ANOVA tests followed by Tukey's HSD test for normal distributions in JMP software (SAS, Cary, NC, USA), or Student's *t*-tests in Igor Pro (Wavemetrics, Portland, OR, USA). For non-normal distributions, we used Wilcoxon/Kruskal–Wallis multiple comparison tests followed by the Benjamini–Hochberg procedure using a false discovery rate (FDR) of 0.05 in JMP software (SAS, Cary, NC, USA) or a Mann–Whitney *U* test in Igor Pro. Multiple-comparison corrections were performed with Excel scripts. *P*-values of <0.05 were considered significant.

RESULTS

Developmentally Transient Torpedoes on Axons of Purkinje Cells that Persist into Adulthood

Focal axonal swellings, or torpedoes, have been observed on the axons of developing Purkinje cell from postnatal rats (Gravel et al., 1986), and have been reported in developing mice (Baurle and Grusser-Cornehls, 1994). To characterize developmental axonal torpedoes found in the developing mouse cerebellum on Purkinje cell axons, we imaged Purkinje cell axons from several postnatal ages (**Figure 1A**) from L7-tau-GFP mice that express a tau-GFP fusion protein in Purkinje cells, resulting in strong axonal labeling, as previously described (Sekirnjak et al., 2003; Watt et al., 2009). To determine how prevalent developmental torpedoes were, we counted their numbers normalized to Purkinje cell number at several ages from both the apex and bank of anterior Lobule III of the vermis. We observed a rapid and transient increase in large focal axonal swellings, or developmental torpedoes, which were largely absent before P9, peaked at P11, and had decreased significantly by P30 (**Figures 1A,B**; P5: 7 torpedoes counted/702 Purkinje cells total, or 1.1 $\pm$ 0.44% normalized to acquisition, see "Materials and Methods" for details; P7: 16 torpedoes/690 Purkinje cells or 2.4 $\pm$ 1.1%; P9: 140 torpedoes/736 Purkinje cells, or 20.0 $\pm$ 4.5%; P11: 273 torpedoes/674 Purkinje cells, or 39.7 $\pm$ 2.5%; P13: 140 torpedoes/633 Purkinje cells, or 22.4 $\pm$ 4.3%; P15:

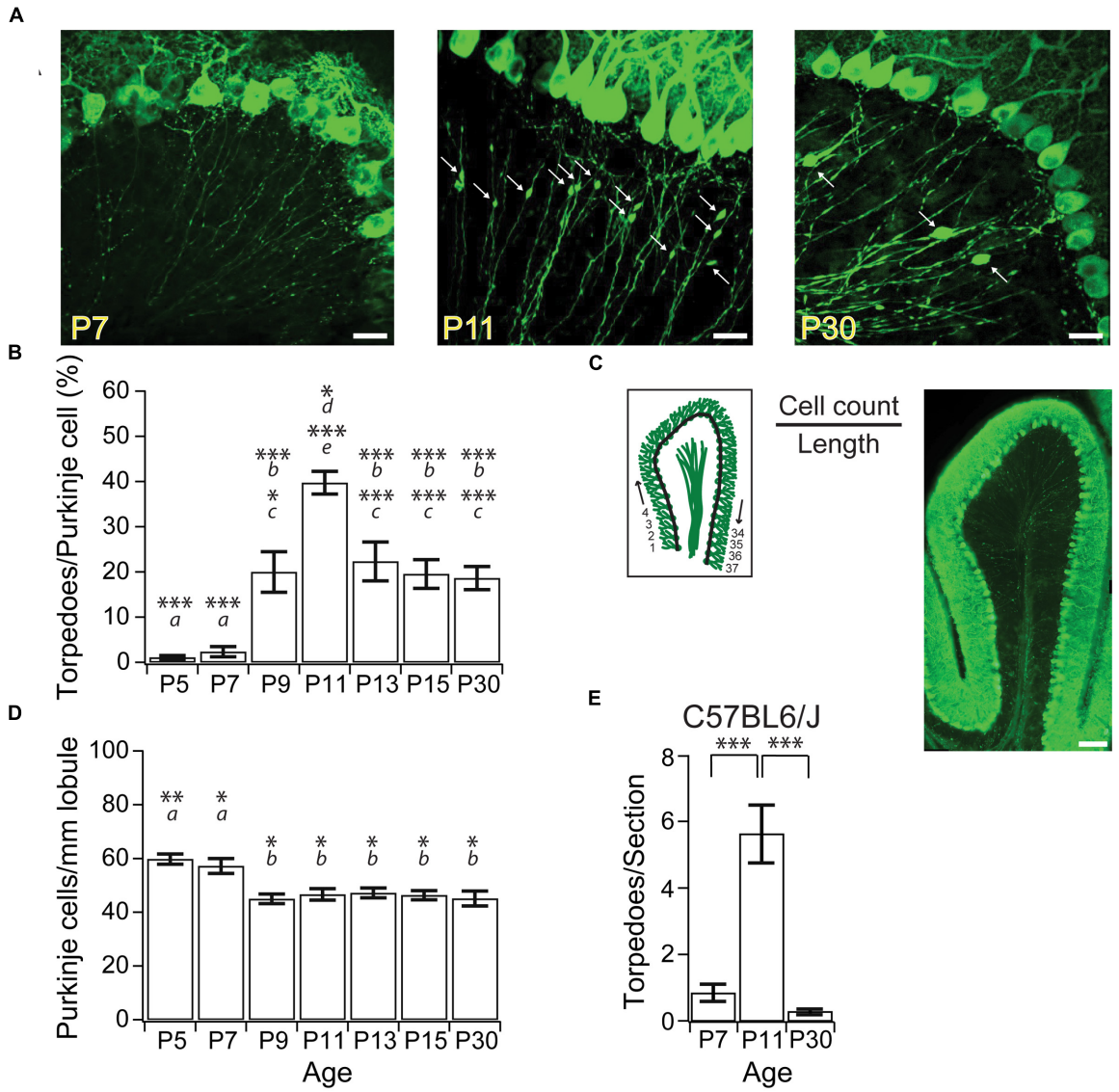

FIGURE 1 | Purkinje cell axonal torpedoes peak at P11 during postnatal mouse development. (A) Sample images highlighting Purkinje cell axons at P7 (left), P11 (middle), and P30 (right) from L7-tau-GFP mice. White arrows point to torpedoes. Note the abundance of Purkinje cell axon torpedoes at P11. Scale bar, 20 μm. **(B)** Summary data showing number of torpedoes peak at P11, with nearly 40% of Purkinje cell soma with a torpedo. Torpedoes are nearly absent during first week (P5-7) of development. Even at P30, there are a significant number of Purkinje cells that harbor axon torpedoes. **(C)** Left, illustration of how cell density measurements were taken. The number of Purkinje cells per length of lobule were counted for the entire Lobule III to calculate total Purkinje cell density, cell count/length. Right, sample image of sagittal slice through lobule III. Note that there are torpedoes present in the white matter that have not been included in our analysis. Scale bar, 100 μm. **(D)** Purkinje cell density (cells/mm lobule) in Lobule III is higher at P5 and P7, but remains constant after P9, consistent with reports that apoptosis is over by P9 in developing mouse Purkinje cells (Jankowski et al., 2009). **(E)** Torpedoes were also transiently enriched in P11 C57BL6/J wild-type (WT) cerebellum, and were low at both P7 and P30. Significance determined by Wilcoxon multiple comparisons followed by Benjamini–Hochberg procedure with the FDR of 0.05 for panel **(B,E)**; significance determined by one-way ANOVA followed by Tukey HSD test for panel **(D)**. Asterisks denote the minimum significance for comparisons where the letter denotes the relevant comparisons: ***a*** = significantly different from P9, P11, P13, P15, and P30; ***b*** = significantly different from P5 and P7; ***c*** = significantly different from P11; ***d*** = significantly different from P9; ***e*** = significantly different from P5, P7, P13, P15, and P30. All comparisons that are non-indicated are not significantly different, $P > 0.05$. *$P < 0.05$; **$P < 0.01$; ***$P < 0.005$.

145 torpedoes/766 Purkinje cells or 19.5 ± 3.2%; P30: 141 torpedoes/774 Purkinje cells, or 18.6 ± 2.6%). Developmental torpedoes could be observed along Purkinje cell axons in both the granule cell layer and white matter (**Figures 1A,C**); however, because of the bundling of the Purkinje cell axons in white matter, which makes individual axons and torpedoes difficult to resolve, we limited our analysis to Purkinje cell axons in the granule cell layer. Interestingly, although torpedoes were not observed in younger ages, Purkinje cell axons in the first postnatal week displayed multiple small varicosities, as previously reported

(Baurle and Grusser-Cornehls, 1994), which were distinguishable from torpedoes based on their smaller size (compare **Figure 1A**, left, middle). We thus restricted our analysis to developmental torpedoes, which showed a similar time course to those reported in rat (Gravel et al., 1986).

We wondered whether the transient changes in Purkinje cell torpedoes we observed were due to the presence of the tau-GFP protein in our transgenic mice, since tau is important for axonal integrity, and overexpressing tau can be pathological in Alzheimer Disease (Duan et al., 2012; Krstic and Knuesel, 2013). To determine whether our results were influenced by overexpression of tau, we examined Purkinje cell axons from C57BL6/J mice and counted the number of developmental torpedoes at three different ages: P7, P11, and P30 (**Figure 1E**; P7: 0.84 ± 0.26 torpedoes/section; P11: 5.6 ± 1.2 torpedoes/section; P30: 0.29 ± 0.08 torpedoes/section). Broadly speaking, we observed a similar shape in the developmental profile of torpedoes from C57BL6/J mice as in L7-tau-GFP mice, with a peak of torpedoes at P11 (significantly different from P7 and P30; $P < 0.0001$). These values are lower than corresponding torpedo counts from L7-tau-GFP mice (P7: 1.1 ± 0.42 torpedoes/section; P11: 18.4 ± 1.7 torpedoes/section; P30: 8.8 ± 1.2 torpedoes/section, data not shown). However, we cannot directly compare these values since image quality varies for calbindin antibody labeling and endogenous GFP expression, and it is possible that calbindin does not label all torpedoes. To address this, we processed a subset of L7-tau-GFP sections for calbindin and counted the number of torpedoes that we observed. Remarkably, we detected only 46.4% of torpedoes with calbindin compared to the same sections examined in the GFP channel ($N = 15$ sections). This suggests that either only a subset of torpedoes are labeled with calbindin, and/or we detect fewer torpedoes with immunocytochemistry due to poorer image quality. Thus, our data indicates that L7-tau-GFP is a good model to study developmental torpedoes because more torpedoes can be detected than with standard immunocytochemistry. Although it is possible that the presence of tau increases torpedo numbers in developing axons, this likely accounts for a relatively small proportion of torpedoes at these ages.

Purkinje cell axon torpedoes have been observed in diseased (Louis et al., 2006, 2009, 2014) and aged cerebellum (Baurle and Grusser-Cornehls, 1994), where they have often been associated with Purkinje cell death (Louis et al., 2014). We wondered whether developmental torpedoes might also be related to Purkinje cell death, since developmental apoptosis of Purkinje cells is a normal part of cerebellar development (Light et al., 2002; Jankowski et al., 2009). To address this question, we measured the number of Purkinje cells in a sagittal slice from an entire lobule III at several ages (**Figure 1C**), and found that Purkinje cell numbers were elevated at both P5 and P7, but remained constant after P9 (P5: 59.8 ± 1.9 Purkinje cells/mm; P7: 57.2 ± 2.8 Purkinje cells/mm; P9: $45.0 \pm 1.8 \times 10^{-2}$ Purkinje cells/mm; P11: 46.7 ± 2.1 Purkinje cells/mm; P13: 47.2 ± 1.8 Purkinje cells/mm; P15: 46.4 ± 1.7 Purkinje cells/mm; P30: 45.1 ± 2.7 Purkinje cells/mm; at least four whole-lobule images from four mice included at each age point). Our findings are in agreement with previous reports demonstrating that developmental Purkinje cell apoptosis peaks at P3 and is complete by P9 (Light et al., 2002; Jankowski et al., 2009). Our results argue that the majority of developmental torpedoes occur on axons of Purkinje cells that will persist into adulthood, since they appear after the peak of Purkinje cell apoptosis. However, the small fraction of torpedoes that appear at or before P9 might arise on axons of Purkinje cells that will undergo developmental apoptosis.

Developmental Torpedoes Are Unlikely to be Associated with Axonal Pruning

Purkinje cell axons extend collaterals that are extensively pruned during the second week of postnatal development (Gianola et al., 2003), and we wondered whether developmental torpedoes are associated with axonal collateral branch points. Collateral-associated torpedoes are structurally distinct, with a triangular rather than oval shape (**Figure 2A**). To address this, we counted how often Purkinje cell torpedoes were associated with an axon collateral (**Figures 2A,B**), and found that only a small fraction of torpedoes are located at collateral branch points (**Figures 2A,B**). Disease-related torpedoes have been characterized morphologically using the axial ratio measurement: length/width of torpedoes (Baurle and Grusser-Cornehls, 1994). We measured the length and width of torpedoes throughout postnatal mouse development (**Figure 2C**), and calculated their axial ratio (**Figure 2D**). We found that both the length and width of torpedoes increased with age (**Figure 2C**) while the axial ratio decreases from P15 onward (**Figure 2D**), suggesting that the torpedoes that persist after P11 increase in width more rapidly than they increase in length. Consistent with their different shape, the axial ratio of the collateral-branch-point-associated triangular torpedoes is significantly lower than non-collateral associated oval torpedoes (**Figure 2E**). Thus, developmental axonal torpedoes are typically not associated with axonal collaterals, and are structurally dynamic across development.

Could Purkinje cell torpedoes be associated with sites of axonal remodeling without being directly associated with a branch point? For example, could the swelling of a torpedo mark where a recent axonal collateral has been pruned? To address this, we examined the localization of activated microglia in the granule cell layer, which have been associated with axonal refinement and pruning during development (Pont-Lezica et al., 2011), and can be recruited to axonal swellings (di Penta et al., 2013; Kato et al., 2016). We looked at two ages: at P11, the peak of developmental torpedo density, and at P30 (**Figure 3A**), when torpedoes are larger but less numerous. We found that microglia density in the granule cell layer increased significantly over this period (**Figure 3B**; P11: 6.52 ± 0.37 cells/10^6 μm^3; P30: 7.71 ± 0.44 cells/10^6 μm^3; significantly different, $P = 0.045$), likely because microglia density throughout the cerebellum overall increases across development (Perez-Pouchoulen et al., 2015). To determine whether microglia were enriched around torpedoes, which might suggest that they are involved in axonal refinement, we measured the local density of microglia around torpedoes (**Figure 3C**) and compared this density to that around Purkinje cell axons that are not in the

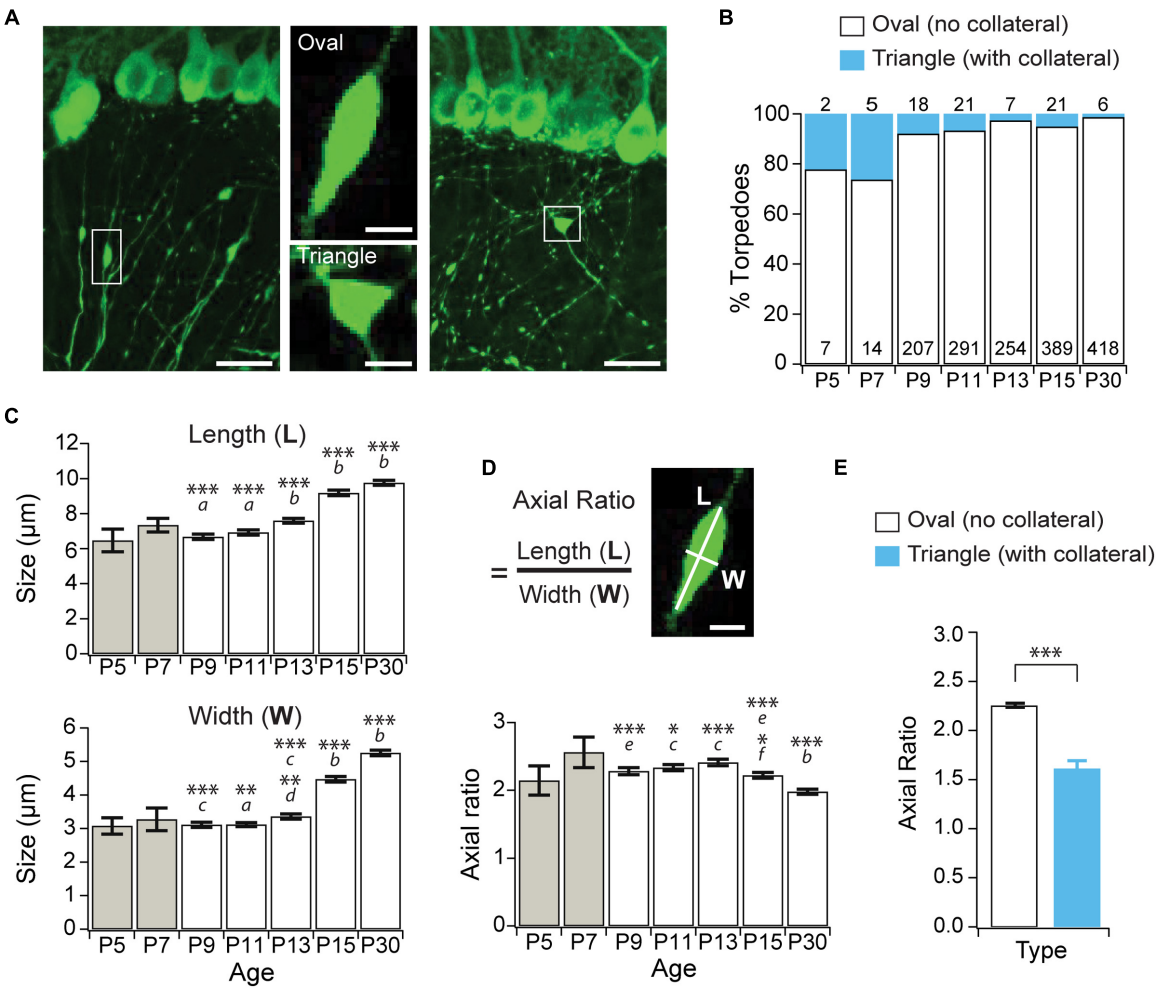

FIGURE 2 | Purkinje cell developmental torpedoes are seldom associated with axonal branch points. (A) Left: sample image showing oval-shaped axonal torpedo (inset, middle top); and right: triangle-shaped torpedo associated with axonal collateral branch point (inset, middle bottom). Scale bar for left and right images, 20 μm; scale bar for insets in middle, 5 μm. **(B)** The majority of torpedoes are not associated with collateral branch points (white bars), with only a subset associated with collaterals (blue bars) at all ages. Number of torpedoes counted indicated in (white) or above (cyan) bars. **(C)** Torpedo length (top) and width (bottom) increased after P13. **(D)** The axial ratio (length, *L*/width, *W*) significantly decreased at P15 and P30 because torpedo width increased more than length at these ages. Scale bar, 5 μm. **(E)** The axial ratio is significantly lower in triangle torpedoes associated with axon collateral branch points than in oval-shaped torpedoes that are not associated with branch points. Note that because there are so few torpedoes at P5 and P7 **(B)**, these ages were not included in the analysis in panels **(C,D)**. They are included in the graph for reference (gray bars). Significance determined by Wilcoxon multiple comparisons followed by Benjamini–Hochberg procedure with the FDR = 0.05 for panels **(C,D)**, and with a Mann–Whitney *U* test for panel **(E)**. Asterisks denote the minimum significance for comparisons where the letter denotes the relevant comparisons: ***a*** = significantly different from P13, P15, and P30; ***b*** = significantly different from all other ages; ***c*** = significantly different from P15, and P30; ***d*** = significantly different from P11; ***e*** = significantly different from P30. ***f*** = significantly different from P11 and P13. All comparisons that are non-indicated are not significantly different, $P > 0.05$. *$P < 0.05$, **$P < 0.01$; ***$P < 0.001$.

proximity of a torpedo (**Figure 3C** shows two examples for each). We found no significant enrichment of microglia around torpedoes compared to axons at either the peak age of torpedo enrichment, P11 (**Figure 3D**, left; P11 torpedo: 25/51 or 49.0% have 0 microglia in proximity, 20/51 or 39.2% are near 1 microglia, and 6/51 or 11.8% are near 2 microglia; P11 axon: 29/51, or 56.9% have 0 microglia in proximity, 21/51 or 41.2% are near 1 microglia, and 1/51 or 1.9% are near 2 microglia; not significantly different $P = 0.84$) or later when torpedoes are less prevalent but larger, P30 (**Figure 3D**, right; P30 torpedo: 11/45 or 24.4% have 0 microglia in proximity, 26/45 or 57.8% are near 1 microglia, and 8/45 or 17.8% are near 2 microglia; P30 axon: 14/48, or 56.9% have 0 microglia in proximity, 28/48 or 58.3% are near 1 microglia, and 6/48 or 12.5% are near 2 microglia; not significantly different $P = 0.84$). Taken together, our findings suggest that torpedoes are unlikely to be associated with axonal damage or refinement.

Developmental Torpedoes Are Unlikely to be Presynaptic Terminals

Some neurons, such as hippocampal dentate gyrus granule cells, have striking focal axonal swellings along their axons that

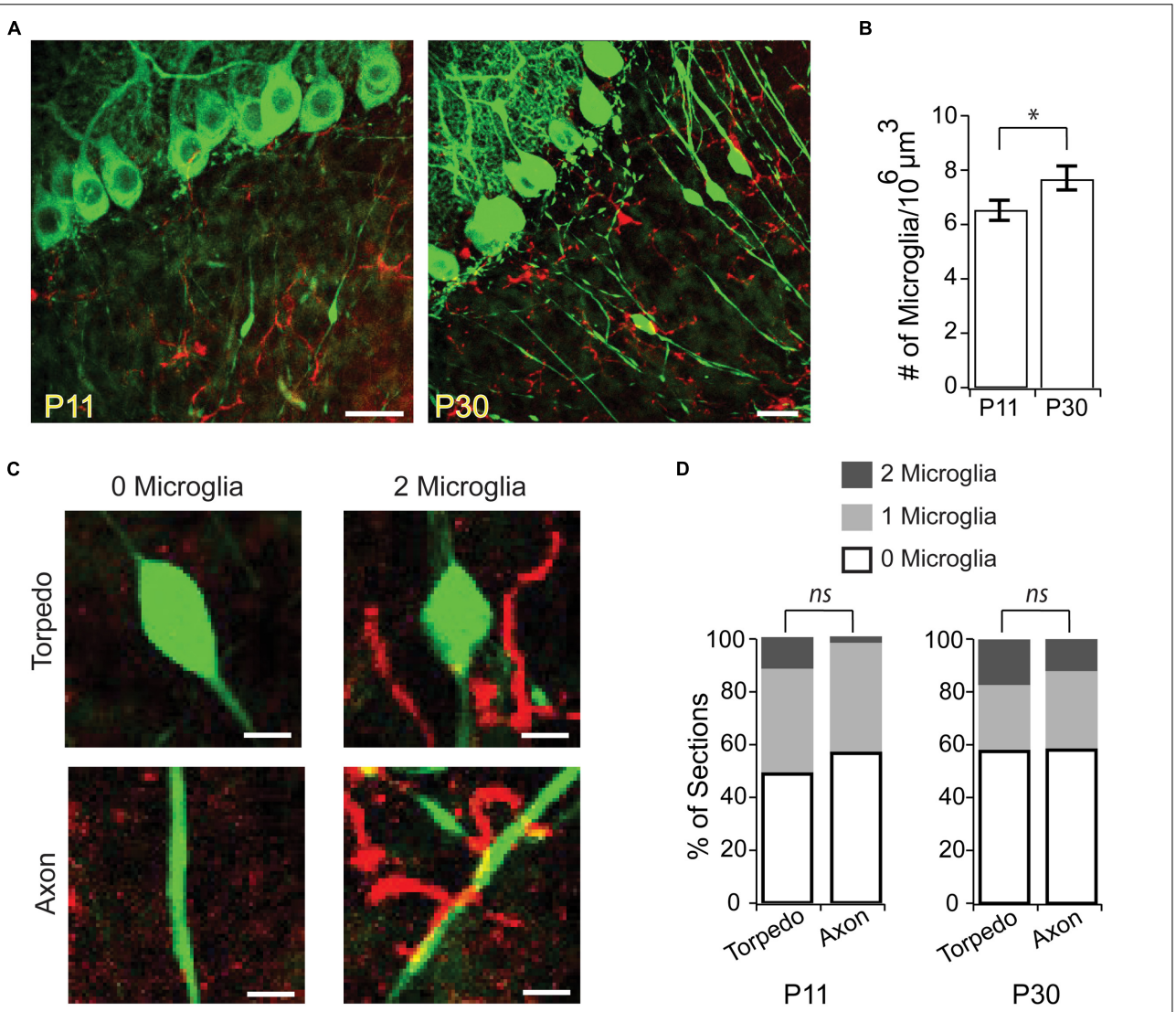

FIGURE 3 | Microglia are not enriched around developmental torpedoes. (A) Sample images from P11 (left) and P30 (right) of Purkinje cells and their axons (green, eGFP), and activated microglia (red, Alexa 594). Scale bar, 20 μm. **(B)** The density of activated microglia increases in the developing granule cell layer between P11 and P30. **(C)** Sample images highlighting how analysis was done. After identifying stretches of axon with torpedoes (top) or without torpedoes (bottom) in the green channel, the red channel was added and the number of nearby microglia (within a 25 μm^3 box centered on the torpedo or axon) were counted: merged examples show 0 microglia (left) and 2 microglia (right). Scale bar, 5 μm. **(D)** Number of microglia in the vicinity of torpedo or axon, from 0 to 2 microglia/section (white–gray). No significant differences were observed between microglia density around torpedoes or non-torpedo axons at either P11 (left; $P = 0.84$), or P30 (right; $P = 0.84$). Significance determined by Student's *t*-test **(B)** or Mann–Whitney *U* test **(D)**. $^*P < 0.05$, *ns* $P > 0.05$.

are the morphological correlates of large presynaptic terminals (Chamberland et al., 2014). These large presynaptic terminals bear a resemblance to Purkinje cell axonal torpedoes. Although ultrastructure analysis of disease-related Purkinje cell axonal torpedoes reveals that they do not contain vesicles (Petito et al., 1973; Yagishita, 1978; Mann et al., 1980; Louis et al., 2009), suggesting that they are not presynaptic release sites, we wondered whether developmental Purkinje cell axonal torpedoes might be the presynaptic structure of a transient synapse that functions during postnatal development. Interestingly, Purkinje cells form transient synapses onto other Purkinje cells during postnatal development (Watt et al., 2009), and transient synapses are thought to be a common feature of developing brain circuits (van Welie et al., 2011), and can also be found in other cerebellar neurons (Trigo et al., 2010). To examine whether developmental torpedoes were axon terminals containing vesicles, we used immunolabeling for vesicular GABA transporter (VGAT; **Figure 4A**) (Watt et al., 2009), and quantified the number of torpedoes that colocalized with this presynaptic marker (**Figures 4A,B**). We found that the vast majority (>80%) of Purkinje cell torpedoes were negative for VGAT staining, both at P11 and P30 (**Figure 4B**; P11: 54/62, or 87.1% of torpedoes were VGAT negative; P30: 124/144, or 86.1% of torpedoes were VGAT negative, not significantly different, $P = 0.62$),

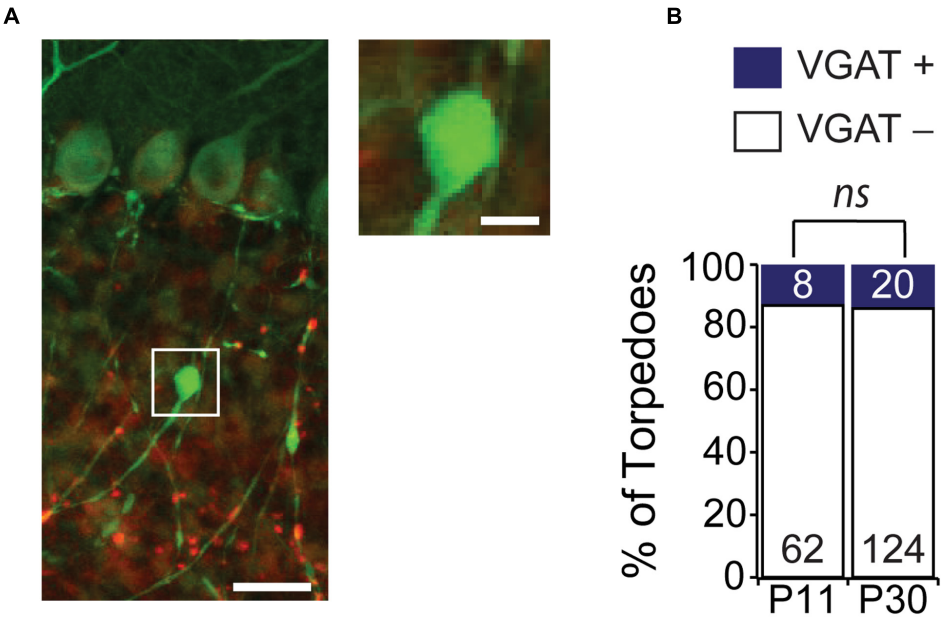

FIGURE 4 | Purkinje cell torpedoes unlikely to be presynaptic terminals. (A) Sample image of Purkinje cell with torpedo (green) that is co-stained with the presynaptic inhibitory terminal marker VGAT (red). Inset shows that torpedo does not label for VGAT. Scale bar for left image, 20 μm; scale bar for insets to right, 5 μm. **(B)** The vast majority of torpedoes at both P11 and P30 are not positive for VGAT (white bars) with only a subset having any VGAT labeling nearby (VGAT+, blue bars), suggesting that they are unlikely to be presynaptic terminals. Number of torpedoes (N) counted is indicated in bars. Significance determined by Mann–Whitney *U* test, *ns* $P > 0.05$.

which suggests that like disease-related torpedoes, developmental torpedoes do not appear to be inhibitory presynaptic terminals.

Structural Distinctions between Developmental and Disease-Related Torpedoes

An understanding of Purkinje cell developmental torpedo function is currently unknown. Since the myelination of Purkinje cell axons is underway during the second postnatal week of development (Gianola et al., 2003), at the age when developmental torpedoes are prevalent, we wondered whether developmental torpedoes occur on myelinated or unmyelinated axons. To examine this, we used MBP to identify myelin, and examined whether torpedoes were surrounded by myelin (MBP+) or not (MBP−; **Figures 5A,B**), at P11, the peak of torpedo density, and at P30, when torpedo numbers are decreased and when Purkinje cell axons are expected to be fully myelinated (Gianola et al., 2003). We found that the vast majority of torpedoes at P11 (102/122, or 85%) and at P30 (78/81, or 96%) were myelinated (**Figure 5B**), with no significant difference in the percentage of non-myelinated axons across ages ($P = 0.13$). While we considered any local enrichment of MBP to be positive for myelin, we typically observed torpedoes to have good myelin coverage (**Figure 5C** shows three successive z-stack images). This suggests that action potential conductance may not be hindered in developing axons by the presence of a developmental axonal torpedo, although it is possible that we missed subtle changes in myelin that could affect propagation. We found no significant differences in the length ($P = 0.41$), width ($P = 0.60$), or axial ratio ($P = 0.62$) of myelinated or unmyelinated torpedoes at P11 (there were too few non-myelinated torpedoes to compare at P30), suggesting that these torpedoes are not distinct subpopulations. Rather, whether a developmental torpedo is myelinated or not is likely to depend on whether its parent axon is myelinated or not, and not on the torpedo. The high percentage of developmental torpedoes that are myelinated is in contrast to what is observed for disease-related torpedoes, which although occurring on both myelinated or non-myelinated axons, (Yagishita, 1978; Takeuchi et al., 1995; Louis et al., 2009), disease-related torpedoes are typically more common on non-myelinated axons (Louis et al., 2009).

One striking feature of disease-related torpedoes that has been observed in several diseases is that they are enriched in disorganized neurofilament (Petito et al., 1973; Yagishita, 1978; Mann et al., 1980; Louis et al., 2009), which may be associated with alterations in axonal transport. We wondered whether developmental torpedoes also contained neurofilament. To address this, we labeled neurofilament 200 kD (NF) and counted the torpedoes that were positive (NF+) and negative (NF−) at both P11 and P30 (**Figure 6A**). At the peak of Purkinje cell torpedo density at P11, although the majority of Purkinje cell axon torpedoes were NF+ (51/80, or 64% of torpedoes), there was a significant fraction that were not (29/80, or 36%; **Figure 6B**). Sometimes neurofilament positive and negative torpedoes were next to each other on the same axon (**Figure 6A**, inset), suggesting that these two types of torpedoes may have distinct functions that are locally determined. Consistent with this, NF+

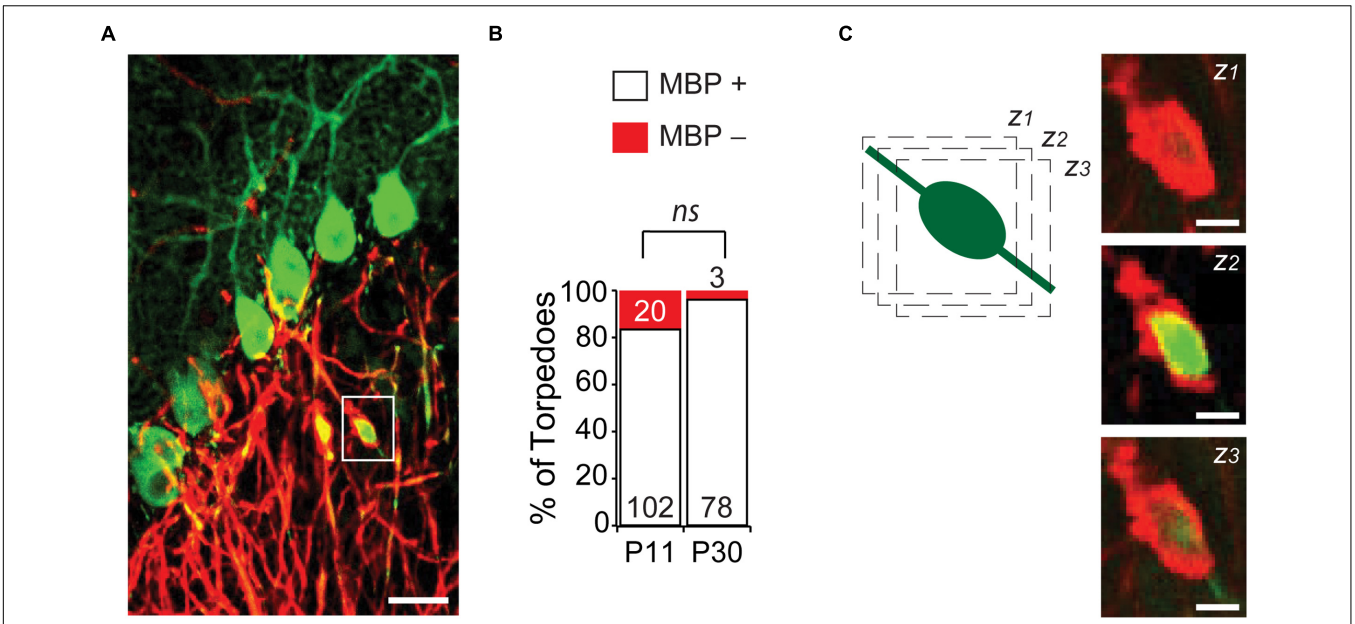

FIGURE 5 | Most developmental torpedoes are myelinated. (A) Sample image showing Purkinje cells and axons (green) as well as myelin basic protein (MBP; red). Scale bar, 20 μm. **(B)** The vast majority of torpedoes at both P11 and P30 are positive for MBP (white bars), with only a fraction negative for MBP (red). Number of torpedoes (N) is indicated in or above each bar. **(C)** Successive z-stack images (z_{1-3}) of region highlighted in panel **(A)**, highlighting that myelin appears to fully wrap around Purkinje axon developmental torpedo. Scale bar, 5 μm. Significance determined by Mann–Whitney *U* test, *ns* $P > 0.05$.

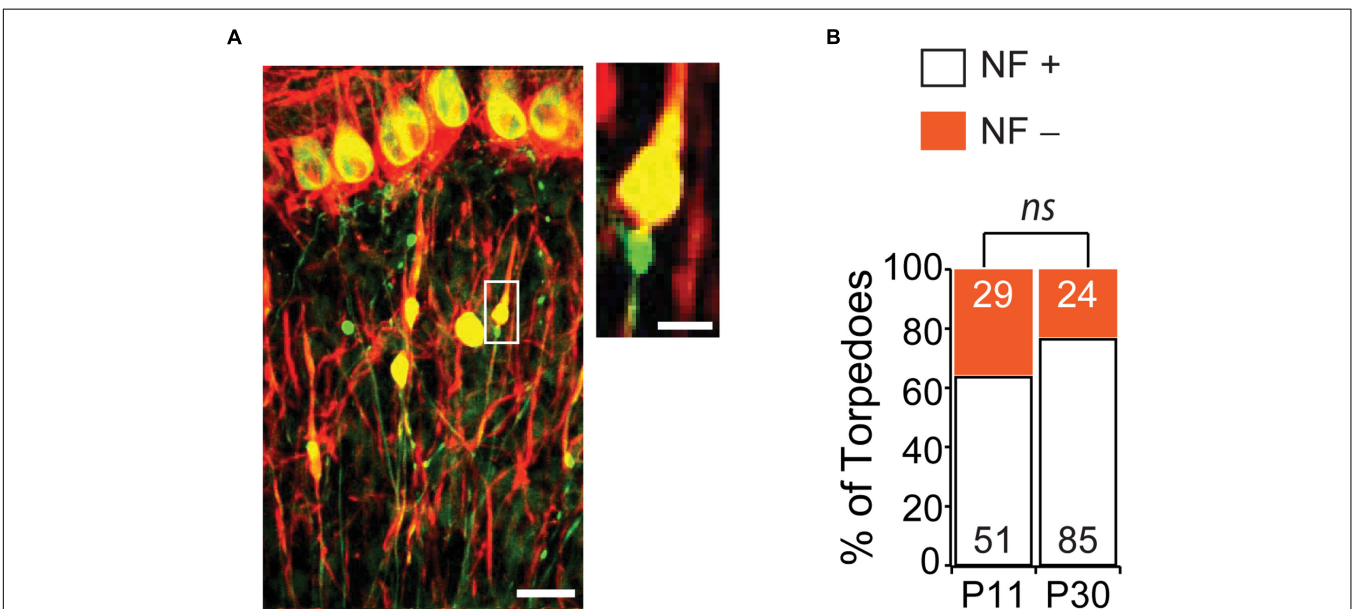

FIGURE 6 | The majority of Purkinje cell torpedoes contain neurofilament (NF). (A) Sample image showing Purkinje cells and their axons (green) and neurofilament (red). Co-labeling appears yellow. Most torpedoes are neurofilament (NF) positive, although some are not. Inset shows even neighboring torpedoes on the same axon can be NF+ and NF−. Scale bar in left image, 20 μm; Scale bar in inset, 5 μm. **(B)** Quantification of NF+ (white bars) and NF− (orange bars) at P11 and P30. A sizeable minority of torpedoes are NF−, especially at P11, suggesting that there may be two populations of developmental torpedoes. Significance determined by Mann–Whitney *U* test, *ns* $P > 0.05$.

torpedoes were significantly larger than NF− torpedoes (NF+ length: 7.6 ± 0.3 μm; NF− length: 6.1 ± 0.2 μm; significantly different, $P = 0.0001$; NF+ width: 3.4 ± 0.2 μm; NF− width 2.7 ± 0.1 μm; significantly different, $P = 0.0007$). Later in development at P30, the proportion of NF+ torpedoes had increased slightly although not significantly from P11 (NF+: 85/109, or 78% of torpedoes; NF−: 24/109, or 22% of torpedoes; not significantly different from P11, $P = 0.09$). Similar to what

was observed at P11, NF+ torpedoes were also larger than NF− at P30 (NF+ length: 8.9 ± 0.3 μm; NF− length: 7.5 ± 0.6 μm; significantly different, $P = 0.036$; NF+ width: 4.7 ± 0.2 μm; NF− width: 3.5 ± 0.3 μm; significantly different, $P = 0.003$). These data raise the possibility that there may be functional subpopulations of developmental torpedoes, with the majority staining positive for neurofilament, and a significant minority that do not, in contrast to reports of disease-related torpedoes, where neurofilament accumulation in torpedoes is robust (Petito et al., 1973; Yagishita, 1978; Mann et al., 1980; Louis et al., 2009). An alternate explanation is that that the distinction between NF+ and NF− torpedoes is less distinct, with a continuum of neurofilament content in torpedoes ranging from low to high, rather than two separate populations.

Recent studies have identified changes in basket cell innervation of Purkinje cells that contain axonal torpedoes in disease states (Erickson-Davis et al., 2010; Kuo et al., 2013). Since basket cell innervation of Purkinje cells is maturing during postnatal development (Ichikawa et al., 2011), we thought that such changes might be associated with developmental torpedoes as well. We identified Purkinje cell neurons that had axonal torpedoes on their axon and examined the extent of basket cell innervation of the parent Purkinje cell [**Figure 7A** shows examples of low (score = 1), medium (score = 3), and high (score = 5) degree of innervation], and compared this with similar neighboring neurons that did not have a torpedo on their proximal axon, using neurofilament labeling to measure basket cell innervation density, since basket cell processes contain neurofilament (Erickson-Davis et al., 2010). In contrast to what has been observed in essential tremor-related torpedoes (Erickson-Davis et al., 2010; Kuo et al., 2013), we found no differences between axonal-torpedo-containing Purkinje cells and those without axonal torpedoes, with both groups being similarly innervated by basket cell processes (**Figures 7B,C**; average basket cell innervation density, scored in arbitrary units from 1 to 5, of Purkinje cells with torpedoes: 2.23 ± 0.26; $N = 13$; average basket cell innervation of Purkinje cells without torpedoes: 2.23 ± 0.28; $N = 13$; not significantly different, $P = 0.92$). Aberrant basket cell innervation of Purkinje cells harboring disease-related axonal torpedoes suggests that circuit rewiring is associated with those neurons. In contrast, our results suggest that developmental torpedoes are not associated with differences in rewiring, but rather appear normally during normal development. Thus, although morphologically similar, there appears to be differences between developmental and disease-related torpedoes.

Normal Developmental Torpedoes in a Mouse Model of SCA6

To understand whether a relationship exists between developmental and disease-related torpedoes, we examined Purkinje cell axons at several time points in a mouse model of SCA6, since torpedoes have been seen in postmortem tissue from SCA6 patients (Sasaki et al., 1998; Yang et al., 2000). We used $SCA6^{84Q/84Q}$ mice harboring an expanded polyglutamine (poly-Q) repeat which have been shown to display ataxic symptoms at 7 months old (Watase et al., 2008; Jayabal et al., 2015). We have previously shown that there is no Purkinje cell loss at 7 months when disease symptoms are first observed, although Purkinje cell loss is detectable at 2 years (Jayabal et al., 2015). We first wondered whether disease-related torpedoes would be observed in these mice at 2 years. To address this, we labeled Purkinje cells with calbindin (**Figure 8A**) and counted the number of torpedoes we observed on Purkinje cell axons in both $SCA6^{84Q/84Q}$ and litter-matched wild-type (WT) controls. We found that torpedo number was greatly increased at 2-years in $SCA6^{84Q/84Q}$ compared to WT mice as predicted from human postmortem studies (2 year WT: 1.09 ± 0.27 torpedoes/section; 2 year $SCA6^{84Q/84Q}$: 4.48 ± 0.68 torpedoes/section; significantly different, $P < 0.0001$) (Sasaki et al., 1998; Yang et al., 2000). Interestingly, we have recently shown that transient functional and morphological changes occur during postnatal development in the developing $SCA6^{84Q/84Q}$ cerebellum at the age when we observe developmental torpedoes (Jayabal et al., 2016b). This led us to wonder whether developmental torpedoes might be altered in these mice as well, since this might suggest that they are related to later pathophysiology. We found, however, that developmental torpedo density was normal in P11 $SCA6^{84Q/84Q}$ mice compared to WT, suggesting that they are not directly related to later pathophysiology (P11 WT: 2.71 ± 0.90 torpedoes/section; P11 $SCA6^{84Q/84Q}$: 2.61 ± 0.54 torpedoes/section; not significantly different, $P = 0.92$; **Figure 8B**, left). We also measured the density of Purkinje cell torpedoes in $SCA6^{84Q/84Q}$ and litter-matched mice at 7 months, when cerebellar-related motor deficits are observed without detectable Purkinje cell loss (Jayabal et al., 2015, 2016a), and found that torpedo density was low at 7 months and similar in both WT and $SCA6^{84Q/84Q}$ mice (7 month WT: 0.57 ± 0.20 torpedoes/section; 7 month $SCA6^{84Q/84Q}$: 0.42 ± 0.13 torpedoes/section; not significantly different; $P = 0.53$; **Figure 8B**, middle). Note that we observe higher torpedo numbers in P11 mice than 7-month-old mice in both WT and $SCA6^{84Q/84Q}$ mice, which is consistent with our observations of a transient developmental peak of torpedoes at P11 (**Figure 1**). These data suggest that developmental torpedoes are unlikely to be linked to later disease-related torpedoes and do not by themselves contribute to later pathogenesis. They furthermore suggest that disease-related torpedoes are not an early symptom of SCA6, but rather are observed later during disease progression, at the same time as Purkinje cell loss.

DISCUSSION

We observed Purkinje cell axonal torpedoes that occurred in the developing mouse cerebellum of both L7-tau-GFP and C57Bl6/J mice, peaking at P11. These torpedoes appear similar to the developmental torpedoes that have been observed in developing rat cerebellum (Gravel et al., 1986). We showed that developmental Purkinje cell axonal torpedoes occur almost exclusively after developmental cell death has occurred when the total density of Purkinje cells was static in Lobule III. Purkinje cell developmental torpedoes were seldom associated with an axon collateral branch point, and microglia were not enriched near

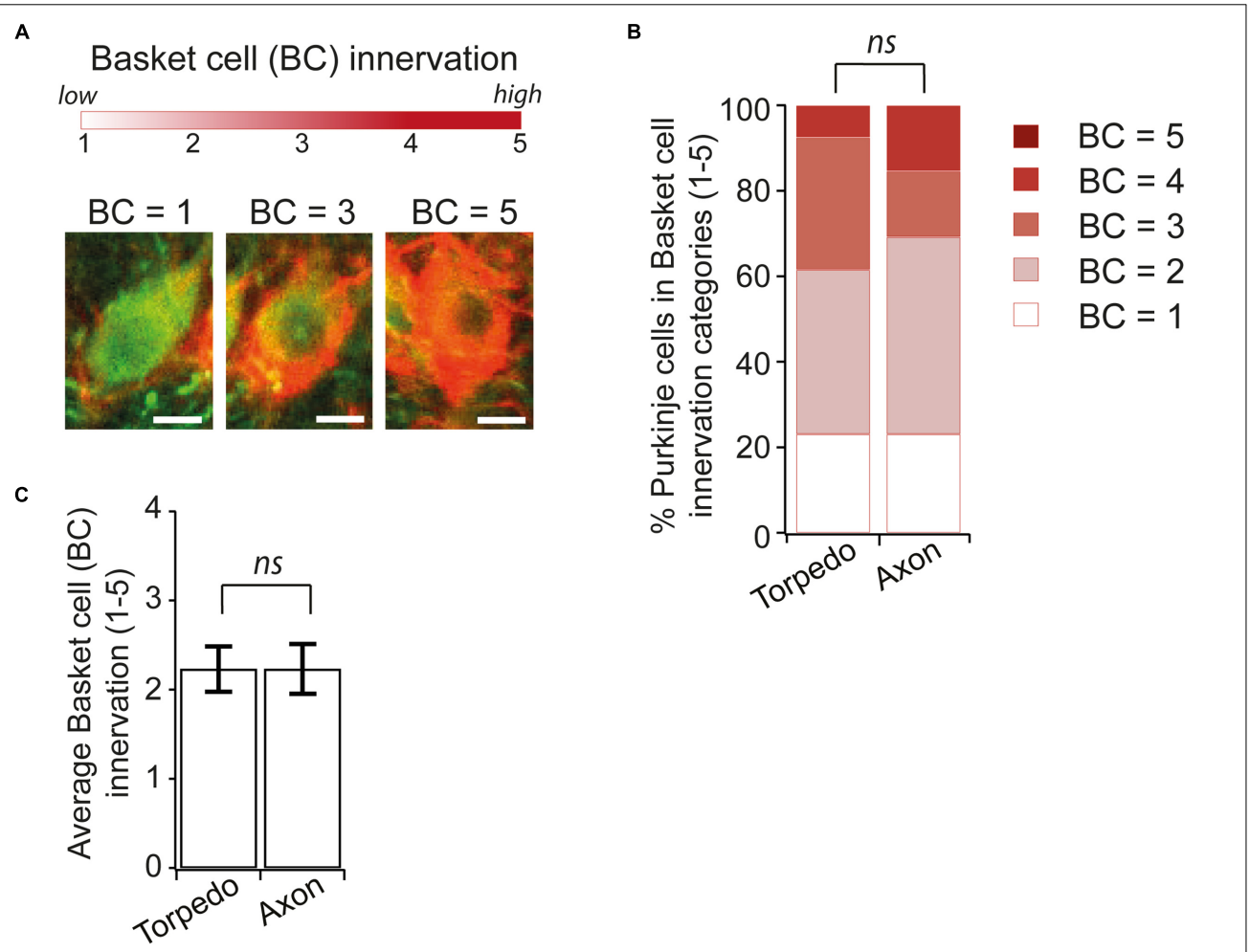

FIGURE 7 | Similar Basket cell innervation of Purkinje cells with and without developmental torpedoes. (A) We are analyzing the extent of Basket cell (BC) innervation on individual Purkinje cell somata, where BC = 1 is low, and BC = 5 is high innervation. Sample images showing representative Purkinje cells (green) innervated by Basket cells (labeled red for neurofilament) for low (BC = 1), medium (BC = 3) and high (BC = 5) innervation. Scale bar, 5 μm. **(B)** We traced torpedoes back to their parent Purkinje cell and measured the innervation of BC cells with and without a torpedo on their axon (Torpedo and axon, respectively). % of Purkinje cell with different basket cell innervation was similar in both cases. **(C)** The average Purkinje cell innervation by Basket cells was not significantly different when a torpedo was or was not present (Torpedo: $N = 13$; Axon: $N = 13$; not significantly different, Mann–Whitney U test, $P = 0.92$). *ns* $P > 0.05$.

developmental torpedoes, suggesting that they are not likely to be associated with axonal pruning. The majority of developmental torpedoes did not label for an inhibitory presynaptic marker, which suggests that they are not the presynaptic element of synapses. Like torpedoes associated with diseases, we found that developmental torpedoes were myelinated and most were enriched with neurofilament, although the presence of a sizeable fraction of non-neurofilament containing torpedoes suggests that there may be two subpopulations of developmental torpedoes. This will be interesting to explore in future studies. Finally, we report that although aged Purkinje cells display disease-related torpedoes in a mouse model of SCA6, we see no differences in the number of developmental torpedoes in these mice, nor are disease-related torpedoes elevated during early disease stages when motor deficits are first observed. Taken together, these results suggest that developmental torpedoes are not pathophysiological in SCA6 mice but rather represent a normal transient morphological feature during the formation of the cerebellar microcircuit.

What function might transient developmental torpedoes serve in the cerebellum? Our findings of neurofilament accumulation in a subset of developmental torpedoes which appear mostly on myelinated axons, suggest that they are involved in normal axonal function, and do not interfere with axonal propagation, for instance, although functional studies are necessary to test this directly. While developmental torpedoes may serve a role in axonal refinement, which is underway at the time point that they are observed (Gianola et al., 2003), the absence of microglia enrichment around developmental torpedoes, and absence of enrichment at axonal collateral branch points argues against this, or at least suggests that their role in axonal refinement is complex. It is thus premature to speculate what role developmental

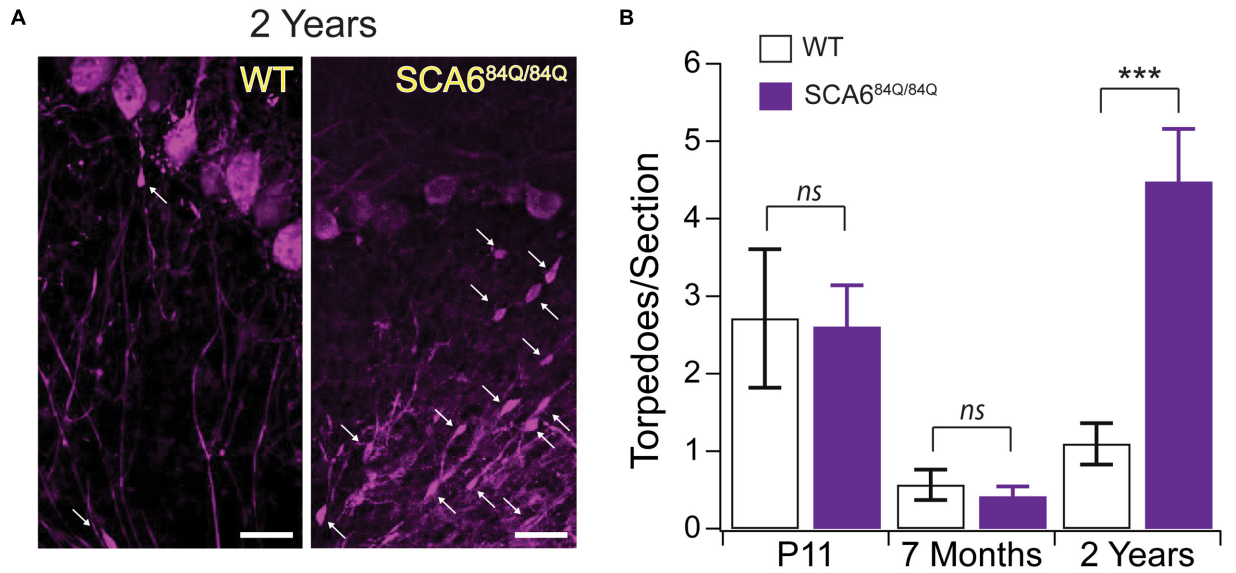

FIGURE 8 | Developmental torpedoes appear normal in SCA6$^{84Q/84Q}$ mice that later develop disease-related torpedoes. (A) Sample images of Purkinje cells (purple, labeled with calbindin) from 2-year-old WT (left) and litter-matched SCA6$^{84Q/84Q}$ mice that have more disease-related Purkinje cell axonal torpedoes. White arrows point to torpedoes. Scale bar, 20 μm. **(B)** Although the number of Purkinje cell axonal torpedoes are high in SCA6$^{84Q/84Q}$ mice (purple) compared to WT mice (white bars) at an age when Purkinje cell death is observed (right) (Jayabal et al., 2015), there are no statistically significant differences in the number of torpedoes observed during development at P11 in these mice (left), and torpedo numbers are low in 7-month-old mice when disease symptoms first appear (middle) (Jayabal et al., 2015). These results suggest that developmental torpedoes are not directly related to disease-related torpedoes, as they appear at normal levels in late-onset disease models. Significance determined by Student's *t*-test, ***$P < 0.001$, *ns* $P > 0.05$.

torpedoes play, although our evidence suggests that they are not occurring on Purkinje cells that undergo developmental apoptosis. Further studies will be needed to elucidate their function.

Why do developmental torpedoes appear transiently a few days after birth and then decrease during a few postnatal weeks of development? The age at which torpedoes occur is a time of great restructuring in the developing cerebellum (McKay and Turner, 2005; van Welie et al., 2011; Hashimoto and Kano, 2013; White and Sillitoe, 2013). Several such transient changes have been identified in developing brain circuits that are thought to be involved in its proper development, including transient depolarization by GABAergic innervation (Ben-Ari, 2001, 2002), and transient electrical synapses (Fulton, 1995). Indeed, just in the developing cerebellum, transient presynaptic miniature currents (Trigo et al., 2010), and transient Purkinje – Purkinje synapses that mediate early network activity [(Watt et al., 2009) but see (Witter et al., 2016)] have been shown. Thus, developmental torpedoes appear to represent a normal morphological specialization during the development of Purkinje cell axons. It will be interesting to determine the temporal properties of developmental torpedoes: how long they persist on an axon, whether they are mobile or not, and what triggers their appearance and disappearance on an axon, since this may give us deeper insight into their function.

Superficially, developmental torpedoes appear to resemble disease-related torpedoes, since they have similar morphology, both contain neurofilament, and both occur on myelinated or unmyelinated axons. It is thus possible that similar physiological conditions exist transiently during development and in several diseases cause similar axonal structures in these conditions. However, careful analysis of developmental torpedoes suggests that there are differences between them and disease-related torpedoes that may be functionally meaningful. For instance, while to our knowledge the accumulation of neurofilament in disease-related torpedoes is robust, we see a significant minority of developmental torpedoes that do not appear to contain neurofilament, and these torpedoes were smaller, suggesting that our population of developmental torpedoes is heterogenous and may have distinct functions. However, an alternate explanation would suggest that there exist torpedoes with a range of neurofilament from low to high, rather than two distinct populations, which would suggest that developmental torpedoes may not be distinct from disease-related torpedoes in this manner. In the disease literature, disease-related torpedoes are most commonly observed on non-myelinated axons (Yagishita, 1978; Louis et al., 2009), which is in stark contrast to our developmental torpedoes, where most torpedoes are myelinated, yet another apparent difference between developmental and disease-related torpedoes. Interestingly, disease-related torpedoes are associated with enhanced basket cell inhibitory input onto the parent Purkinje cell (Erickson-Davis et al., 2010; Kuo et al., 2013), which we thought might also occur for developmental torpedoes since basket cell innervation is forming at the ages when developmental torpedoes are observed (Ichikawa et al., 2011). However, we observed no differences in the extent of basket cell innervation between Purkinje cells with torpedoes and without. This suggests

that torpedoes may not affect the cerebellar microcircuit to the same extent as disease-related torpedoes. Given the differences existing in the cerebellar microcircuit during development and during disease, it seems more likely that these superficially similar morphological structures have different properties and serve different functions. In a similar vein, although disease-related torpedoes are observed in several diseases, there is evidence that they may have distinct properties in different diseases (Louis et al., 2014). It remains possible, however, that the differences we have identified do not strongly influence cerebellar function and that the similarities between developmental and disease-related torpedoes are enough to produce similar functional consequences. Future experiments are required to resolve this question.

Are developmental torpedoes, which closely resemble disease-related torpedoes, somehow involved in cellular pathophysiology? Our data in normal L7-tau-GFP and C57Bl6/J mice suggest that they are not, but we wanted to address this by examining developmental torpedoes in a disease model that shows enhanced disease-related torpedoes at later ages. We used a mouse model of SCA6 that we have previously characterized in our lab to address this. These mice show initial motor symptoms at 7 months, which progressively worsen (Jayabal et al., 2015). Purkinje cell death is not observed at 7 months, but is seen at 2-years-old (Jayabal et al., 2015). We found that although disease-related torpedoes were highly enriched in 2-year-old mice when Purkinje cell death was observed, there were no differences in torpedo numbers at P11, suggesting that developmental torpedoes are not related to later disease-onset torpedoes. Interestingly, torpedo numbers were elevated at P11 compared to 7 months, consistent with the existence of a transient developmental peak in these mice. Although disease-related torpedoes are likely to differ in different diseases (Louis et al., 2014), but these results suggest that developmental torpedoes are normal and non-pathological, since they appear at normal levels in a mouse that later shows high levels of disease-related torpedoes at old age.

At present, we lack a good understanding of the function of torpedoes, and how they act in Purkinje cells. Interestingly, careful analysis of disease-related torpedoes in essential tremor brains reveals that these structures are simply one of a number of related morphometric changes occurring in Purkinje cells (Babij et al., 2013), suggesting that although perhaps the most notable morphological change, they may not be the most salient change for cerebellar function. What role developmental torpedoes play in circuit formation remains to be seen, but our findings argue that it is not a pathological role. One interpretation of our data suggests that there may be different populations of developmental torpedoes, which might thus serve more than one function in the developing brain. To understand the role of developmental torpedoes, we will need to have a deeper understanding of their functional properties and how they contribute to cerebellar development.

AUTHOR CONTRIBUTIONS

LL performed immunocytochemistry, collected and analyzed the data, made figures, and helped to write the manuscript, DL-O performed immunocytochemistry, collected and analyzed the data, and helped to write the manuscript, AY performed immunocytochemistry and analyzed the data, SJ prepared tissue, collected and analyzed the data, and helped to write the manuscript, SQ performed immunocytochemistry and analyzed the data, and AW analyzed the data, made figures, and wrote the manuscript.

FUNDING

This work was funded by a CFI Leaders Opportunity Fund 29127 (AW), a CIHR operating grant, MOP-299921 (AW), and an FRQNT Nouveau-Chercheur grant (AW).

ACKNOWLEDGMENTS

We thank S. du Lac and M. Hausser for the generous gift of the L7-tau-GFP mice, which originated in S. du Lac's lab. We thank D. Dankort for the use of his Leica upright fluorescent microscope to generate whole lobule images, as shown in **Figure 1C**, and R. Krahe for the use of his Leica Vibratome 3000. We thank K. Murai and W. T. Farmer for help with immunocytochemistry. We thank A. McKinney, J. Sjöström, A. Fournier, E. Ruthazer, H. Durham, B. Brais, R. Larivière, V. Ady, B. Toscano Marquez, A. Metzger, M. Nath, S. Quilez, C. Rosen, and M. Virdee for useful discussions about this project.

REFERENCES

Babij, R., Lee, M., Cortes, E., Vonsattel, J. P., Faust, P. L., and Louis, E. D. (2013). Purkinje cell axonal anatomy: quantifying morphometric changes in essential tremor versus control brains. *Brain* 136, 3051–3061. doi: 10.1093/brain/awt238

Baurle, J., and Grusser-Cornehls, U. (1994). Axonal torpedoes in cerebellar Purkinje cells of two normal mouse strains during aging. *Acta Neuropathol.* 88, 237–245. doi: 10.1007/BF00293399

Ben-Ari, Y. (2001). Developing networks play a similar melody. *Trends Neurosci.* 24, 353–360. doi: 10.1016/S0166-2236(00)01813-0

Ben-Ari, Y. (2002). Excitatory actions of gaba during development: the nature of the nurture. *Nat. Rev. Neurosci.* 3, 728–739. doi: 10.1038/nrn920

Bouman, L. (1918). *Die Histopathologie Der Psychosen*. Amsterdam: Springer.

Chamberland, S., Evstratova, A., and Toth, K. (2014). Interplay between synchronization of multivesicular release and recruitment of additional release sites support short-term facilitation at hippocampal mossy fiber to CA3 pyramidal cells synapses. *J. Neurosci.* 34, 11032–11047. doi: 10.1523/JNEUROSCI.0847-14.2014

di Penta, A., Moreno, B., Reix, S., Fernandez-Diez, B., Villanueva, M., Errea, O., et al. (2013). Oxidative stress and proinflammatory cytokines contribute to demyelination and axonal damage in a cerebellar culture model of neuroinflammation. *PLoS ONE* 8:e54722. doi: 10.1371/journal.pone.0054722

Duan, Y., Dong, S., Gu, F., Hu, Y., and Zhao, Z. (2012). Advances in the pathogenesis of Alzheimer's disease: focusing on tau-mediated neurodegeneration. *Transl. Neurodegener.* 1:24. doi: 10.1186/2047-9158-1-24

Erickson-Davis, C. R., Faust, P. L., Vonsattel, J. P., Gupta, S., Honig, L. S., and Louis, E. D. (2010). "Hairy baskets" associated with degenerative Purkinje cell changes in essential tremor. *J. Neuropathol. Exp. Neurol.* 69, 262–271. doi: 10.1097/NEN.0b013e3181d1ad04

Fulton, B. P. (1995). Gap junctions in the developing nervous system. *Perspect. Dev. Neurobiol.* 2, 327–334.

Gianola, S., Savio, T., Schwab, M. E., and Rossi, F. (2003). Cell-autonomous mechanisms and myelin-associated factors contribute to the development of Purkinje axon intracortical plexus in the rat cerebellum. *J. Neurosci.* 23, 4613–4624.

Gravel, C., Leclerc, N., Plioplys, A., and Hawkes, R. B. (1986). Focal axonal swellings in rat cerebellar Purkinje cells during normal development. *Brain Res.* 363, 325–332. doi: 10.1016/0006-8993(86)91018-8

Hashimoto, K., and Kano, M. (2013). Synapse elimination in the developing cerebellum. *Cell Mol. Life Sci* 70, 4667–4680. doi: 10.1007/s00018-013-1405-2

Hirano, A., Dembitzer, H. M., Ghatak, N. R., Fan, K. J., and Zimmerman, H. M. (1973). On the relationship between human and experimental granule cell type cerebellar degeneration. *J. Neuropathol. Exp. Neurol.* 32, 493–502. doi: 10.1097/00005072-197310000-00002

Ichikawa, R., Yamasaki, M., Miyazaki, T., Konno, K., Hashimoto, K., Tatsumi, H., et al. (2011). Developmental switching of perisomatic innervation from climbing fibers to basket cell fibers in cerebellar Purkinje cells. *J. Neurosci.* 31, 16916–16927. doi: 10.1523/JNEUROSCI.2396-11.2011

Jankowski, J., Miething, A., Schilling, K., and Baader, S. L. (2009). Physiological purkinje cell death is spatiotemporally organized in the developing mouse cerebellum. *Cerebellum* 8, 277–290. doi: 10.1007/s12311-009-0093-9

Jayabal, S., Chang, H. H. V., Cullen, K. E., and Watt, A. J. (2016a). 4-Aminopyridine alleviates ataxia and reverses cerebellar output deficiency in a mouse model of spinocerebellar ataxia type 6. *Sci. Rep.* 6, 29489. doi: 10.1038/srep 29489

Jayabal, S., Ljungberg, L., Erwes, T., Cormier, A., Quilez, S., El Jaouhari, S., et al. (2015). Rapid onset of motor deficits in a mouse model of spinocerebellar ataxia type 6 precedes late cerebellar degeneration. *eNeuro* 2, 1–18. doi: 10.1523/ENEURO.0094-15.2015

Jayabal, S., Ljungberg, L., and Watt, A. J. (2016b). Transient cerebellar alterations during development prior to obvious motor phenotype in a mouse model of spinocerebellar ataxia type 6. *J. physiol.* doi: 10.1113/JP273184 [Epub ahead of print].

Kato, G., Inada, H., Wake, H., Akiyoshi, R., Miyamoto, A., Eto, K., et al. (2016). Microglial contact prevents excess depolarization and rescues neurons from excitotoxicity. *eNeuro* 3, 1–9. doi: 10.1523/ENEURO.0004-16.2016

Kato, T., and Hirano, A. (1985). A Golgi study of the proximal portion of the human Purkinje cell axon. *Acta Neuropathol.* 68, 191–195. doi: 10.1007/BF00688636

Krstic, D., and Knuesel, I. (2013). Deciphering the mechanism underlying late-onset Alzheimer disease. *Nat. Rev. Neurol.* 9, 25–34. doi: 10.1038/nrneurol.2012.236

Kuo, S. H., Tang, G., Louis, E. D., Ma, K., Babji, R., Balatbat, M., et al. (2013). Lingo-1 expression is increased in essential tremor cerebellum and is present in the basket cell pinceau. *Acta Neuropathol.* 125, 879–889. doi: 10.1007/s00401-013-1108-7

Lariviere, R., Gaudet, R., Gentil, B. J., Girard, M., Conte, T. C., Minotti, S., et al. (2015). Sacs knockout mice present pathophysiological defects underlying autosomal recessive spastic ataxia of Charlevoix-Saguenay. *Hum. Mol. Genet.* 24, 727–739. doi: 10.1093/hmg/ddu491

Light, K. E., Belcher, S. M., and Pierce, D. R. (2002). Time course and manner of Purkinje neuron death following a single ethanol exposure on postnatal day 4 in the developing rat. *Neuroscience* 114, 327–337. doi: 10.1016/S0306-4522(02)00344-5

Louis, E. D., Faust, P. L., Ma, K. J., Yu, M., Cortes, E., and Vonsattel, J. P. (2011). Torpedoes in the cerebellar vermis in essential tremor cases vs. controls. *Cerebellum* 10, 812–819. doi: 10.1007/s12311-011-0291-0

Louis, E. D., Kuo, S. H., Vonsattel, J. P., and Faust, P. L. (2014). Torpedo formation and Purkinje cell loss: modeling their relationship in cerebellar disease. *Cerebellum* 13, 433–439. doi: 10.1007/s12311-014-0556-5

Louis, E. D., Vonsattel, J. P., Honig, L. S., Ross, G. W., Lyons, K. E., and Pahwa, R. (2006). Neuropathologic findings in essential tremor. *Neurology* 66, 1756–1759. doi: 10.1212/01.wnl.0000218162.80315.b9

Louis, E. D., Yi, H., Erickson-Davis, C., Vonsattel, J. P., and Faust, P. L. (2009). Structural study of Purkinje cell axonal torpedoes in essential tremor. *Neurosci. Lett.* 450, 287–291. doi: 10.1016/j.neulet.2008.11.043

Mann, D. M., Stamp, J. E., Yates, P. O., and Bannister, C. M. (1980). The fine structure of the axonal torpedo in Purkinje cells of the human cerebellum. *Neurol. Res.* 1, 369–378. doi: 10.1080/01616412.1980.11739567

McKay, B. E., and Turner, R. W. (2005). Physiological and morphological development of the rat cerebellar Purkinje cell. *J. Physiol.* 567, 829–850. doi: 10.1113/jphysiol.2005.089383

Perez-Pouchoulen, M., VanRyzin, J. W., and McCarthy, M. M. (2015). Morphological and phagocytic profile of microglia in the developing rat cerebellum(1,2,3). *eNeuro* 2. doi: 10.1523/ENEURO.0036-15.2015

Petito, C. K., Hart, M. N., Porro, R. S., and Earle, K. M. (1973). Ultrastructural studies of olivopontocerebellar atrophy. *J. Neuropathol. Exp. Neurol.* 32, 503–522. doi: 10.1097/00005072-197310000-00003

Pioro, E. P., and Cuello, A. C. (1988). Purkinje cells of adult rat cerebellum express nerve growth factor receptor immunoreactivity: light microscopic observations. *Brain Res.* 455, 182–186. doi: 10.1016/0006-8993(88)90131-X

Pologruto, T. A., Sabatini, B. L., and Svoboda, K. (2003). ScanImage: flexible software for operating laser scanning microscopes. *Biomed. Eng. Online* 2, 13. doi: 10.1186/1475-925X-2-13

Pont-Lezica, L., Bechade, C., Belarif-Cantaut, Y., Pascual, O., and Bessis, A. (2011). Physiological roles of microglia during development. *J. Neurochem.* 119, 901–908. doi: 10.1111/j.1471-4159.2011.07504.x

Ramon, Y., and Cajal, S. (1991). *Cajal's Degeneration and Regeneration of the Nervous System*. New York, NY: Oxford University Press.

Rossi, F., Borsello, T., and Strata, P. (1994). Exposure to kainic acid mimics the effects of axotomy in cerebellar Purkinje cells of the adult rat. *Eur. J. Neurosci.* 6, 392–402. doi: 10.1111/j.1460-9568.1994.tb00282.x

Sarna, J. R., and Hawkes, R. (2011). Patterned Purkinje cell loss in the ataxic sticky mouse. *Eur. J. Neurosci.* 34, 79–86. doi: 10.1111/j.1460-9568.2011.07725.x

Sasaki, H., Kojima, H., Yabe, I., Tashiro, K., Hamada, T., Sawa, H., et al. (1998). Neuropathological and molecular studies of spinocerebellar ataxia type 6 (SCA6). *Acta Neuropathol.* 95, 199–204. doi: 10.1007/s004010050787

Sekirnjak, C., Vissel, B., Bollinger, J., Faulstich, M., and du Lac, S. (2003). Purkinje cell synapses target physiologically unique brainstem neurons. *J. Neurosci.* 23, 6392–6398.

Sotelo, C. (1990). Axonal abnormalities in cerebellar Purkinje cells of the 'hyperspiny Purkinje cell' mutant mouse. *J. Neurocytol.* 19, 737–755. doi: 10.1007/BF01188042

Takahashi, N., Iwatsubo, T., Nakano, I., and Machinami, R. (1992). Focal appearance of cerebellar torpedoes associated with discrete lesions in the cerebellar white matter. *Acta Neuropathol.* 84, 153–156. doi: 10.1007/BF00311388

Takeuchi, I. K., Aoki, E., and Takeuchi, Y. K. (1995). Axonal swellings in cerebellar white matter of groggy mutant rat. *Acta Neuropathol.* 90, 486–492. doi: 10.1007/BF00294810

Trigo, F. F., Bouhours, B., Rostaing, P., Papageorgiou, G., Corrie, J. E., Triller, A., et al. (2010). Presynaptic miniature GABAergic currents in developing interneurons. *Neuron* 66, 235–247. doi: 10.1016/j.neuron.2010.03.030

van Welie, I., Smith, I. T., and Watt, A. J. (2011). The metamorphosis of the developing cerebellar microcircuit. *Curr. Opin. Neurobiol.* 21, 245–253. doi: 10.1016/j.conb.2011.01.009

Volk, B., and Kirchgassner, N. (1985). Damage of Purkinje cell axons following chronic phenytoin administration: an animal model of distal axonopathy. *Acta Neuropathol.* 67, 67–74. doi: 10.1007/BF00688125

Watase, K., Barrett, C. F., Miyazaki, T., Ishiguro, T., Ishikawa, K., Hu, Y., et al. (2008). Spinocerebellar ataxia type 6 knockin mice develop a progressive neuronal dysfunction with age-dependent accumulation of mutant CaV2.1 *channels. Proc. Natl. Acad. Sci. U.S.A.* 105, 11987–11992. doi: 10.1073/pnas.0804350105

Watt, A. J., Cuntz, H., Mori, M., Nusser, Z., Sjöström, P. J., and Häusser, M. (2009). Traveling waves in developing cerebellar cortex mediated by asymmetrical Purkinje cell connectivity. *Nat. Neurosci.* 12, 463–473. doi: 10.1038/nn.2285

White, J. J., and Sillitoe, R. V. (2013). Development of the cerebellum: from gene expression patterns to circuit maps. *Wiley Interdiscip. Rev. Dev. Biol.* 2, 149–164. doi: 10.1002/wdev.65

Witter, L., Rudolph, S., Pressler, R. T., Lahlaf, S. I., and Regehr, W. G. (2016). Purkinje cell collaterals enable output signals from the cerebellar cortex to feed back to Purkinje cells and interneurons. *Neuron* 91, 312–319. doi: 10.1016/j.neuron.2016.05.037

Yagishita, S. (1978). Morphological investigations on axonal swellings and spheroids in various human diseases. *Virchows Arch. A Pathol. Anat. Histol.* 378, 181–197. doi: 10.1007/BF00427359

Yang, Q., Hashizume, Y., Yoshida, M., Wang, Y., Goto, Y., Mitsuma, N., et al. (2000). Morphological Purkinje cell changes in spinocerebellar ataxia type 6. *Acta Neuropathol.* 100, 371–376. doi: 10.1007/s004010000201

Conflict of Interest Statement: The authors declare that the research was conducted in the absence of any commercial or financial relationships that could be construed as a potential conflict of interest.

ANNEX II

Title: Purkinje cell axonal swellings enhance axonal action potential fidelity and cerebellar function

Authors list: Daneck Lang-Ouellette, François G. C. Blot, Chloe Stewart, Pauline de Vanssay de Blavous, Connie H. Li, Carter Van Eitrem, Charlotte Rosen, Martijn Schonewille, and Alanna J. Watt

Under review at: Nature Communications

Date: August 2020

Purkinje cell axonal swellings enhance action potential fidelity and cerebellar function.

Daneck Lang-Ouellette[1], François G. C. Blot[2], Chloe A. Stewart[1,3], Pauline de Vanssay de Blavous[1], Connie H. Li[1], Carter Van Eitrem[1], Charlotte Rosen[1], Phyllis L. Faust[4], Martijn Schonewille[2], and Alanna J. Watt[1*]

[1]Biology Department, McGill University, Montreal, QC, Canada.

[2]Erasmus University Medical Center, Rotterdam, ZH, Netherlands.

[3]Integrated Neuroscience Program, McGill University, Montreal, QC, Canada.

[4]Department of Pathology and Cell Biology, Columbia University, New York, NY, United States.

*Correspondence: alanna.watt@mcgill.ca

Abstract

Axonal plasticity allows neurons to control their output, which critically determines the flow of information in the brain. Axon diameter can be regulated by activity, yet an understanding of how morphological changes in an axonal structure impact its function remains poorly understood. Axonal swellings have been found on Purkinje cell axons in the cerebellum both in healthy development and in neurodegenerative diseases where they have been thought to contribute to axonal pathophysiology. Here we report that Purkinje cell axons with swellings propagated action potentials with higher fidelity than those without, and that axonal swellings form when axonal failures are high. Furthermore, we observed that healthy young adult mice with more axonal swellings learned better on cerebellar-related tasks than mice with fewer swellings. Our findings suggest that axonal swellings underlie a novel form of axonal plasticity that optimizes the fidelity of action potential propagation in axons, resulting in enhanced learning.

Keywords

Axon, morphology, plasticity, Purkinje cell, cerebellum, two-photon imaging, light-sheet imaging, action potential, spike failures, motor learning, torpedoes.

Introduction

Information is transmitted in the nervous system primarily by action potentials traveling along axons. This means that a neuron's ability to maintain high-fidelity axonal propagation is of fundamental importance for its function[1]. Indeed, instances when axonal propagation is delayed or interrupted can produce devastating consequences. For example, in multiple sclerosis (MS), axonal

impairments resulting from the break-down of myelin that surrounds axons lead to severe sensory and motor symptoms. Conversely, alterations in axonal structure can also be adaptive: for example, neurons respond to elevated levels of activity by restructuring their axon initial segment (AIS) to homeostatically regulate their excitability[2].

Since Purkinje cell axons carry information out of the cerebellar cortex, changes in the structure of their axons could impact cerebellar function dramatically. Purkinje cell axonal swellings appear transiently during cerebellar development[3,4] and are observed during normal aging[5], including in healthy human samples[6,7]. These data suggest that axonal swellings play a physiological role in the brain. However, axonal swellings have also been associated with axon dysfunction in several neurodegenerative diseases[8-11], indicating that axonal swellings may be implicated in pathological function. Likewise, computational modeling has proposed that axonal swellings serve a pathophysiological role, as models predict that action potentials will be delayed, filtered, or fail when propagating across an axonal swelling[12-14].

To determine the impact of axonal swellings on Purkinje cell axonal function, we performed visually-targeted dual recordings from the soma and axon of individual Purkinje cells from young mice, and found that Purkinje cell axonal failures were reduced in axons with swellings. In other words, axonal propagation was more reliable when swellings were present. Pharmacologically mimicking high levels of axonal failures led to the formation of focal axonal swellings, and we uncovered that their formation is Ca^{2+}-dependent and requires Ca^{2+} entry through voltage-gated Ca^{2+} channels. Finally, by examining cerebellar-related behavior, we observed that mice exhibiting higher levels of cerebellar learning had higher numbers of axonal swellings. These data suggest that the enhancement of action potential propagation associated with axonal swellings in healthy young animals positively impacts behaviour.

Results

Action potential propagation is enhanced in axons with swellings

Purkinje cell axonal swellings are present in healthy developing rodents[4] and are also observed in several neurodegenerative diseases[8-11]. However, functional measurements of the impact of axonal swellings on axons have been lacking. We used dual targeted loose-patch recordings with fluorescently-tagged Quantum dot-coated glass electrodes[15] to measure action potentials simultaneously in Purkinje cell somata and axons (**Fig. 1a**) in acute brain slices prepared from the cerebellar vermis of juvenile, healthy transgenic mice expressing GFP in Purkinje cells, including in their axons[16,17]. Since computational models suggest that axonal swellings increase axonal failure rates[13], we monitored action potential failures in Purkinje cells with and without focal axonal swellings (**Fig. 1b**). Approximately 30% of axons display swellings at this age[4], and the vast majority of these were single swellings (98.7%; **Supplementary Fig. 1**), which we targeted for our recordings of axonal swellings. Axons without swellings were recorded as control axons at similar distances from the soma (**Supplementary Fig. 2; Supplementary Table 1**). Surprisingly, we found that the axonal failure rate in Purkinje cells with swellings was significantly lower than that in Purkinje cells without axonal swellings (Control Axon: 6.07 ± 1.36 per 1000 spike; n = 11; Axon with Swelling: 1.12 ± 0.41 per 1000 spike; n = 9; Mann Whitney *U* test, P = 0.002; **Fig. 1c**). A large proportion of axons with swellings propagated action potentials with very high fidelity (having very few axonal failures), whereas only the occasional axon without a swelling propagated with similar fidelity (9.1% of control axons were high-fidelity; 55.5% of axons with swellings were high-fidelity; Mann Whitney *U* test, P = 0.05; **Fig. 1d**). We found no differences in the propagation speed in axons with swelling and control axons, suggesting that

swellings do not change the propagation speed of action potentials, or at least not over the relatively short distances that we have measured (**Supplementary Fig. 2; Supplementary Table 1**). Taken together, these data argue that axonal swellings enhance rather than impair axonal propagation.

We wondered whether firing properties would differ in Purkinje cells with axonal swellings, since changes in Purkinje cell firing properties are observed in diseases where Purkinje cell axon swellings are observed[18-21]. We found that Purkinje cells with axonal swellings fired action potentials at rates that were indistinguishable from those with axons without swellings and observed no changes in regularity (**Supplementary Fig. 3**). Furthermore, we observed no relationship between baseline firing rate and axonal failure rate for axons with or without swellings (**Supplementary Fig. 3**). This was surprising because axonal failures are enhanced when Purkinje cell firing is driven at extremely high frequencies (> 250 Hz)[22-24]. This observation suggests that baseline axonal failure rate is regulated in a manner that is distinct from the processes that contribute to axonal failures at high frequencies.

To examine axonal swellings in greater detail, we studied their ultrastructure by imaging anterior lobules of cerebellar vermis with transmission electron microscopy (TEM; from N = 7 mice). We identified 15 myelinated spheroid-shaped structures with smallest diameters greater than 4 μm as putative axonal swellings (**Fig. 2a, b;** swelling diameter average = 8.1 μm; range from 4.1 to 11.8 μm). We found no evidence of presynaptic or postsynaptic specializations, confirming that axonal swellings are not presynaptic terminals or specialized postsynaptic structure for axo-axonal synapses. Axonal swellings were myelinated and we fortuitously found two instances where an axonal swelling had intact flanking axonal segments (one example shown in **Fig. 2a**) which revealed that the myelin surrounding the axonal swelling was similar to that around flanking axons.

Occasionally, we observed perinodal protrusions proximal to an axonal swelling (**Fig. 2a**, white asterisk), which agrees with our findings that about half of axonal swellings are near the paranodal protein CASPR (contactin-associated protein 1; n = 58 axonal swellings; **Supplementary Fig. 4**), suggesting that swellings are frequently found close to paranodal junction, and therefore are proximal to nodes of Ranvier. Additionally, we occasionally observed periaxonal oligodendrocyte cytoplasm associated with axonal swellings (**Fig. 2a** cyan box inset, observed in ~20% of swellings), as has been previously described[25]. Although the function of specialized oligodendrocytic structures like perinodal protrusions is poorly understood, it suggests that axonal swellings may preferentially form close to them. Given that perinodal and internodal structures play a role in saltatory conduction[26], our results suggest that oligodendrocytic specialization and perinodal protrusions proximal to axonal swellings may contribute to enhanced action potential propagation in Purkinje cell axons.

TEM revealed that axonal swellings are rich in intracellular organelles including mitochondria and endoplasmic reticulum (ER) (**Fig. 2a, b** yellow box inset). We also found that the majority (~80 %) of axonal swellings were positive for ER-located IP3R (inositol 1,4,5-trisphosphate receptors) using immunocytochemistry (**Supplementary Fig. 5**), as previously reported[27]. Furthermore, the majority of axonal swelling contained close co-localization of ER and mitochondria (**Fig. 2b** yellow box inset), which has been linked to axonal repair in peripheral axons[28]. Surprisingly, we did not observe a significant enrichment in the density of intracellular organelles in axonal swellings compared to control axons (**Fig. 2c; Supplementary Table 1**), although dense packing of organelles has been reported for axonal swellings in disease models[29], suggesting that swellings in healthy and diseased brains differ in their subcellular composition. Even without enrichment, however, all swellings contained intracellular organelles such as mitochondria and ER, which may

lead to specialized biochemical signaling which could contribute to the enhancement of action potential propagation that we have observed (**Fig. 1**).

A distinguishing morphological feature of disease-related axonal swellings in human post-mortem tissue is disorganized neurofilament[29]. Interestingly, we detected disorganized neurofilament in most axonal swellings from healthy young mice (**Fig. 2b** inset). The prevailing interpretation of disorganized neurofilament as a marker of impaired axonal transportation appears incongruous with our observation of their presence in axonal swellings that enhance axonal function, and highlight that some similarities exist between swellings in healthy brains and diseased states.

We determined that axons flanking axonal swellings were similar in diameter to control axons without swellings, suggesting that axonal swellings occur on axons that are not morphologically distinct (**Supplementary Fig. 6**). Axonal propagation is influenced not only by the size of the axonal diameter, but also by the thickness of the myelin sheath surrounding it, which is reflected in an axon's g-ratio (g-ratio = axonal diameter / (axonal diameter + total diameter including myelin sheath))[30]. In agreement with what has been reported for axons with large diameters[31,32], the myelin sheath around axonal swellings is thicker than that around thin axons (**Supplementary Fig. 6**). However, the increase in myelin thickness is modest, and not proportional to the increase in diameter, and as a result the g-ratio for axonal swellings is higher and farther from the theoretical optimal g-ratio (**Fig. 2d; Supplementary Table 1**). This data appears at odds with our findings of unchanged propagation velocity (**Supplementary Fig. 2**), since higher g-ratios are thought to be associated with decreased propagation velocity[30]. Interestingly, despite enhanced myelination, large central axons tend to have larger g-ratios than smaller axons[33,34], which is reminiscent to what we have reported for axonal swellings, and suggests that optimal g-ratios may differ for different classes of axons[24]. Since dynamic regulation of myelin structure may impact axonal

propagation[35], the modest increase in myelination we measured around putative axonal swellings, together with their close proximity to nodes of Ranvier, could contribute to the enhanced propagation fidelity that we have observed (**Fig. 1**).

Axonal swellings form when action potential failure rate is high in the axon

Recent and classic studies have determined that axonal diameter can vary in response to changes in activity[36,37]. Since axonal swellings are associated with reduced axonal propagation failures, we predicted that axonal failures might be involved in their formation. To test this, we perfused a sub-saturating concentration of tetrodotoxin (10 nM; "*low TTX*", which is estimated to block ~ 75% of the Na^+ current in Purkinje cells)[38,39] onto live acute cerebellar slices. By recording spontaneous activity from the soma and/or axon of Purkinje cells, we observed that perfusing *low TTX* significantly reduced firing in axons more extensively than in Purkinje cell somas (**Fig. 3a-c**; n = 17 for somatic and axonal recordings), thereby mimicking high axonal failures pharmacologically. Through time-lapse imaging of GFP-expressing Purkinje cell axons, we discovered that swellings formed on a subset of Purkinje cell axons after 3 hours of *low TTX* application (*low TTX*: 7.11 ± 0.94 new swellings per 100 Purkinje cells; significant difference over time, $P < 0.0001$; n = 38 acquisitions; **Fig. 3d-f**; **Supplementary Movie 1**), while no swelling formation was observed in axons imaged over a 3 hour time period without TTX (*no TTX*: 1.45 ± 0.95 new swellings per 100 Purkinje cells; n = 6; no difference over time, $P = 0.74$; **Fig. 3d-f**). To confirm that the TTX-induced formation of focal axonal swellings was due to differential activity in the soma and axon, and not the binding of Na^+ channels, we applied saturating levels of TTX (200 nM, "*high TTX*") and found that swelling formation was minimal (*high TTX*: 2.26 ± 0.79 new swellings; n = 6; not significantly different over time, $P = 0.74$; **Fig. 3d-f**). This posits that the swellings formed in *low TTX* arise from axonal failures. To gain insight into the time window over which axonal failures

are integrated, we applied *low TTX* briefly for 30 minutes followed with a firing blockade by applying *high TTX* for 90 minutes, or reversed the order, perfusing of *high TTX* first for 30 minutes followed by *low TTX* for 90 minutes. We observed that in both cases, shorter periods of axonal failure produced no formation of new swellings **(Supplementary Fig. 7**), suggesting that swellings only form when a sufficient number of axonal failure has occurred.

Upon pharmacologically mimicking axonal failures, we observed that axonal swellings form on a subset of axons, and wondered whether this selectivity arose from morphological differences between axons. We created 3-D reconstructions from time-lapse images, in *low TTX* conditions, of axons that formed new swellings and neighboring axons that did not (**Fig. 3g**). Over time, the axonal volume increased as axonal swellings formed. However, at time zero, their initial volume was indistinguishable from that of neighboring axons (control axon: 12.5 ± 3.4 μm^3; axon before swelling formed: 19.2 ± 7.7 μm^3; n = 8; P = 0.96; **Fig. 3h, i**). As expected, we observed that following three hours of *low TTX* perfusion, axons that formed swellings had significantly larger volumes than those that did not (control axon: 20.9 ± 6.8 μm^3; axon with a newly-formed swelling: 71.4 ± 17.4 μm^3; n = 8; P = 0.0047; **Fig. 3h, j**). The similarity in volume at the initial time point suggests that there is no obvious morphological signature for axons that will form a swelling, and that swellings do not originate from the local rearrangement of axoplasm in already-thicker axons.

If axonal swellings develop in response to axonal failures, what is the signal that reports when failure occurs? Since activity is implicated, we wondered whether calcium might be playing a role. To address this, we perfused *low TTX* in artificial cerebrospinal fluid (ACSF) without calcium (0 mM Ca^{2+}), and found that the absence of calcium was sufficient to block the formation of axonal swellings (1.86 ± 0.58%; n = 15; not significantly different over time, P = 0.16, **Fig. 4a-c**). Meanwhile, both 2 mM (the concentration in ACSF used in all other experiments) and 3 mM of

calcium resulted in robust swelling formation (2 mM Ca^{2+}: 5.99 ± 1.14%; n = 14; 3 mM Ca^{2+}: 6.81 ± 1.23%; n = 12; both are significantly different over time, P < 0.0001 for both, **Fig. 4a-c**). Importantly, 0 mM Ca^{2+} in the absence of *low TTX* did not cause formation of axonal swellings (0 mM Ca^{2+}: 1.65 ± 0.56%; n = 12; no difference over time, P = 0.25, **Fig. 4a-c).** If extracellular calcium is critical for axonal swelling formation, how might it be involved in signaling? Since voltage-dependent calcium channels are found in Purkinje cell axons, including T-type[40], we predicted that they might be implicated. We applied a saturating concentration of Ni^{2+} (1 mM) that blocks most T-type calcium channels[40-42], but may also impact other voltage-dependent calcium channels as well[43]. We found that 1 mM Ni^{2+} in the presence of *low TTX* prevented the formation of axonal swellings (Ni^{2+} + *low TTX*: 1.19 ± 0.61%; n = 8; *low* TTX: 6.09 ± 1.39%; n = 14 ; *low* TTX significantly different from Ni^{2+}+ *low* TTX, Mann-Whitney U-test, P = 0.0027; **Fig. 4d, e**) while Ni^{2+} without TTX had no effect (1 mM Ni^{2+}: 1.58 ± 0.81%; n = 6; **Fig. 4d, e**). A sub-saturating concentration of Ni^{2+} partially blocked the formation of axonal swellings, (**Supplementary Fig. 8**). These findings suggest that axonal action potential failures trigger axonal swelling via calcium entry through voltage-dependent calcium channels.

Elevated numbers of axonal swellings are linked to enhanced cerebellar learning

Does the increase in axonal action potential propagation fidelity associated with axonal swellings have an impact on cerebellar function? To address potential functional changes, we assayed mice with Rotarod (**Fig. 5a**), a motor task implicated in motor coordination and learning[19], and took advantage of the natural variability in learning that is observed across young adult mice (**Fig. 5b**). After performing behavioral assays, we quantified the number of Purkinje cell axonal swellings found in the granule cell layer in lobule III of the vermis, a cerebellar region that is important for locomotion[44]. We observed variability in the number of swellings across animals (**Fig. 5b**) which

positively correlated with the amount of learning on the Rotarod task (R = 0.544; P = 0.011; **Fig. 5c**). High-learning mice had significantly more axonal swellings (**Fig. 5d**) than low-learning mice (low learner: 29.8 ± 3.3% axonal swellings; n = 10; high learners: 39.2 ± 3.0% axonal swellings; n = 11; P = 0.046; **Fig. 5e**). These results highlight the positive effect that axonal swellings have on cerebellar-related motor learning. Based on these data, we developed a Monte Carlo simulation to understand the differences in information content in a cerebellar network with varying numbers of axonal swellings. This model enabled us to estimate the amount of learning that can be accounted for by variation in axonal swelling occurrence. The amount of learning that the model predicted varied dramatically depending on the number of swellings (**Supplementary Fig. 9**).

We further investigated the difference in motor learning with a cerebellar-specific assay, the Erasmus ladder[45]. We trained mice to cross an Erasmus ladder every day for 4 days (**Fig. 5f**), noting the amount of learning that occurred. As we observed for Rotarod, there was significant heterogeneity in learning across mice (**Fig. 5g**). Still, learning was positively correlated with the number of axonal swellings found in lobule III of the cerebellar vermis (R = 0.776; P = 0.008; **Fig. 5h, i**). When mice were grouped into low and high learners on the Erasmus ladder, we found that high learners had significantly more axonal swellings than low learners (low learners: 34.9 ± 4.2%; n = 5; high learners: 46.6 ± 2.2%; n = 5; P = 0.039; **Fig. 5j**).

To determine whether axonal swellings influence behavior in a cerebellar region with a well-defined associated behavior, we tested the adaptation of the vestibular ocular reflex (VOR; **Fig. 5k**). VOR adaptation is known to be encoded by Purkinje cells in the flocculus[46], which differ in intrinsic firing rate from those in lobule III[47,48]. There is relatively little variability across animals for VOR adaptation (**Fig. 5l**). These experiments were also conducted in C57Bl/6J mice and axonal swellings were labeled with IP3R, which we have shown labels the majority (~ 80%), but not all,

of axonal swellings in both Lobule III and the flocculus (**Supplementary Fig. 3**). We observed a positive correlation between the number of axonal swellings and learning in the flocculus that was reminiscent of the correlation seen in the anterior vermis, although not significant (R = 0.627; P = 0.052; **Fig. 5m, n**); furthermore, no significant difference was observed between the low and high learners (low learners: 13.2 ± 1.5%; n = 5; high learners: 17.8 ± 2.2%; n = 5; P = 0.12; **Fig. 5o**). This suggests that variability in axonal swellings in the flocculus does not account for the variability in learning in this task. However, taken together, our data suggest that axonal swellings have a modest but positive impact on cerebellar function, a trend that is consistent with their ability to ameliorate axonal spike fidelity.

As we observed fewer axonal swellings in the flocculus than in the anterior vermis of mice, we harnessed tissue clearing and light-sheet imaging techniques to determine whether the number of swellings varied across cerebellar region (**Supplementary Movie 2**). Focusing on the cerebellar vermis, we found that the number of swellings varied dramatically across cerebellar lobules, with lower numbers of swellings in posterior lobules (**Supplementary Fig. 10**). Having conducted the Rotarod task prior to imaging, we were also able to observe the positive correlation between the density of axonal swellings and learning: greater density of swellings tended to coincide with more learning (**Supplementary Fig. 10**).

Discussion

Here we describe the unexpected observation that Purkinje cell axonal swellings in young mice are associated with enhanced axonal fidelity and cerebellar performance. Using targeted paired recordings, we report that Purkinje cell axons presenting focal swellings have significantly fewer axonal failures than Purkinje cell axons without swellings, with no detectable changes in firing

properties. Purkinje cell axonal swellings are myelinated, show no evidence of being synaptic structure, but are frequently observed in proximity to nodes of Ranvier or at locations enriched with oligodendrocytic cytoplasm, and have a moderately thicker myelin sheath than those surrounding smaller axons, as well as a higher g-ratio. These characteristics of swellings observed at the ultrastructure level may contribute to the enhanced action potential fidelity observed in axons with swellings. We wondered if axonal failures are instrumental in the formation of axonal swellings, and found that by mimicking high axonal failures, we could induce the formation of swellings on Purkinje cell axons within 2 to 3 hours. Axonal swelling formation required extracellular calcium entry and was blocked by a voltage-dependent Ca^{2+} channel blocker, suggesting that neurons detect axonal failures by the integration of calcium influx through voltage-dependent channels. Finally, using three different cerebellar-related behavioral assays, we demonstrated a positive correlation between motor learning and the number of axonal swellings in related cerebellar structures in young adult mice. Light-sheet imaging revealed that the density of axonal swellings even varies within an animal across cerebellar lobules. These data suggest that there is a behavioral read-out to the enhancement of axonal propagation associated with axonal swellings.

Modeling studies have mostly predicted that action potentials moving across axons that swell will be delayed, filtered, or fail to propagate[12-14], although this depends greatly on the precise geometry of the swelling, with small differences leading to large and at times opposite outcomes[14]. Furthermore, these models have typically focused on non-myelinated axons, so it is unclear how they apply to myelinated axons like those of Purkinje cells. For myelinated axons, the g-ratio is a concept that relates the thickness of myelination to an axon's diameter, and has been studied extensively. Theoretically, there is an optimal g-ratio that produces the fastest propagation

velocity[30]. However, since g-ratios assume regular shape[30], it is difficult to interpret g-ratios for axonal swellings. These pitfalls may explain why our experimentally-determined findings of enhanced action potential propagation fidelity – without detectable change in propagation velocity – appear at odds with model predictions.

Does the ultrastructural composition of axonal swellings impact axonal propagation? There are several possible ways this may occur. First, enriched organelles found in disease-related swellings[29] may alter axonal axial resistance, although we did not observe significant enrichment in axonal swellings from young healthy mice. Moreover, IP3 receptors in axonal swellings on ER in proximity to mitochondria likely result in biochemical signal compartmentalization in the axon swelling. Whether the proximity of these signaling cascades to perinodal structures directly impacts saltatory conduction is an unresolved but exciting possibility that is suggested by recent findings from Cohen and colleagues, who report that perinodal structures play a role in saltatory conduction[26]. It is possible that the enhancement of action potential propagation fidelity in the axon by axonal swellings results more from the compartmentalization of intracellular signaling in swellings, rather than from biophysical properties conferred by their morphology.

Axonal plasticity enables neurons to modulate their excitability and optimize neuronal output. For example, activity-dependent modulation of the axon initial segment (AIS), where action potentials are initiated, enables neurons to homeostatically adapt to alterations in their activity[2,49,50,51]. The formation of axonal swellings is reminiscent of homeostatic synaptic and intrinsic alterations like synaptic scaling or firing rate homeostasis that optimize network output[52,53]. For axonal swellings, however, axon propagation fidelity appears to be the output that is being optimized. Additionally, activity-dependent myelination has been observed in several brain regions, where axons with heightened activity trigger oligodendrocytes to increase myelination[54-56]. We observed differences

in the density of axonal swellings across individual mice that relates to behavior, suggesting that axonal swellings represent a novel form of structural plasticity that the nervous system utilizes to influence its function. Understanding how neurons decode axonal failures leading to the formation of axonal swellings is an important question to be answered. The signaling pathway involving calcium influx may take place directly in the axon, since voltage-dependent calcium channels are expressed in axons[40]. However, it is also possible that signals occur in distal locations that are then are relayed to the axon, or that signaling originate from the surrounding myelin sheath rather than from the axon itself[57], perhaps explain the relatively slow time course of swelling formation.

We observed a correlation between the density of axonal swellings and different cerebellar-related forms of behavioral learning. These findings were surprising to us, since learning and memory are thought to be largely determined by synaptic plasticity[58]. Yet many factors contribute to successful learning, including the reliable transmission of information. Indeed, we found that the number of axonal swellings correlates with motor performance on the last day of the motor assay as well with the amount of learning, albeit this correlation was weaker for some behaviour (data not shown). A parsimonious explanation of our data is that the correlation between learning and axonal swellings arises because information becomes more reliably propagated in the cerebellum, and that the effect on learning could thus be indirect. Chaisanguanthum and colleagues recently showed that even a single extra action potential in Purkinje cells in the cerebellar flocculus could impact eye-movement behavior variability[59]. These data argue that reliable transmission of action potentials in axons is essential for the engagement of appropriate forms of synaptic plasticity in the brain.

Purkinje cells transmit information in vivo with two distinct patterns: simple spikes and complex spikes. Purkinje cell axons have been reported to have relatively low propagation failure rates for simple spikes with higher failures for complex spikes[23,38,40]. Our study has focused on spontaneous

action potentials, which correlate with simple spikes. How and if axonal swellings impact complex spike propagation down the axon is an intriguing question to be explored.

Purkinje cell axons are important because they transmit information from the cerebellar cortex to downstream targets. Interestingly, similar axonal swellings, or spheroids, have been observed in several locations, including frontal lobe white matter[60,61], hippocampus[62], basal ganglia[63], brain stem[64], and spinal cord[65,66]. Axonal swellings in other brain regions have frequently been associated with neurodegenerative diseases[60-63,65], although axonal swellings have also been reported in other brain regions from healthy humans[64,66] and animal models[66]. Whether axonal swellings on axons in other brain regions cause enhanced action potential propagation as we have observed, or whether our results arise from a unique property of Purkinje cell axons remains to be determined.

Axonal swellings in neurodegenerative diseases have typically been regarded as morphological signatures of neuronal dysfunction[8-11]. Although one suggestion raised by our findings is that disease-related axonal swellings might also serve an adaptive role, several alternative explanations exist. It is possible that disease-related axonal swellings differ from those observed in healthy states, as mice used in our study were young and healthy and did not suffer from a neurodegenerative disease. Furthermore, axonal swellings in neurodegenerative diseases exhibit heterogeneity in their myelination; that is, some diseases are associated with axonal swellings that are myelinated while others are associated with predominantly unmyelinated swellings[67]. Differences in underlying axonal dysfunction may produce axonal swellings that look similar at the light-microscopic level, but that are nonetheless structurally and functionally distinct. It would be interesting to test the functional properties of axonal swellings arising from disease models to gain insight into whether disease-related swellings show similar properties to those characterized

here. Regardless of whether they are similar or distinct from one another, our findings highlight the importance of empirically determining the impact of morphological specializations on neuronal function.

In conclusion, our data demonstrate that Purkinje cell axonal swellings constitute an adaptive alteration to morphology that maintains optimal axonal propagation. In light of the central role that Purkinje cell axonal conductance plays in transmitting information from the cerebellar cortex, it appears that axonal swellings are structures that can form dynamically and enable a Purkinje cell to maintain axonal propagation fidelity, thereby optimizing cerebellar function[53].

Methods

Animals: We used *pcp2-tau-eGFP* mice[16,17] to characterize the functional properties of axonal swellings as well as for time-lapse visualization of their formation and for Rotarod and Erasmus Ladder behavioral studies. C57BL/6J mice were used for vestibular ocular reflex (VOR) behavioral study. All animal procedures were approved either by the McGill Animal Care Committee, in accordance with guidelines established by the Canadian Council on Animal Care, or for experiments from **Fig. 5k-o** by the Dutch Ethical Committee for animal experiments in accordance with the Institutional Animal Care and Use committee at the Erasmus Medical Centre.

Behavior: Mice were used at 1-2 months of age for all behavioral studies. *Rotarod Assay.* We used a Rotarod (Stoelting Europe, Dublin, Ireland) as previously described [19] to assess the natural variability of individual mice motor coordination. After an hour of acclimatization, mice were placed on an accelerating (from 4 to 40 RPM, over 5 min) Rotarod and latency to fall (4 trials/day for 7 days) was recorded. Motor learning was determined by subtracting the average time on the rod of the last two trials for day 1 from day 7. *Erasmus Ladder Assay*. We used the Erasmus Ladder (Noldus Inc., Wageningen, GE, Netherlands) to assess motor learning[45]. Mice walked across a horizontal ladder (42 trials/day for 4 days), which consisted of 2 parallel rows of 37 pressure monitored rungs between two dark chambers. Mice typically used short steps (stepping between two upper rungs) to traverse the ladder. The change in the number of short steps across days was used to measure motor learning in individual animals. *VOR Assay*. Mice were equipped with a construct for immobilization ("pedestal") under general anesthesia with isoflurane/O_2. After a 2–3 days of recovery, mice were head-fixed with the body loosely restrained in a custom-made restrainer and placed in the center of a turntable (diameter: 60 cm) in the experimental set-up. A round screen (diameter 63 cm) with a random dotted pattern ('drum') surrounded the mouse during

the experiment. VOR Phase reversal was induced by training mice over 4 days (6 x 5 min. per day) using in-phase sinusoidal drum and table rotation at 0.6 Hz (amplitude table 5° on all days, drum 5° on day 1, 7.5° on day 2, 10° on day 3-4) and probed by recording VOR in the dark before and after training sessions. A CCD camera fixed to the turntable monitored the eyes of the mice using eye-tracking software (ETL-200, ISCAN systems, Burlington, NA, USA). For eye illumination during the experiments, two infrared emitters (output 600 mW, dispersion angle 7°, peak wavelength 880 nm) were fixed to the table and a third emitter, which produced the tracked corneal reflection, was mounted to the camera and aligned horizontally with the optical axis of the camera. Eye movements were calibrated by moving the camera left-right (peak-to-peak 20°) during periods that the eye did not move[48]. Gain and phase values of eye movements were calculated using custom-made Matlab routines (MathWorks, Natick, MA, USA).

Acute Slice Preparation: Acute slices were prepared from young juvenile mice (postnatal (P)9-14), when axonal swellings are numerous[4]. Mice were deeply anesthetized using isoflurane and checked for foot-paw reflex. Mice were decapitated, and the brain quickly removed in ice-cold artificial cerebrospinal fluid (ACSF; in mM: 125 NaCl, 2.5 KCl, 2 $CaCl_2$, 1 $MgCl_2$, 1.25 NaH_2PO_4, 26 $NaHCO_3$ and 20 glucose, bubbled with 95% O_2 and 5% CO_2 to maintain pH at 7.3; Osmolarity 320 ± 5 mOsm). Parasagittal cerebellar vermis slices (200 μm thick) were made using a Leica VT 1000S vibratome. Slices were incubated in ACSF at 37°C for 45 min and then incubated at room temperature (RT) until used for experiments. All chemicals were purchased from Sigma-Aldrich (Oakville, ON, Canada).

Electrophysiology: All recordings were taken in lobule III from the cerebellar vermis, using a Multiclamp 700B amplifier (Molecular Devices, Sunnyvale, CA, USA), at 33°C. An upright microscope (Scientifica, Uckfield, UK) combined with a custom-built two-photon Ti:Sapphire

laser (MaiTai; Spectra Physics, Santa Clara, CA, USA) was used to identify Purkinje cells soma with intact axons (GFP). Glass pipette dipped in CdSeS/ZnS alloyed quantum dots (Sigma-Aldrich, Oakville ON, CA) were visually positioned using the scanning two-photon laser as previously described[15]. Loose cell-attached or extracellular recording of Purkinje cells soma and axons was performed using a custom-designed Igor Pro acquisition and data analysis software (Wavemetrics, Portland, OR, USA). Axons were recorded in the granule cell layer, downstream from axonal swellings (50-200 μm from the parent soma), or an equivalent distance down a control axon without swellings. Approximately 30% of axons display swellings at this age[4]. We only recorded from axons with single swellings, which were the majority of axons with swellings (98.7%, or 950/963 of axons with swellings had single swellings, N = 4 animals; **Supplementary Fig. 1**).

Imaging: Parasagittal cerebellar slices were imaged with a custom-built two-photon microscope (Scientifica) with a Ti:Sapphire laser (MaiTai; Spectra Physics, Santa Clara. CA, USA) tuned to 890 nm (GFP) or 775 nm (non-GFP). Images acquisition was done using ScanImage running in MatLab (Mathworks, Natick, MA, USA). For live imaging, cerebellar slices were kept alive by continuously perfusing buffered ACSF (with drugs) at 33°C. For fixed tissue, slices from the vermis were imaged on a LSM800 laser scanning confocal microscope (Zeiss, Oberkochen, Germany), while slices from the flocculus were imaged using an LSM700 laser scanning confocal microscope (Zeiss).

Pharmacology: Tetrodotoxin (TTX; Biotium Inc., Fremont, CA, USA) was used at a concentration of 10 nM (*low TTX*) or 200 nM (*high TTX*) and Nickel chloride (NiCl; Sigma-Aldrich, Oakville, ON, Canada) was used at a concentration of 1 mM in ACSF. Extracellular Ca^{2+}

was also manipulated by changing its concentration in the ACSF (3 mM or 0 mM) while keeping the concentration of other positively-charged divalent ions (e.g. Mg^{2+}) constant.

Immunocytochemistry: Mice were anesthetized using an intraperitoneal (IP) injection of Avertin (2,2,2-tribromoethanol; dosage: 0.25 mL/10 g body weight), and transcardially perfused with 4 % paraformaldehyde (PFA; Electron Microscopy Sciences, Hatfield, PA, USA). Perfused brains were removed and stored at 4°C on a rotary shaker at 70 RPM for 24 hours in 4 % PFA. Brains were then transferred into phosphate-buffered saline (PBS) with 0.05 % sodium azide. Brain were sliced on a Leica vibratome 3000 into 100 μm-thick parasagittal slices or on a cryostat Leica CM into 40 μm-thick coronal slices. In some cases, brain slices were briefly washed in a 0.1mg/ml pepsin solution dissolve in 1x phosphate buffer (PB), for 5min at RT for antigen retrieval. Slices were washed in 1x PBS - 0.4% Triton X, blocked with 5 % BSA, and primary antibodies (anti-mouse CASPR, used at a dilution of 1:200, Antibodies Incorporated, Davis, CA, US, Cat#75-001; anti-rabbit IP3R, used at a dilution of 1:200, Abcam, Cambridge, UK, abID#5804) were applied to slices for 3 days while incubated on a rotary shaker at 70 RPM at RT. After washing, secondary donkey anti-mouse or anti-rabbit antibodies conjugated to Alexa Fluor-594 (1:500, Life Technologies, Carlsbad, CA, USA, product # A12203; Jackson Immunoresearch Labs, West Grove, PA, USA, product # 711-585-152, respectively) were applied to slices while incubated on the rotary shaker for 90 min at RT. Slice were mounted on slides with Prolong gold anti-fade mounting media (Life Technologies). For imaging of axonal swellings in the flocculus, experiments differed from above in the following manner: mice were deeply anesthetized through IP administration of sodium pentobarbital, and brains were post-fixed for 1 hour instead of 24 hours, and were subsequently transferred to a 10% sucrose solution overnight at 4ºC. The following day they were embedded with 10% sucrose/14% gelatin (Wako) and placed in a 30%

sucrose/10% formaldehyde for 1 hour at RT, and then were switched to a 30% sucrose solution overnight at 4ºC. Embedded brains were sectioned transversally into 40 μm-thick slices with a freezing microtome. Sections were rinsed with 0.1 M PB and incubated for 2 hours in 10 mM sodium citrate (pH 6) at 80 ºC for 2 hours for antigen retrieval. 10% horse serum was used instead of 5% BSA to block non-specific binding, and antibodies were applied for 2 instead of 3 days. Primary antibodies used were Calbindin (1:7000 mouse monoclonal, Sigma C9848), and IP3R (1:1000 rabbit polyclonal, Abcam 5804). Secondary antibodies used were coupled to Alexa Fluor-488 or Cy3 (1:200). Sections were mounted on coverslips in Chromaluin (genatin/chromate) and covered with Mowiol mounting medium (Polysciences Inc., Bergstrasse, Germany).

Electron Microscopy: Mice were anesthetized using an IP injection of Avertin and transcardially perfused with a combination of 2% Glutaraldehyde (Electron Microscopy Sciences) and 2% paraformaldehyde (Electron Microscopy Sciences) in 1X PBS at a perfusion rate of 5mL/min. The brain was then removed and placed in 2.5% Glutaraldehyde in 0.1M sodium cacodylate (Electron Microscopy Sciences) buffer at 4°C, overnight. Brains were dissected to isolate the anterior lobules of the cerebellar cortex. TEM was performed of axons located in the anterior cerebellar lobules 3, 4, and 6. Lobules were kept at 4ºC in fixative no longer than a week before being processed for TEM. Subsequently, samples were washed 3 times with 0.1M sodium cacodylate washing buffer (Electron Microscopy Sciences) for 1 hour. The samples were then post-fixed using 1% aqueous osmium tetraoxide (Mecalab, Montreal, QC, Canada) and 1.5% aqueous potassium ferrocyanide for 2 hours, followed by 3 washes of washing buffer for a total of 15 minutes. Then, samples were dehydrated with acetone (Fisher Scientific) in increasing concentrations (30%, 50%, 70%, 80%, 90%, 3 X 100%) for 8-15 min per concentration. Samples were then infiltrated with Epon (Mecalab) in acetone as follows: 1:1 overnight, 2:1 the next day,

3:1 the following night, and pure Epon the last day for 4 hours. Samples were embedded and allowed to polymerize in a 60ºC oven for 48 hours. Samples were trimmed and cut at 90-100 nm thick sections with UltraCut E ultramicrotome (Leica Microsystems, Wetzlar, HE, Germany, formerly Reichert-Jung) and placed onto slotted grids (Electron Microscopy Sciences). Finally, sections were stained with uranyl acetate (Electron Microscopy Sciences) for 8 min, followed by Reynold's lead (Electron Microscopy Sciences) for 5 min. Samples were imaged using FEI Tecnai G2 Spirit Twin Cryo-TEM (FEI Company, Hillsboro, OR, USA) at 120 kV and visualized with an AMT XR80C 8 megapixel CCD camera (Advanced Microscopy Techniques, Woburn, MA, USA).

Tissue Clearing: Mice were anesthetized and transcardially perfused as above. The brain was removed and transferred into 4% PFA and stored at 4°C on a rotary shaker at 70RPM for 24 hours after which the cerebellar cortex was isolated and transferred into a hydrogel solution (10% v/v 10X PBS, 10% v/v 40% Acrylamide; 0.025% v/v 10% VA-044 and filled up to 15ml with ddH_2O) at 4°C for 24h. The cerebella were then transferred to the X-Clarity Polymerization system (Logos Biosystem, Annandale, VA, USA) at 37°C, under 90 kPa vacuum for 3 hours, followed by the X-Clarity Tissue Clearing system, using the electrophoretic tissue clearing solution (Logos Biosystem, Annandale, VA, USA) set at a current of 1 Amp at 37°C for 24h. A Lightsheet Z.1 with the Zen 2014 SP1 (black edition) software (Zeiss, Oberkochen, Germany) was used to image the whole cerebellum.

Monte Carlo Simulation: A Monte Carlo simulation was created in Python (python.org). Purkinje cell firing and failure rate modelling was done with a tkinter graphical user interface. The network simulates the convergence of 40 Purkinje cells upon a single DCN cell[68] for a 200,000-Purkinje cell network. Firing rates were taken from our previously published WT datasets[19, 20] and failure rates were drawn from our experimental data (**Fig. 1**). Each simulation was repeated 5000

times. Behavioral simulation is done using a linear regression calculated from experimental data to simulate to link between expected learning and expected spike failures rate.

Data Analysis: We used a custom-designed Igor Pro 8 software for electrophysiology data analysis of spike timing, frequency, regularity and failures. Image analysis of 2-photon image stacks was conducted out with Fiji/ImageJ2 or Zen 2014 SP1 (black edition: Zeiss). Lightsheet image processing was done using Zen 2.5 (blue edition), Imaris File Converter and Stiching 9.2.1 software, and analysis was completed using Imaris 9.3.0 software (Bitplane Inc., Zurich, Switzerland). For axonal reconstructions in **Fig. 3**, we used Neurolucida software (MBF Biosciences, Williston, VT, USA) to reconstruct an axonal swelling and the sections of axon flanking both sides of the swelling, in addition to an equivalent length of neighboring axon without a swelling. For measurement of velocity, axons were reconstructed from the recording location to the soma using Simple Neurite Traces, a plugin for ImageJ. For EM images, axons were unbiasedly identified and imaged using the presence of myelin. Using Fiji/ImageJ2, the axonal circumference was traced and minimum Feret diameter was measured. In one case where minimum Feret diameter was not applicable (i.e. in **Fig. 2a** when the axon was not spherical but rather was observed in cross-section, and thus rectangular in shape), the diameter was taken by averaging 4 diameters along the axon. Myelin thickness was quantified by measuring myelin width at 4 cartesian points, although care was taken to avoid locations where myelin infiltration occurred. Organelle density was measured by tracing organelle bodies and was quantified as the ratio between the area covered by organelles to the total axonal area. Organelles included mitochondria, ER, and putative endosomes and lysosomes, and excluded neurofilament.

Statistics: Data normality and equality of variance were determine using Shapiro-Wilk and Levene's test. Multiple comparisons with repeated measures ANOVA were performed using IBM

SPSS Statistics (IBM Corp., Armonk, NY, USA). All reported data are interaction effect of conditions over time corrected for sphericity using Greenhouse-Geisser test, with post-hoc analysis with Bonferroni correction were performed between all conditions over time. Due to low degree of freedom, the assumption of normality is not always respected. To address that concern, non-parametric multiple comparisons were made using Kruskal-Wallis *H* test to compare all conditions at the last time point, followed by Mann-Whitney *U* test corrected with Bonferroni. Simple comparison were made using either paired or unpaired two-tailed Student's *T* tests for parametric data, or the Mann Whitney *U* test for non-parametric data, and correlations were made using the Pearson (r) correlation test in SPSS software. Data were reported as mean ± SEM. Statistical comparisons were made with the level of significance (α) set at P* < 0.05; P** < 0.01; P*** < 0.005, unless corrected with Bonferroni.

Acknowledgements

We thank S. du Lac and M. Häusser for generously providing the mice, which originated in the du Lac lab. We thank J. Sjöström for custom software for action potential failure analysis, E. Ruthazer, R. A. McKinney, J. Sjöström, and A. Fournier for thoughtful input on the project, and comments from D. Jaarsma. We thank members of the Watt lab (past and present) for input, support and feedback on the project and the manuscript as well as N. Recio and A. Huang for technical contribution. We thank Claire Brown and other members of the McGill University Life Sciences Complex Advanced BioImaging Facility (ABIF) and Jackie Vogel and other members of the McGill University Integrated Quantitative Biology Initiative (IQBI) for technical resources and support with X-clarity, lightsheet and confocal imaging and image analysis. We thank the members of the McGill University Facility for Electron Microscopy Research (FEMR) for

technical assistance with TEM. We thank members of the McGill GCC animal care facility for technical assistance, and L. Post and S. Sahin for technical contributions to the VOR data. This work was supported by a Postgraduate PGS-D Scholarship-Doctoral (D.L.-O.) and Summer Undergraduate Research Awards (C.L. and C.R.) from the Natural Science and Engineering Research Council of Canada (NSERC), a McGill Integrated Program in Neuroscience (IPN) Returning Student Award (C.S.), and a New Investigator (Nouveau Chercheur) Grant from the Fonds de Recherche Nature et Technologies de Quebec (AJW, 189153), a European Research Council grant (MS, ERC-Stg No. 680235), a Canadian Institutes of Health Research (CIHR) Operating Grant (AJW, 130570) and Project Grant (AJW, 153150), an NSERC Discovery Grant (AJW, 05118), and a Canadian Foundation for Innovation (CFI) Leaders Opportunity Fund (AJW, 29127).

Author contributions

D. L.-O. designed and ran experiments and analyzed data for all Figures, and helped write the manuscript, F.C.G.B. designed and ran experiments for Fig. 5 and helped write the manuscript, C.A.S. designed, ran experiments and analyzed data for Fig. 2 and helped write the manuscript. P.V.B. ran experiments for Fig. 5. C.H.L. designed and ran experiments for Fig. 3 and Fig. S10 and helped write the manuscript. C.V.E. designed and ran Monte Carlo simulation for Fig. S9. C.R. ran experiments for Fig. 1. P.L.F. helped interpret data for Fig. 2 and helped write the manuscript. M.S. designed experiments and analyzed data for Fig. 5 and helped write the manuscript. A.J.W. conceived of the project, designed experiments and analyzed data, supervised the project, and wrote the manuscript.

Supplementary Information

Supplementary Figs. 1-10

Supplementary Table 1

Supplementary Movies 1-2

Data Availability

The authors declare that the data supporting the findings and custom code used to analyze the findings of this study are available from the corresponding author upon reasonable request. Source data are provided as a Source Data file.

References

1. Debanne, D. Information processing in the axon. *Nat Rev Neurosci* **5**, 304-316 (2004).
2. Grubb, M.S. & Burrone, J. Activity-dependent relocation of the axon initial segment fine-tunes neuronal excitability. *Nature* **465**, 1070-1074 (2010).
3. Gravel, C., Leclerc, N., Plioplys, A. & Hawkes, R.B. Focal axonal swellings in rat cerebellar Purkinje cells during normal development. *Brain Res* **363**, 325-332 (1986).
4. Ljungberg, L., *et al.* Transient Developmental Purkinje cell axonal torpedoes in healthy and ataxic mouse cerebellum. *Frontiers in cellular neuroscience*, 1-15 (2016).
5. Baurle, J. & Grusser-Cornehls, U. Axonal torpedoes in cerebellar Purkinje cells of two normal mouse strains during aging. *Acta neuropathologica* **88**, 237-245 (1994).
6. Kato, T. & Hirano, A. A Golgi study of the proximal portion of the human Purkinje cell axon. *Acta neuropathologica* **68**, 191-195 (1985).
7. Louis, E.D., Faust, P.L., Vonsattel, J.P. & Erickson-Davis, C. Purkinje cell axonal torpedoes are unrelated to advanced aging and likely reflect cerebellar injury. *Acta neuropathologica* **117**, 719-721 (2009).
8. Louis, E.D., Kuo, S.H., Vonsattel, J.P. & Faust, P.L. Torpedo formation and Purkinje cell loss: modeling their relationship in cerebellar disease. *Cerebellum* **13**, 433-439 (2014).
9. Babij, R., *et al.* Purkinje cell axonal anatomy: quantifying morphometric changes in essential tremor versus control brains. *Brain* **136**, 3051-3061 (2013).
10. Louis, E.D., *et al.* Torpedoes in Parkinson's disease, Alzheimer's disease, essential tremor, and control brains. *Mov Disord* **24**, 1600-1605 (2009).
11. Redondo, J., *et al.* Purkinje Cell Pathology and Loss in Multiple Sclerosis Cerebellum. *Brain Pathol* **25**, 692-700 (2015).
12. Manor, Y., Koch, C. & Segev, I. Effect of geometrical irregularities on propagation delay in axonal trees. *Biophys J* **60**, 1424-1437 (1991).
13. Maia, P.D., *et al.* Diagnostic tools for evaluating the impact of Focal Axonal Swellings arising in neurodegenerative diseases and/or traumatic brain injury. *J Neurosci Methods* **253**, 233-243 (2015).
14. Goldstein, S.S. & Rall, W. Changes of action potential shape and velocity for changing core conductor geometry. *Biophys J* **14**, 731-757 (1974).

15. Andrasfalvy, B.K., *et al.* Quantum dot-based multiphoton fluorescent pipettes for targeted neuronal electrophysiology. *Nat Methods* **11**, 1237-1241 (2014).
16. Sekirnjak, C., Vissel, B., Bollinger, J., Faulstich, M. & du Lac, S. Purkinje cell synapses target physiologically unique brainstem neurons. *J Neurosci* **23**, 6392-6398 (2003).
17. Watt, A.J., *et al.* Traveling waves in developing cerebellar cortex mediated by asymmetrical Purkinje cell connectivity. *Nature neuroscience* **12**, 463-473 (2009).
18. Walter, J.T., Alvina, K., Womack, M.D., Chevez, C. & Khodakhah, K. Decreases in the precision of Purkinje cell pacemaking cause cerebellar dysfunction and ataxia. *Nature neuroscience* **9**, 389-397 (2006).
19. Jayabal, S., Chang, H.H., Cullen, K.E. & Watt, A.J. 4-aminopyridine reverses ataxia and cerebellar firing deficiency in a mouse model of spinocerebellar ataxia type 6. *Sci Rep* **6**, 29489 (2016).
20. Ady, V., *et al.* Altered Synaptic and Intrinsic properties of cerebellar Purkinje cells in a mouse model of ARSACS. *Journal of Physiology* **596**, 4253-4267 (2018).
21. Stoodley, C.J., *et al.* Altered cerebellar connectivity in autism and cerebellar-mediated rescue of autism-related behaviors in mice. *Nature neuroscience* **20**, 1744-1751 (2017).
22. Khaliq, Z.M. & Raman, I.M. Axonal propagation of simple and complex spikes in cerebellar Purkinje neurons. *J Neurosci* **25**, 454-463 (2005).
23. Monsivais, P., Clark, B.A., Roth, A. & Hausser, M. Determinants of action potential propagation in cerebellar Purkinje cell axons. *J Neurosci* **25**, 464-472 (2005).
24. Hirono, M., *et al.* BK Channels Localize to the Paranodal Junction and Regulate Action Potentials in Myelinated Axons of Cerebellar Purkinje Cells. *J Neurosci* **35**, 7082-7094 (2015).
25. Watanabe, S., *et al.* Glycosphingolipid synthesis in cerebellar Purkinje neurons: roles in myelin formation and axonal homeostasis. *Glia* **58**, 1197-1207 (2010).
26. Cohen, C.C.H., *et al.* Saltatory Conduction along Myelinated Axons Involves a Periaxonal Nanocircuit. *Cell* **180**, 311-322 e315 (2020).
27. Ishibashi, T., Kodama, A. & Baba, H. Disruption of paranodal axo-glial interaction and/or absence of sulfatide causes irregular type I inositol 1,4,5-trisphosphate receptor deposition in cerebellar Purkinje neuron axons. *J Neurosci Res* **93**, 19-27 (2015).

28. Lee, S., Wang, W., Hwang, J., Namgung, U. & Min, K.T. Increased ER-mitochondria tethering promotes axon regeneration. *Proc Natl Acad Sci U S A* **116**, 16074-16079 (2019).
29. Louis, E.D., Yi, H., Erickson-Davis, C., Vonsattel, J.P. & Faust, P.L. Structural study of Purkinje cell axonal torpedoes in essential tremor. *Neurosci Lett* **450**, 287-291 (2009).
30. Rushton, W.A. A theory of the effects of fibre size in medullated nerve. *The Journal of physiology* **115**, 101-122 (1951).
31. Michailov, G.V., *et al.* Axonal neuregulin-1 regulates myelin sheath thickness. *Science* **304**, 700-703 (2004).
32. Fraher, J.P. Axon-myelin relationships in rat cranial nerves III, IV, and VI: a morphometric study of large- and small-fibre classes. *The Journal of comparative neurology* **286**, 384-390 (1989).
33. Chomiak, T. & Hu, B. What is the optimal value of the g-ratio for myelinated fibers in the rat CNS? A theoretical approach. *PloS one* **4**, e7754 (2009).
34. Guy, J., Ellis, E.A., Kelley, K. & Hope, G.M. Spectra of G ratio, myelin sheath thickness, and axon and fiber diameter in the guinea pig optic nerve. *The Journal of comparative neurology* **287**, 446-454 (1989).
35. Dutta, D.J., *et al.* Regulation of myelin structure and conduction velocity by perinodal astrocytes. *Proc Natl Acad Sci U S A* **115**, 11832-11837 (2018).
36. Chereau, R., Saraceno, G.E., Angibaud, J., Cattaert, D. & Nagerl, U.V. Superresolution imaging reveals activity-dependent plasticity of axon morphology linked to changes in action potential conduction velocity. *Proc Natl Acad Sci U S A* **114**, 1401-1406 (2017).
37. Costa, A.R., Pinto-Costa, R., Sousa, S.C. & Sousa, M.M. The Regulation of Axon Diameter: From Axonal Circumferential Contractility to Activity-Dependent Axon Swelling. *Front Mol Neurosci* **11**, 319 (2018).
38. Khaliq, Z.M. & Raman, I.M. Relative contributions of axonal and somatic Na channels to action potential initiation in cerebellar Purkinje neurons. *J Neurosci* **26**, 1935-1944 (2006).
39. Swensen, A.M. & Bean, B.P. Robustness of burst firing in dissociated purkinje neurons with acute or long-term reductions in sodium conductance. *J Neurosci* **25**, 3509-3520 (2005).
40. Grundemann, J. & Clark, B.A. Calcium-Activated Potassium Channels at Nodes of Ranvier Secure Axonal Spike Propagation. *Cell reports* **12**, 1715-1722 (2015).

41. Mouginot, D., Bossu, J.L. & Gahwiler, B.H. Low-threshold Ca2+ currents in dendritic recordings from Purkinje cells in rat cerebellar slice cultures. *J Neurosci* **17**, 160-170 (1997).
42. Isope, P. & Murphy, T.H. Low threshold calcium currents in rat cerebellar Purkinje cell dendritic spines are mediated by T-type calcium channels. *The Journal of physiology* **562**, 257-269 (2005).
43. Zamponi, G.W., Bourinet, E. & Snutch, T.P. Nickel block of a family of neuronal calcium channels: subtype- and subunit-dependent action at multiple sites. *J Membr Biol* **151**, 77-90 (1996).
44. Reeber, S.L., Otis, T.S. & Sillitoe, R.V. New roles for the cerebellum in health and disease. *Front Syst Neurosci* **7**, 83 (2013).
45. Vinueza Veloz, M.F., *et al.* Cerebellar control of gait and interlimb coordination. *Brain Struct Funct* (2014).
46. Ito, M. Cerebellar control of the vestibulo-ocular reflex--around the flocculus hypothesis. *Annual review of neuroscience* **5**, 275-296 (1982).
47. Zhou, H., *et al.* Cerebellar modules operate at different frequencies. *Elife* **3**, e02536 (2014).
48. Wu, B., *et al.* TRPC3 is a major contributor to functional heterogeneity of cerebellar Purkinje cells. *Elife* **8**(2019).
49. Evans, M.D., Dumitrescu, A.S., Kruijssen, D.L.H., Taylor, S.E. & Grubb, M.S. Rapid Modulation of Axon Initial Segment Length Influences Repetitive Spike Firing. *Cell reports* **13**, 1233-1245 (2015).
50. Kuba, H., Ishii, T.M. & Ohmori, H. Axonal site of spike initiation enhances auditory coincidence detection. *Nature* **444**, 1069-1072 (2006).
51. Kuba, H., Yamada, R., Ishiguro, G. & Adachi, R. Redistribution of Kv1 and Kv7 enhances neuronal excitability during structural axon initial segment plasticity. *Nat Commun* **6**, 8815 (2015).
52. Turrigiano, G.G. & Nelson, S.B. Homeostatic plasticity in the developing nervous system. *Nat Rev Neurosci* **5**, 97-107 (2004).
53. Marder, E. & Goaillard, J.M. Variability, compensation and homeostasis in neuron and network function. *Nat Rev Neurosci* **7**, 563-574 (2006).

54. Purger, D., Gibson, E.M. & Monje, M. Myelin plasticity in the central nervous system. *Neuropharmacology* **110**, 563-573 (2016).
55. Chorghay, Z., Karadottir, R.T. & Ruthazer, E.S. White Matter Plasticity Keeps the Brain in Tune: Axons Conduct While Glia Wrap. *Frontiers in cellular neuroscience* **12**, 428 (2018).
56. Gibson, E.M., *et al.* Neuronal activity promotes oligodendrogenesis and adaptive myelination in the mammalian brain. *Science* **344**, 1252304 (2014).
57. Yin, X., *et al.* Myelin-associated glycoprotein is a myelin signal that modulates the caliber of myelinated axons. *J Neurosci* **18**, 1953-1962 (1998).
58. Suvrathan, A. Beyond STDP-towards diverse and functionally relevant plasticity rules. *Current opinion in neurobiology* **54**, 12-19 (2019).
59. Chaisanguanthum, K.S., Joshua, M., Medina, J.F., Bialek, W. & Lisberger, S.G. The Neural Code for Motor Control in the Cerebellum and Oculomotor Brainstem. *eNeuro* **1**(2014).
60. Jin, C., Washimi, Y., Yoshida, K., Hashizume, Y. & Yazawa, I. Characterization of spheroids in hereditary diffuse leukoencephalopathy with axonal spheroids. *J Neurol Sci* **352**, 74-78 (2015).
61. Trapp, B.D., *et al.* Axonal transection in the lesions of multiple sclerosis. *N Engl J Med* **338**, 278-285 (1998).
62. Galvin, J.E., Uryu, K., Lee, V.M. & Trojanowski, J.Q. Axon pathology in Parkinson's disease and Lewy body dementia hippocampus contains alpha-, beta-, and gamma-synuclein. *Proc Natl Acad Sci U S A* **96**, 13450-13455 (1999).
63. Ohgami, T., Kitamoto, T. & Tateishi, J. Alzheimer's amyloid precursor protein accumulates within axonal swellings in human brain lesions. *Neurosci Lett* **136**, 75-78 (1992).
64. Liberski, P.P. & Budka, H. Neuroaxonal pathology in Creutzfeldt-Jakob disease. *Acta neuropathologica* **97**, 329-334 (1999).
65. Carpenter, S. Proximal axonal enlargement in motor neuron disease. *Neurology* **18**, 841-851 (1968).

66. Clark, A.W., Parhad, I.M., Griffin, J.W. & Price, D.L. Neurofilamentous axonal swellings as a normal finding in the spinal anterior horn of man and other primates. *J Neuropathol Exp Neurol* **43**, 253-262 (1984).
67. Yagishita, S. Morphological investigations on axonal swellings and spheroids in various human diseases. *Virchows Arch A Pathol Anat Histol* **378**, 181-197 (1978).
68. Person, A.L. & Raman, I.M. Purkinje neuron synchrony elicits time-locked spiking in the cerebellar nuclei. *Nature* **481**, 502-505 (2012).

Figures and Figure Legends

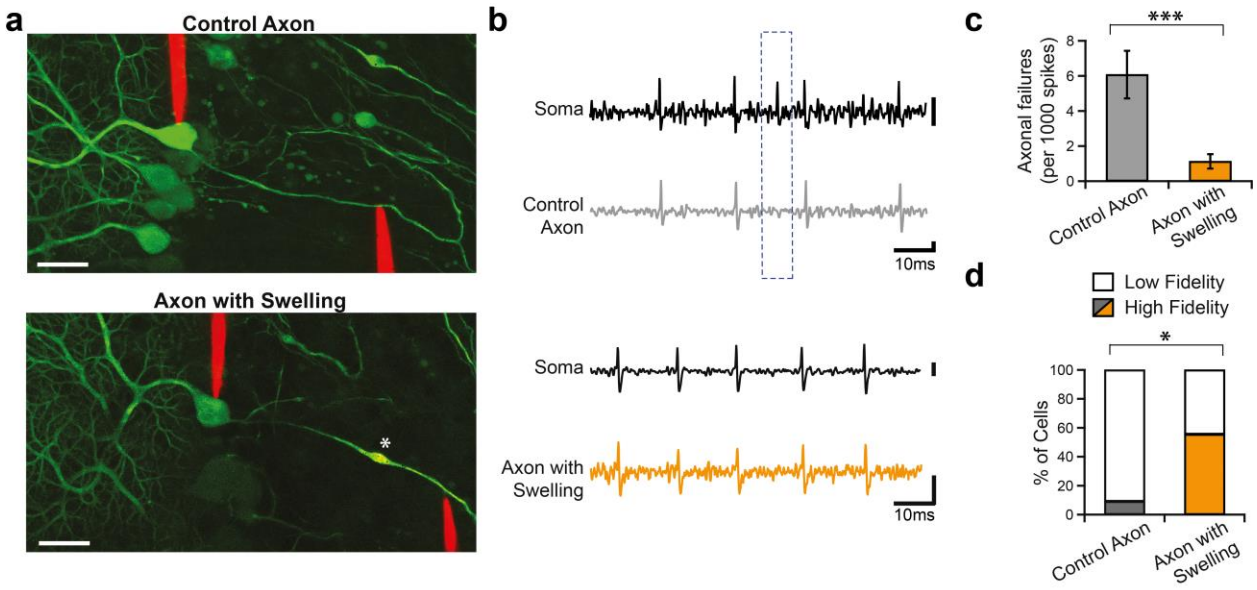

Fig. 1. Axonal swellings are associated with improved axonal propagation of action potentials. (**a**) Representative images of a Purkinje cell with placement of electrodes showing simultaneous dual recording from Purkinje cells soma (left electrode) and axon (right electrode) from a control axon (top) and an axon with a swelling (bottom; asterisk indicates swelling). Scale bar, 25 μm. (**b**) Representative traces of dual recordings from soma (black) and axon corresponding to Purkinje cell axons without (top, grey) and with (bottom, orange) an axonal swelling. Scale bar: 0.5 mV for top two traces, 1 mV and 0.5 mV for bottom two traces, respectively. (**c**) Axonal spike failure rate is significantly reduced in axons with swellings (Control Axon, n= 11; Axon with Swelling, n=9; significantly different, Mann Whitney *U* test; ***P < 0.005). (**d**) Purkinje cell axons with swellings are more likely to be high fidelity transmitters (high fidelity: < 1 of 1000 action potentials fail; low fidelity > 1 in 1000 action potentials fail) than axons

without swellings (Mann Whitney *U* test; P* < 0.05). Source data are provided as a Source Data file.

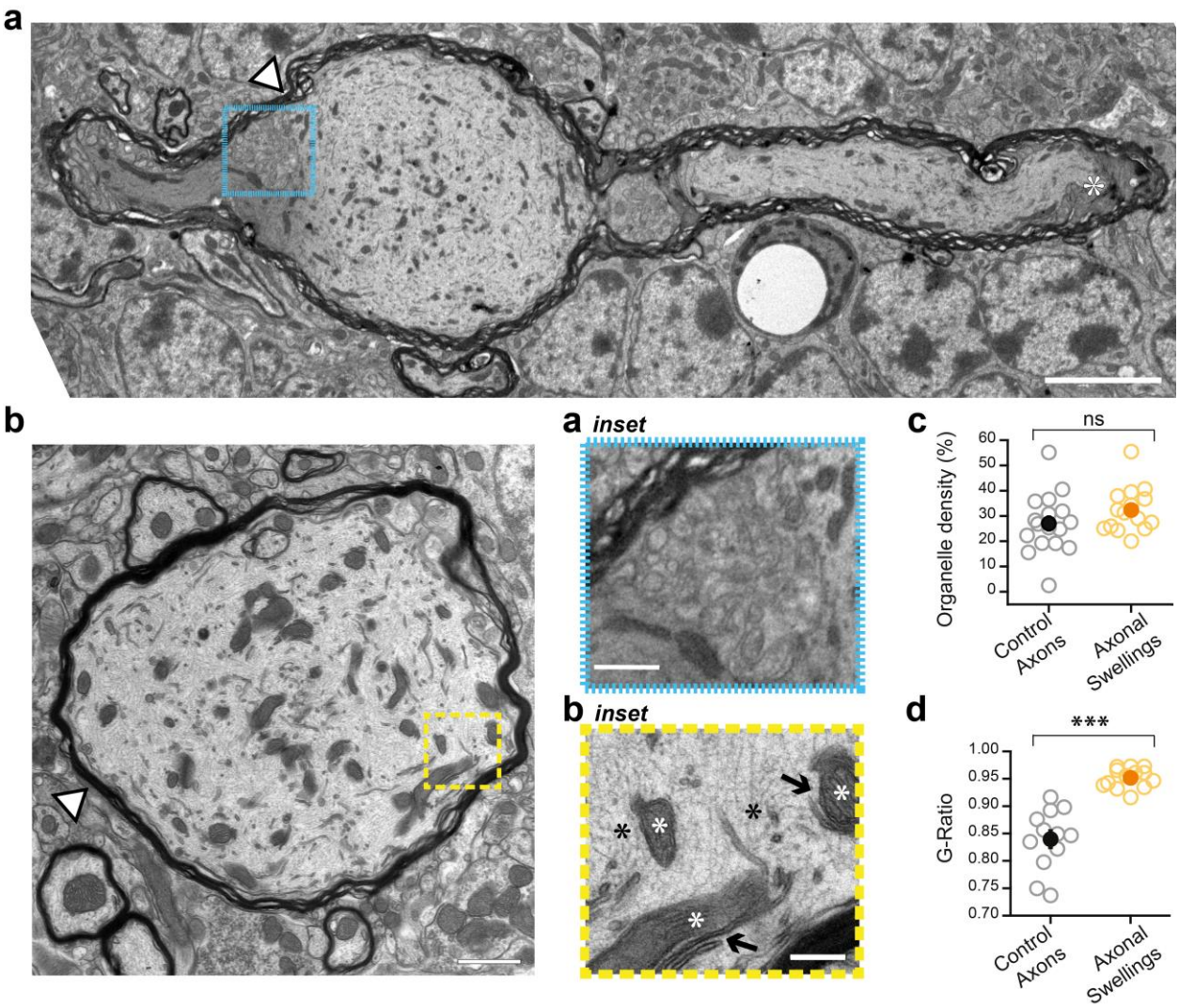

Fig. 2. Purkinje cell axonal swellings are myelinated and are not synaptic structures. (**a**) Representative TEM image showing longitudinal cut of axon with swelling and non-swollen sections extending from both sides of swelling. White asterisk shows perinodal protrusions (PNP) indicating proximity of node of Ranvier. Axon dips out of plane of image to the right of the swelling. Scale bar, 5 μm. Inset below middle: Region of interest delineated by cyan dashed outline in (**a**) shows periaxonal oligodendrocyte cytoplasm. Scale bar, 1 μm. (**b**) Representative TEM image showing crosswise cut of a putative axonal swelling (centre) with 5 neighbouring control

axons, discernable by presence of dark myelin outline. Scale bar, 1 μm. Inset right: Region of interest delineated by yellow dashed outline in (**b**) shows mitochondria (white asterisks) that is in close proximity to EM (black arrows), and disorganized neurofilament (black asterisks). Scale bar, 500 nm. (**c**) Axonal swellings are not enriched in organelles compared to control axons. (Organelles were predominantly mitochondria and ER; n = 17 control axons; n = 15 putative axonal swellings, independent Student *T* test, P = 0.162). (**d**) G-ratio as a function of axonal diameter of control axons (grey) and axonal swellings (orange). Myelin is measured only in compact regions, indicated by the white arrowheads in (**a**) and (**b**). Axonal swellings have a larger g-ratio than smaller axons do. (n = 12 control axons; n = 13 putative axonal swellings, Mann Whitney *U* test; *** P < 0.001). Source data are provided as a Source Data file.

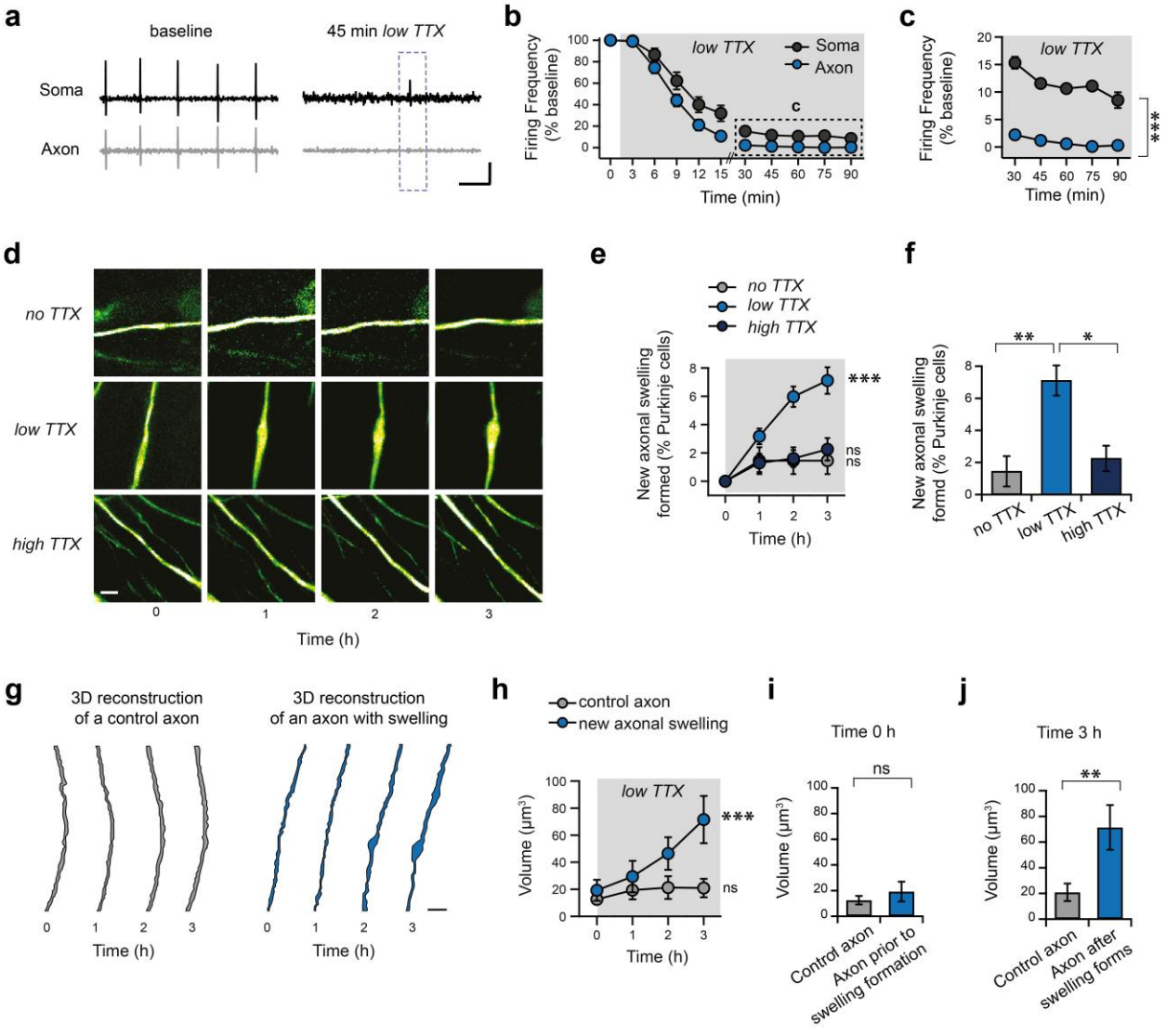

Fig. 3. Enhancing axonal failures causes axonal swellings to form. (**a**) Sample recordings from Purkinje cell soma (top, black) and axon (bottom, grey) prior to (left) and 45 minutes after (right) *low TTX* has been applied onto an acute cerebellar slice. Action potential amplitudes are reduced and axonal failures become prominent. Scale bar, 1 mV, 25 ms. n = 17 for both soma and axon recordings. (**b**) Summary data showing that firing in Purkinje cell axons is reduced to a greater extent than in the soma, mimicking axonal failures. In some cases, axons and soma recordings were not from the same cell. Frequency was normalized to initial frequency prior to TTX wash-in

in order to compare these cases. (**c**) Replotting data in panel (**b**) showing expanded y-axis. Axonal firing rates are significantly lower than somatic firing rates, indicating that more failures occur in the axon and that this persists throughout the recording (repeat-measured ANOVA followed by pairwise comparisons using Bonferroni correction shows significant difference at each timepoint, *** $P < 0.001$). (**d**) Representative images of axons at 1-hour intervals after bath application of regular ACSF (*no TTX*, top); *low TTX* (10nM) and *high TTX* (200nM). Scale bar, 5 μm. **(e)** *Low TTX* treatment results in the formation of new axonal swellings (*no TTX*, n = 6; *low TTX*, n = 38; *high TTX*, n = 6; repeated measures ANOVA showed a significant difference over time for low TTX but not the other conditions, *** $P < 0.001$). (**f**) Summary data showing significant differences in the number of swellings formed in low TTX condition after 3 hours. (Kruskal-Wallis *H* test followed by Mann-Whitney *U* test, with Bonferroni correction; * $\alpha = 0.016$; ** $\alpha = 0.0033$). (**g**) 3-D reconstruction of new axonal swelling (right) and neighbouring axons without the formation of swellings (left) demonstrate that axons that later produce swellings are not morphologically distinct at the initial timepoint (time 0). Scale bar, 5 μm. (**h**) Summary data from 3-D reconstructions reveals that volume of axons with swellings differs after 3 hours, but is not different from control axons at time 0 (control axon, n = 8; new axonal swelling, n = 8; repeated measures ANOVA followed by pairwise comparison corrected with Bonferroni ; P*** < 0.005). (**i**) No differences in axon volume were observed between controls and those that will form new swellings at time 0 (Mann-Whitney *U* test, $P = 0.959$), whereas (**j**) significant differences were observed once the swelling formed after 3 hours (Mann-Whitney *U* test, $P = 0.0047$). Source data are provided as a Source Data file.

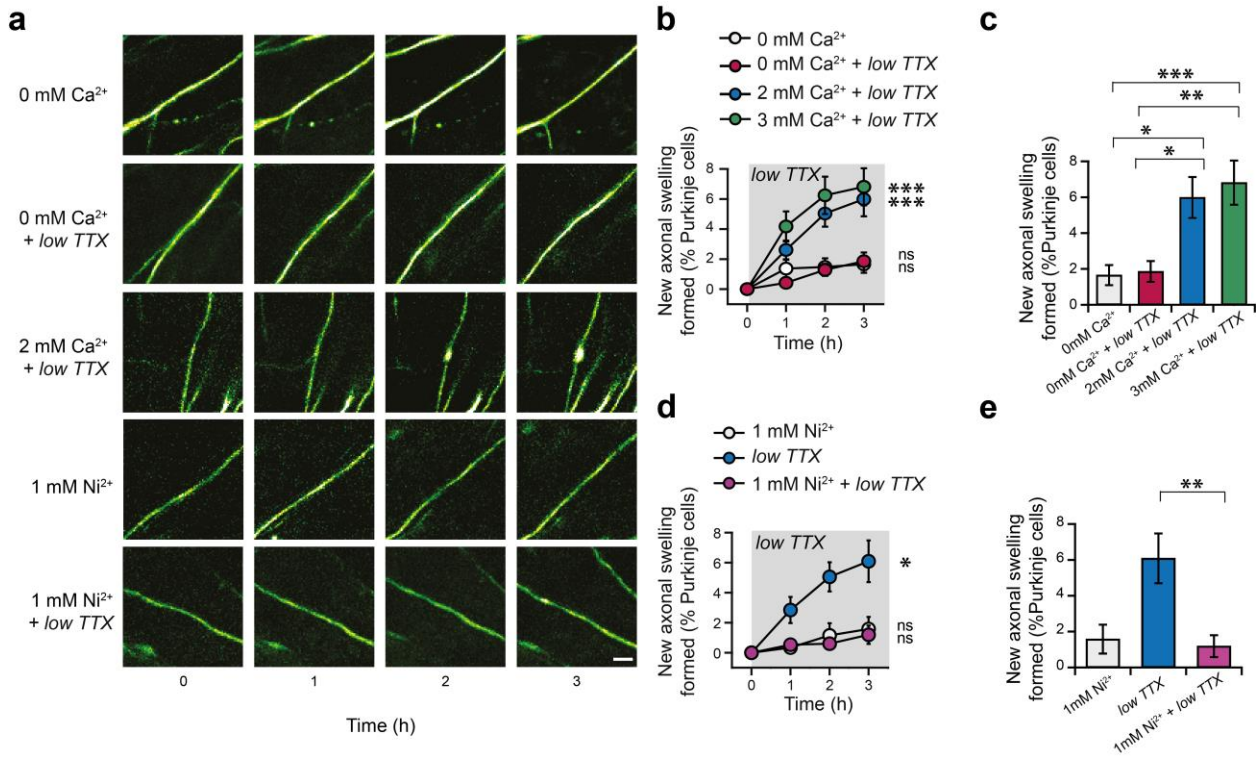

Fig. 4. Axonal swelling formation requires calcium influx through voltage-gated Ca^{2+} channels. (**a**) Representative time-lapse images during bath application of ACSF containing no Ca^{2+} (0 mM Ca^{2+}, top), 0 mM Ca^{2+} with *low TTX* (second row), *low TTX* with 2 mM Ca^{2+} (third row). The formation of axonal swellings in *low TTX* is occluded by the presence of 1 mM Ni^{2+} (fourth row), and Ni^{2+} without TTX does not produce axonal swelling formation. Scale bar, 5 μm. (**b**) Axonal swellings do not form in *low TTX* with 0 mM Ca^{2+}, but do form in both 2 mM and 3 mM Ca^{2+} (repeated measures ANOVA; 0 mM Ca^{2+}, n = 12, P = 0.25; 0 Ca^{2+} + *low TTX*, n = 15, P = 0.16; 2 mM Ca^{2+} (2mM) + *low TTX*, n = 14, P < 0.001; 3 mM Ca^{2+} + *low TTX*, n = 12, P < 0.001). (**c**) Summary data showing that after 3 hours, significantly fewer swellings are observed with 0 mM Ca^{2+} and with 0 mM Ca^{2+} + *low TTX* compared to higher concentrations of Ca^{2+} (2 mM and 3 mM; one-way ANOVA, P = 0.0004, followed by Mann-Whitney *U* tests with Bonferroni

correction). * $\alpha = 0.0083$; ** $\alpha = 0.00167$; *** $\alpha = 0.00083$, data is not significantly different if not shown. (**d**) Summary data showing *low TTX* ACSF containing 1 mM Ni^{2+} occludes the formation of axonal swellings. (repeated measures ANOVA; ACSF containing 1 mM Ni^{2+}, n = 6, P = 0.78; *low TTX*, n = 14, P < 0.001; 1mM Ni^{2+} + *low TTX*, n = 8, P = 0.80). (**e**) Summary data showing that after 3 hours, the number of new axonal swellings is significantly reduced in Ni^{2+} + *low TTX* compared to *low TTX* alone (one-way ANOVA, P = 0.0027). ** $\alpha = 0.00333$; data is not significantly different if not shown. Source data are provided as a Source Data file.

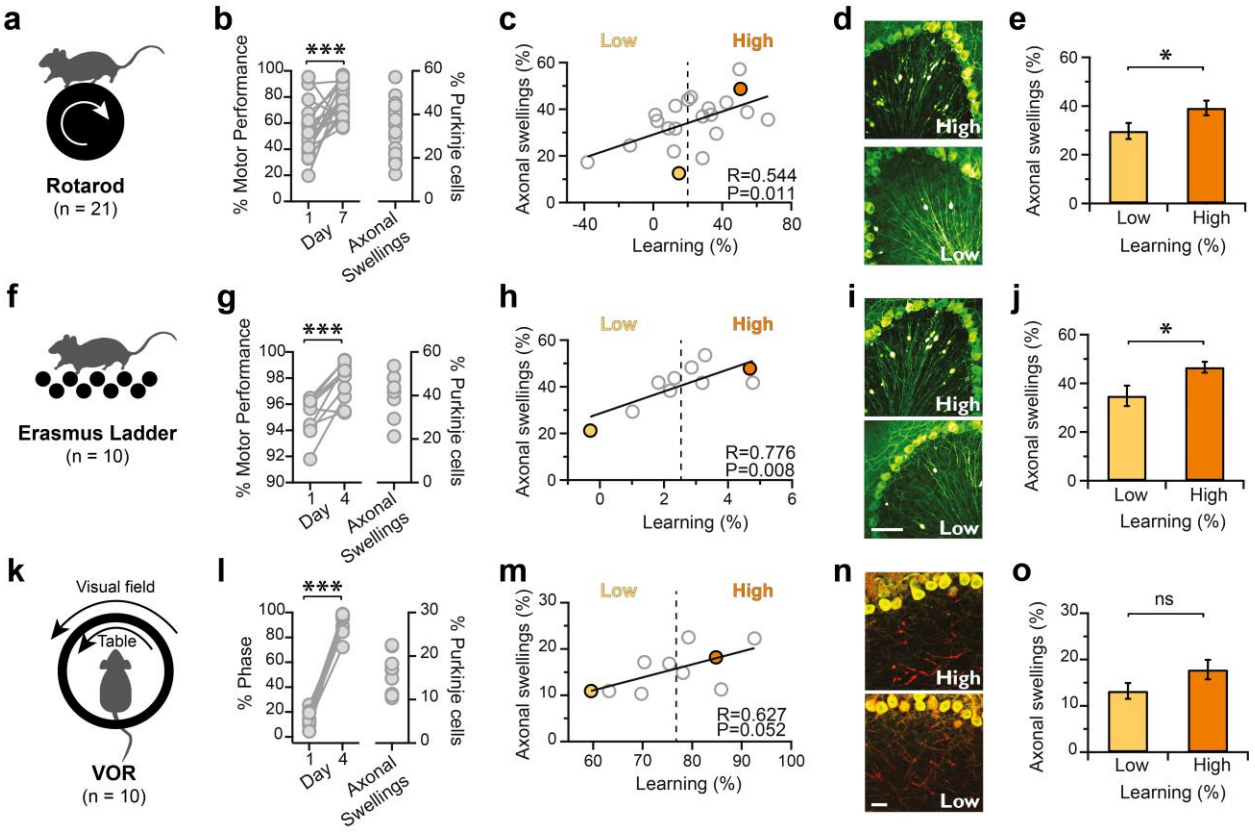

Fig. 5. Axonal swelling density is positively correlated with cerebellar-related learning. (**a**) Rotarod assay. (**b**) Variability in motor learning (left; ***P < 0.005) and the density of axonal swellings in anterior vermis lobule III (right) across mice. (**c**) The variability in motor learning is positively correlated with the density of axonal swellings. The filled orange marker indicates representative high learner in **(d)**, while the yellow marker indicates the low learner in **(d)**. (**d**) Representative images of anterior cerebellar vermis from high learners (top) and low learners (bottom). Note the differences in the number of axonal swellings. (**e**) When mice are separated into high and low learner groups, they have significantly different numbers of axonal swelling, with high learners having more than low learners. (**f**) Erasmus ladder assay. (**g**) Variability in motor learning (left) and anterior lobule swelling density (right) are also observed with Erasmus ladder. (**h**) This variability is positively correlated across animals. (**i**) Representative images from high

(top) and low (bottom) learners on the Erasmus ladder assay. (**j**) High learners on Erasmus ladder show more axonal swellings in lobule III of the vermis than low learners. (**k**) VOR assay. (**l**) Some but less variability in learning is observed in VOR (left) and in the density of axonal swellings in the flocculus (right). (**m**) Variability in learning and axonal swelling density in the flocculus is correlated across animals for VOR. (**n**) Representative images showing axonal swellings (stained with IP3R) in high learners (top) and low learners (bottom) for VOR task. (**o**) The density of axonal swellings in the flocculus is not significantly different in low and high VOR learners, perhaps because only a subset of swellings are labelled with IP3R, although the same trend is observed as for the Rotarod and Erasmus ladder tasks. Source data are provided as a Source Data file.